Regulation of brown adipose tissue metabolism by TP53INP2

Regulació del metabolisme del teixit adipós marró per mitja de TP53INP2

Alba Sabaté Pérez

UNIVERSITAT DE BARCELONA

FACULTAT DE BIOLOGIA

DEPARTAMENT DE BIOQUÍMICA I BIOMEDICINA MOLECULAR

Regulation of brown adipose tissue metabolism by TP53INP2

Regulació del metabolisme del teixit adipós marró per mitjà de TP53INP2

Alba Sabaté Pérez

Barcelona, 2019

UNIVERSITAT DE BARCELONA

FACULTAT DE BIOLOGIA

DEPARTAMENT DE BIOQUÍMICA I BIOMEDICINA MOLECULAR

INSTITUTE FOR RESEARCH IN BIOMEDICINE (IRB BARCELONA)

PROGRAMA DE DOCTORAT EN BIOMEDICINA

Regulation of brown adipose tissue metabolism by TP53INP2

Regulació del metabolisme del teixit adipós marró per mitjà de TP53INP2

Memòria presentada per Alba Sabaté Pérez per optar al grau de doctora per la Universitat de Barcelona.

Alba Sabaté Pérez	Antonio Zorzano Olarte	Xavier Testar Ymbert
Doctoranda	Director i tutor	Director

Barcelona, 2019

CONTENTS

FIGURE CONTENTS

INTRODUCTION

RESULTS

DISCUSSION

MATERIALS AND METHODS

RESUM EN CATALÀ

TABLE CONTENTS

ABBREVIATIONS

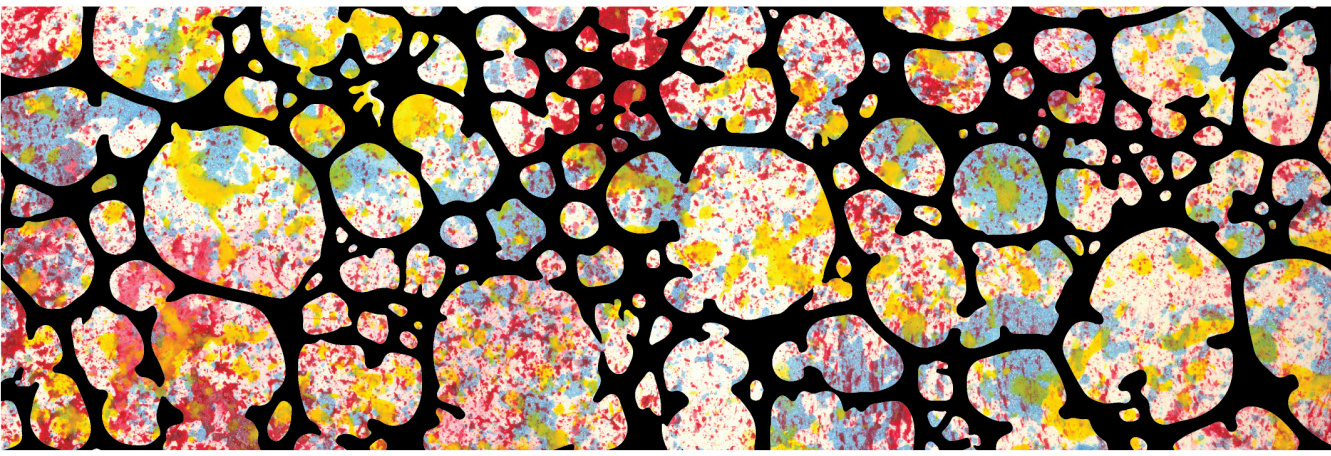

A
aBAT: axillar brown adipose tissue
Ad: adenovirus
Adipo: adipocytes
ADP: adenosine diphosphate
ANCOVA: analysis of covariance
aP2: fatty acid binding protein
AR: adrenergic receptor
ARP: actin related protein
asWAT: anterior subcutaneous white adipose tissue
ATF-2: activating transcription factor 2
ATGL: adipose triglyceride lipase
ATP: adenosine triphosphate
AUC: area under the curve

B
BCA: bicinchoninic acid
BMI: body mass index
BMP: bone morphogenetic protein
BSA: Bovine serum albumin

C
C: control
C I: mitochondrial complex I
C II: mitochondrial complex II
C/EBP: CCCAAT/enhancer-binding protein
cAMP: cyclic adenosine monophosphate
cBAT: cervical brown adipose tissue
CCCP: carbonyl cyanide m-chlorophenyl hydrazone
CD: chow diet
cDNA: complementary deoxyribonucleic acid
Cidea: cell death inducing DFFA like effector A
CL: CL-316,243
Cox: cytochrome c oxidase subunit
CREB: cyclic adenosine monophosphate response element-binding protein

D
Dio2: type II iodothyronine deiodinase
DMEM: Dulbecco's modified Eagle medium
DMSO: dimethyl sulfoxide
DNA: deoxyribonucleic acid
DOR: diabetes and obesity regulated gene
DTT: dithiothreitol

E
E: epoxomicin
E1: ubiquitin-activating enzyme
E2: ubiquitin-conjugation enzyme
E3: ubiquitin ligase enzyme
EBF2: early B cell factor 2
EDTA: ethylenediaminetetraacetic acid
EE: energy expenditure
EGTA: ethylene glycol tetraacetic acid
EHMT1: euchromatic histone-lysine methyltransferase 1
ELISA: enzyme-linked immunosorbent assay
Elovl3: elongation of very long chain fatty acids protein 3
EN1: engrailed 1
ER: estrogen receptor

F
FBS: fetal bovine serum
FFA: free fatty acids
FGF21: fibroblast growth factor 21

G
GABARAP: gamma-aminobutyric acid receptor-associated protein
GABARAPL1: gamma-aminobutyric acid receptor-associated protein-like 1
Gastro: gastrocnemoius muscle
GATE16: gamma-aminobutyric acid receptor-associated protein-like 2
GFP: green fluorescent protein
GLUT1: glucose transporter 1
GLUT4: glucose transporter 4
GR: glucocorticoid receptor
GSEA: gene set enrichment analysis
GTT: glucose tolerance test

H
HBSS: Hanks' balanced salt solution
HDAC3: histone deacetylase 3
HEPES: 4-(2-hydroxyethyl)-1-piperazineethanesulfonic acid
HFD: high fat diet
HRP: horseradish peroxidase
HSL: hormone-sensitive lipase

I
iBAT: interscapular brown adipose tissue
IBMX: 3-isobutyl-1-methylxanthine
IGF-1: insulin-like growth factor 1
IL-6: interleukin-6

ingWAT: inguinal white adipose tissue
ITT: insulin tolerance test

K
KO: knockout
KO^{Myf5}: Myf5-specific TP53INP2 knockout mice
KO^{Ubc}: global-TP53INP2 knockout mice

L
LAMP1: lysosome-associated membrane glycoprotein 1
LB: Luria broth
LC3: microtubule-associated proteins 1A/1B light chain 3B
LD: lipid droplet
LIR: LC3-interacting region
LoxP: locus of X-over P1
LSB: Laemmli sample buffer

M
MEF: mouse embryonic fibroblasts
MFN2: mitofusin 2
MOI: multiplicity of infection
mRNA: messenger ribonucleic acid
mTOR: mammalian target of rapamycin
mWAT: mesenteric white adipose tissue
Myf5: myogenic factor 5
MYOD: myoblast determination protein

N
NCoR1: nuclear receptor co-repressor 1
NCS: newborn calf serum
NE: norepinephrine
NEDD4: E3 ubiquitin-protein ligase NEDD4
Neo: neomycin
NES: nuclear export signal
NLS: nuclear localization signal
NoLS: nucleolar localization signal

O
O/N: overnight
OCR: oxygen consumption rate

P
p38 MAPK: p38 mitogen-activated protein kinase
Pax7: paired box protein 7
PBS: phosphate buffered saline

PCR: polymerase chain reaction
PEI: polyethylenimine
PET/CT: positron emission tomography–computed tomography
PGC1α: peroxisome proliferator-activated receptor gamma coactivator 1-α
pgWAT: perigonadal white adipose tissue
PKA: protein kinase A
PKG: cGMP–dependent protein kinase G
PML: promyelocytic leukemia
PPAR: peroxisome proliferator-activated receptor
PPRE: peroxisome proliferator-activated receptor response element
prBAT: perirenal brown adipose tissue
PRDM16: PR domain zinc-finger protein 16
Pread: preadipocytes
Pref1: preadipocyte factor-1
PTM: post-translational modifications
Puro: puromycin

Q
qPCR: quantitative real-time polymerase chain reaction
Quadri: quadriceps muscle

R
RER: respiratory exchange ratio
RNA: ribonucleic acid
RNAseq: ribonucleic acid sequencing
Rosi: rosiglitazone
rpm: revolutions per minute
rWAT: retroperitoneal white adipose tissue

S
SDS: sodium dodecyl sulfate
siRNA: small interfering ribonucleic acid
SKM: skeletal muscle
SKM-KO: skeletal muscle specific TP53INP2 knockout mice
SKM-Tg: skeletal muscle specific TP53INP2 overexpressing mice
SNS: sympathetic nervous system
SV40-LT: simian vacuolating virus 40 large T antigen
SVF: stromal vascular fraction

T
T3: thyroid hormone triiodothyronine
TAG: triglycerides
TAM: 4-hydroxy-tamoxifen
TBP: TATA box-binding protein-like protein 1
TBS: tris-buffered saline

TCA cycle: tricarboxylic acid cycle
TCF/LEF: T cell factor/lymphoid enhancer
Tibial: tibialis anterior muscle
TIM44: mitochondrial import inner membrane translocase subunit 44
TP53INP1: tumor protein p53 inducible nuclear protein 1
TP53INP2: tumor protein p53 inducible nuclear protein 2
TR: thyroid hormone receptor
TRAF6: tumor necrosis factor receptor-associated factor 6
TRAIL: tumor necrosis factor-related apoptosis-inducing ligand
TRE: thyroid hormone receptor elements

U
UCP: uncoupling protein
UIM: ubiquitin-interacting motif

V
VCO_2: carbon dioxide production
VDR: vitamin D receptor
VO_2: oxygen consumption

W
WT: wild type

^{18}F-FDG: fluorodeoxyglucose (^{18}F)

INTRODUCTION

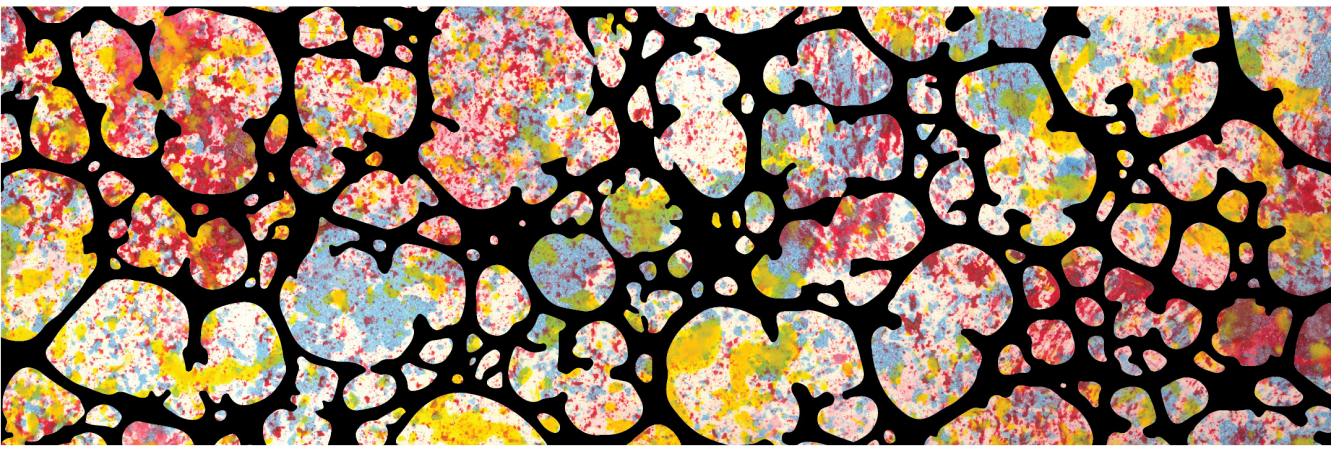

2.1. The adipose organ

The adipose tissue, once considered a passive organ involved in fat accumulation, it is nowadays clear that is a dynamic tissue involved in several physiological processes. It is a highly heterogeneous tissue distributed in depots all around the body, differing from morphology, composition and function. Traditionally it has been classified into two main types, white adipose tissue and brown adipose tissue.

On the one hand, white adipose tissue accounts for the majority of the depots present in mammals and it is the main site for energy storage in the form of triglycerides (TAG). White adipose cells are characterized by the presence of a big lipid droplet which occupies the majority of the cytoplasm. This induces the compression of the nucleus between the plasma membrane and the lipid droplet. The cytosolic compartment has few and non-dense mitochondria. In addition to being an energy repository organ, white adipose tissue also releases cytokines that modulate whole-body metabolism and insulin sensitivity (Kershaw and Flier, 2004).

On the other hand, brown adipose tissue is specialized in energy dissipation through thermogenesis and has reduced capacity for energy storage. It is composed of brown adipocytes that contain several small lipid droplets. They also contain a centrally located nucleus surrounded by the cytoplasm and by a large number of mitochondria, which are densely packed with cristae. In fact, this huge amount of mitochondria containing iron pigmented cytochromes confers brown adipocytes its brown color.

Albeit of their opposite functions, white and brown adipose cells are directly involved in the control of fat mass, and a correct equilibrium between their functions is required in order to preserve energy balance.

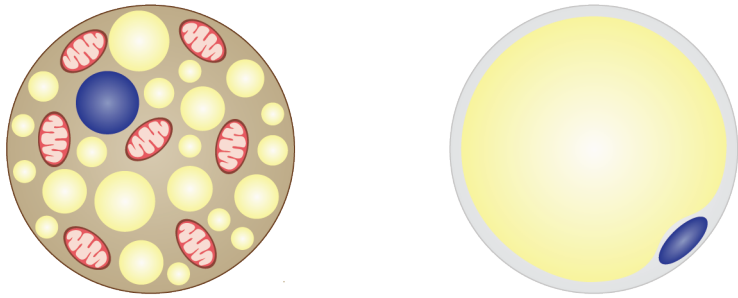

Figure 1. Morphological characteristics of brown and white adipocytes. Brown adipocytes have small and multilocular lipid droplets and high number of mitochondria, whereas white adipocytes are unilocular and have few mitochondrial content.

This thesis is focused on the understanding of brown adipose tissue development and metabolism.

2.2. Brown adipose tissue

2.2.1. Brown adipose tissue structure and physiological relevance

Brown adipose tissue was described for the first time as *nec pinguitudo nec caro* (neither fat nor flesh) by Kornad Gessner in 1551. But it was not till the last century when it was realized that brown adipose tissue is a unique organ that is present in all mammals, including humans.

In rodents and in hibernators, brown adipose tissue can be found during the entire lifespan. However, in other species, including humans, it decreases with ageing. The main brown adipose depot, in mice or rats, is localized in the interscapular region, but other smaller depots can also be found in cervical, axillary, perirenal and periaortic regions (Waldén et al., 2012; Zhang and Bi, 2015). Brown adipocytes themselves constitute the main volume of the tissue and provide a source of heat

to protect newborns against cold exposure (Géloën et al., 1990), but they are accompanied by several cell types. Contrary to white adipose tissue, brown adipose tissue is highly vascularized as it needs significant amount of oxygen and nutrients for its function and has to distribute the heat produced throughout the whole body (Cinti, 2005). It is also densely innervated by the sympathetic nervous system, which exerts the central control of brown adipose tissue activity (Fawcett, 1952; Cannon and Nedergaard, 2004). Precursor adipose cells, or preadipocytes, are distributed within the tissue, and are induced to proliferate and differentiate under conditions of high thermogenic demand (Géloën et al., 1990). In such situations, not only the number of preadipocytes and adipocytes are increased, but also the capillaries and nerve innervation are expanded in order to satisfy energy needs. These morphological rearrangements of the tissue upon prolonged conditions of increased thermogenesis demand, as cold exposure, are known as brown adipose tissue recruitment. In addition to the classical brown adipose depots, brown-like adipocytes, or also called "beige" or "brite" adipocytes, can be recruited in white adipose tissue depots under conditions requiring increased heat production (Young et al., 1984; Cousin et al., 1992; Wu et al., 2012).

The physiological role of brown adipose tissue is to protect the body against environmental changes such as cold exposure or lipid overload. Under these conditions, non-shivering thermogenesis is induced in brown adipocytes in order to maintain body temperature or to prevent an excessive accumulation of energy in the body. These two processes are also referred as cold- or diet-induced thermogenesis respectively. Thus, the thermogenic potential of brown adipose tissue allows small mammals to live in cold environments without relying on the shivering process to maintain body temperature (Himms-Hagen, 1990).

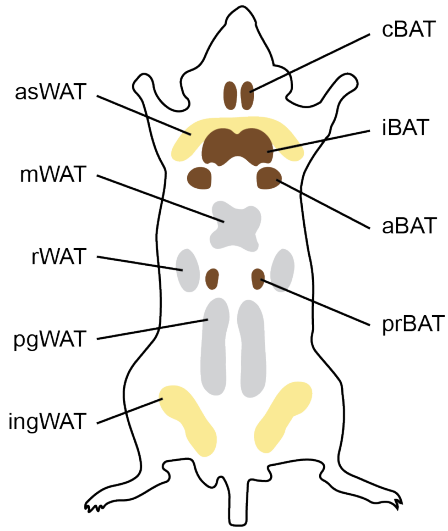

Figure 2. Adipose tissue depots in mice. Subcutaneous depots: cervical, interscapular and axillar brown adipose tissue (cBAT, iBAT and aBAT), anterior subcutaneous and inguinal white adipose tissue (asWAT and ingWAT). Visceral depots: perirenal brown adipose tissue (prBAT), perigonadal, mesenteric and retroperitoneal white adipose tissue (pgWAT, mWAT and rWAT).

The concept of diet-induced thermogenesis emerged in the 1970s by Rothwell and Stock. At that time, they observed that rats that were fed with a hypercaloric diet underwent an increased oxygen consumption and gained less weight than the expected from the excess caloric intake. With such a diffuse definition, it is not surprising that some studies have questioned the truly existence of a diet-induced thermogenic effect different to the obligatory diet thermic effect, referred as the thermogenic response to food intake including digestion and absorption (Maxwell et al., 1987; Kozak, 2010). It was some years ago when stringent approaches were used to directly identify and characterize the nature of diet-induced thermogenesis (Feldmann et al., 2009; von Essen et al., 2017), which is now defined as the facultative (directly induced by food intake) and adaptive (as it develops during periods of lipid overload) capacity to increase energy expenditure in response to caloric excess.

Thermogenic activity in brown adipocytes is possible due to the activity of the

mitochondrial proton transport uncoupling protein 1 (UCP1), which is located in the inner mitochondrial membrane and uncouples oxidative phosphorylation from ATP production to release energy in the form of heat (Lowell and Spiegelman, 2000; Cannon and Nedergaard, 2004). UCP1, previously referred as thermogenin, was the first uncoupling protein identified, and was found to be expressed exclusively in brown or beige adipocytes (Lin and Klingenberg, 1980; Cannon et al., 1982). Other uncoupling proteins have been described (UCP2 and UCP3) and are expressed also in other tissues than brown adipose tissue (Fleury et al., 1997; Vidal-Puig et al., 1997), but UCP1 is considered the only one capable of inducing thermogenesis (Matthias et al., 2000).

Energy balance is the resultant of energy intake, and energy expenditure, through basal metabolism, exercise and thermogenesis. Thus, obesity develops when energy intake exceeds energy waste during prolonged periods. In this regard, brown adipose tissue activity can directly impact on energy balance preventing an excessive fat mass gain. Moreover, brown adipose tissue dysfunction has been related to the development of obesity as a result of decreased energy expenditure (Lowell et al., 1993). Further evidences supporting the role of brown adipose tissue in the control of body weight came from the studies using UCP1 knockout mice, which in the presence of a high fat diet and in the absence of cold-stress develop an obese phenotype (Feldmann et al., 2009). Conversely, genetic or pharmacological elevation of brown and/or beige fat activity in animal models has been reported to protect against obesity (Kopecky et al., 1995; Guerra et al., 1998; Cederberg et al., 2001).

2.2.2. Brown adipogenesis

Brown adipose tissue develops and differentiates during fetal life, since newborns require the presence of active thermogenesis to survive. Lineage tracing studies have demonstrated that brown and white adipose cells, in opposite to what was expected, do not arise from the same precursor, but instead, brown precursor cells

share more similarities with myoblasts. Classical brown preadipocytes originate from precursor mesenchymal stem cells that express myogenic factor 5 (Myf5), paired box protein 7 (Pax7) and engrailed 1 (EN1) (Atit et al., 2006; Timmons et al., 2007; Lepper and Fan, 2010; Sanchez-Gurmaches and Guertin, 2014). Beige adipose cells have a distinct origin than brown adipocytes, and its differentiation will not be discussed in this thesis. The determination between brown adipocyte versus muscle fate is mediated by the activation of a group of genes that control brown preadipocyte commitment and induce the stable silencing of the muscle-specific gene program. These group of genes include the early B cell factor 2 (EBF2), the euchromatic histone-lysine methyltransferase 1 (EHMT1) and the PR domain zinc-finger protein 16 (PRDM16). For instance, EBF2 represses the expression of myoblast determination protein (MYOD) and myogenin (Wang et al., 2014). EHMT1 is a crucial enzymatic component of the PRDM16 complex, which together with its binding partners CCCAAT/enhancer-binding protein-β (C/EBPβ) and peroxisome proliferator-activated receptor-γ (PPARγ) configure a transcriptional complex to induce the thermogenic program of brown fat cells (Seale et al., 2007, 2008; Kajimura et al., 2009; Ohno et al., 2013). Thus, genetic ablation of EHMT1 substantially impairs brown adipogenesis but also induces the ectopic expression of skeletal muscle selective genes (Ohno et al., 2013). Another protein that is required for progenitor cells to commit to brown lineage is bone morphogenetic protein 7 (BMP7). It is expressed early during the process of differentiation, and suppresses adipogenic inhibitors such as necdin and preadipocyte factor-1 (Pref1). Consequently, it induces the expression of brown fat regulators as PRDM16 and triggers brown adipocyte phenotype with UCP1 expression (Tseng et al., 2008; Schulz et al., 2013).

Despite different physiological functions and developmental origins, white and brown adipogenesis are mainly controlled by PPARγ and C/EBPs transcription factors (Barak et al., 1999; Rosen et al., 1999; Karamitri et al., 2009). However, their expression and activity are differentially regulated by cell type-selective regulators

which results into two distinct phenotypes. C/EBPβ is induced early during differentiation, and induce the expression of both PPARγ, C/EBPα. Subsequently, PPARγ and C/EBPα activate each other's expression to coordinate the expression of a several genes that will define the differentiated adipocyte (Farmer, 2006). In addition, C/EBPβ interaction with PRDM16 is essential to co-activate the transcriptional activity of the mitochondrial biogenesis nuclear coactivator factor PPARγ coactivator 1α gene (PGC1α) (Kajimura et al., 2009).

PPARγ is considered the master adipogenic transcription factor adipocyte differentiation from preadipocytes. It is considered an essential protein for both white and brown adipogenesis, as PPARγ-deficient mouse models showed no formation of white or brown adipose tissues (Barak et al., 1999; Rosen et al., 1999; Koutnikova et al., 2003). However, ectopic expression of PPARγ into non-adipose cells drives them into white but not brown adipocyte like cells, proving that additional transcriptional factors are required to cooperate with PPARγ in order to induce brown fat features (Tontonoz et al., 1994; Kajimura et al., 2010). PPARγ appears to be dispensable for brown fat cell commitment (Barak et al., 1999), however genetic mutations lowering PPARγ activity have been associated to a reduction in brown adipose tissue development and thermogenic activity (Gray et al., 2006), indicating that its function is required for brown fat maturation and function. Several post-translational modifications have been described to modulate the transcriptional activity of PPARγ, including phosphorylation (Hu et al., 1996), sumoylation (Floyd and Stephens, 2004; Ohshima et al., 2004; Qiang et al., 2012), acetylation (Qiang et al., 2012) and ubiquitination (Hauser et al., 2000; Kilroy et al., 2009). Nonetheless, these studies were mainly performed in white adipose cells and whether PPARγ is similarly regulated in brown adipocytes remains to be determined. In addition, PPARγ activation by its specific ligands has been reported to enhance the thermogenic machinery of brown adipose tissue and to induce the browning of white fat by stabilizing PRDM16 protein (Petrovic et al., 2008; Ohno et al., 2012).

Although C/EBPβ and PPARγ are clearly necessary for brown adipogenesis, their overexpression is not sufficient to completely induce the brown adipogenic transcriptional program, evidencing that other brown fat-specific transcriptional regulators are required for this process (Tapia et al., 2018).

PRDM16 is a transcriptional co-activator that binds to and activates the transcriptional activity of PPARγ, peroxisome proliferator-activated receptor-α (PPARα), C/EBPs and PGC1α (Seale et al., 2008; Hondares et al., 2011a; Harms et al., 2015). It is involved in the early determination of brown fat lineage, as it induces the expression of brown fat thermogenic program, and also represses the muscle and white adipose specific gene programs. Mechanistically, it has been also reported that PRDM16 induces the expression of UCP1 through its interaction with PGC1α (Iida et al., 2015). Hence, overexpression of PRDM16 into white adipocytes is sufficient to induce the expression of the thermogenic gene program, and also to repress the expression of white adipose selective genes (Seale et al., 2007; Kajimura et al., 2008, 2009). Moreover, mice that overexpress PRDM16 under the control of the fatty acid binding protein (aP2), showed brown features into white adipose depots, increased whole body oxygen consumption and protection against diet-induced obesity (Seale et al., 2011). Nonetheless, PRDM16 deletion in Myf5-positive precursor cells does not affect embryonic development of brown adipose tissue. This was explained by a compensatory mechanism mediated by PRDM3, a protein from the PRDM family that shows high homology to PRDM16 (Harms et al., 2014). However, PRDM16 ablated mice showed a decline in brown adipose tissue with age, demonstrating a role for PRDM16 in the maintenance of brown adipocyte identity. This resulted in cold intolerance, which reveals a defective non-shivering thermogenesis by the lack of PRDM16 in brown precursor cells.

PGC1α was described in the late 1990s as an interacting partner of PPARγ that was able to induce UCP1 expression (Puigserver et al., 1998). Since then, several studies have characterized PGC1α function and nowadays it is known as a regulator of brown adipocyte fate through the interaction with different transcription factors to

induce the expression of genes involved in mitochondrial biogenesis, peroxisome remodeling and β-oxidation (Wu et al., 1999a; Puigserver and Spiegelman, 2003; Bagattin et al., 2010). In addition, its overexpression in white adipocytes is sufficient to induce brown fat characteristics in these cells, including UCP1 expression and increased mitochondrial content (Puigserver et al., 1998; Tiraby et al., 2003).

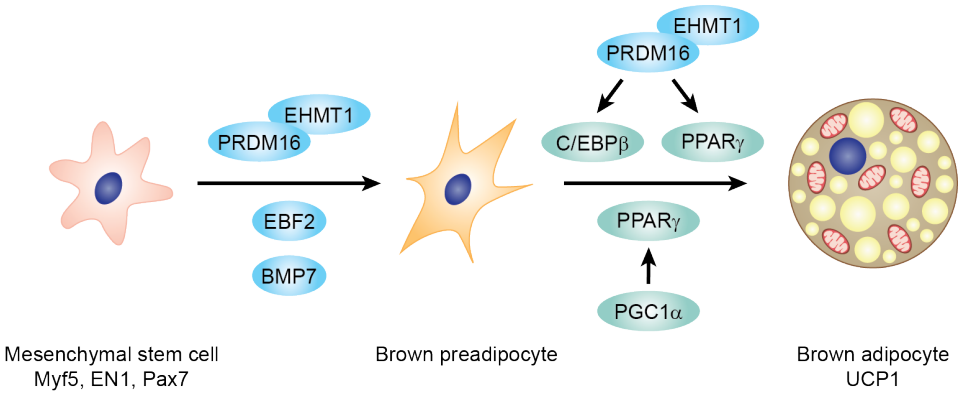

Figure 3. Brown adipocyte differentiation. Brown preadipocyte commitment is regulated by BMP7, EBF2 and EHMT1 interaction with PRDM16. Brown adipogenesis is initiated by the interaction of the transcriptional co-activator PRDM16 with transcription factors C/EBPβ and PPARγ. These interactions induce the acquisition of the brown adipocyte features and promotes mitochondrial biogenesis through the transcriptional co-activator PGC1α. UCP1 expression in brown adipocytes is stimulated by PPARγ together with PGC1α.

2.2.3. Regulation of thermogenesis and UCP1

Non-shivering thermogenesis is the process by which energy from the oxidative phosphorylation is released in the form of heat mediated by UCP1, a proton transporter located in the inner mitochondrial membrane of brown and beige adipocytes. The sympathetic nervous system (SNS) is the major regulator of this process under acute and prolonged brown adipose tissue activation, by the release of catecholamines upon cold or diet exposure. Norepinephrine (NE), the catecholamine with higher activity in the context of brown adipose tissue, is released by the innervated adrenergic nerves and interacts with adrenergic receptors of brown adipocytes cell membrane to activate thermogenesis.

Brown adipocytes express different types of adrenergic receptors, i.e. β, α1 and α2, all of them being activated by NE. Among them, β-adrenergic receptors are the most significant and the most studied pathways involving thermogenic stimulation. Of the three subtypes of β-adrenergic receptors (β1, β2 and β3), β3-adrenergic receptor appears to be the most relevant in mediating brown adipocyte activation in rodents (Granneman and Lahners, 1995; Cannon and Nedergaard, 2004). β1-adrenergic receptors are also expressed in brown adipocytes, but under physiological conditions they are not coupled to thermogenesis signaling (Susulic et al., 1995; Bronnikov et al., 1999). Despite being present in brown adipose tissue, β2-adrenergic receptors are not expressed by brown adipocytes, but predominantly found in vascular cells (Rothwell et al., 1985; Bengtsson et al., 2000).

The next step of the adrenergic signaling is mediated via adenylate cyclase: NE stimulation of β3-adrenergic receptors results in the accumulation of cAMP (Zhao et al., 1997). Increased cAMP concentration induce the activation of protein kinase A (PKA), which in turns phosphorylates the hormone-sensitive lipase (HSL) and the lipid droplet-associated protein perilipin, leading to the hydrolysis of the stored TAG (Holm, 2003; Souza et al., 2007). Thus, the activation of lipolysis increases intracellular free fatty acids (FFA) levels that can directly activate UCP1 function (Prusiner et al., 1968). In these regard, alterations in the adipose triglyceride lipase activity (ATGL), that mediates the hydrolysis of TAG to diglycerides, result in cold intolerance due to insufficient FFA levels to enhance UCP1 activity (Haemmerle, 2006). PKA induces the phosphorylation of several signaling molecules that will mediate the thermogenic response. The transcription factor cAMP response element-binding protein (CREB) is activated by PKA phosphorylation in order to induce target gene expression, including UCP1, the final effector of heat release (Thonberg et al., 2002). Also, the p38 mitogen-activated protein kinase (p38 MAP kinase or MAPK) pathway is induced upon PKA activation. p38 MAPK phosphorylates the activating transcription factor 2 (ATF-2), which results in PGC1α expression and mitochondrial biogenesis. But also, p38

MAPK phosphorylates and activates PGC1α which enhances UCP1 expression (Cao et al., 2001, 2004). p38 MAPK is also activated by the atrial and ventricular natriuretic peptides released upon cold exposure. They signal through guanylyl cyclase-coupled receptors, inducing cGMP–protein kinase G (PKG), upstream of p38 MAPK. Finally, generated FFA are channeled towards the mitochondria, serving as a substrate for β-oxidation and so for thermogenesis.

The SNS also allows the switching off of thermogenesis. In this sense, when sympathetic tone decreases, lipolysis is diminished and FFA levels are reduced. Hence, the limited availability of FFA will decrease UCP1 function.

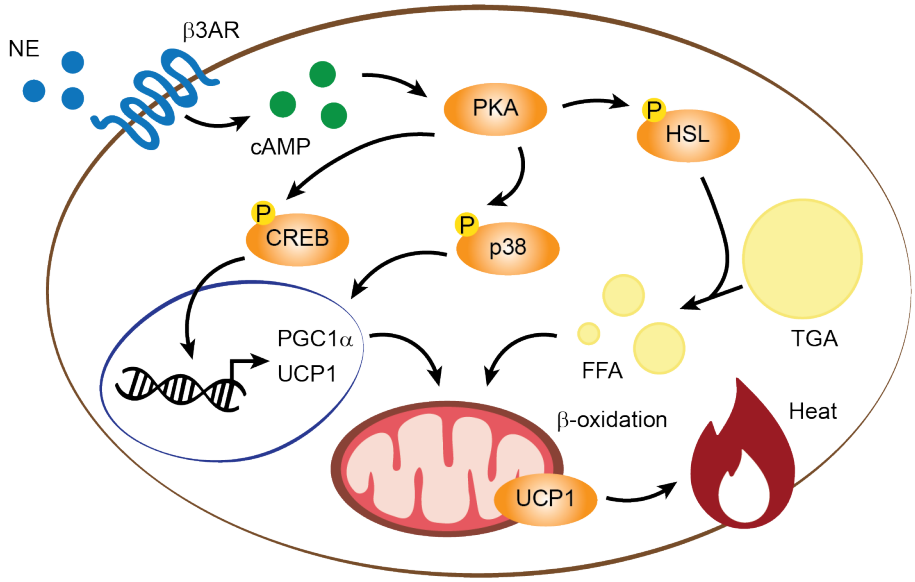

Figure 4. Non-shivering thermogenesis. Upon cold or diet exposure, the SNS releases NE that will activate β3-adrenergic receptors (β3AR). This will result in an increase of the intracellular cyclic AMP levels, which in turn will activate PKA. On one hand, PKA phosphorylates (P) HSL that will activate lipolysis. On the other hand, PKA phosphorylates transcription factors p38 MAPK and CREB that control PGC1α and UCP1 expression. Finally, FFA are oxidized and with the protein UCP1 energy is finally released as heat.

Overall, the signals that are activated to induce thermogenesis converge on the expression and activation of UCP1, which allows the transformation of stored energy into heat by uncoupling oxidative phosphorylation from ATP production. UCP1 is a transmembrane protein that allows the entrance of the protons

accumulated in the intermembrane space from the electron transport chain to the mitochondrial matrix, avoiding thus the pass through ATP synthase. By doing so, activated UCP1 decreases the inner mitochondrial membrane potential. Therefore, the potential of brown adipose tissue to perform thermogenesis is only limited by nutrient availability (Cannon and Nedergaard, 2004).

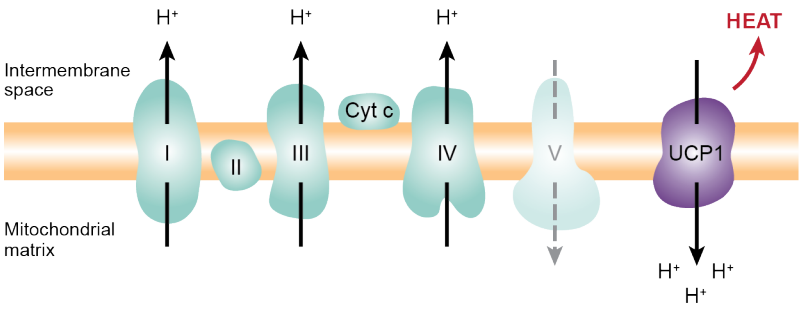

Figure 5. Electron transport chain and UCP1 uncoupled respiration. During electron transport chain, protons (H^+) are released to the mitochondrial intermembrane space though complex I, II and IV. To decrease the inner mitochondrial membrane potential, UCP1 redirects H^+ to the mitochondrial matrix, uncoupling oxidative phosphorylation from ATP production mediated by complex V.

In addition to being regulated at transcriptional level by PPARγ, PGC1α and thyroid hormone receptor (TR), UCP1 activity can also be regulated by intracellular molecules. Under conditions of no thermogenic demand, UCP1 is inhibited by purine nucleotides. Upon adrenergic stimulation however, FFA generated through lipolysis can displace purine nucleotides to bind and activate UCP1 function (Nicholls, 1974; Nicholls and Locke, 1984; Klingenberg and Echtay, 2001).

2.2.4. Brown adipose tissue in the control of glucose metabolism

FFA are the principal substrate for brown adipocyte thermogenesis. They can preferentially be generated through intracellular lipolysis, but also taken up from circulation, a process that is mainly regulated by the fatty acid translocase CD36 and by fatty acids transporter proteins. Therefore, the restoration of intracellular

lipid levels is essential to sustain thermogenesis (Zimmermann, 2004; Anderson et al., 2015; Khedoe et al., 2015).

Besides FFA, brown adipose tissue also uses glucose, especially during sympathetic activation (Cannon and Nedergaard, 2004). Glucose uptake in brown adipose tissue can be mediated by insulin-dependent or insulin-independent mechanisms. Even though the cellular pathways of insulin signaling in brown adipose tissue have not been studied deeply, several observations show that the pathways involved are really similar to the ones in white adipocytes. Thus, when plasma insulin levels are high, glucose uptake in brown adipocytes is increased, and on the contrary, under states of low plasma insulin, glucose uptake is decreased (Smith et al., 1992; Sugden and Holness, 1993). In fact, one of the most insulin-stimulated glucose uptake responsive tissues is brown adipose tissue (Storlien et al., 1986). Insulin induces the expression of the glucose transporter 4 (GLUT4) and its translocation to the plasma membrane to enhance glucose uptake (Slot et al., 1991; Omatsu-Kanbe et al., 1996). Then, glucose can be either stored in the form of lipids or as glycogen (McCormack, 1982). The relevance of brown adipose tissue insulin-induced glucose clearance was clearly demonstrated with the brown adipose tissue-specific insulin receptor knockout mice, which presented fasting hyperglycemia and decreased glucose tolerance (Guerra et al., 2001).

In addition to the stimulatory role of insulin in glucose uptake, this process is also induced during active thermogenesis by the SNS, independently of insulin levels (Shibata et al., 1989). However, the mechanisms by which NE induces glucose uptake are not clarified yet. Cold exposure markedly promotes glucose uptake, while denervation prevents it, which proves that the adrenergic signaling is involved (Shimizu et al., 1993). Some evidences show that NE enhances glucose uptake through glucose transporter 1 (GLUT1) instead of GLUT4, without altering its cellular localization (Shimizu et al., 1998). Under these conditions, glucose can be converted to pyruvate, in order to sustain ATP levels during thermogenesis, or into TGA or fatty acids to refill intracellular lipid stores (Ma and Foster, 1986).

Studies aimed at testing the role of brown adipose tissue in the direct regulation of glucose metabolism through brown adipose tissue transplantation have revealed that this tissue releases several endocrine signals. Standford and colleagues transplanted brown adipose tissue from male donor mice into the visceral cavity of age-matched male recipient mice and observed improved glucose tolerance and insulin sensitivity (Stanford et al., 2013). Also, recipient mice presented lower body weight, decreased fat mass and a reversal of insulin resistance induced by high fat diet. However, the beneficial effects of brown adipose transplants were more likely to be a result of metabolic changes in endogenous tissues though endocrine signals from the transplanted depot, rather than to the thermogenic capacity acquired by the transplant itself. Among brown adipose tissue secreted endocrine molecules, also called batokines (Villarroya et al., 2017a, 2017b), the main candidates of mediating insulin sensitizing effects are fibroblast growth factor 21 (FGF21), insulin-like growth factor 1 (IGF-1), interleukin-6 (IL-6), thyroid hormone triiodothyronine (T3) and bone morphogenetic protein 8B (BMP8B). FGF21 is secreted in an IL-6 dependent manner, and they both are secreted by brown adipocytes stimulated with NE (Burýšek and Houštěk, 1997; Hondares et al., 2011b). Indeed, FGF21 acts centrally inducing energy expenditure into several tissues (including liver, skeletal muscle and white adipose tissue), and in brown adipose tissue induces glucose uptake and substrate oxidation (Hondares et al., 2010; Owen et al., 2014). IGF-1 acts as an endocrine factor resembling insulin actions, and it is able to reverse diabetes symptoms into streptozotocin-induced diabetic mice (Gunawardana and Piston, 2012, 2015). The release of T3 or BMP8B is associated to thermogenesis activation (de Jesus et al., 2001; Whittle et al., 2012).

2.2.5. Human brown adipose tissue and relevance for human diseases

During years it was assumed that in humans brown adipose tissue was only present in newborn infants (Aherne and Hull, 1966; Hull, 1966) or in adult individuals with hibernomas o catecholamine-secreting tumors such as pheochromocytomas

(Sutherland et al., 1952; Lean et al., 1986). However, with the use of the techniques of nuclear medicine, in the last decade became clear that adult humans have active brown adipose tissue depots. Positron emission tomography combined with computed tomography (PET/CT) investigations that were initially aimed at detecting metabolically active tumors with the glucose analogue fluorodeoxyglucose (^{18}F-FDG), revealed symmetrical labelling in the supraclavicular, cervical an paraspinal regions of the body, that have been demonstrated to be active brown adipose depots (Nedergaard et al., 2007; Cypess et al., 2009; van Marken Lichtenbelt et al., 2009; Virtanen et al., 2009; Zingaretti et al., 2009). Since then, brown adipose tissue field attracted scientific interest, and nowadays, the available information regarding brown adipose biology has increased exponentially.

In mice, the interscapular depot is the main site for non-shivering thermogenesis, while in humans the supraclavicular depot is the one that shows higher activity. Some studies have proposed different markers genes that are expressed specifically in mouse brown or beige adipocytes, and they have been used as a way to classify human UCP1 positive depots. Gene expression profile in brown adipose tissue from human infants shows similarities with the mouse interscapular depot, although some markers of beige adipocytes are also expressed (Sharp et al., 2012; Lidell et al., 2013). In adult humans brown adipose depots show heterogeneity. The supraclavicular depot shows a mixed gene expression profile of both beige and classical brown adipocytes (Sharp et al., 2012; Jespersen et al., 2013; Lidell et al., 2013; Lee et al., 2014). However, the depots from the cervical and perirenal regions present adipocytes that express classical brown fat markers (Cypess et al., 2013; Nagano et al., 2015).

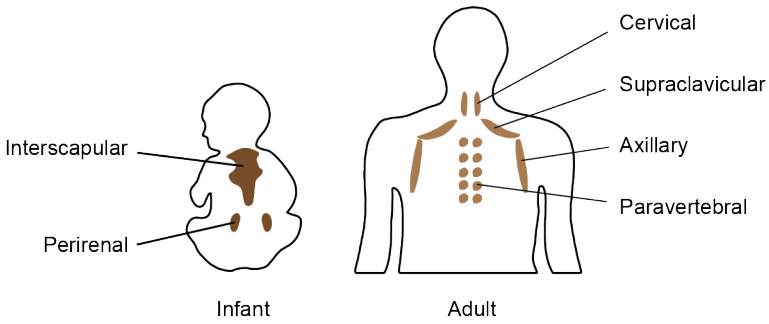

Figure 6. Human brown adipose tissue depots. In human infants, brown adipose tissue is localized in the interscapular and perirenal region. However, in adult humans the main depots detected are the cervical, the supraclavicular, the axillar and the paravertebral.

It is not surprising that brown adipose tissue in adult humans has been unnoticed for years. In fact, in adulthood a decrease in brown adipose tissue mass and activity has been observed both in males and in females (Pfannenberg et al., 2010; Yoneshiro et al., 2011). Nevertheless, activation of brown adipose tissue by cold exposure has been clearly demonstrated in human subjects. The volume of active tissue can be increased by mild cold exposure (10°C for 2 hours/day during 4 weeks, or 15°C for 6 hours/day during 10 days), even in patients without detectable brown fate depots before cold intervention (Lans et al., 2013; Yoneshiro et al., 2013; Blondin et al., 2014).

Taking into account that in rodents brown adipose tissue activity is positively correlated with weight loss and improved glucose metabolism, human brown adipose tissue has emerged as a novel target for the treatment of obesity and metabolic disorders associated to this condition it, which includes insulin resistance. Human studies have demonstrated a negative correlation between brown adipose tissue activity and fat mass or body mass index (BMI) (van Marken Lichtenbelt et al., 2009; Saito et al., 2009; Vijgen et al., 2011). In the same direction, obese subjects showed reduced brown adipose tissue amount and activity (Orava et al., 2013), and individuals with detectable brown adipose tissue weighed on an average 4 kg less

than subjects without detectable brown fat (Lee et al., 2010). Healthy subjects also presented increased resting energy expenditure by cold exposure (Chondronikola et al., 2014). In addition, in newborns, an increased brown fat thermogenesis has been related to decreased body fat accumulation during the first months of life (Entringer et al., 2017).

The relation between human adipose tissue metabolism and glucose homeostasis is also being extensively studied. In this regard, experiments in adult humans revealed that the rate of cold-induced glucose uptake in brown adipose tissue exceeds the rate of insulin-stimulated glucose uptake in skeletal muscle. Cold exposure is able to enhance by 12-fold glucose uptake in brown adipose tissue, while insulin induces a 5-fold increase (Saito et al., 2009). In addition, brown adipose tissue activation by cold is associated with improved insulin sensitivity and reduced FFA levels in circulation (Iwen et al., 2017). Thus, a positive correlation between brown adipose tissue ^{18}F-FDG uptake and decreased blood glucose levels has also been documented (Lee et al., 2010; Jacene et al., 2011; Ouellet et al., 2011). This idea was further supported by the observation that brown adipose tissue glucose uptake is reduced in diabetic patients compared to healthy subjects (Blondin et al., 2015).

Overall available data regarding human brown adipose tissue metabolism strongly suggest that activating brown adipose thermogenesis could be a powerful tool to reduce glucose and FFA levels from circulation, to increase energy expenditure and to decrease fat mass. In consequence, a better understanding of its development and thermogenic activation seems key to design efficient treatments of metabolic disorders such as obesity and type 2 diabetes.

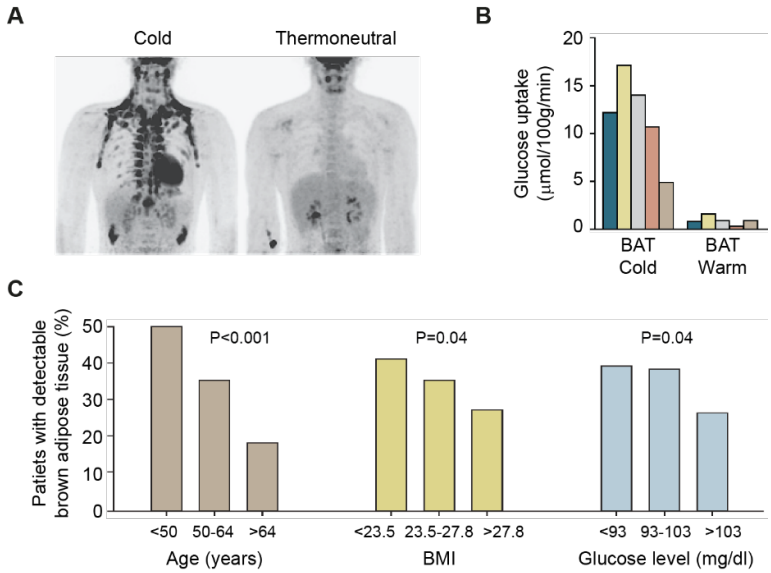

Figure 7. Human brown adipose tissue activity is correlated with metabolic health. (A) PET-CT ^{18}F-FDG scanning images from a lean subject exposed to cold or to thermoneutral conditions. Black areas represent active ^{18}F-FDG uptake. (B) Glucose uptake rates in supraclavicular brown adipose tissue (BAT) from 5 different subjects exposed to a cold or a warm environment, calculated with the use of graphical analysis of PET data. (C) Age, BMI and fasting plasma glucose level are correlated with the prevalence of maximal activity of brown adipose tissue in adult humans. Adapted from (Cypess et al., 2009; van Marken Lichtenbelt et al., 2009; Virtanen et al., 2009).

2.3. TP53INP2

The laboratory of Antonio Zorzano has studied some of the mechanisms involved in the development of metabolic disorders. With the objective to identify genes involved in the pathophysiology of type 2 diabetes mellitus and obesity, a gene screen was performed in muscle from obese-diabetic and non-diabetic lean rats (Dani Bach, PhD thesis, 2002). From this screen, our laboratory described the gene Tumor protein p53 inducible nuclear protein 2 (*Tp53inp2)*, initially named *DOR* (from Diabetes and Obesity Regulated), which was strongly repressed in skeletal muscle from obese-diabetic rats (Baumgartner et al., 2007). Its nomenclature in mouse is TRP53INP2, but since now one, we well refer to it as TP53INP2 for simplicity. *TP53INP2* expression was also downregulated in the skeletal muscle

from obese or diabetic patients, which somehow links TP53INP2 with this two metabolic alterations (Figure 8A) (Baumgartner et al., 2007; Sala et al., 2014). Posterior studies characterized *Tp53inp2* mRNA levels in different tissues. Its higher expression was found in the skeletal muscle from human or rat samples, but also, *Tp53inp2* expression was detected in metabolically active tissues like heart, liver, brain or white adipose tissue (Figure 8B) (Baumgartner et al., 2007). TP53INP2 transcript and protein levels profile was similar in mouse tissues (Figure 8C and D) (Sala et al., 2014).

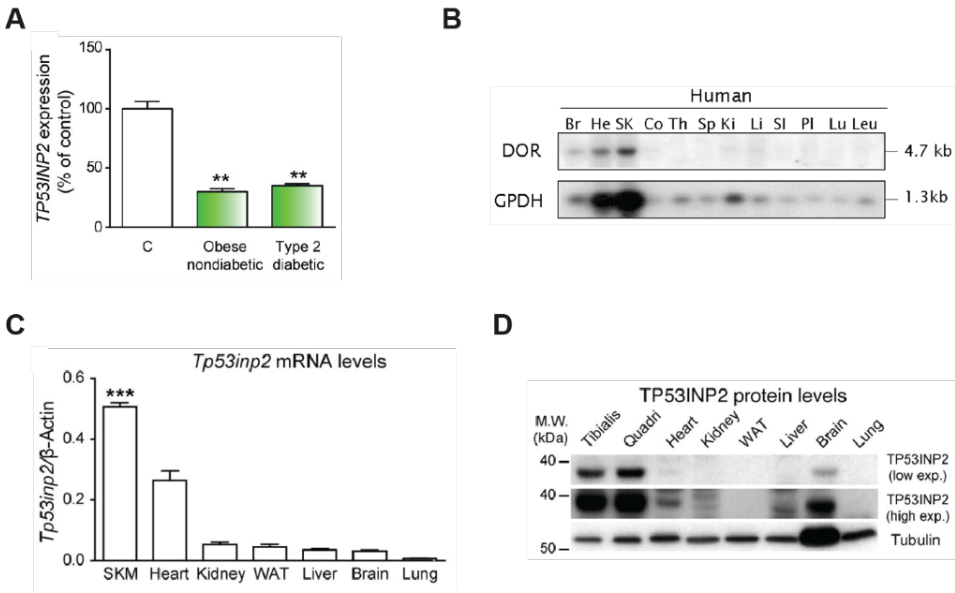

Figure 8. TP53INP2 is expressed in metabolically active tissues and is repressed in obese and type 2 diabetic patients. *TP53INP2* mRNA levels in (A) skeletal muscle from control, obese nondiabetic or type 2 diabetic patients, and (B) in different human tissues. TP53INP2 (C) mRNA levels and (D) protein abundance in different mouse tissues. TP53INP2 is referred as DOR in panel (B). Data are mean ± SEM. *p<0.05 vs. C or vs. other tissues. From (Baumgartner et al., 2007; Sala et al., 2014).

This gene encodes for a protein of 220 amino acids in humans or 221 amino acids in mouse or rat, and its sequence is highly conserved among these species. Mouse and rat TP53INP2 sequences showed 85% identity, mouse and human presented an 84%, while human TP53INP2 and its sequence in rat displayed 83% identity. Tumor protein p53 inducible nuclear protein 1 (TP53INP1 or also named SIP)

is the only homologue of TP53INP2, and they show 36% of identity in the case of humans (Baumgartner et al., 2007). Phylogenic studies performed in our laboratory showed that TP53INP2 and TP53INP1 are only present in metazoan species and not in other kingdoms. Invertebrate species possess only *Tp53inp2* gene, demonstrating that it is the ancestor and that *Tp53inp1* may have originated by gene duplication (Sancho et al., 2012).

Based on the phylogenic analysis, two well conserved regions were identified in TP53INP2 sequence, which were found unique to TP53INP2 family and did not show identity with other protein sequences in databases. The first region is localized between position 28-42 (region 1) and the second in 67-112 (region 2). Region 1 is rich in negatively charged amino acids, while region 2 in the C-terminal part shows a strong positive charge and facilitates the α-helix structure that has been postulated for this region. However, region 1 does not have a defined tendency to acquire a secondary structure. Moreover, structural examination have determined that TP53INP2 contains a nuclear export signal (NES, residues 32-40) and a nuclear localization signal (NLS), which will account for its nuclear and cytoplasmic localization (Mauvezin et al., 2010). A functional conserved LC3-interacting region (LIR) was also identified in region 1 (residues 35-38) overlapping with the NES motive (Figure 9) (Sancho et al., 2012).

The first TP53INP2 functional characterization studies were published in 2007 (Baumgartner et al., 2007). TP53INP2 is able to co-activate the transcriptional activity of nuclear hormone receptors (Baumgartner et al., 2007; Francis et al., 2010; Sancho et al., 2012). In addition, TP53INP2 was described as a protein that undergoes nuclear cytoplasmic shuttling under stress conditions, such as amino acid starvation, to induce autophagy (Mauvezin et al., 2010). Recently, our laboratory has described that TP53INP2 also contributes to the signaling promoted by the death receptor leading to apoptosis (Ivanova et al., 2019). At the molecular level, TP53INP2 has been reported to bind to the E3 ubiquitin ligase TRAF6 as well as its substrate caspase 8 leading to enhanced ubiquitination (Ivanova et

al., 2019). From the physiological perspective, TP53INP2 regulates muscle mass through the control of the degradation of ubiquitinated proteins (Sala et al., 2014), and TP53INP2 negatively regulates adiposity (Romero et al., 2018).

Figure 9. Mouse T53INP2 sequence and motifs identified. The nuclear export signal is in red letters (NES), the nuclear localization signal (NLS) is in orange letters and the LC3-interacting domain is highlighted in yellow. Regions 1 and 2 are highlighted in green. α-Helix structure is marked from amino acid 86 to 112. From Caroline Mauvezin, PhD thesis, 2011.

2.3.1. TP53INP2 as a nuclear coactivator

Originally, TP53INP2 was described as a nuclear protein that is co-localized in the promyelocytic leukemia (PML) bodies (Baumgartner et al., 2007). Moreover, *in vitro* TP53INP2 overexpression is able to trans-activate in a dose dependent manner the transcriptional activity of nuclear receptors such as TRα1, glucocorticoid receptor (GR), PPARγ, vitamin D receptor (VDR) and estrogen receptor (ERα) (Figure 10A and B) (Baumgartner et al., 2007; Sancho et al., 2012). The authors also characterized a physical binging between TP53INP2 and TRα1, while no interaction was detected with the others in the conditions assayed (Figure 10C). Additionally, by chromatin immunoprecipitation experiments it was demonstrated that TP53INP2 binds to the T3-responsive promoters.

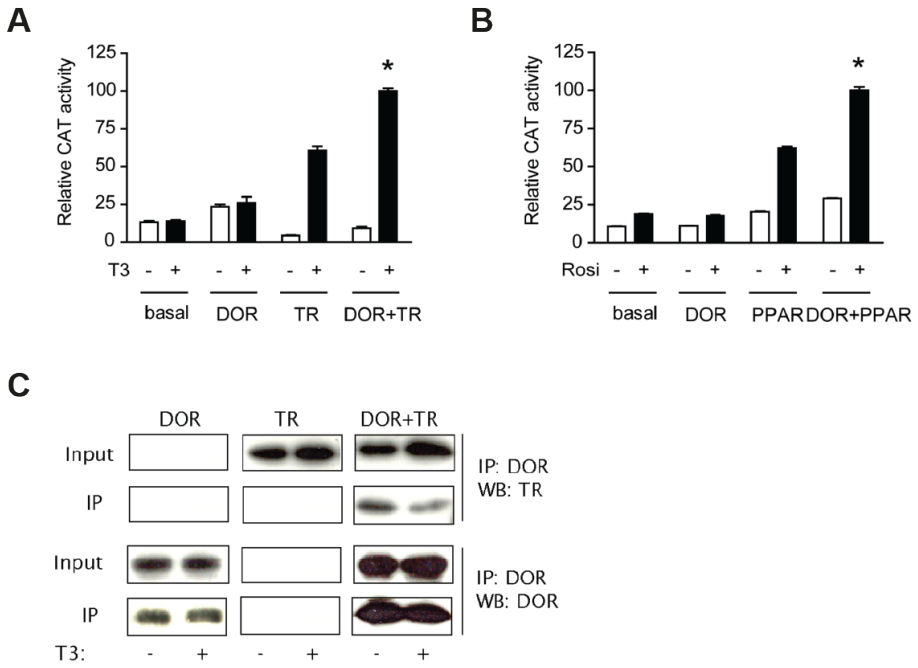

Figure 10. TP53INP2 co-activates TR and PPAR transcriptional activity. Transcriptional (A) TR or (B) PPAR activity in HeLa cells transfected with indicated plasmids and treated with respective nuclear receptor ligands. (C) Physical interaction between TP53INP2 and TR in HeLa cells transfected with indicated plasmids and treated with thyroid hormone (T3). TP53INP2 is referred as DOR in panels. Data are mean ± SEM. *p<0.05 vs. control group. From (Baumgartner et al., 2007; Sancho et al., 2012).

Downregulation of TP53INP2 by siRNA into C2C12 muscle cells also decreases the activity of TRα1, and reduces the expression of target genes like *myogenin*, *creatine kinase* and *caveolin-3*. In fact, C2C12 myoblasts present delayed myogenic differentiation capacity by the lack of TP53INP2, a process directly impacted by thyroid hormone signaling (Baumgartner et al., 2007).

A posterior publication demonstrated the capacity of TP53INP2 to co-activate nuclear receptors in *Drosophila melanogaster* as an *in vivo* model. In this case, it was shown that the orthologous of TP53INP2 in *Drosophila* (dTP53INP2) is able to activate the ecdysone receptor, a hormone receptor fundamental during metamorphosis. Thus, dTP52INP2 knockdown flies present decreased ecdysone receptor target gene expression, partial lethality during pupation and reduced

triglyceride content (Francis et al., 2010).

Previous observations from our laboratory also revealed that when TP53INP2 leaves the nucleus and goes to the cytoplasm, it does so by passing through the nucleolus (Mauvezin et al., 2012). This conclusion was also validated in a recent article, which describes a nucleolar localization signal (NoLS) located at the C-terminal domain of TP53INP2. This study also uncovered a novel nuclear function of and demonstrates that TP53INP2 binds to the ribosomal DNA and promotes ribosome biogenesis (Xu et al., 2016).

2.3.2. Role of TP53INP2 in autophagy

A highly relevant publication from our laboratory demonstrated a new function of TP53INP2 as a regulator of autophagy (Mauvezin et al., 2010). As said above, under basal conditions TP53INP2 is mainly localized into the nucleus, and under stress situations, such as mTOR inhibition by amino acid starvation, it moves to the cytoplasm. This suggested a possible role of TP53INP2 in the process of autophagy.

Autophagy is a catabolic process that mediates the degradation of intracellular components engulfed inside a double membrane vesicle, called autophagosome, and subsequent fusion with lysosomes (forming the autolysosome vesicle). Together with other proteolytic systems, autophagy is involved in the maintenance of cellular homeostasis by removing misfolded proteins and damaged or dysfunctional organelles, and producing building blocks for the synthesis of new components (Martinez-Vicente and Cuervo, 2007).

In this regard, it was described that TP53INP2 participates in the initial steps of autophagy through directly binding to LC3, GABARAP, GABARAPL1 and GATE16, all proteins required for autophagosome formation. TP53INP2 co-localizes with LC3 in the autophagosome membrane until it fuses with the lysosome,

as no TP53INP2 is detected in LAMP1 positive vesicles, a protein marker for lysosomes and autolysosomes (Nowak et al., 2009; Mauvezin et al., 2010; Sancho et al., 2012). The interaction of TP53INP2 with autophagy related proteins facilitates the degradation of proteins through autophagy. Thus, TP53INP2 overexpression in HeLa cells results in a higher number of LC3 positive puncta per cell and an accumulation of autophagosomes. On the contrary, TP53INP2 downregulation by siRNA in C2C12 cells reduces autophagosome formation and protein degradation through this pathway (Mauvezin et al., 2010). The role of TP53INP2 in autophagy has also been validated in *Drosophila* and in mouse skeletal muscle and white adipose tissue (Francis et al., 2010; Sala et al., 2014; Romero et al., 2018).

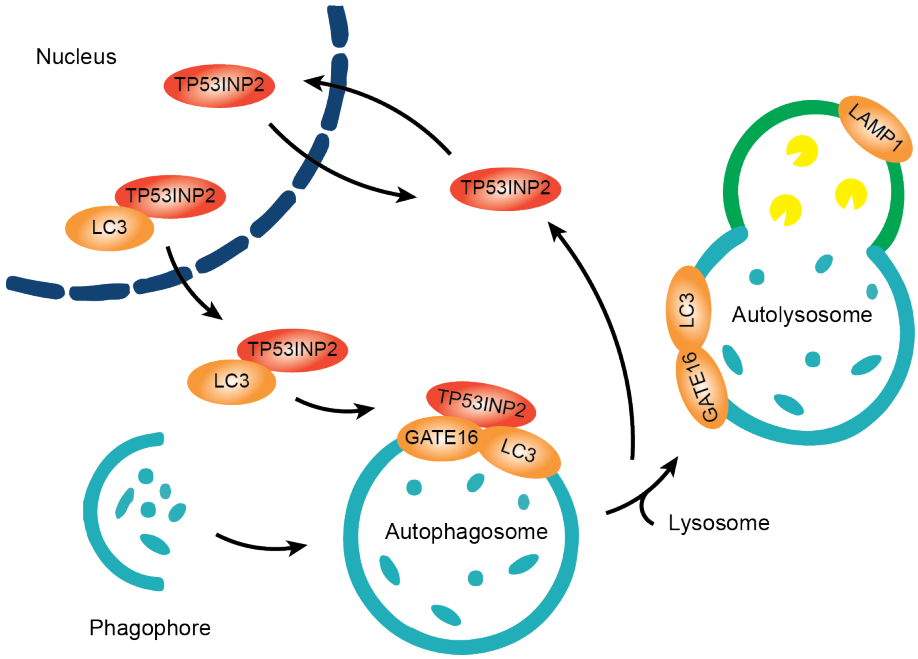

Figure 11. Role of TP53INP2 in autophagy. Under basal conditions, TP53INP2 is shuttling between the nucleus and the cytoplasm. Upon amino acid starvation, LC3 is deacetylated and binds to TP53INP2. They exit from the nucleus to the cytoplasm to promote autophagosome formation, were they also bind to GATE16. When lysosomes fuse to autophagosomes TP53INP2 leaves LC3 and GATE16.

Coherent with this data, another study demonstrated that TP53INP2 is able to bind LC3 in the nucleus dependent on its acetylation. Under starvation conditions,

the deacetylase sirtuin 1 gets activated, deacetylates nuclear LC3 and allows the interaction with TP53INP2. LC3 and TP53INP2 have been reported to translocate together from the nucleus to the cytoplasm to participate in autophagosome formation (Huang et al., 2015).

2.3.3. Role of TP53INP2 in apoptosis

The most recent function of TP53INP2 that has been described is its ability to modulate apoptosis through death receptor signaling (Ivanova et al., 2019). Apoptosis is a process of programmed cell death that is crucial for maintaining homeostasis, and its deregulation occurs in several pathologies (Jacobson et al., 1997; Vaux and Korsmeyer, 1999). Activation of apoptosis can be triggered either an intrinsic or an extrinsic pathway (Ferri and Kroemer, 2001; Fulda and Debatin, 2006). In the extrinsic pathway, death ligands such as FasL or TRAIL bind to their respective receptors and activate caspase-8 that in turn will activate other caspases that will execute apoptosis (Medema et al., 1997; Li et al., 1998; Luo et al., 1998). In this study, it has been shown that TP53INP2 sensitizes various cancer cell lines to death receptor-induced apoptosis. Thus, TP53INP2 binds to and activates caspase-8 by increasing its ubiquitination levels in a manner that was dependent on the activity of the E3 ubiquitin ligase TRAF6. A TRAF6-interacting motif has also been identified in TP53INP2 sequence, which upon mutation abrogates TP53INP2 interaction with TRAF6 and caspase-8. Moreover, TP53INP2 protein levels are positively correlated with higher TRAIL-induced apoptosis, which indicates that TP53INP2 might be a potential biomarker for personalized TRAIL treatment in cancers characterized by decreased caspase-8 activity (Ivanova et al., 2019).

2.3.4. TP53INP2 and ubiquitinated proteins

Another function of TP53INP2 that our laboratory has uncovered, that is

partially dependent on the capacity to induce autophagy, is its ability to regulate the degradation of ubiquitinated proteins (Sala et al., 2014; Ivanova et al., 2019; Xu and Wan, 2019). In transgenic mice overexpressing TP53INP2 specifically in the skeletal muscle, TP53INP2 was shown to accelerate the degradation of ubiquitinated proteins through the autophagic machinery, which suggested that TP53INP2 could act as an autophagy adaptor for ubiuitinated proteins. Thus, TP53INP2 interaction with ubiquitin and ubiquitinated proteins was evaluated. This study demonstrated that TP53INP2 is able to immunoprecipitate with ubiquitin, and this is not associated to TP53INP2 ubiquitination, but through a direct binding with ubiquitin and poliubiquitin chains (Sala et al., 2014).

In a recent publication, our laboratory has also described that TP53INP2 interacts with the E3 ubiquitin ligase TRAF6 to facilitate caspase-8 ubiquitination (Ivanova et al., 2019). This is coherent with a previous observation from our laboratory that showed that TP53INP2 can modulate mitochondrial-specific autophagy, referred as mitophagy, by interacting with parking, a crucial E3 ubiquitin ligase in the regulation of mitophagy (Yuliana Enciso, PhD thesis, 2017).

This last article also described an ubiquitin-interacting motif (UIM) responsible for its interaction with ubiquitin and poliubiquitin chains. In this regard, TP53INP2 UIM mutation partially reduced its ability to interact with ubiquitin, assessed by pull-down experiments (Ivanova et al., 2019). This observation has been validated few months ago by another laboratory (Xu and Wan, 2019). The authors identified the same UIM in TP53INP2 sequence and document that it is essential for TP53INP2 interaction with ubiquitinated proteins to mediate its autophagic degradation. Consequently, overexpression of mutants forms of TP53INP2 either lacking the UIM domain or with several mutations in this motif resulted in the accumulation of ubiquitinated proteins, which was dependent on autophagy activation (Xu and Wan, 2019).

2.3.5. Physiological roles of TP53INP2

Our laboratory has analyzed the physiological impact of TP53INP2 expression modulation in mice. With that idea, and taking into account that the skeletal muscle is the tissue harboring higher TP53INP2 expression levels, two mouse models were generated: one with skeletal muscle specific TP53INP2 overexpression (SKM-Tg) and another one with skeletal muscle specific TP53INP2 ablation (SKM-KO). This investigation revealed that SKM-Tg mice had reduced muscle mass, while SKM-KO displayed muscle hypertrophy. SKM-Tg animals exhibited enhanced muscle wasting in streptozotocin-induced diabetes that was dependent on autophagy. However, SKM-KO mice presented mitigated experimental diabetes-associated muscle loss. Overall these results show that under *in vivo* conditions, TP53INP2 negatively regulates muscle mass through the activation of autophagy (Sala et al., 2014).

Later, it was also described that TP53INP2 expression was repressed in the adipose tissue of obese subjects, which suggested a role of TP53INP2 in the regulation of white adipose tissue biology. In these regard, an inducible global-TP53INP2 knockout mouse model was generated (KO^{Ubc}). Global TP53INP2 ablation resulted in an obese phenotype characterized by an expansion of white adipose tissue depots. The cell-specific effect of TP53INP2 in the negative regulation of white preadipocyte differentiation was validated *in vitro* using human and mouse preadipocyte cell lines. The action of TP53INP2 was dependent on the activation of the T cell factor/lymphoid enhancer (TCF/LEF) transcription factors (Romero et al., 2018). These findings revealed that, in spite of low levels of TP53INP2 in white adipose tissue, its role is this tissue of crucial importance in the prevention of obesity.

OBJECTIVES

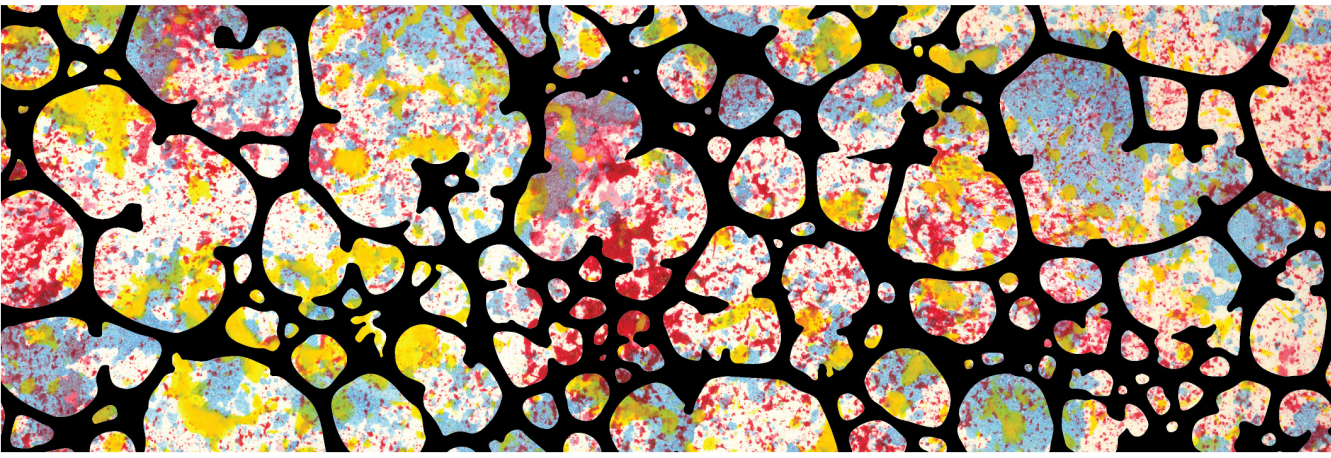

In 2007 TP53INP2 was identified in the laboratory of Antonio Zorzano as a gene that is downregulated in the skeletal muscle from Zucker diabetic and obese rats (Baumgartner et al., 2007). Since then, several efforts have been performed in order to determine the physiological role of TP53INP2 in the development of obesity and type 2 diabetes. The first studies using cellular models unraveled a role of TP53INP2 in the modulation of transcriptional activity of nuclear receptors as the TR and the GR, both of crucial importance in mediating insulin sensitivity in skeletal muscle (Francis et al., 2010; Sancho et al., 2012). Later, TP53INP2 was also described as a positive regulator of autophagy in cellular models and in *Drosophila melanogaster* as *in vivo* model (Mauvezin et al., 2010, 2012). With the objective of characterizing the role of TP53INP2 in complex organisms, such as mammals, mouse models with genetic mutations in the gene TP53INP2 were developed. From this investigation it was demonstrated that in the skeletal muscle TP53INP2 negatively regulates muscle mass through the activation of autophagy, and that TP53INP2 repression is part of an adaptive mechanism aimed at preserving muscle mass in conditions of decreased insulin sensitivity (Sala et al., 2014).

At the beginning of this PhD thesis, the laboratory had also obtained strong evidences showing that TP53INP2 represses white adipogenesis in cellular models and in an inducible TP53INP2 global-knockout mice, which at the present are already published (Romero et al., 2018).

Taking into account the described action of TP53INP2 in the skeletal muscle, and because brown adipose tissue and skeletal muscle arise from a common precursor cell, a conserved function of TP53INP2 in this cell type was speculated. Moreover, the information available in the regulation of white adipose tissue biology by TP53INP2, suggested that TP53INP2 may have the capacity to modulate energy balance and body weight, parameters that can be directly impacted by brown adipose tissue activity.

Considering all the antecedents mentioned, the main aim postulated in this PhD thesis was to investigate the functional role of TP53INP2 in brown adipose tissue metabolism. To do so, we pursued the following specific objectives:

1. To study the regulation of TP53INP2 expression in brown adipose tissue and the function of TP53INP2 in brown preadipocyte cell cultures.

2. To evaluate the impact of TP53INP2 ablation in brown adipose tissue using *in vivo* mouse models.

3. To determine the molecular mechanisms involved in the regulation of brown adipose cells by TP53INP2.

RESULTS

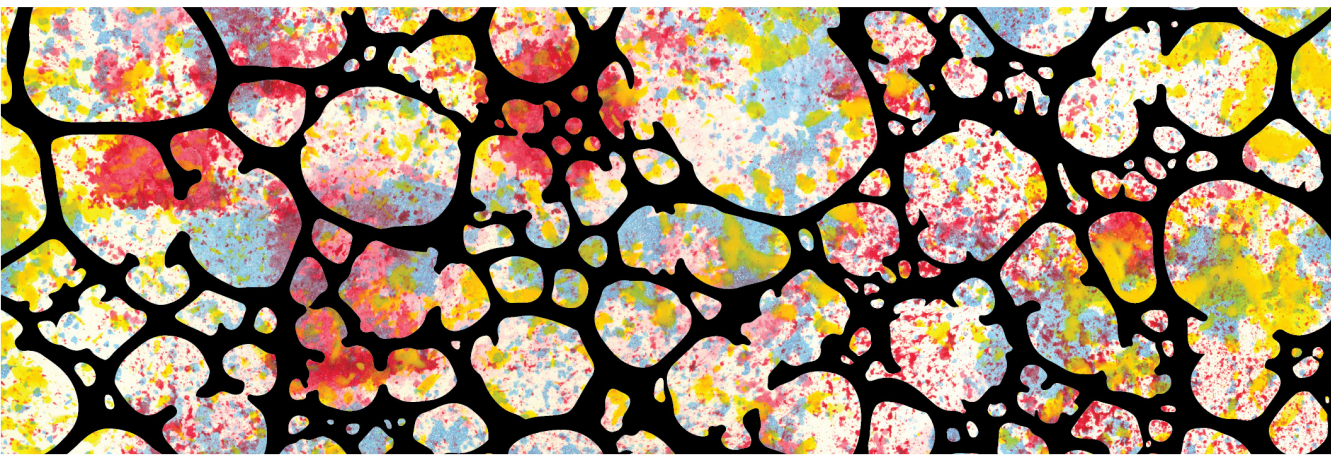

4.1. Analysis of TP53INP2 expression in brown adipose tissue

TP53INP2 is expressed in metabolically active tissues including skeletal muscle, heart, brain and white adipose tissue. In 2014 our laboratory reported the expression levels of TP53INP2 in several mouse tissues, in which the skeletal muscle showed the higher TP53INP2 levels (Sala et al., 2014). However, brown adipose tissue, a tissue that also has a high metabolic rate, was not included in this screen. With the aim of studying whether TP53INP2 was also expressed in mouse brown adipose tissue we evaluated *Tp53inp2* mRNA levels in this depot. Analysis by qPCR revealed that *Tp53inp2* mRNA levels were also very high in interscapular brown adipose tissue (iBAT), being superior to white adipose tissue and comparable to those present in skeletal muscle (Figure 12). This is coherent with the fact that both the skeletal muscle and brown adipose tissue originate from a common mesenchymal precursor cell (Timmons et al., 2007).

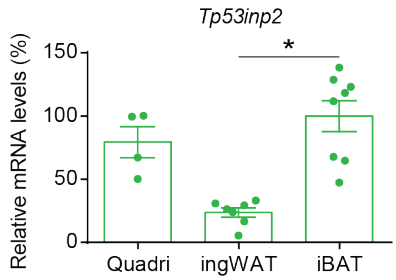

Figure 12. *Tp53inp2* expression levels in iBAT and skeletal muscle is comparable. *Tp53inp2* relative mRNA levels in mouse quadriceps (Quadri), inguinal white adipose tissue (ingWAT) and interscapular brown adipose tissue (iBAT) (n=4-8). Data are mean ± SEM. *p<0.05 vs. ingWAT.

Having determined that TP53INP2 expression in brown adipose tissue is high, our next step was to study *Tp53inp2* mRNA levels were modulated under situations characterized by different thermogenic activity.

4.1.1. Regulation of TP53INP2 expression by diet

Brown adipose tissue responds to energy overload by increasing the thermogenic activity in order to avoid an excessive accumulation of fat and to protect from weight gain. In fact, fatty acids can directly activate UCP1 expression and function to promote non-shivering thermogenesis (Mercer and Trayhurn, 1987; Cannon and Nedergaard, 2004; Divakaruni et al., 2012; Fedorenko et al., 2012). Thus, we analyzed TP53INP2 expression in brown adipose tissue from mice that were fed with a standard chow diet (CD) or with a high fat diet (HFD) for 16 weeks. To validate that HFD was really increasing thermogenesis we also measured the expression of the classical brown adipocyte marker genes *Ucp1*, *Pgc1α* and *Prdm16*. qPCR results revealed that the mRNA levels of both *Tp53inp2* and *Ucp1* were upregulated by HFD administration (Figure 13). As previously described, *Prdm16* that is associated to brown adipocyte differentiation, was not affected by HFD (García-Ruiz et al., 2015). *Pgc1α* showed a trend to be increased by HFD although it did not reach statistical significance.

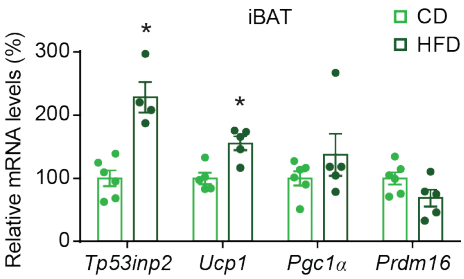

Figure 13. *Tp53inp2* expression is enhanced by HFD. *Tp53inp2*, *Ucp1*, *Pgc1α* and *Prdm16* relative mRNA levels in interscapular brown adipose tissue (iBAT) from control mice subjected to a chow diet (CD) or to a high fat diet (HFD) for 16 weeks (n=5-6). Data are mean ± SEM. *p<0.05 vs. CD.

Moreover, we evaluated TP53INP2 expression at protein level. The increased non-shivering thermogenesis induced by HFD was again validated by an increase in UCP1 protein levels (Figure 14). Under these conditions TP53INP2 expression was also upregulated (Figure 14), showing that HFD regulates both TP53INP2 transcript and protein levels. These results suggest that TP53INP2 has a role in the regulation of brown adipose tissue activity.

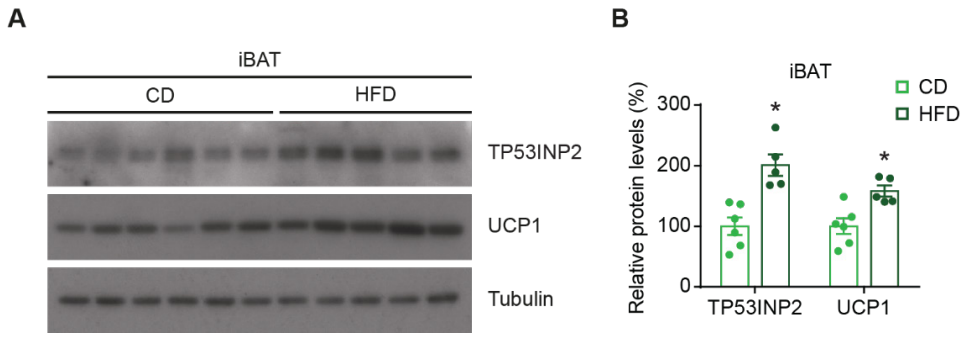

Figure 14. TP53INP2 protein levels are modulated by HFD. TP53INP2 and UCP1 (A) western blot and (B) quantification in interscapular brown adipose tissue (iBAT) from control mice subjected to a chow diet (CD) or to a high fat diet (HFD) for 16 weeks (n=5-6). Data are mean ± SEM. *p<0.05 vs. CD.

4.1.2. Regulation of TP53INP2 expression by temperature

Environmental temperature is the major stimulus that impacts brown adipose thermogenesis. In this sense, cold exposure induces an increase in the thermogenic activity by the release of catecholamines from the sympathetic nervous system in order to maintain body temperature. This results in the accumulation of cAMP which in turns activates mitochondrial biogenesis, directed by PGC1α expression, and β-oxidation of the stored fatty acids. Finally, UPC1 gets activated to uncouple oxidative phosphorylation from ATP production, which results in heat release (Cannon and Nedergaard, 2004). The contrary situation is named thermoneutrality, which is the temperature in which an animal does not need to expend energy in maintaining body temperature. Thus, brown adipose tissue non-shivering thermogenesis is mainly inactive as there is no need for heat generation (Gordon, 1990).

Keeping these in mind, we decided to study TP53INP2 expression under two conditions with different cold-induced thermogenesis. First, as a high thermogenic rate condition we compared mice that were housed at standard temperature (22°C) with mice that were acutely cold exposed for 10 hours (4°C). *Tp53inp2* mRNA

levels in brown adipose tissue were doubled by low temperature environment (Figure 15). The strong induction of the thermogenic genes *Ucp1* and *Pgc1α* validated the increased thermogenic activity of the experimental setup (Carmona et al., 2005; Hondares et al., 2011a) (Figure 15).

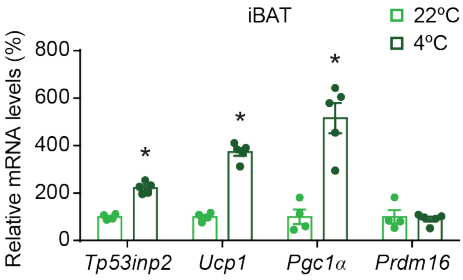

Figure 15. *Tp53inp2* mRNA levels are induced by cold exposure. *Tp53inp2*, *Ucp1*, *Pgc1α* and *Prdm16* relative mRNA levels in interscapular brown adipose tissue (iBAT) from control mice housed at 22°C or 4°C for 10 hours (n=4-5). Data are mean ± SEM. *p<0.05 vs. 22°C.

Protein levels were not evaluated in these samples, as we considered that 10 hours of cold exposure would not be long enough to modulate TP53INP2 protein expression.

In addition, brown adipose tissue cold-induced thermogenesis was inhibited by housing animals at thermoneutrality (30°C) for 5 months. Brown adipose tissue gene expression of these mice was compared to 22°C housed mice from the same age. *Tp53inp2* mRNA levels were decreased under thermoneutral environment in parallel to the expected downregulation of the master brown adipocyte marker gene *Ucp1* (Goldgof et al., 2014; Xiao et al., 2015; Cui et al., 2016; Kalinovich et al., 2017) (Figure 16).

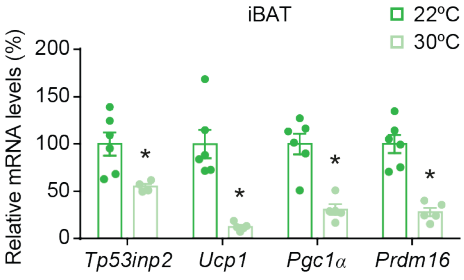

Figure 16. *Tp53inp2* mRNA levels are downregulated by thermoneutrality. *Tp53inp2*, *Ucp1*, *Pgc1α* and *Prdm16* relative mRNA levels in interscapular brown adipose tissue (iBAT) from control mice housed at 22°C or 30°C for 5 months (n=5-6). Data are mean ± SEM. *p<0.05 vs. 22°C.

Pgc1α and *Prdm16* genes were also repressed under thermoneutrality. Prior studies using shorter protocols of thermoneutrality have reported no modulation for these two genes (Goldgof et al., 2014; Xiao et al., 2015; Cui et al., 2016).

These observations show that *Tp53inp2* mRNA levels are positively correlated with cold-induced thermogenesis activity, and that *Tp53inp2* expression is, probably, regulated by the adrenergic signaling pathway.

UCP1 protein levels were also downregulated by thermoneutrality (Figure 17), although TP53INP2 protein abundance showed comparable levels between 22°C and 30°C (Figure 17). It is likely that TP53INP2 protein levels under thermoneutrality are maintained by factors other than the adrenergic signaling pathway, or that TP53INP2 protein also plays other roles in addition to thermogenesis.

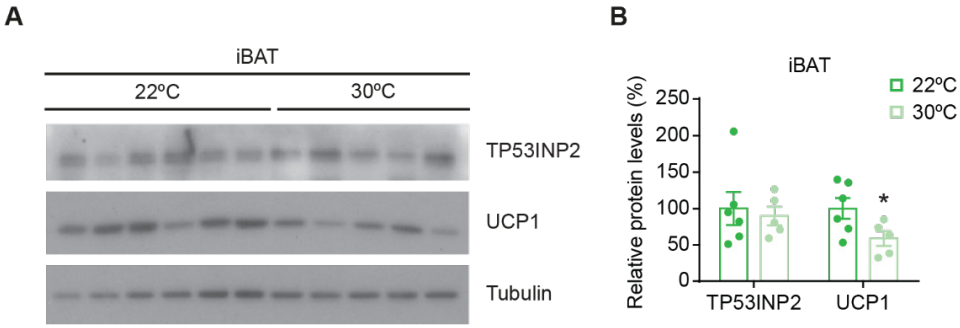

Figure 17. TP53INP2 protein levels are not modulated by thermoneutrality. TP53INP2 and UCP1 (A) western blot and (B) quantification in interscapular brown adipose tissue (iBAT) from control mice housed at 22°C or 30°C for 5 months (n=5-6). Data are mean ± SEM. *p<0.05 vs. 22°C.

4.1.3. Regulation of TP53INP2 by an adrenergic agonist

To determine whether the adrenergic signaling was involved in the modulation of TP53INP2, we analyzed TP53INP2 regulation in cultured brown adipocytes. To mimic thermogenic activation conditions, brown adipocytes were treated with the β3-adrenergic agonist CL-316,243 (CL) or with PBS as vehicle for 4 hours. Adrenergic stimulation induced the expression of *Ucp1* and *Pgc1α* by 8 and 4 fold

respectively, as described (Klein et al., 1999; Cao et al., 2001, 2004) (Figure 18). More importantly, *Tp53inp2* mRNA levels were also upregulated about 50% from basal levels (Figure 18), reinforcing the idea of a specific regulation of TP53INP2 in brown adipocytes by the adrenergic signaling pathway.

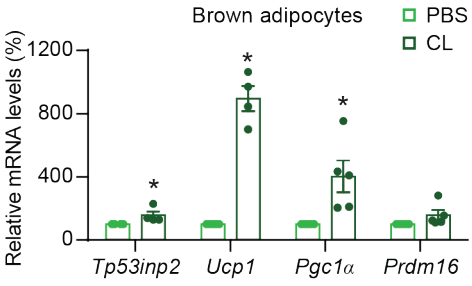

Figure 18. *Tp53inp2* expression is enhanced by adrenergic stimulation. *Tp53inp2*, *Ucp1*, *Pgc1α* and *Prdm16* relative mRNA levels in mature brown adipocytes treated with vehicle (PBS) or with the β3-adrenergic agonist CL-316,243 (CL) for 4 hours (n=4). Data are mean ± SEM. *p<0.05 vs. PBS.

4.2. Study of the role of TP53INP2 in brown adipogenesis

Our laboratory has recently described that TP53INP2 controls adiposity by repressing white adipogenesis (Romero et al., 2018). Following this idea, and taking in to account that TP53INP2 expression is increased upon brown adipose tissue recruitment, we wanted to study the possible involvement of TP53INP2 in the regulation of brown adipogenesis.

4.2.1. Generation and validation of the brown preadipocyte cellular model

Different brown preadipocyte cell lines have been reported and characterized in the literature, both from mouse and human origin. In spite of that, the cellular models that have been extensively used are primary cultures from brown adipose tissue. Preadipocytes are the principal component of the brown fat stromal vascular fraction (SVF), and they have been proved to be an excellent model for studying brown adipogenesis. However, they show a limited capacity to undergo cellular divisions and require continuous isolation of cells from tissue. To avoid these

limitations, the immortalization of primary cultures has become the principal tool to generate brown preadipocyte cell lines for the *in vitro* study of brown adipocyte biology.

Taking into account this information, we decided to generate an immortalized brown preadipocyte cell line for the *in vitro* experiments of this thesis. We isolated the SVF from brown adipose tissue from TP53INP2$^{loxP/loxP}$ mice, already available in the laboratory, and immortalized them by infection of the large T antigen of the SV40 virus (see detailed description in materials and methods section 7.2.2.2). The validation of the generated cellular model was based on the capacity to accumulate lipid droplets during the differentiation process (Figure 19A), and on the expression of the classical brown adipocyte markers *Ucp1*, *Pgc1α* and *Prdm16* (Figure 19B).

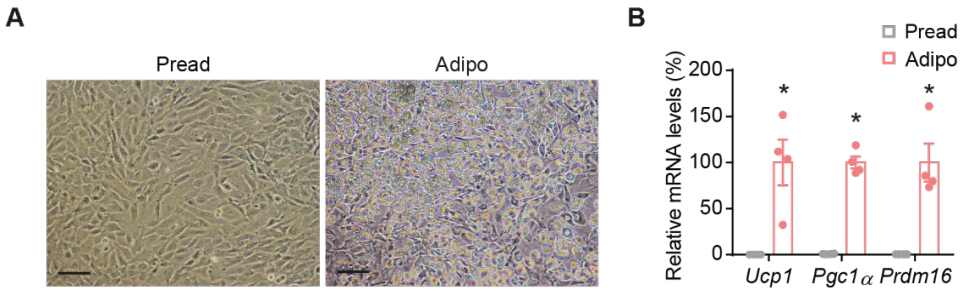

Figure 19. Brown preadipocyte cellular model validation. (A) Optical microscopy images and (B) expression of *Ucp1*, *Pgc1α* and *Prdm16* relative to housekeeping gene *ARP* in undifferentiated (Pread) and differentiated (Adipo) cells (n=4-5). Data represent mean ±SEM. *p<0.05 vs Pread. Scale bar, 100μm.

4.2.2. TP53INP2 is a positive regulator of brown adipogenesis

The differentiation of mouse brown preadipocytes was linked to a marked induction of *Tp53inp2* mRNA levels (Figure 20), which further suggested a potential role in the regulation of this process.

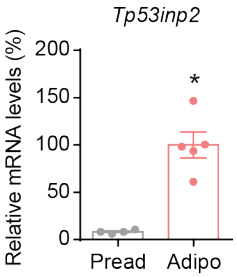

Figure 20. *Tp53inp2* expression is higher in brown adipocytes than in preadipocytes. *Tp53inp2* relative mRNA levels in undifferentiated (Pread) and differentiated (Adipo) cells (n=4). Data are mean ± SEM. *p<0.05 vs. Pread.

Based in all the previous observations, we aimed to characterize the functional role of TP53INP2 in the regulation of brown adipogenesis. To this end, a TP53INP2 knockout (KO) cell line was generated by an adenoviral infection with the Cre-recombinase enzyme fused to GFP into TP53INP2$^{loxP/loxP}$ preadipocytes. A GFP adenovirus was used to generate control cells (C) in the same cellular context. The validation of the model showed undetectable TP53INP2 mRNA (Figure 21A) and protein expression (Figure 21B) in KO cells compared to control ones.

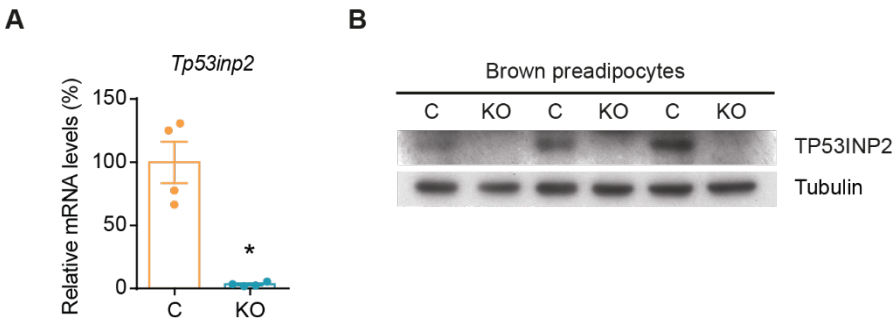

Figure 21. Validation of TP53INP2 depletion in brown preadipocytes. TP53INP2 (A) mRNA and (B) protein levels in control (C) and TP53INP2 knockout (KO) brown preadipocytes (n=3-4). Data represent mean ±SEM. *p<0.05 vs C.

Then, control and KO preadipocytes were induced to differentiate to evaluate whether TP53INP2 loss-of-function had an impact on the adipogenic capacity. Morphological analysis of differentiated brown adipocytes revealed that KO brown preadipocytes presented decreased capacity to undergo differentiation (Figure 22).

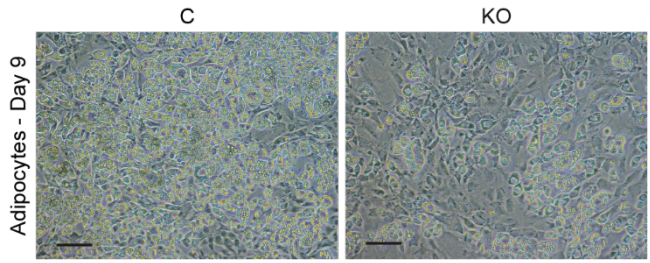

Figure 22. Decreased adipogenic capacity by TP53INP2 ablation. Optical microscopy images of control (C) and TP53INP2 knockout (KO) brown adipocytes at day 9 of differentiation. Scale bar, 100μm.

Gene and protein expression during the process was also evaluated in C and KO cells. The expression of *Prdm16* and *PPARγ1* genes, both involved in differentiation, were decreased in KO cells (Figure 23C). We were unable to detect endogenous PRDM16 protein levels with the antibodies available in the laboratory, however, the two isoforms of PPARγ protein were also downregulated by TP53INP2 ablation (Figure 23A and B). Also, the specific marker of brown adipocytes *Cidea* was found downregulated in KO adipocytes (Figure 23C). Brown adipogenesis involves an increase in mitochondrial biogenesis, mainly controlled by the expression of the transcription factor PGC1α. TP53INP2 deficiency did not alter *Pgc1α* mRNA levels, and its protein levels seemed decreased in KO adipocytes (Figure 23A, B and C). As a result, the induction of the mitochondrial genes *Cox8b* and *Cox7a1*, and the mitochondrial proteins TIM44 and MFN2 were blunted by TP53INP2 loss-of-function (Figure 23A, B and C). More importantly, the thermogenic protein UCP1, which expression is mainly controlled by PGC1α and PPARγ, was dramatically reduced both at mRNA and protein level (Figure 23A, B and C). All these results are coherent with a positive role of TP53INP2 in brown adipocyte differentiation.

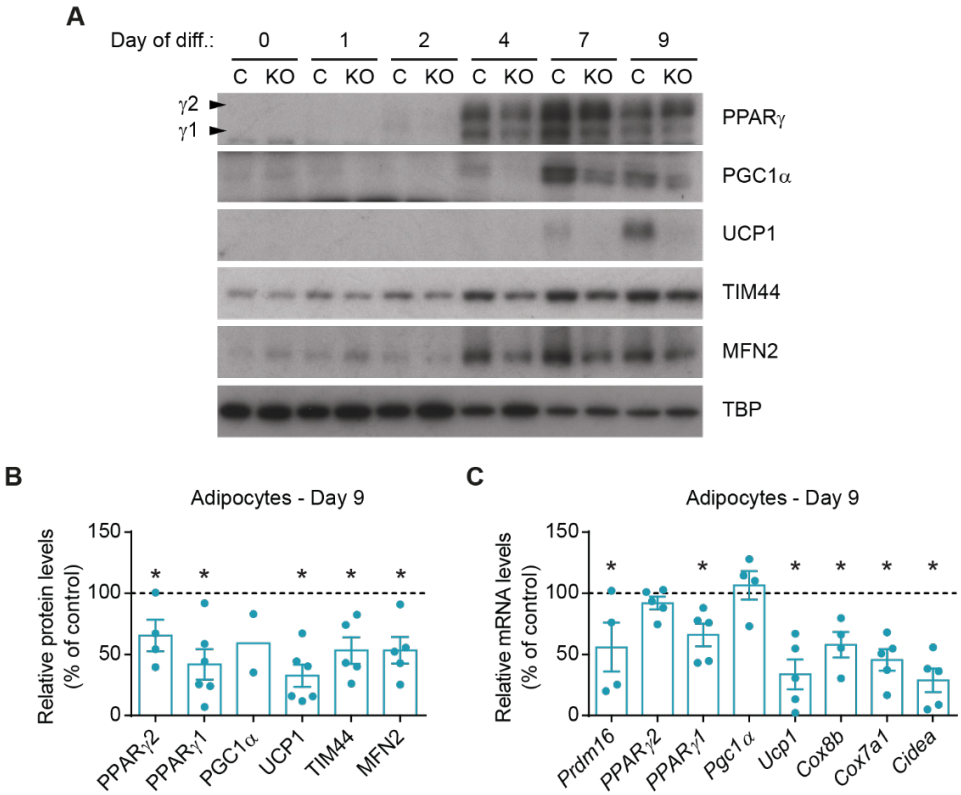

Figure 23. Brown adipogenesis is positively regulated by TP53INP2. Differentiation of control (C) and TP53INP2 knockout (KO) mouse brown preadipocytes. (A) PPARγ, PGC1α, UCP1, TIM44 and MFN2 protein abundance during differentiation and (B) western blot quantification at day 9 of differentiation (n=2–6). (C) Relative mRNA levels of adipogenic and thermogenic genes at day 9 of differentiation (n=4–5). Values of KO cells are represented relative to C group. Data are mean ± SEM. *p<0.05 vs. C.

4.2.3. TP53INP2 ablated brown adipocytes present impaired adrenergic response

Our next objective was to examine the impact of TP53INP2 ablation in the functionality of differentiated adipocytes, or in other words, in the thermogenic capacity of brown adipocytes. With that idea, mature adipocytes were treated with the β3-adrenergic agonist CL in other to activate the signaling pathway involved in thermogenesis. The stimulation of the adrenergic pathway during 4 hours was able to strongly induce *Ucp1* gene expression by 9-fold in control cells, while in KO this

response was significantly reduced (Figure 24A). The same result was obtained for the expression of *Prdm16* (Figure 24B), although the expression induction of this gene was much milder than *Ucp1*.

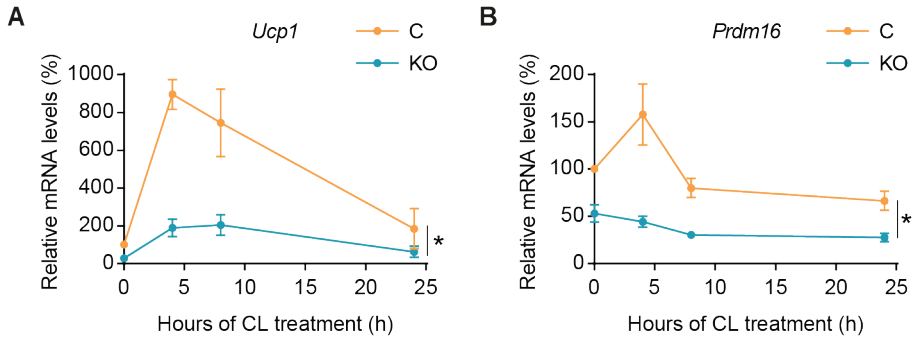

Figure 24. Impaired adrenergic signaling in TP53INP2 depleted brown adipocytes. (A) *Ucp1* and (B) *Prdm16* relative mRNA levels in brown adipocytes treated with CL-316,243 (CL) at different times (n=4). Data are mean ± SEM. *p<0.05 vs.C.

To ensure that both cell lines have the same ability to respond to the stimulus, the expression of the β3-adrenergic receptor (β3AR) was evaluated. No statistically significant differences were found in the receptor expression between control and KO cells, but a tendency to be increased was found in KO cells, probably due to a compensatory mechanism (Figure 25). This results further proves that the decreased adrenergic response in TP53INP2 ablated adipocytes is not dependent on decreased β3AR levels due to deficient differentiation, but arise from a defective intracellular signaling.

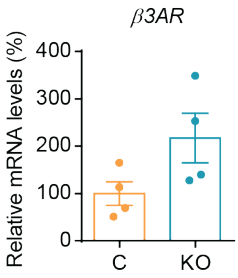

Figure 25. Normal β3AR expression in TP53INP2 knockout adipocytes. **β3AR** relative mRNA levels in control (C) and TP53INP2 knockout (KO) brown adipocytes (n=4). Data are mean ± SEM.

Following this direction and aiming at having functional data, mitochondrial respiratory profile was also analyzed in differentiated brown adipocytes by the XF24 Extracellular Flux Analyzer (Seahorse Bioscience). This system allows the measurement of oxygen consumption in intact adherent cells by the successive addition of different cellular permeable compounds. First, under basal conditions, cells are consuming oxygen through the oxidation of nutrients available in cellular media (Basal respiration). Second, oligomycin is added to inhibit ATP synthase, which abolishes all the ATP-linked mitochondrial respiration and obtaining uncoupled respiration (Proton leak). Then the uncoupling agent CCCP is added to measure the maximal electron transport capacity (Maximal respiration). Mitochondrial respiration associated to ATP production (ATP production) is calculated by the difference between basal and maximal respiration. Finally, rotenone and antimycin A are added to inhibit complex I and III respiration which reveals the oxygen that is been consumed by non-mitochondrial processes (this value is subtracted to obtain the previous measurements).

Surprisingly, KO adipocytes presented increased basal respiration compared to control cells, as well as an enhanced ATP production. No differences between groups were observed in the maximal respiration or proton leak (Figure 26).

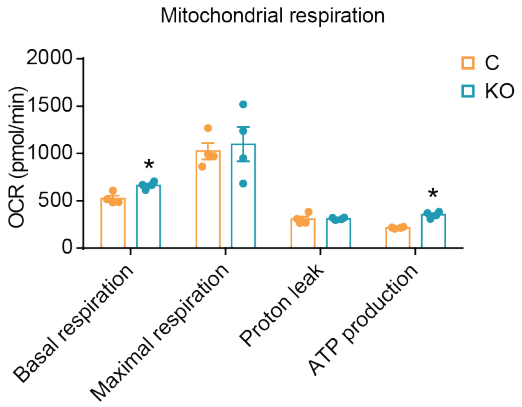

Figure 26. Mitochondrial respiration profile in adipocytes. Oxygen consumption rates (OCR) measured in differentiated control (C) and TP53INP2 knockout (KO) brown adipocytes (Day 9) (n=4). Data are mean ± SEM. *p<0.05 vs.C.

Next, the capacity to increase mitochondrial respiration by an adrenergic stimulus was also evaluated. NE is a catecholamine able to interact with β1-, β2- and β3-adrenergic receptors. This interaction results in the accumulation of cAMP, which in turn activates lipolysis. Thus, free fatty acids will directly activate UCP1 and promote thermogenesis (Cannon and Nedergaard, 2004). As evidenced in control cells, NE was able to increase oxygen consumption, indicative of an activation of thermogenesis. Nevertheless, this stimulation was significantly blunted in TP53INP2 ablated brown adipocytes (Figure 27), further proving that TP53INP2 deficiency results in a decreased thermogenic capacity that emanates from the differentiation defect.

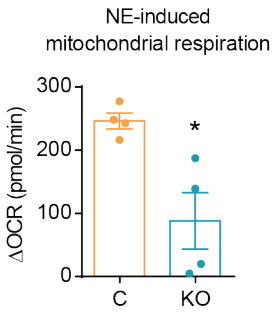

Figure 27. Decreased NE-induced mitochondrial respiration in TP53INP2 ablated adipocytes. Norepinephrine (NE)-induced oxygen consumption increase (ΔOCR) in differentiated control (C) and TP53INP2 knockout (KO) brown adipocytes (Day 9) (n=4). Data are mean ± SEM. *p<0.05 vs.C.

4.3. Characterization of Myf5-specific TP53INP2 knockout mice

Having determined that *in vitro* TP53INP2 ablation in brown preadipocytes reduces their adipogenic capacity, we wanted to study whether TP53INP2 was also required for the *in vivo* development of brown adipose in mice.

4.3.1. Animal model validation

In order to evaluate the impact of *in vivo* TP53INP2 ablation in brown adipogenesis a Myf5-specific TP53INP2 knockout mice (KO^{Myf5}) was generated by crossing homozygous $TP53INP2^{loxP/loxP}$ mice (Sala et al., 2014), which have floxed exon 3 and

4 to eliminate the translation initiation codon, with a Cre-recombinase expressing mice under the control of *Myf5* promoter. The selection of the Cre expressing mice was based on the fact that we were interested on studying brown adipogenesis and it was the only commercially available Cre mice that could induce gene knockout at brown preadipocyte level. In spite of that, the model we generated was not brown adipose tissue specific, because *Myf5* is also expressed in skeletal muscle, so TP53INP2 would be ablated in both tissues. However, our laboratory has previously described a skeletal muscle specific TP53INP2 knockout, which did not show any alterations in body composition, energy homeostasis or glucose metabolism (Sala et al., 2014).

Mice used were always homozygous for the LoxP sequences, and were divided into control (LoxP) or knockout (KO^{Myf5}) group depending on Cre expression (negative or positive respectively). Both strains were bred in a C57BL/6J genetic background and were born in normal Mendelian ratios. Deletion of exons 3 and 4 driven by Cre-recombinase caused the ablation of *Tp53inp2* expression in both brown adipose tissue (iBAT) and in the different muscles analyzed (Figure 28A). TP53INP2 protein levels were also undetectable in iBAT from KO^{Myf5} mice (Figure 28B). However *Tp53inp2* mRNA levels remained unchanged in all other tissues tested, including white adipose tissue, liver, heart or brain (Figure 28C).

4.3.2. General phenotyping: normal body weight and body composition in Myf5-specific TP53INP2 knockout mice

Brown adipose tissue function is of crucial importance after birth when mice are exposed for the first time to environment temperature and need to maintain their body temperature (Cannon and Nedergaard, 2004). Then, as mice get older, start to develop their skeletal muscle and white adipose organs which will allow for different mechanisms for heat generation, as for example shivering thermogenesis. That is why brown adipose tissue activity declines with age.

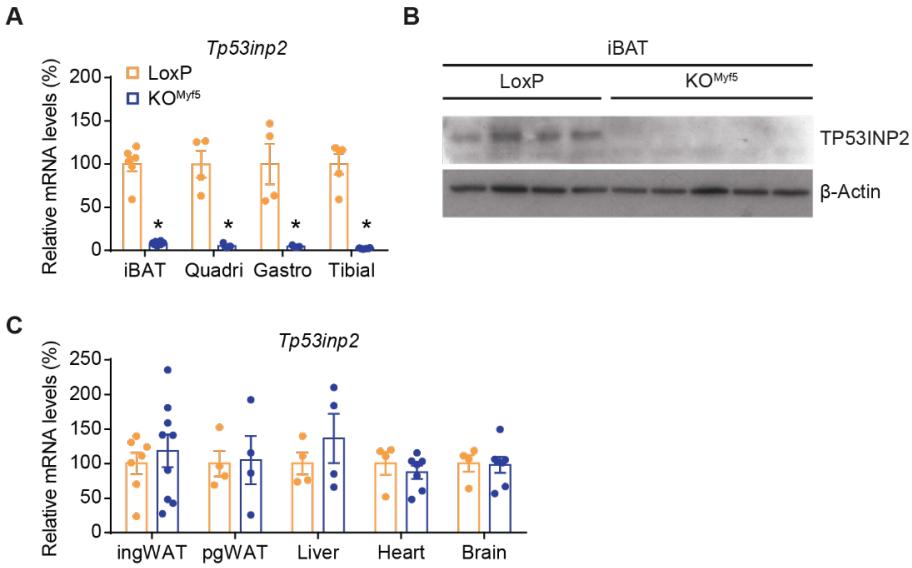

Figure 28. Myf5-specific TP53INP2 knockout mouse model validation. Control (LoxP) and Myf5-specific TP53INP2 knockout mice (KO^{Myf5}) at 3-months of age housed at 22°C and subjected to a chow diet (n=4-9). (A) *Tp53inp2* relative mRNA levels in mouse interscapular brown adipose tissue (iBAT), quadriceps (Quadri), gastrocnemius (Gastro) and tibialis (Tibial) muscles. (B) TP53INP2 protein abundance in iBAT. (C) *Tp53inp2* relative mRNA levels in mouse inguinal or perigonadal white adipose tissue (ingWAT or pgWAT), liver, heart and brain. Data are mean ± SEM. *p<0.05 vs. control LoxP group.

Based on this, we wanted to evaluate the impact of TP53INP2 elimination in a young age in which brown adipose tissue function is significantly relevant. At 3 months of age, no changes were found in body weight or body composition both in male and in female TP53INP2 deficient mice (Figure 29).

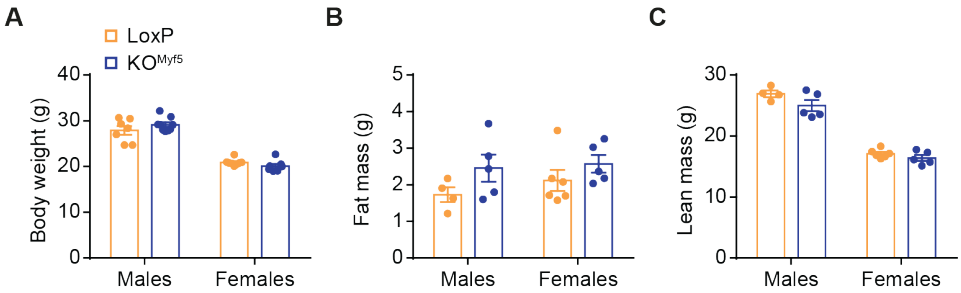

Figure 29. Normal body weight and body composition in Myf5-specific TP53INP2 knockout young mice. Control (LoxP) and Myf5-specific TP53INP2 knockout male or female mice (KO^{Myf5}) at 3-months of age housed at 22°C and subjected to a chow diet (n=5-9). (A) Body weight, (B) total fat mass and (C) total lean mass. Data are mean ± SEM.

However, when adipose depots were studied in detail, an increased iBAT weight was found in male KO^{Myf5} mice, but not in females, (Figure 30A) suggesting an early alteration in this tissue. On the contrary, two major white adipose depots, inguinal white adipose tissue (ingWAT) or perigonadal white adipose tissue (pgWAT) showed similar weights in both sexes and genotypes (Figure 30B and C). The same weight between genotypes and sexes was also found in the weight of quadriceps, gastrocnemius and tibialis muscles, which suggest no alteration in skeletal muscle development by TP53INP2 ablation (Figure 30D and E). No changes were observed in other tissues in which TP53INP2 expression was not altered, including liver, heart, kidney or brain (Figure 30D and E).

4.3.3. Gene expression profile of brown adipose tissue from Myf5-specific TP53INP2 ablated mice shows decreased thermogenic potential

In order to study which are the alterations in iBAT by TP53INP2 depletion, microarray gene expression profile was performed using iBAT samples from KO^{Myf5} and LoxP mice for control (at 3 months of age). 702 genes were significantly upregulated and 464 were downregulated by TP53INP2 ablation. Gene set enrichment analysis (KEGG) showed that, among the top ten downregulated pathways with the greatest statistically significance we found Fatty Acid Metabolism, Peroxisomes and TCA cycle, all coherent with a decreased oxidative phenotype (Figure 31).

In addition, Adipogenesis signaling pathway (Broad Hallmarks) was also downregulated by TP53INP2 ablation in brown adipose tissue (Figure 32A). Brown and white specific gene sets have been previously described according to genes whose expression is significantly enriched in one adipose depot compared to the other (Alvarez-Dominguez et al., 2015). In this sense, KO^{Myf5} presented decreased expression of the gene set defined as BAT-specific (Figure 32B), supporting the idea of a decreased brown adipogenesis *in vivo* upon deletion of TP53INP2.

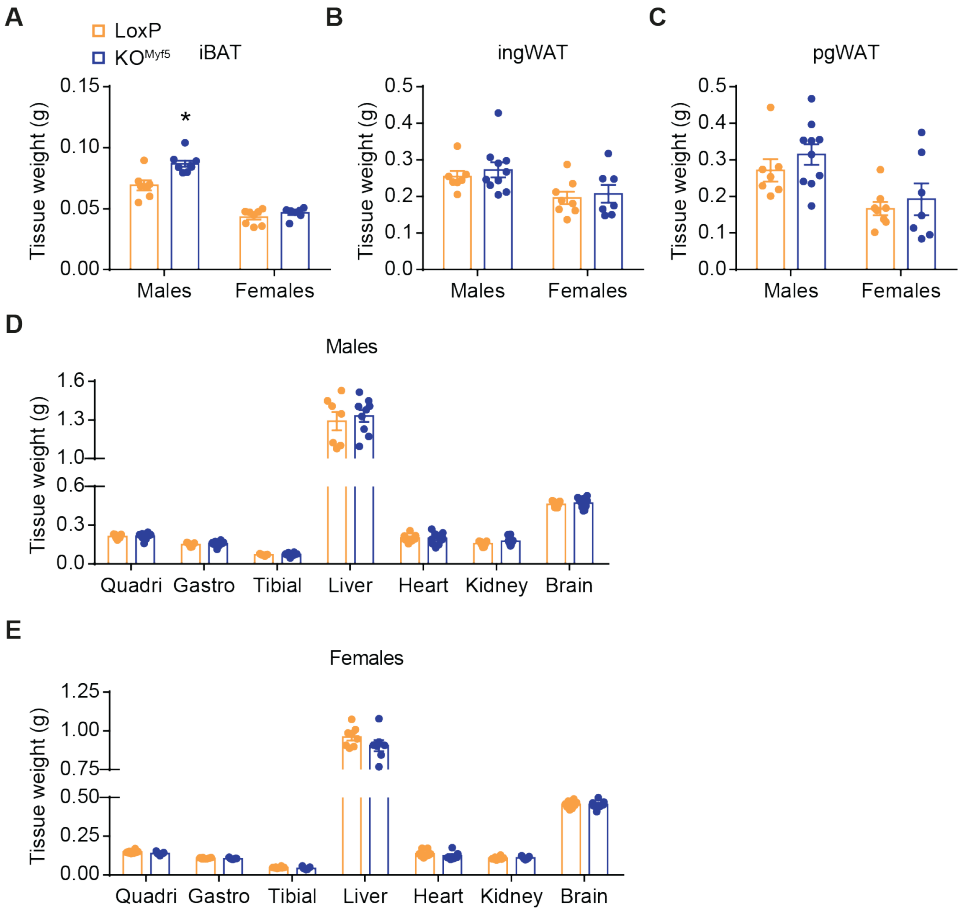

Figure 30. Increased iBAT weight in male Myf5-specific TP53INP2 knockout young mice. Control (LoxP) and Myf5-specific TP53INP2 knockout male or female mice (KO^{Myf5}) at 3-months of age housed at 22°C and subjected to a chow diet (n=7-9). Weight of (A) interscapular brown adipose tissue (iBAT), (B) inguinal white adipose tissue (ingWAT), (C) perigonadal white adipose tissue (pgWAT), (D) quadriceps (Quadri), gastrocnemius (Gastro), tibialis (Tibial), liver, heart, kidney and brain. Data are mean ± SEM. *p<0.05 vs. control LoxP group.

To further study whether TP53INP2 deletion resulted in a profile characterized by decreased thermogenic capacity, our microarray data were compared to an already published RNAseq study (Bai et al., 2017) aimed to examine the impact of thermoneutrality on brown adipose tissue modulation.Thus, the authors compared gene expression from iBAT samples of mice housed at 30°C for 7 days with mice housed at standard conditions (22°C). Interestingly, around 40% of the genes

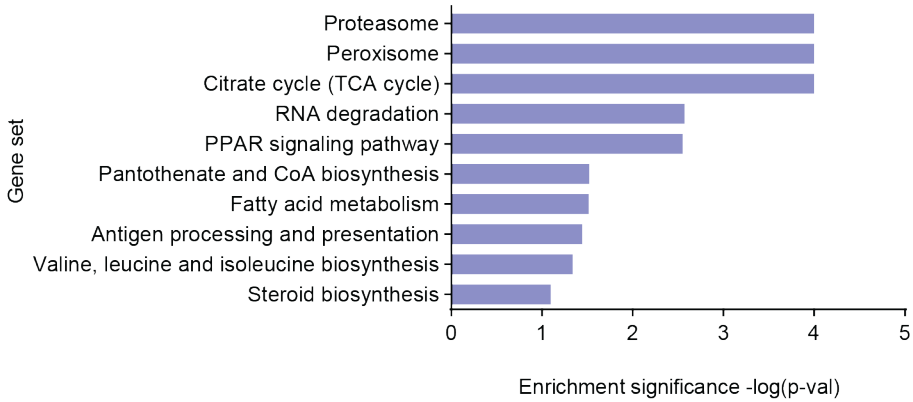

Figure 31. Gene sets downregulated in iBAT by TP53INP2 ablation. Transcriptomic analysis and Gene Set Enrichment Analysis (GSEA) performed in interscapular brown adipose tissue from control (LoxP) (n=4) or Myf5-specific TP53INP2 knockout (KO^{Myf5}) mice (n=4). Enrichment significance (-log(p-value)) of downregulated gene sets (KEGG).

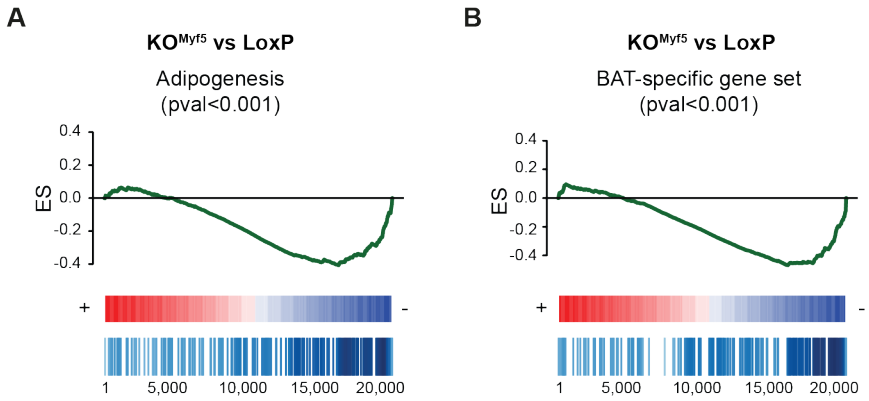

Figure 32. Enrichment plots of adipogenesis and brown adipose tissue specific genes. Transcriptomic analysis and Gene Set Enrichment Analysis (GSEA) performed in interscapular brown adipose tissue from control (LoxP) (n=4) or Myf5-specific TP53INP2 knockout (KO^{Myf5}) mice (n=4). Enrichment plots of (A) adipogenesis (Broad Hallmarks) and (B) custom gene set for brown adipose tissue (BAT)-specific genes.

modulated by the lack of TP53INP2 in iBAT were also naturally modified by the physiological inhibition of thermogenesis (Figure 33A). Moreover, gene expression showed a positive correlation (r=0.145) between both transcriptomic studies (Figure 33B), indicating that in both conditions (thermoneutrality and TP53INP2 ablation) gene variation showed a similar pattern.

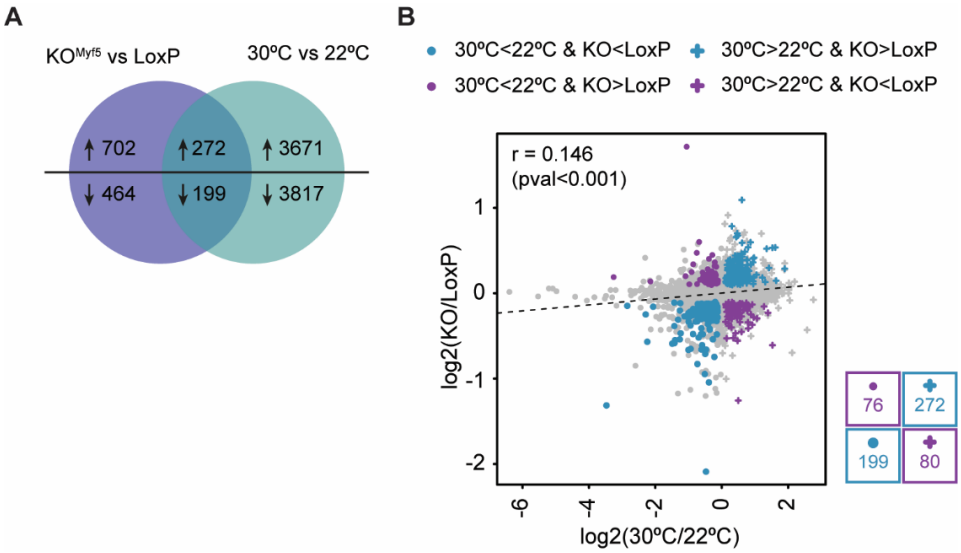

Figure 33. Gene modulation by TP53INP2 ablation is comparable to thermoneutrality. Transcriptomic analysis performed in interscapular brown adipose tissue from control (LoxP) (n=4) or Myf5-specific TP53INP2 knockout (KO^{Myf5}) mice (n=4) and compared to transcriptomic analysis from WT mice housed at 22°C (n=2) or 30°C (n=2) (Bai et al., 2017). (A) Number of genes upregulated or downregulated and (B) fold change correlation plot (KO/LoxP and 30°C/22°C) between both transcriptomic studies.

The expression of selected genes was also subjected to validation by qPCR. Our results confirm a reduced expression of the adipogenic genes *Prdm16*, *C/EBPβ*, *PPARγ1* and *PPARγ2* in TP53INP2 deficient brown adipose tissue from male mice (Figure 34A). The mRNA levels of *Pref1*, which is known to be expressed in preadipocytes to inhibit adipogenesis, was also significantly enhanced in KO^{Myf5} mice compared to control ones, further supporting the idea of a differentiation defect induced by TP53INP2 depletion (Figure 34B). In addition, genes involved in BAT thermogenesis such as *Ucp1*, *Pgc1α*, *Cox8b*, *Dio2* and *Elovl3* were also downregulated in KO^{Myf5} mice (Figure 34A), which goes in parallel with GSEA results.

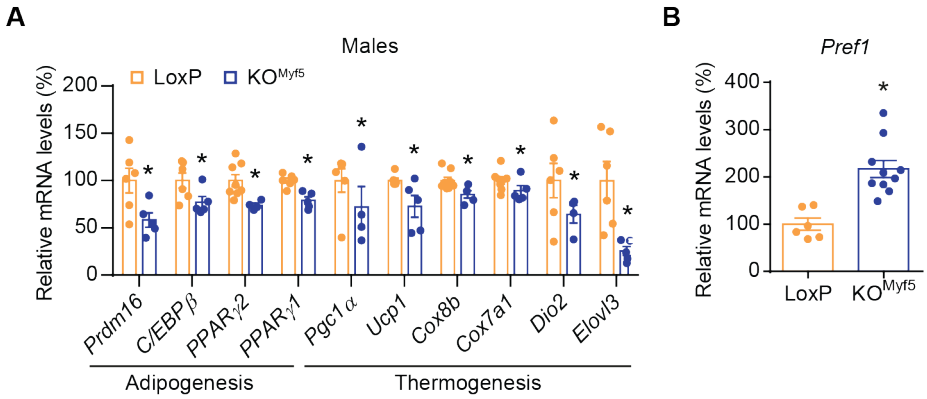

Figure 34. Downregulated expression of adipogenic and thermogenic genes by T53INP2 ablation. Control (LoxP) and Myf5-specific TP53INP2 knockout male mice (KO^{Myf5}) at 3-months of age housed at 22°C and subjected to a chow diet (n=7-9). Expression of (A) adipogenic and thermogenic genes, and (B) preadipocyte factor 1 (*Pref1*) in interscapular brown adipose tissue. Data are mean ± SEM. *p<0.05 vs. control LoxP group.

Female KO^{Myf5} mice showed a similar tendency of decreased expression of adipogenic and thermogenic genes in brown adipose tissue (Figure 35). However none of them reached statistically significance, probably because female KO^{Myf5} have a milder phenotype compared to male mice, or due to a low statistical potency.

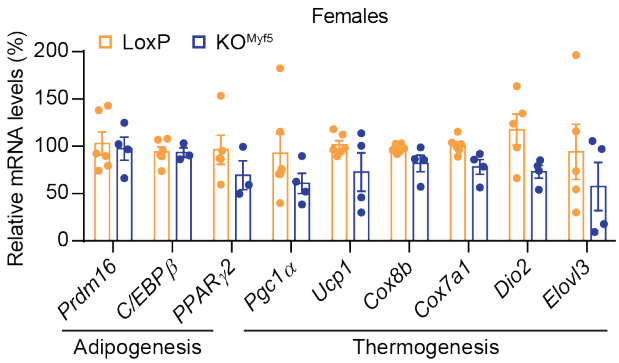

Figure 35. Expression of adipogenic and thermogenic genes by T53INP2 deletion in female mice. Expression of adipogenic and thermogenic genes in interscapular brown adipose tissue from control (LoxP) and Myf5-specific TP53INP2 knockout female mice (KO^{Myf5}) at 3-months of age housed at 22°C and subjected to a chow diet (n=4-5). Data are mean ± SEM.

4.3.4. TP53INP2 loss-of-function in Myf5 precursor cells impairs the morphological characteristics of brown adipose tissue

The morphology of brown adipocytes is linked to its thermogenic state, being multilocular under thermogenically active conditions and unilocular when thermogenesis is inhibited (Cui et al., 2016; Small et al., 2018). Taking into account that our gene expression results suggested that TP53INP2 ablation results in a thermogenically inactive brown adipose tissue, we decided to evaluate tissue histology. Quantification of lipid droplet (LD) number and LD area was used as a measure of multilocularity. Both males and females KO^{Myf5} mice showed a loss of multilocularity in hematoxylin and eosin iBAT stained sections (Figure 36A), characterized by a reduction in LD number per area and an increase in LD size (Figure 36B and C).

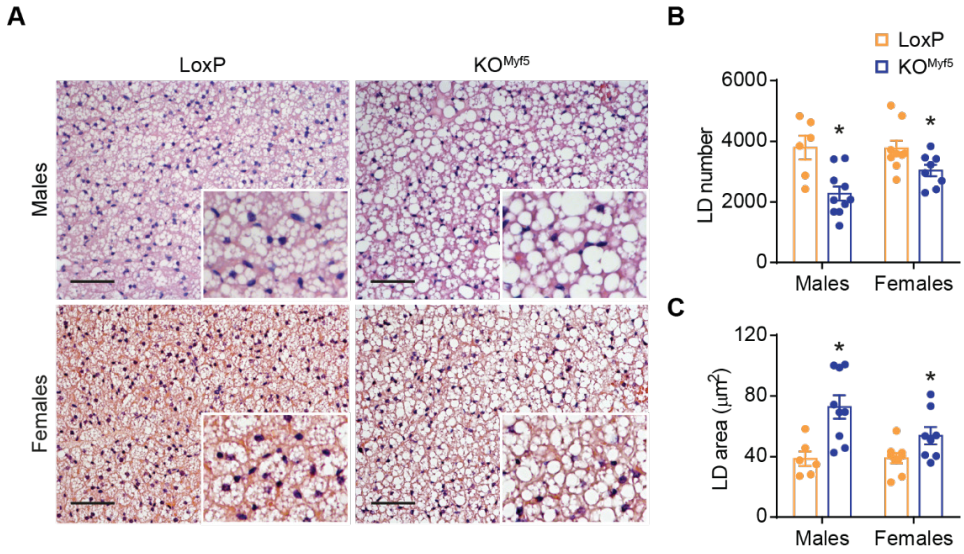

Figure 36. Myf5-specific TP53INP2 knockout mice have altered iBAT morphology. Control (LoxP) and Myf5-specific TP53INP2 knockout male or female mice (KO^{Myf5}) at 3-months of age housed at 22°C and subjected to a chow diet (n=6-9). (A) Hematoxylin-eosin staining of interscapular brown adipose tissue sections, (B) lipid droplet (LD) number and LD average area measurements. Data are mean ± SEM. *p<0.05 vs. control LoxP group. Scale bar, 100μm.

4.3.5. Myf5-specific TP53INP2 ablated mice show decreased energy expenditure

From different animal and human studies it has become clear that brown adipose tissue non-shivering thermogenesis can have an impact in overall energy balance (Wijers et al., 2009). In cold exposed mice (5°C), when brown adipose tissue is fully active, 60% of all the energy expenditure of a mouse is performed in brown adipocytes (Cannon and Nedergaard, 2011; Golozoubova et al., 2004). Conversely, animal models with defective brown adipose tissue thermogenesis develop an obese phenotype as a result of decreased energy expenditure (Feldmann et al., 2009).

Thus, we next asked whether energy balance was altered upon ablation of TP53INP2 in brown adipose tissue. We evaluated energy expenditure in male mice at 3 months of age, as they have previously shown a stronger phenotype compared to female, and if so, we expected higher differences between genotypes. Oxygen consumption (VO_2), carbon dioxide production (VCO_2) and energy expenditure (EE) were corrected by an adjusted body weight of 29.4714g determined using ANCOVA. This correction has been reported as a good method to eliminate variance in metabolic parameters derived from differences in body weight between animals, as a bigger animal will expend more energy than a smaller one (Tschöp et al., 2012). Thus, we performed indirect calorimetry assays and we found that KO^{Myf5} mice showed a significant reduction of VO_2, VCO_2 and EE, independently of body weight (Figure 37A, C and E). When we plotted the different metabolic parameters evaluated (VO_2, VCO_2 and EE) as a function of body weight, we could clearly observe that their relation was statistically different in LoxP and KO^{Myf5} mice (Figure 37B, D and F).

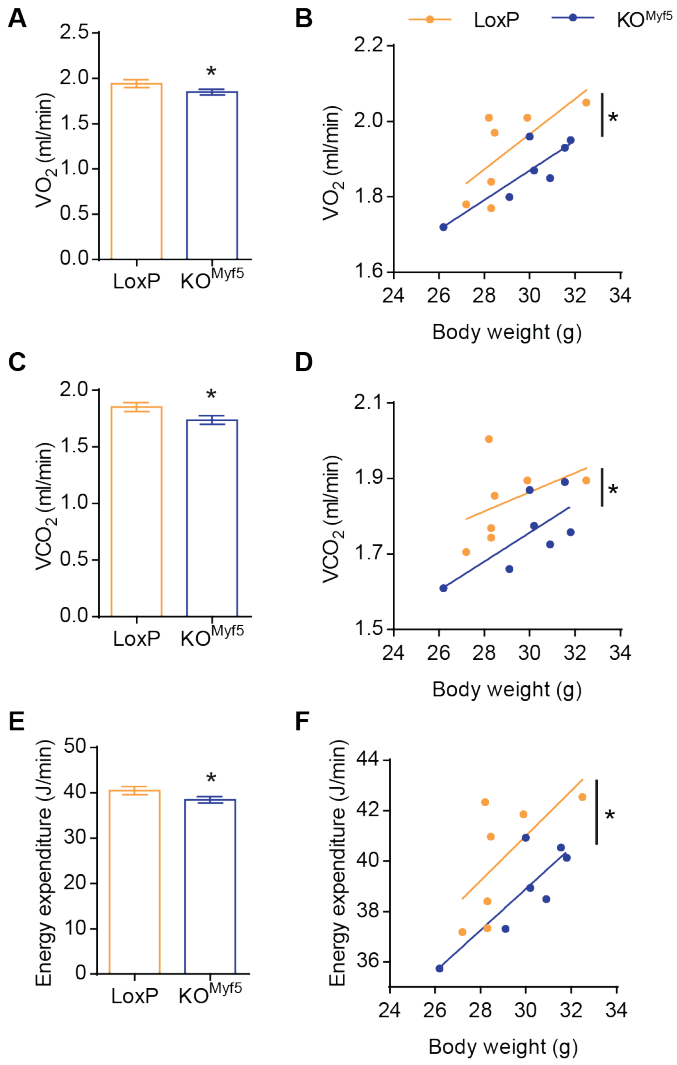

Figure 37. Decreased oxygen consumption, carbon dioxide production and energy expenditure in Myf5-specific TP53INP2 knockout mice. Control (LoxP) and Myf5-specific TP53INP2 knockout (KO^{Myf5}) male mice at 3-months of age housed at 22°C and subjected to a chow diet (n=7). (A) and (B) oxygen consumption (VO_2); (C) and (D) carbon dioxide production (VCO_2); (E) and (F) energy expenditure. Adjusted means (based on a normalized mouse weight of 29.4714g determined using ANCOVA) or correlation with body weight. Data are mean ± SEM. *p<0.05 vs. control LoxP group.

The reduction in energy expenditure was mainly detected in the light phase (in which mice are resting), which suggests a defect in thermogenesis (Figure 38A). These alterations were observed in the absence of changes in the locomotor activity (Figure 38B). No changes were seen in the respiratory exchange ratio (RER) nor in nutrient oxidation (Figure 38C, D and E).

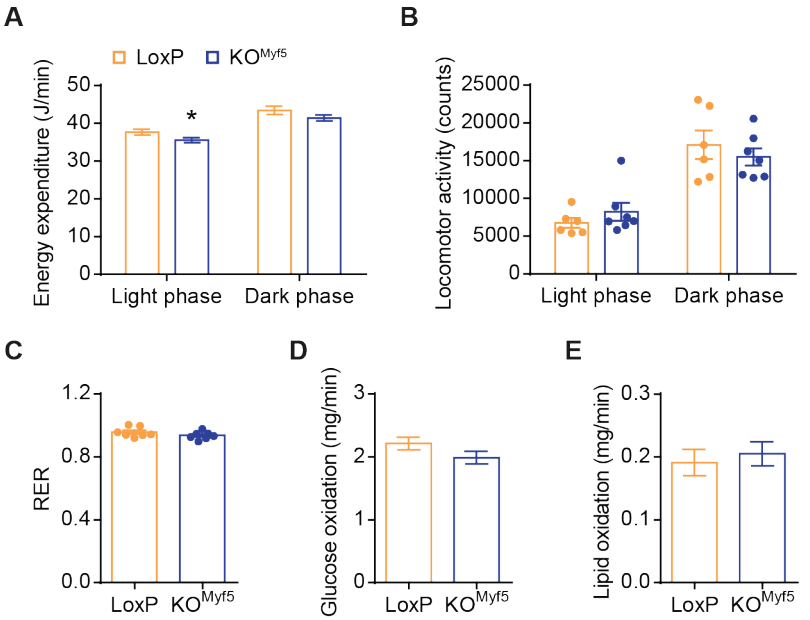

Figure 38. Metabolic parameters in control and Myf5-specific TP53INP2 knockout mice. Control (LoxP) and Myf5-specific TP53INP2 knockout (KO^{Myf5}) male mice at 3-months of age housed at 22°C and subjected to a chow diet (n=7). (A) Energy expenditure adjusted means (based on a normalized mouse weight of 29.4714g determined using ANCOVA) and (B) locomotor activity during light (inactive) and dark (active) phase. (C) Respiratory exchange ratio (RER). (D) Glucose and (E) lipid oxidation adjusted means (ANCOVA). Data are mean ± SEM. *p<0.05 vs. control LoxP group.

Moreover, we also wanted to evaluate whether the differences in energy balance could be influenced by energy intake. For that, we placed LoxP and KO^{Myf5} into metabolic chambers to measure food and water intake. The same daily consumption of food and water was found in LoxP and KO^{Myf5} mice (Figure 39A and B), proving that the decreased energy expenditure was not a result of differences in energy intake. Urine and faeces excretion were also unaltered by TP53INP2 ablation (Figure 39C and D).

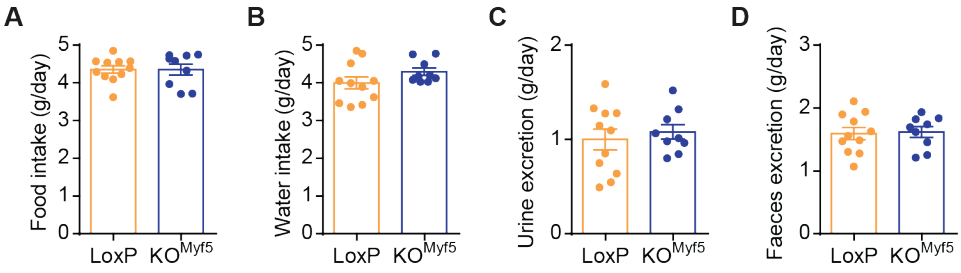

Figure 39. Food or water intake and urine or faeces excretion are not altered in Myf5-specific TP53INP2 knockout mice. Control (LoxP) and Myf5-specific TP53INP2 knockout (KO^{Myf5}) male mice at 3-months of age housed at 22°C and subjected to a chow diet (n=9-11). Daily (A) food and (B) water intake. Daily (C) urine and (D) faeces excretion. Data are mean ± SEM.

4.3.6. Brown adipose specific thermogenic capacity is reduced by TP53INP2 depletion

The results above document that TP53INP2 ablation in brown adipose tissue decrease energy expenditure without modifying energy intake. However, indirect calorimetry is a measure of the global metabolic rate of an animal. Thus, our next aim was to directly determine whether the maximal thermogenic capacity is compromised in KO^{Myf5} animals, which measures the quantity of heat that a mouse can produce compared to the energy that is being produced under free-living conditions evaluated by indirect calorimetry. To assess maximal thermogenic capacity, a supramaximal dose of a thermogenic drug (usually NE or the β3-adrenergic agonist CL) is administered to an animal to induce maximal brown adipose tissue activation. However, other organs like skeletal muscle, liver or white adipose tissue will also respond to this adrenergic stimulus. That is why, in order to identify brown adipose tissue specific thermogenesis it is necessary to measure maximal thermogenic capacity in animals acclimated at two different environment temperatures (Virtue and Vidal-Puig, 2013). Thus, the difference between adrenergic stimulated energy expenditure under two different temperatures is directly dependent on the presence of UCP1 (Golozoubova et al., 2006).

With this idea, we measured VO_2 upon NE injection in male mice at 4 months of age acclimated either to 22°C or at 30°C. Mice were acclimated to the corresponding temperature after weaning for 2 months, to ensure that brown adipose tissue had reached a steady state with respect to its level of thermogenic capacity (Virtue and Vidal-Puig, 2013). In addition, mice were anesthetized before performing the measurements to avoid noise due to energy consuming processes such as physical activity or the stress derived from the mice manipulation, and to decrease endogenous sympathetic tone. When anesthetized, mice were placed inside a chamber at 30°C in order to prevent them from hypothermia. Under low thermogenic conditions (30°C) both LoxP and KO^{Myf5} mice showed similar maximal thermogenic capacity (Figure 40A), which was low coherent with their acclimation temperature. However, when VO_2 measurement upon NE injection was performed in mice that were housed at 22°C, their maximal thermogenic capacity was significantly enhanced compared to 30°C, consistent with the fact that at this temperature there is active thermogenesis to maintain body temperature. More importantly, we could also observe that VO_2 increase (ΔVO_2) upon NE treatment was significantly diminished in KO^{Myf5} mice compared to control littermates (Figure 40A). Area under the curve quantification showed the same profile (Figure 40B). Our results demonstrate a defective brown adipose tissue specific non-shivering thermogenesis due to the lack of TP53INP2.

4.3.7. Decreased brown adipose tissue and normal skeletal muscle mitochondrial respiration in Myf5-specific TP53INP2 knockout mice

To further confirm that brown adipose tissue dysfunction was contributing to the decrease in whole body energy expenditure, we directly measured mitochondrial respiration using high-resolution respirometry. To do so, mitochondrial enriched fractions were obtained from LoxP and KO^{Myf5} mice and the same amount of mitochondrial protein was used. Basal mitochondrial respiration (Leak) in the presence of glutamate and malate showed no differences between genotypes.

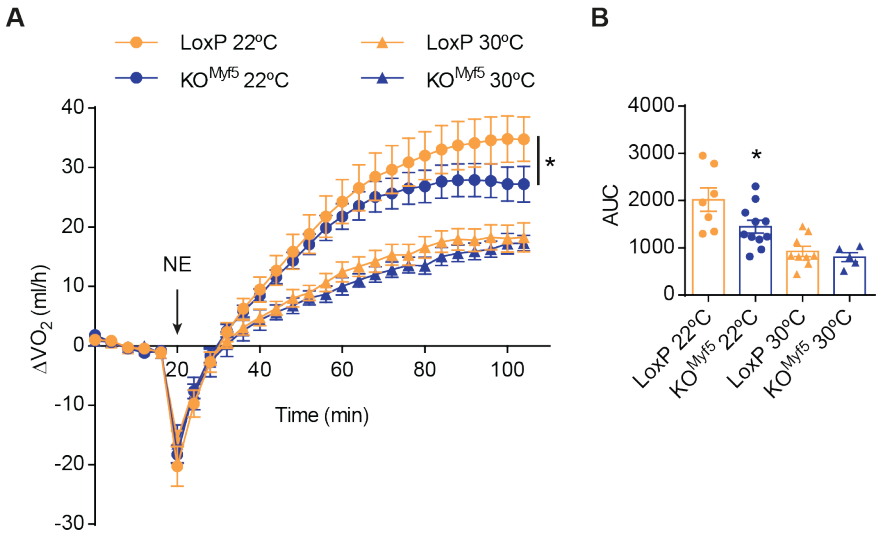

Figure 40. TP53INP2 enhances BAT specific non-shivering thermogenesis. Control (LoxP) and Myf5-specific TP53INP2 knockout (KO^{Myf5}) male mice at 4-months of age housed at 22°C or 30°C for 2 months and subjected to a chow diet (n=5-11). (A) Oxygen consumption increase (ΔVO2) upon norepinephrine injection (NE) and (B) area under the curve quantification in anesthetized mice at 30°C. Data are mean ± SEM. *p<0.05 vs. control LoxP group.

The addition of ADP to the chamber to induce complex I activity (C I) induced a slight increase in coupled respiration but also showed the same oxygen flux in both groups. However the addition of succinate significantly enhanced mitochondrial coupled respiration in LoxP and KO^{Myf5} mitochondria, but this induction was slightly blunted by T53INP2 ablation (Figure 41A).

Given that the animal model used in these experiments also presents TP53INP2 depletion in skeletal muscle, and taking into account that skeletal muscle metabolism can account for over the 30% of energy expenditure, we also evaluated mitochondrial respiration in this tissue. For these experiments, we used permeabilized fibers from tibialis anterior muscle, because it represents a mixed muscle with oxidative and glycolytic fibers. Under these conditions, no alterations in mitochondrial respiration were detected in any of the parameters assessed (Figure 41B).

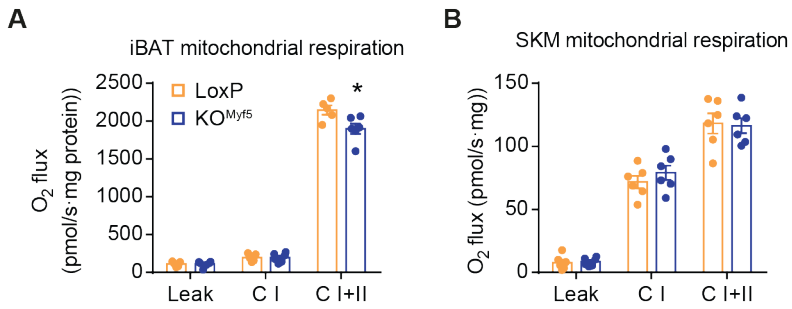

Figure 41. Decreased brown adipose tissue and normal skeletal muscle mitochondrial respiration in Myf5-specific TP53INP2 knockout mice. Control (LoxP) and Myf5-specific TP53INP2 knockout (KO^{Myf5}) male mice at 3-months of age housed at 22°C and subjected to a chow diet (n=5-6). High resolution respirometry in (A) isolated interscapular brown adipose tissue (iBAT) mitochondria or in (B) tibialis anterior muscle (SKM) permeabilized fibers. Data are mean ± SEM. *p<0.05 vs. control LoxP group.

Altogether, with these data and with previous reports from our laboratory demonstrating that the muscle-specific TP53INP2 knockout mice did not have any alteration in energy balance (David Sala, PhD thesis, 2013), we postulate that brown adipose tissue dysfunction due to the lack of TP53INP2 is the key factor involved in the phenotype of Myf5-specific KO mice.

4.3.8. Normal body temperature in Myf5-specific TP53INP2 ablated mice

Having determined that the absence of TP53INP2 in brown adipose tissue results in dysfunctional non-shivering thermogenesis, we speculated that KO^{Myf5} would present decreased body temperature as a result of a defective thermoregulation. Following this idea, LoxP and KO^{Myf5} mice were familiarized to a rectal prove daily during one weak to avoid body temperature increase due to the stress induced by the manipulation. After the habituation week, rectal body temperature was measured in LoxP and KO^{Myf5} littermates. Surprisingly, no statistical differences were observed between genotypes (Figure 42).

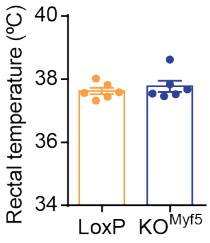

Figure 42. Normal body temperature in TP53INP2 ablated mice. Rectal temperature of control (LoxP) and Myf5-specific TP53INP2 knockout (KO^{Myf5}) male mice at 3-months of age housed at 22°C and subjected to a chow diet (n=6). Data are mean ± SEM.

Maintaining body temperature is a must for the survival of animals and because of that several mechanism are involved in body thermoregulation, like shivering thermogenesis performed by skeletal muscle, the browning of white adipose tissue or increasing uncoupling in liver. These results manifest that in spite of brown adipose tissue dysfunction, KO^{Myf5} show adaptive mechanisms to maintain their body temperature. This is of importance, as an increased energy expenditure from some tissue could influence the overall phenotype.

4.3.9. Myf5-specific TP53INP2 ablation results in glucose intolerance and insulin resistance

Brown adipose tissue metabolism is also involved in the regulation of glucose balance. It presents a very high uptake of glucose per unit of tissue mass, so it can potentially take a significant amount of glucose from circulation. Brown adipose tissue glucose uptake is induced by two opposite situations, stimulated 5-fold by insulin during anabolic processes and increased by 10-fold under conditions of active thermogenesis (Cannon and Nedergaard, 2004; Orava et al., 2011). In this regard, it has been described that brown adipose tissue transplantation in mice improves glucose tolerance and insulin sensitivity (Stanford et al., 2013). Also, brown adipose tissue activation by cold exposure, β3-adrenergic agonists or by thyroid hormones was shown to improve glucose homeostasis and insulin sensitivity (Forest et al., 1987; Peirce and Vidal-Puig, 2013). In adult humans, a positive correlation between blood glucose levels and brown adipose tissue has been documented (Cypess et al., 2009; van Marken Lichtenbelt et al., 2009; Zhang

et al., 2013), and cold can also induce an increase in brown adipose tissue glucose uptake (Ouellet et al., 2012; Chondronikola et al., 2014).

Activation of brown adipose tissue is not only associated to an increase in its glucose uptake rate, but also to the release of autocrine and endocrine adipokines (called batokines), like FGF21 and Neuregulin 4, which will modulate glucose metabolism into target tissues (Hondares et al., 2011b; Whittle et al., 2012; Villarroya et al., 2017a, 2017b).

Evidences obtained in regard to the thermogenesis dysfunction by T53INP2 lead us to speculate whether glucose metabolism could be compromised in KO^{Myf5} mice. In keeping with this, an intraperitoneal glucose tolerance test (GTT) was performed in control and KO^{Myf5} male mice (Figure 43). No differences between genotypes were observed in basal fasting glycaemia. However, glucose administration increased significantly blood glucose levels in KO^{Myf5} animals after 30 mins of injection compared to control littermates (Figure 43A). Thereafter, blood glucose clearance was similar in both groups, however the differences between them were maintained (Figure 43A). The same tendency was found when assessed in female mice, but once again, the phenotype was much milder than in male mice (Figure 43B).

Increased insulinemia was found under basal fasting conditions in KO^{Myf5} male mice, while it remained the same in female mice (Figure 44A and B). Nonetheless insulin release upon glucose injection was not impaired by TP53INP2 ablation in both sexes (Figure 44A and B).

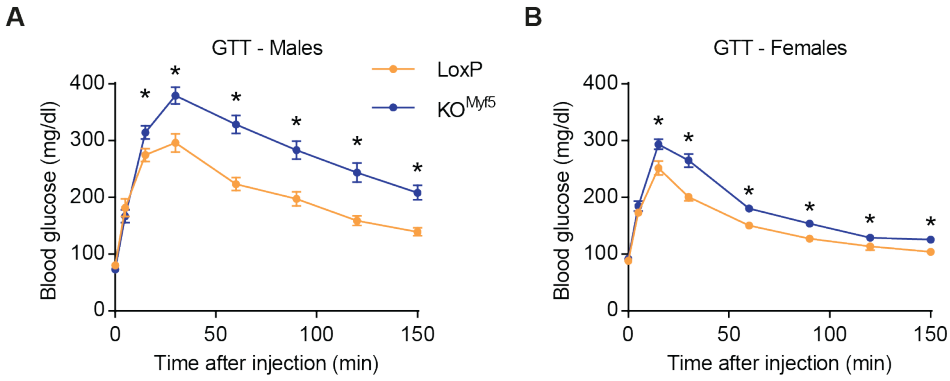

Figure 43. Glucose intolerance by TP53INP2 deletion. Blood glucose levels during glucose tolerance test (GTT 2g/kg) in control (LoxP) and Myf5-specific TP53INP2 knockout (KO^{Myf5}) (A) male or (B) female mice at 3-months of age housed at 22°C and subjected to a chow diet (n=9-10). Data are mean ± SEM. *p<0.05 vs. control LoxP group.

These results suggested that insulin resistance could be the responsible for the glucose intolerance. With that aim, we analyzed insulin sensitivity through an intraperitoneal insulin tolerance test (ITT). While insulin injection was able to reduce 40% the initial blood glucose levels in control animals, insulin was not efficient in doing so in KOMyf5 male mice (Figure 45A and C). In female mice, only a small increase in glycaemia was found in KOMyf5 animals after 30 min of insulin injection (Figure 45B and D).

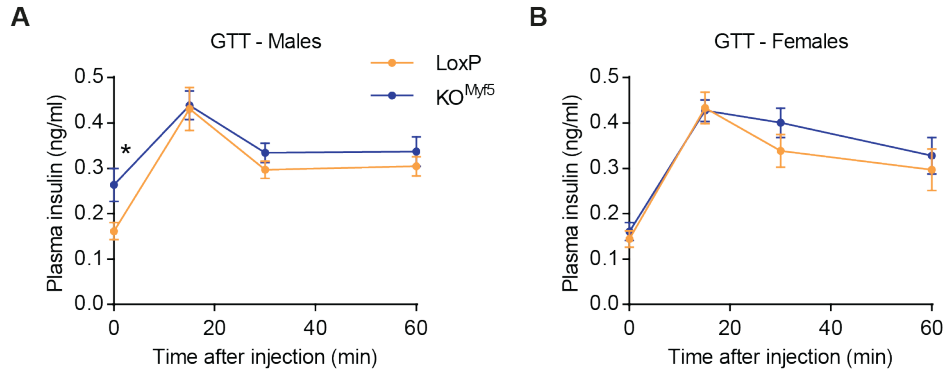

Figure 44. Increased basal insulinemia in Myf5-specific TP53INP2 knockout male mice. Plasma insulin levels during glucose tolerance test (GTT 2g/kg) in control (LoxP) and Myf5-specific TP53INP2 knockout (KO^{Myf5}) (A) male or (B) female mice at 3-months of age housed at 22°C and subjected to a chow diet (n=9-10). Data are mean ± SEM. *p<0.05 vs. control LoxP group.

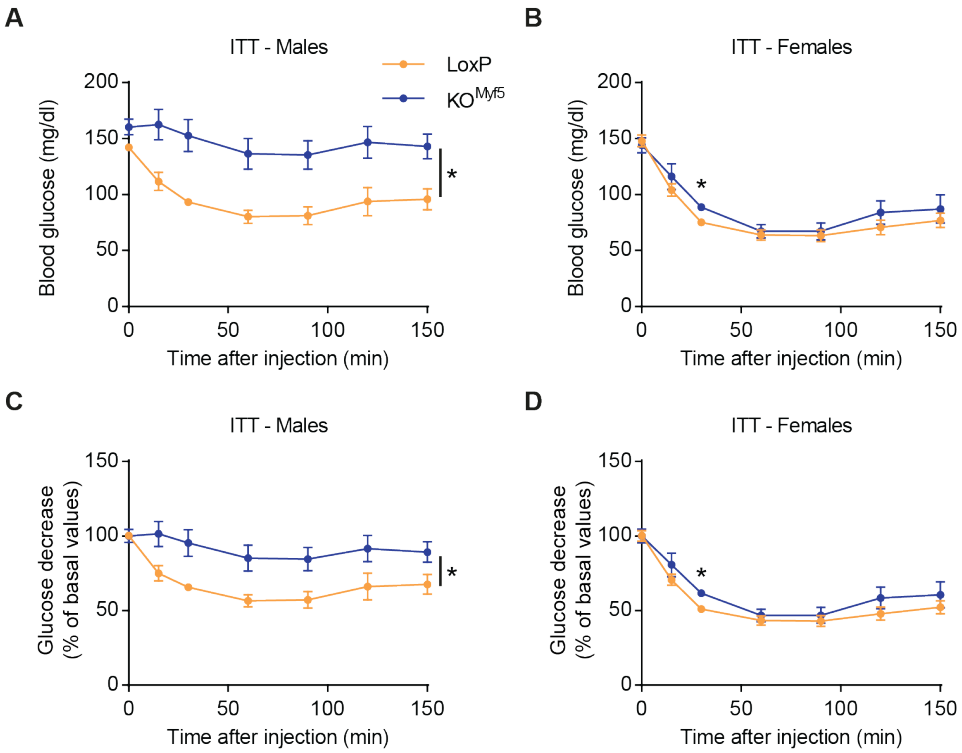

Figure 45. Insulin resistance in Myf5-specific TP53INP2 ablated mice. Insulin tolerance test (ITT 0.7U/kg) in control (LoxP) and Myf5-specific TP53INP2 knockout (KO^{Myf5}) (A) and (C) male or (B) and (D) female mice at 3-months of age housed at 22°C and subjected to a chow diet (n=7-9). (A) And (B) blood glucose levels and (C) and (D) glucose decrease (%) during ITT. Data are mean ± SEM. *p<0.05 vs. control LoxP group.

Overall these results exhibit that Myf5-specific TP53INP2 ablation results in glucose intolerance and insulin resistance. Taking into consideration that previous results of our laboratory have demonstrated normal glucose and insulin metabolism in the skeletal muscle-specific TP53INP2 knockout mice (David Sala, PhD thesis, 2013), we assume that the phenotype is driven directly by the lack of TP53INP2 in brown adipose tissue. However, whether the defects in glucose uptake are occurring in brown adipocytes or in other tissues due to an interruption of an endocrine signaling (from brown adipose tissue to other metabolically active tissues) due to the dysfunction induced by TP53INP2 depletion would need further investigation.

4.3.10. Development of obesity in 6 months old Myf5-specific T53INP2 knockout mice

Based on the fact that 3 months old KO^{Myf5} mice showed a phenotype characterized by decreased energy expenditure without alterations in energy intake, we expected that this energy excess would accumulate with age in the form of lipids. Thus, we decided to study older mice. At 6 months of age we detected that male KO^{Myf5} mice presented increased body weight compared to control littermates, while in females no differences were observed (Figure 46A). Body composition analysis showed that an increase of the total fat mass was the responsible for the body weight increase (Figure 46B). In spite of the lack of differences in body weight, female KO^{Myf5} mice also exhibited enhanced fat mass (Figure 46B), while lean mass remained the same in both groups (Figure 46C).

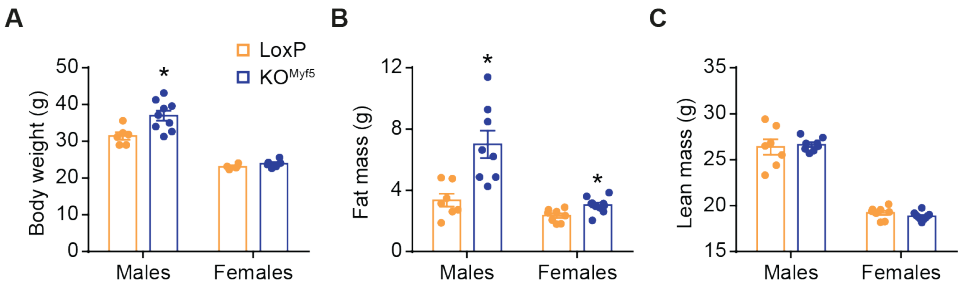

Figure 46. Increased body weight and fat mass in 6-months old knockout mice. Control (LoxP) and Myf5-specific TP53INP2 knockout male or female mice (KO^{Myf5}) at 6-months of age housed at 22°C and subjected to a chow diet (n=6-9). (A) Body weight, (B) total fat mass and (C) total lean mass. Data are mean ± SEM. *p<0.05 vs. control LoxP group.

In addition, under these conditions, iBAT from both male and female TP53INP2 ablated mice weighed twice as much as the LoxP's (Figure 47A). Moreover, expansion of the major white adipose tissue depots ingWAT and pgWAT were markedly greater in KO^{Myf5} compared to controls (Figure 47B and C). The weight of quadriceps, gastrocnemius and tibialis muscles, or the weight of the liver was unaltered by TP53INP2 ablation in both sexes (Figure 47D, E and F).

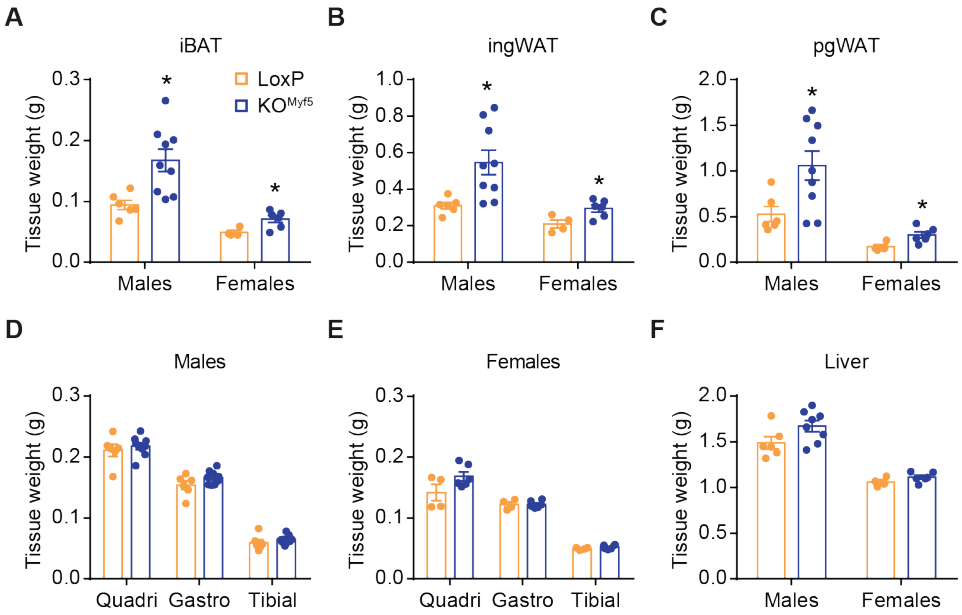

Figure 47. TP53INP2 ablation results in increased adiposity. Control (LoxP) and Myf5-specific TP53INP2 knockout male or female mice (KO^{Myf5}) at 6-months of age housed at 22°C and subjected to a chow diet (n=6-9). Weight of (A) interscapular brown adipose tissue (iBAT), (B) inguinal white adipose tissue (ingWAT), (C) perigonadal white adipose tissue (pgWAT), (D) and (E) quadriceps (Quadri), gastrocnemius (Gastro) and tibialis (Tibial) muscles, and (F) liver. Data are mean ± SEM. *p<0.05 vs. control LoxP group.

Histological analysis of iBAT sections stained with hematoxylin and eosin confirmed that tissue morphology was dramatically impaired in older mice (Figure 48A). The loss of multilocularity was further disrupted both in male and in female KO^{Myf5} mice assessed by a decrease in LD number per area and an increase in LD size (Figure 48B and C).

Under these conditions the expression of UCP1 protein was also evaluated. Protein abundance showed decreased levels in KO^{Myf5} mice compared with control littermates (Figure 49). This is coherent with the decreased thermogenic capacity of Myf5-specific TP53INP2 mice, a property that is directly UCP1-dependent, and supports the idea that the body weight increase in 6-months old mice is due to a defect in non-shivering thermogenesis.

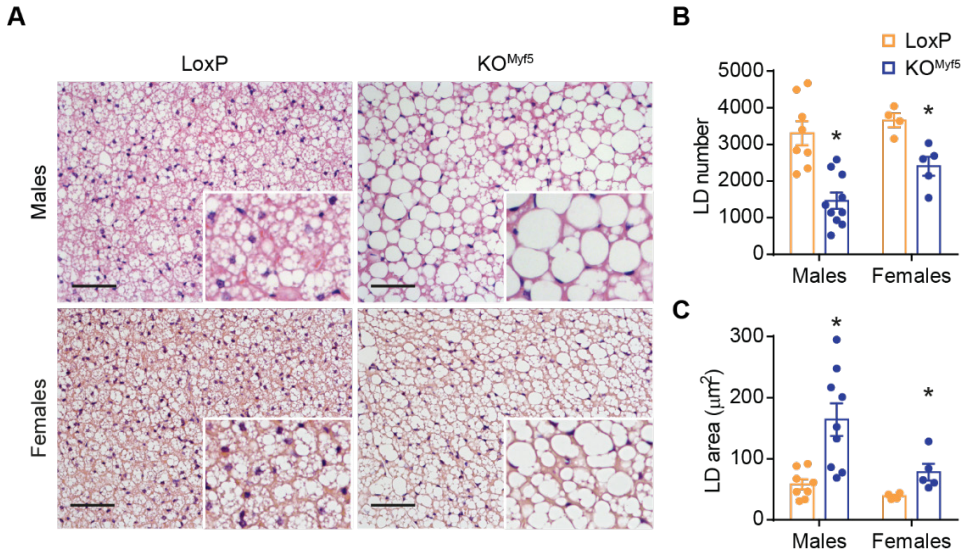

Figure 48. Older Myf5-specific TP53INP2 knockout mice have a dramatic loss of iBAT multilocularity. Control (LoxP) and Myf5-specific TP53INP2 knockout male or female mice (KO^{Myf5}) at 6-months of age housed at 22°C and subjected to a chow diet (n=4-10). (A) Hematoxylin-eosin staining of interscapular brown adipose tissue sections, (B) lipid droplet (LD) number and LD average area measurements. Data are mean ± SEM. *p<0.05 vs. control LoxP group. Scale bar, 100μm.

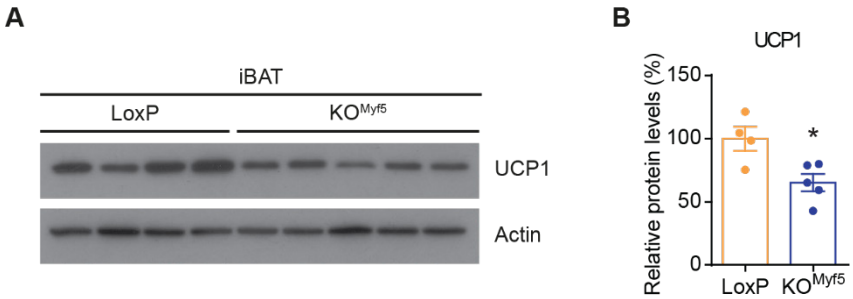

Figure 49. Decreased UCP1 protein levels in KO^{Myf5} mice. UCP1 (A) western blot and (B) quantification in interscapular brown adipose tissue (iBAT) from control (LoxP) and Myf5-specific TP53INP2 knockout male mice (KO^{Myf5}) at 6-months of age housed at 22°C and subjected to a chow diet (n=4-5).

4.3.11. High fat diet administration enhances body weight differences between control and Myf5-specific TP53INP2 knockout mice

As we had previously determined that TP53INP2 ablation in brown adipose tissue results in decreased thermogenic capacity, we speculated that the capacity to increase brown adipose tissue thermogenesis due to lipid overload would be also altered. With that idea, we subjected control and KO^{Myf5} male mice to a high fat diet for 16 weeks. We monitored body weight and body composition after 8 or 16 weeks of diet administration (at 3 and 6 months of total age respectively). Finally, adipose depots were examined at the end of the treatment (6 months of age).

HFD administration resulted in an increase in body weight and total fat mass in KO^{Myf5} mice already at 3 months of age (8 weeks of HFD), while lean mass remained the same between genotypes (Figure 50). This is in contrast with the unaltered body weight at the same age when receiving a normal CD (Figure 29). At older ages, this effect was even more pronounced, and knockout animals presented increased fat expansion due to HFD compared with control mice (Figure 50). Almost a 40% of the body weight of KO^{Myf5} was fat mass, which clearly demonstrates a severe phenotype.

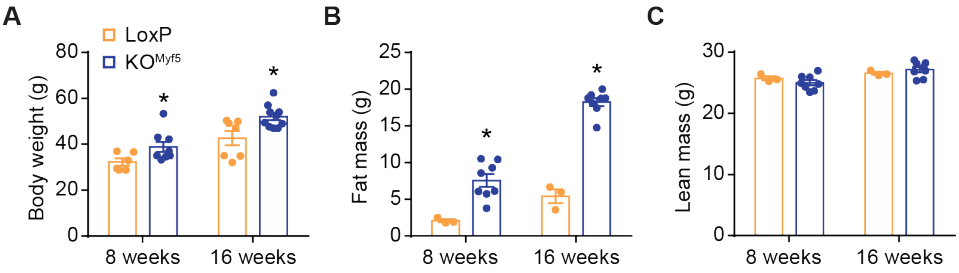

Figure 50. TP53INP2 ablated mice are susceptible to diet-induced obesity. Control (LoxP) and Myf5-specific TP53INP2 knockout male mice (KO^{Myf5}) housed at 22°C and subjected to a high fat diet for 8 or 16 weeks (n=6-10). (A) Body weight, (B) total fat mass and (C) total lean mass. Data are mean ± SEM. *p<0.05 vs. control LoxP group.

Following 16 weeks of HFD, knockout animals also showed enhanced weight of iBAT and ingWAT (Figure 51A and B). However, pgWAT showed the same weight

in both genotypes. (Figure 51C). While no differences in the weight of muscles were detected between LoxP and KO^{Myf5} mice, an increase in the weight of the liver was observed by the lack of TP53INP2 (Figure 51D and E). This clearly shows that TP53INP2 ablation results in an impairment of lipid handling, which results in adipose expansion and lipotoxicity in liver, probably because the adipose tissue has reached its maximal capacity.

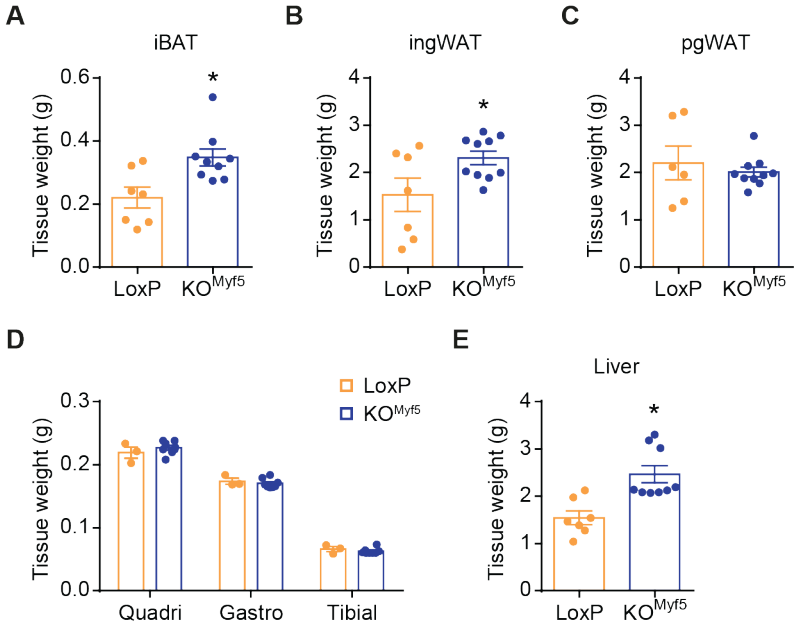

Figure 51. Loss of TP53INP2 enhances diet-induced fat accumulation. Control (LoxP) and Myf5-specific TP53INP2 knockout male mice (KO^{Myf5}) at 6-months of age housed at 22°C and subjected to a high fat diet for 16 weeks (n=7-10). Weight of (A) interscapular brown adipose tissue (iBAT), (B) inguinal white adipose tissue (ingWAT), (C) perigonadal white adipose tissue (pgWAT), (D) quadriceps (Quadri), gastrocnemius (Gastro) and tibialis (Tibial) muscles, and (E) liver. Data are mean ± SEM. *p<0.05 vs. control LoxP group.

4.4. Characterization of Myf5-specific TP53INP2 knockout mice under thermoneutral environment

Maintaining body temperature is an unavoidable necessity in homeotherms animals, as already mentioned above. Upon cold exposure, brown adipose tissue oxidative metabolism requires substantial blood supply to maintain nutrient and

oxygen levels, to remove waste products and to redistribute heat. To this end, angiogenesis within brown adipose tissue is induced by cold exposure (Xue et al., 2009). Metabolic rearrangements are also implemented in tissues other than brown adipose tissue. For instance, animals increase their heart weight and their cardiac frequency to provide more blood flow to either brown adipose tissue for non-shivering thermogenesis, or to skeletal muscle to perform shivering thermogenesis (Shechtman et al., 1990). In pathological conditions in which brown adipose thermogenesis is impaired, different adaptations are also activated to generate heat by other means and maintain body temperature. One clear example is the UCP1 KO mice, which as a result of its inability to perform non-shivering thermogenesis relies on shivering for heat generation and prevents it from becoming obese (Golozoubova et al., 2001). The acquisition of brown features in white adipocytes, a phenomena known as browning, can also be induced in conditions of non-shivering thermogenesis dysfunction. That is the case of the type 1A BMP receptor (*Bmpr1a*) Myf5-specific ablated mice, which present a paucity of brown adipose tissue. This in turns increases sympathetic output to white adipose tissue to promote the recruitment of beige adipocytes and to restore non-shivering thermogenesis to maintain body temperature (Schulz et al., 2013).

The thermoneutral zone is defined as the environment temperature in which an organism does not have to expend energy in maintaining body temperature. In mice, thermoneutrality is found between 28 and 33°C depending on mice strain, gender and age (Cannon and Nedergaard, 2011). Under standard conditions, mice are usually housed at a temperature between 20-22°C, which means that there is chronically active thermogenesis to defend body temperature. However, under thermoneutral temperature brown adipose tissue non-shivering thermogenesis is mainly inactive.

Having determined that TP53INP2 ablation in brown adipose tissue results in a defective brown adipose tissue thermogenic capacity, we considered of importance to characterize the phenotype under thermoneutral conditions and to study the

overall phenotype in the absence of cold stress.

4.4.1. Thermoneutrality abolishes body weight and body composition differences between control and Myf5-specific TP53INP2 knockout mice

In order to be sure that the cold stress induced by housing mice at 22°C was not influencing the global phenotype, we housed LoxP and KO^{Myf5} under thermoneutrality (30°C), starting after weaning. We phenotyped animals after 5 months of thermoneutral environment, being 6-months of age. For these experiments, male mice were used as they exhibited a stronger phenotype when housed below thermoneutrality.

By using this experimental setup, body weight differences between genotypes disappeared, as control and knockout mice presented the same body weight and lean mass (Figure 52A and C). In spite of that, KO^{Myf5} still presented a slight increase in total fat mass (Figure 52B).

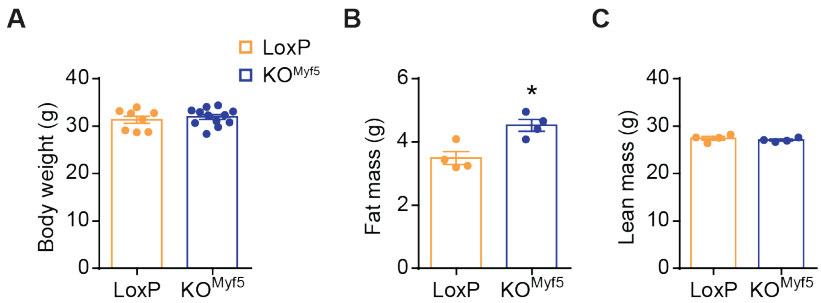

Figure 52. Thermoneutrality reduces body weight differences between control and Myf5-specific TP53INP2 knockout mice. Control (LoxP) and Myf5-specific TP53INP2 knockout male mice (KO^{Myf5}) at 6-months of age housed at 30°C and subjected to a chow diet (n=8-12). (A) Body weight, (B) total fat mass and (C) total lean mass. Data are mean ± SEM. *p<0.05 vs. control LoxP group.

Adipose tissue was examined and showed no differences on the weight of iBAT and pgWAT (Figure 53A and C). The ingWAT, however, presented a minor increased weight in knockout group (Figure 53B).

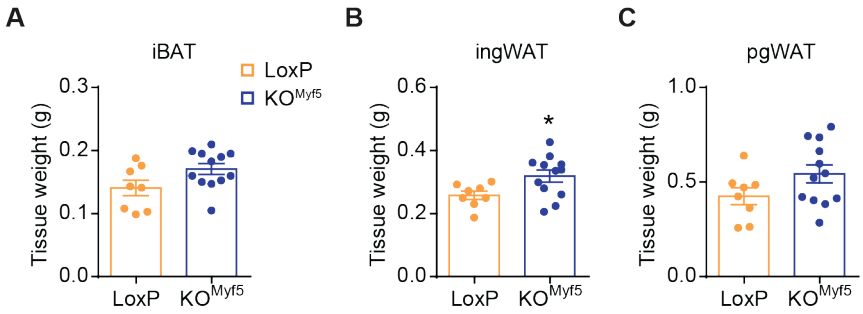

Figure 53. Similar adipose tissue depots in control and Myf5-specific TP53INP2 ablated mice under thermoneutrality. Control (LoxP) and Myf5-specific TP53INP2 knockout male mice (KO^{Myf5}) at 6-months of age housed at 30°C and subjected to a chow diet (n=8-12). Weight of (A) interscapular brown adipose tissue (iBAT), (B) inguinal white adipose tissue (ingWAT) and (C) perigonadal white adipose tissue (pgWAT). Data are mean ± SEM. *p<0.05 vs. control LoxP group.

Histology of iBAT was also analyzed under these conditions. Control mice presented the typical morphology associated to an inactive brown adipose tissue, with unilocular adipocytes (Figure 54A). Again, the morphology between genotypes was similar, and both groups presented the same LD number and size (Figure 54B and C).

If we compare these images with the ones obtained at 22°C (Figure 48), we can see that iBAT morphology in KO^{Myf5} mice is not modified by temperature, and that is the same as the one that control mice present at thermoneutrality.

Overall these results further support the idea of a decreased thermogenic activity by TP53INP2 ablation. In this sense, by decreasing thermogenic requirement, the differences between LoxP and KO^{Myf5} are lost. In fact, under thermoneutral conditions *Tp53inp2* expression is downregulated (Figure 16), which allow us to postulate that thermoneutrality phenocopies TP53INP2 deletion.

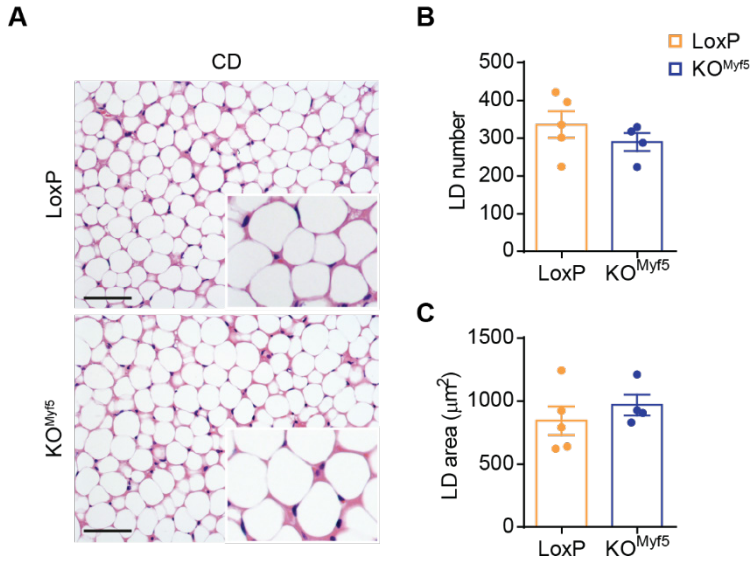

Figure 54. Inactive iBAT morphology under thermoneutral environment. Control (LoxP) and Myf5-specific TP53INP2 knockout male mice (KO^{Myf5}) at 6-months of age housed at 30°C and subjected to a chow diet (n=4-5). (A) Hematoxylin-eosin staining of interscapular brown adipose tissue sections, (B) lipid droplet (LD) number and LD average area measurements. Data are mean ± SEM. Scale bar, 100µm.

4.4.2. Thermoneutrality environment reduces gene expression differences between genotypes

Next, we also evaluated whether gene expression profile in iBAT was modulated by environment temperature. Thus, we measured the mRNA levels of the same genes that we have previously analyzed at standard housing conditions (Figure 34). Interestingly, the majority of the differences in gene expression between control and KO^{Myf5} mice were blunted when housed at 30°C (Figure 55). Nonetheless, a significant reduction in the expression of *Prdm16* and *Cox8b* was still detectable in knockout animals (Figure 55).

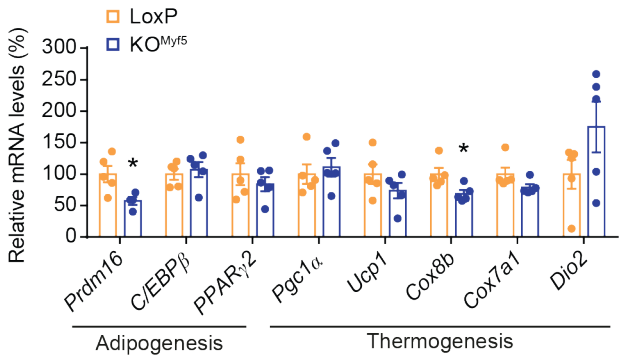

Figure 55. Gene expression differences between control and Myf5-specific TP53INP2 knockout mice are diminished by thermoneutrality. Expression of adipogenic and thermogenic genes in interscapular brown adipose tissue from control (LoxP) and Myf5-specific TP53INP2 knockout male mice (KO^{Myf5}) at 6-months of age housed at 30°C and subjected to a chow diet (n=5). Data are mean ± SEM. *p<0.05 vs. control LoxP group.

As a matter of fact, the expression of adipogenic and thermogenic genes is decreased by thermoneutral environment, as there is no need for heat generation (Goldgof et al., 2014; Xiao et al., 2015; Cui et al., 2016; Kalinovich et al., 2017). It is likely that, the loss of differences between genotypes is due to a decreased expression of these genes in control mice, which makes then more similar to the ones in which TP53INP2 has been depleted. The reduced expression of *Prdm16* and *Cox8b* under thermoneutral conditions may arise as a result of a direct regulation by TP53INP2, but further studies would be required to validate this hypothesis.

4.4.3. High fat diet administration reveals impaired diet-induced thermogenesis in Myf5-specific TP53INP2 ablated mice

Lipid overload can significantly induce brown adipose thermogenesis in order to prevent an excessive accumulation of fat (Cannon and Nedergaard, 2004; Divakaruni et al., 2012; Fedorenko et al., 2012; García-Ruiz et al., 2015). Thus, in a parallel experimental series, mice at 1 month of age were subjected to thermoneutrality and to HFD (60% of calories coming from fat). Finally, mice were studied at the age of 6 months.

Upon 20 weeks of HFD feeding at 30°C, body weight differences were restored between control and knockout mice (Figure 56A). We could determine that the body weight increase in KO^{Myf5} mice was a result of an increased total fat mass (Figure 56B), while no changes were detected in lean mass (Figure 56C).

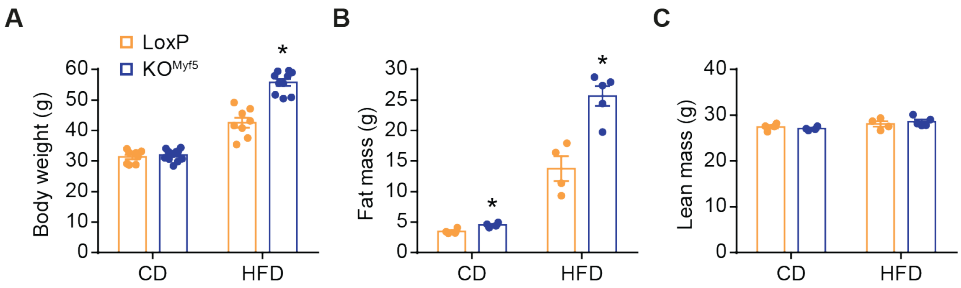

Figure 56. High fat diet administration restores body weight differences between control and Myf5-specific TP53INP2 knockout mice. Control (LoxP) and Myf5-specific TP53INP2 knockout male mice (KO^{Myf5}) at 6-months of age housed at 30°C and subjected to a chow diet (CD) or to a high fat diet (HFD) (n=8-12). (A) Body weight, (B) total fat mass and (C) total lean mass. Data are mean ± SEM. *p<0.05 vs. control LoxP group.

The challenge of a HFD also resulted in differences in the weight of adipose depots. iBAT and ingWAT were significantly expanded in knockout animals (Figure 57A and B), but no changes were found in pgWAT (Figure 57C).

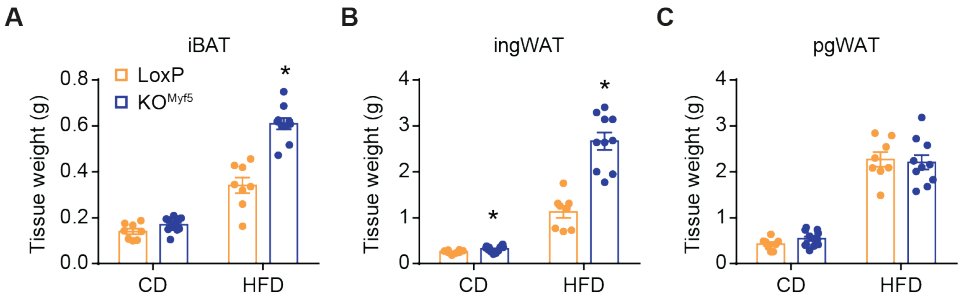

Figure 57. Diet-induced thermogenesis is reduced by TP53INP2 ablation. Control (LoxP) and Myf5-specific TP53INP2 knockout male mice (KO^{Myf5}) at 6-months of age housed at 30°C and subjected to a chow diet (CD) or to a high fat diet (HFD) (n=8-12). Weight of (A) interscapular brown adipose tissue (iBAT), (B) inguinal white adipose tissue (ingWAT) and (C) perigonadal white adipose tissue (pgWAT). Data are mean ± SEM. *p<0.05 vs. control LoxP group.

The fact that ingWAT was getting enlarged in KO^{Myf5} compared to control animals, and not the pgWAT, probably shows a defect in the browning capacity of the small subset of *Myf5* positive white adipocytes that are found in ingWAT. This would mean that in control animals, an active browning mediated by HFD could be preventing a dramatic accumulation of lipids in this depot, however, by the lack of TP53INP2 this adaptation may be blunted, but further examination would be required in this regard.

Increased thermogenic activity induced by HFD was evidenced in control animals by the appearance of multilocular adipocytes in iBAT (Figure 58A), which resulted in a reduction in the LD size (Figure 58C). However, no modifications by HFD administration were seen in KO^{Myf5} mice, as no multilocular adipocytes were detected in this group. Furthermore, LD number and LD size were maintained in knockout animals (Figure 58A, B and C).

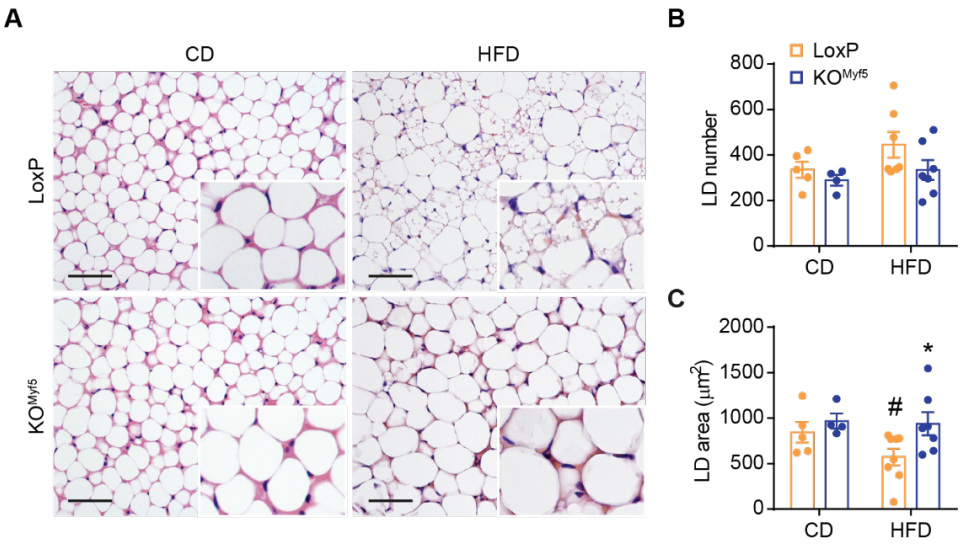

Figure 58. High fat diet induces multilocularity in control but not in knockout mice. Control (LoxP) and Myf5-specific TP53INP2 knockout male mice (KO^{Myf5}) at 6 months of age housed at 30°C and subjected to a chow diet (CD) or to a high fat diet (HFD) (n=4-7). (A) Hematoxylin-eosin staining of interscapular brown adipose tissue sections, (B) lipid droplet (LD) number and LD average area measurements. Data are mean ± SEM. *p<0.05 vs. control LoxP group. #p<0.1 vs. CD group. Scale bar, 100µm.

In general these data expose the protective role of diet-induced thermogenesis in preventing the excessive accumulation of lipids in whole organism. In addition, also reveals that TP53INP2 ablated mice present impaired diet-induced thermogenesis, a property exclusive of UCP1 expressing adipocytes.

4.4.4. Diet-induced thermogenesis is decreased upon TP53INP2 depletion

In order to directly determine whether diet-induced thermogenesis is impaired by TP53INP2 ablation, thermogenic capacity was evaluated (as described in section 4.3.6) in mice acclimated to thermoneutrality. As a high thermogenic activity condition we used mice that were subjected to a HFD, and the CD fed group (the same animals than the ones used in section 4.3.6) was used as a low thermogenic condition. Control animals that had received a HFD showed an increased thermogenic capacity compared with the CD group, coherent with an increased brown adipose tissue thermogenic activity due to lipid overload (Figure 59).

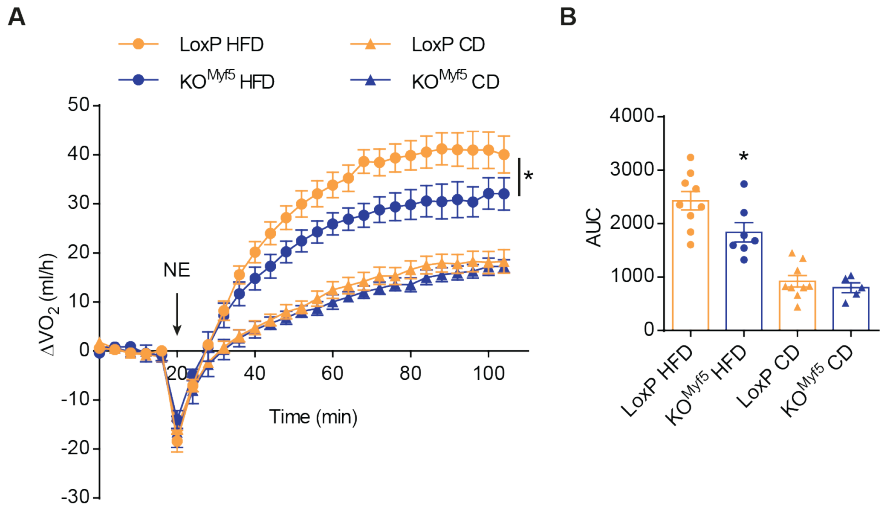

Figure 59. TP53INP2 enhances diet-induced thermogenesis. Control (LoxP) and Myf5-specific TP53INP2 knockout (KO^{Myf5}) male mice at 4-months of age housed at 30°C and subjected to a chow diet (CD) (n=5-9) or to a high fat diet (HFD) (n=7-9). (A) Oxygen consumption increase (ΔVO_2) upon norepinephrine injection (NE) and (B) area under the curve quantification in anesthetized mice at 30°C. Data are mean ± SEM. *p<0.05 vs. control LoxP group.

However, KO^{Myf5} animals fed with a HFD presented a decreased NE-induced ΔVO_2 when compared with control littermates (Figure 59). Again these results demonstrate that diet-induced thermogenesis is decreased by TP53INP2 depletion in brown adipose tissue.

4.4.5. Glucose intolerance and insulin resistance are modulated by TP53INP2 in brown adipose tissue

Housing temperature has been reported to affect several physiological parameters, like energy intake and adiposity. However, there is not a clear consensus on the effect of thermoneutrality in glucose metabolism. Some studies have reported that by lowering environmental temperature glucose tolerance is decreased due to a reduced insulin secretion (Uchida et al., 2010). In the same direction, some evidences point that thermoneutrality improves glucose tolerance in respect to 22°C housed mice (Xiao et al., 2015). On the contrary, other studies support that glucose metabolism is not altered at thermoneutrality when compared to standard housing temperatures (Cui et al., 2016; Tian et al., 2016; Small et al., 2018).

Aiming at evaluating whether brown adipose tissue dysfunction was contributing to the glucose intolerance and insulin resistance that we determined in standard conditions housed KO^{Myf5} mice, we performed GTT and ITT experiments under thermoneutrality. On one hand, in the group receiving a standard CD, there were no major differences in body weight nor in body composition, as both groups presented an inactive thermogenesis. On the other, HFD administration was able to induce non-shivering thermogenesis in control mice, but this was blunted in knockout animals. With these evidences, we speculated that if brown adipose tissue dysfunction induced by TP53INP2 ablation was contributing to glucose intolerance, inhibiting iBAT function to the same level (30°C with CD) will diminish differences between groups. Moreover, by feeding mice with a HFD we would expected a worsening in the phenotype.

In the CD fed group, KO^{Myf5} presented less glucose tolerance when compared to control mice, while insulin sensitivity was the same in both genotypes (Figure 60A, B and C). Feeding with a HFD impaired significantly glucose intolerance in both control and knockout animals (Figure 60B), however, the effect was more dramatic for the KO^{Myf5} mice, as most of them presented a blood glycaemia higher than 600mg/dl (the glucometer was getting saturated). Again, insulin resistance was the responsible for the glucose intolerance, which was also enhanced in KO^{Myf5} mice (Figure 60E and F).

At first sight, insulin sensitivity seems to be improved in the HFD feed group compared to the ones receiving CD. However, this apparent confusion was due to the requirement of using a higher insulin dose in the HFD group in order to be able to detect a decrease in blood glucose levels.

We could not directly assess whether thermoneutrality modifies glucose metabolism because mice used in these experiments were from different age than the ones used at 22°C. Our observations show that control mice housed at 30°C presented better glucose handling compared to standard conditions housed LoxPs in spite of being older at the time of the GTT, which will support the idea of increased insulin sensitivity by increasing environment temperature. Nonetheless, parallel groups with age-matched mice would be necessary to further prove this hypothesis.

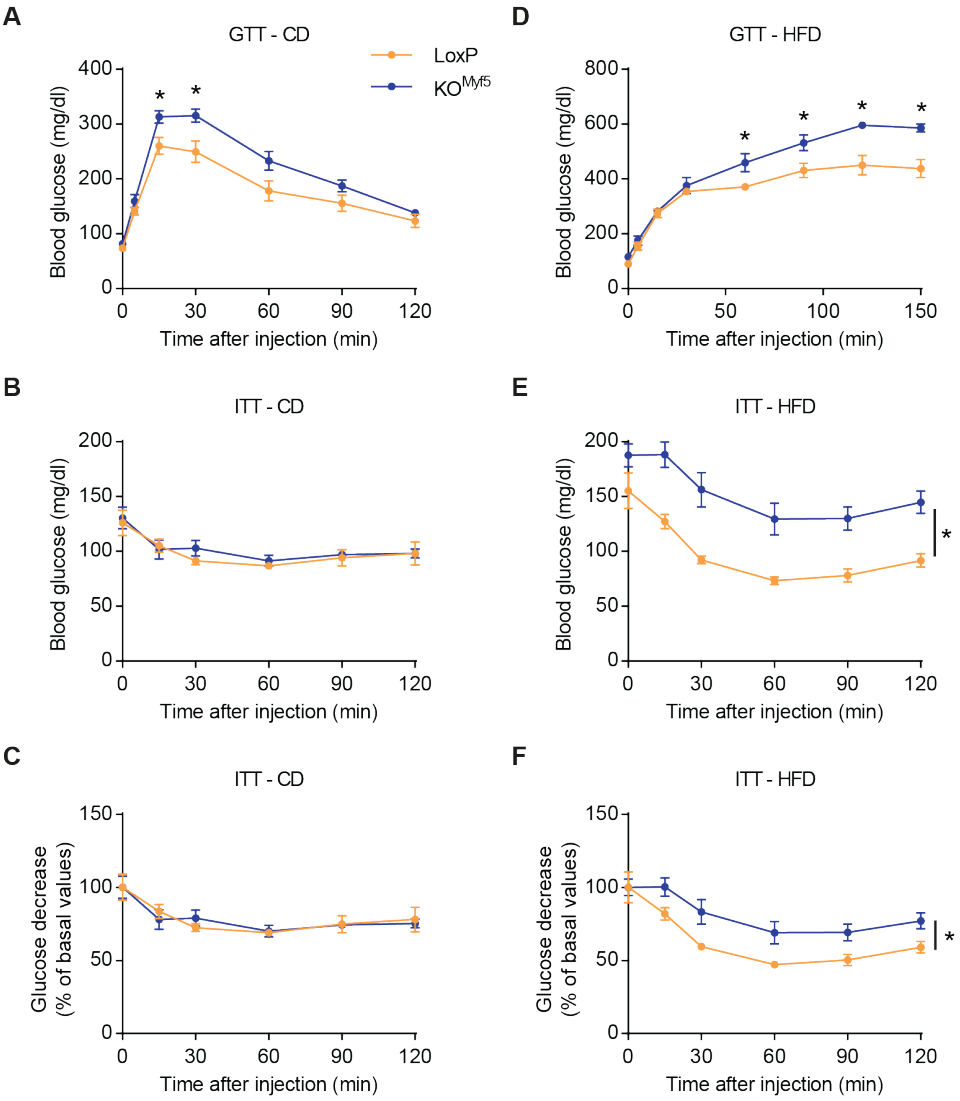

Figure 60. Glucose intolerance and insulin resistance are modulated by brown adipose tissue functionality. Control (LoxP) and Myf5-specific TP53INP2 knockout male mice (KO^{Myf5}) at 6-months of age housed at 30°C and subjected to a chow diet (CD) or to a high fat diet (HFD) (n=4). (A) And (D) blood glucose levels during glucose tolerance test (GTT 2g/kg). (B) Blood glucose levels and (C) glucose decrease (%) during insulin tolerance test (ITT 1U/kg). (E) Blood glucose levels and (F) glucose decrease (%) during insulin tolerance test (ITT 1.5U/kg). Data are mean ± SEM. *p<0.05 vs. control LoxP group.

4.5. Characterization of inducible global-TP53INP2 knockout mice

Previous studies in our laboratory have described the role of TP53INP2 in the biology of white adipose tissue using an inducible global-TP53INP2 knockout mice (KO^{Ubc}) (Romero et al., 2018). Tamoxifen inducible system was chosen to target TP53INP2 ablation in white adipose precursor cells.

The phenotyping of these mice showed increased body weight as a consequence of white adipose tissue hyperplasia already two months after the induction of TP53INP2 knockout by tamoxifen diet administration, which was characterized by an enhanced mass of the inguinal and perigonadal adipose depots (Romero et al., 2018). This was a result of an enhanced adipogenic capacity in white preadipocytes, demonstrated using different *in vitro* approaches. Moreover, older KO^{Ubc} mice presented augmented fat accumulation which lead to an enlargement of the body weight phenotype. In spite of all these alterations, glucose tolerance was not affected by global TP53INP2 ablation in any of the previous conditions evaluated (Romero et al., 2018).

Based on the observations that Myf5-specific TP53INP2 ablated mice show dysregulation of brown adipose tissue development and non-shivering thermogenesis, next we analyzed whether TP53INP2 deletion in brown adipose tissue from the KO^{Ubc} mouse was also contributing to the overall phenotype.

As explained above, brown adipose tissue develops embryonically and its full activity is reached after birth. In the KO^{Ubc} mice model, TP53INP2 is ablated in adult mice when brown adipocytes are already differentiated. In consequence, this experimental model allows the assessment of the possible role of TP53INP2 in the maintenance of the differentiation state in mature brown adipocytes, independently of its role in the regulation of the tissue development.

This section has been performed in collaboration with Dr. Montserrat Romero, who generated the KO^{Ubc} mice model and characterized the role of TP53INP2 in white adipose tissue biology.

4.5.1. Animal model validation

Global-TP53INP2 knockout mice were generated by crossing homozygous TP53INP2$^{loxP/loxP}$ mice (Sala et al., 2014), with Cre-recombinase expressing mice under the control of ubiquitin (Ubc) promoter fused to the estrogen receptor (ERT2) (Ruzankina et al., 2007). In order to induce TP53INP2 knockout, Cre negative (LoxP) and Cre positive (KO^{Ubc}) mice, as control and knockout respectively, were fed with a tamoxifen containing diet for one month to induce Cre-recombinase expression. Tamoxifen administration downregulated *Tp53inp2* in iBAT (Figure 61A) but also in all other tissues studied, including ingWAT and pgWAT (Romero et al., 2018). TP53INP2 protein levels were undetectable in iBAT samples from KO^{Ubc} mice (Figure 61B).

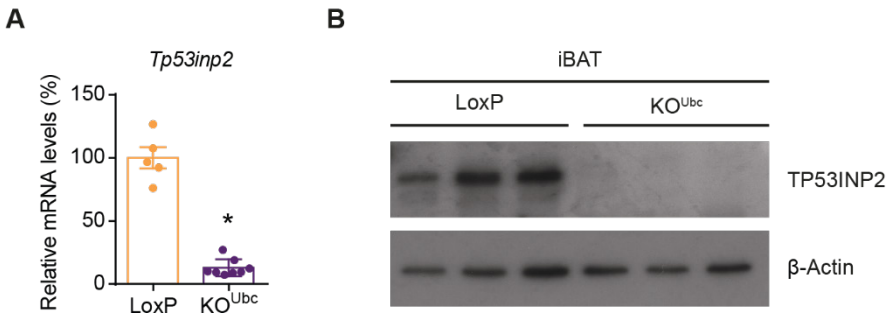

Figure 61. Global-TP53INP2 knockout mouse model validation. Control (LoxP) and global-TP53INP2 knockout mice (KO^{Ubc}) at 4-months of age housed at 22°C and subjected to a chow diet. (A) *Tp53inp2* relative mRNA levels in mouse interscapular brown adipose tissue (iBAT) (n=5-8), (B) TP53INP2 protein abundance in iBAT (n=3). Data are mean ± SEM. *p<0.05 vs. control LoxP group.

4.5.2. General phenotyping: body and adipose tissue weight of inducible global-TP53INP2 knockout mice

In order to evaluate the role of TP53INP2 in brown adipose tissue in the global-TP53INP2 depleted mice and to avoid possible alterations in mice development by the use of tamoxifen, two months old control and knockout mice were fed with a tamoxifen diet for one month. Then, animals were studied one month later in order to ensure tamoxifen wash out (4 months of total age). In addition to the already described body and white adipose tissue weight increase in both male and female knockout mice (Romero et al., 2018), iBAT depot was also significantly expanded in male KO^{Ubc} mice, while remained the same in female mice (Figure 62).

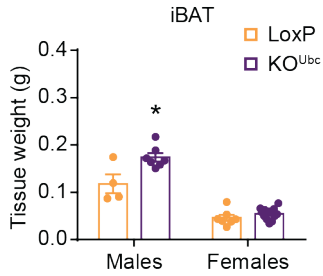

Figure 62. Global-TP53INP2 ablated mice present increased iBAT mass. Weight of interscapular brown adipose tissue (iBAT) in control (LoxP) and global-TP53INP2 knockout male or female mice (KO^{Ubc}) at 4-months of age housed at 22°C and subjected to a chow diet (n=4-12). Data are mean ± SEM. *p<0.05 vs. control LoxP group.

The overall phenotype was also analyzed at older ages, in this case, 6 months after the onset of tamoxifen diet (8 months of total age). As already described, at that point the body weight increase in KO^{Ubc} mice was enhanced, but also the two major adipose tissue depots ingWAT and pgWAT were also significantly expanded in both sexes (Romero et al., 2018). More importantly, iBAT weight was also higher in KO^{Ubc} mice compared with control littermates, both in male and in female mice (Figure 63).

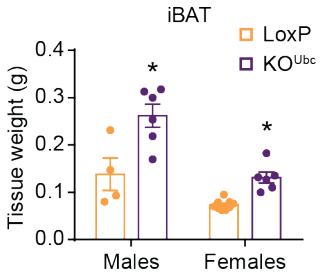

Figure 63. Increased adiposity in older KO^{Ubc} mice. Weight of interscapular brown adipose tissue (iBAT) in control (LoxP) and global-TP53INP2 knockout male or female mice (KO^{Ubc}) at 8-months of age housed at 22°C and subjected to a chow diet (n=4-9). Data are mean ± SEM. *p<0.05 vs. control LoxP group.

These results are in the same line than the ones observed in KO^{My5} mice model. This indicates that TP53INP2 ablation both in brown precursor cells and in mature adipocytes dysregulates brown adipose tissue metabolism and results in an increased tissue mass.

4.5.3. Gene expression profile of brown adipose tissue from global-TP53INP2 ablated mice is comparable to the one observed in Myf5-specific TP53INP2 knockout mice

Following the idea of an impaired brown adipose tissue metabolism in KO^{Ubc} mice, gene expression profile was evaluated. To do so, microarray analysis was performed in iBAT samples from LoxP and knockout mice (at 4 months of total age). TP53INP2 ablation in adult mice resulted in mild a gene expression modulation, with 291 genes being upregulated and 250 downregulated (Figure 64A). Transcriptomic data from both animal models (KO^{Ubc} and KO^{Myf5}) was compared and showed a similar trend, although KO^{Ubc} showed decreased number of genes with a differential expression between genotypes when compared with KO^{Myf5} (Figure 64A). In spite of that, gene expression showed a positive correlation (r=0.311) between both transcriptomic studies, demonstrating that the genes that were being modulated in both animal models were doing so in the same direction

(Figure 64B).

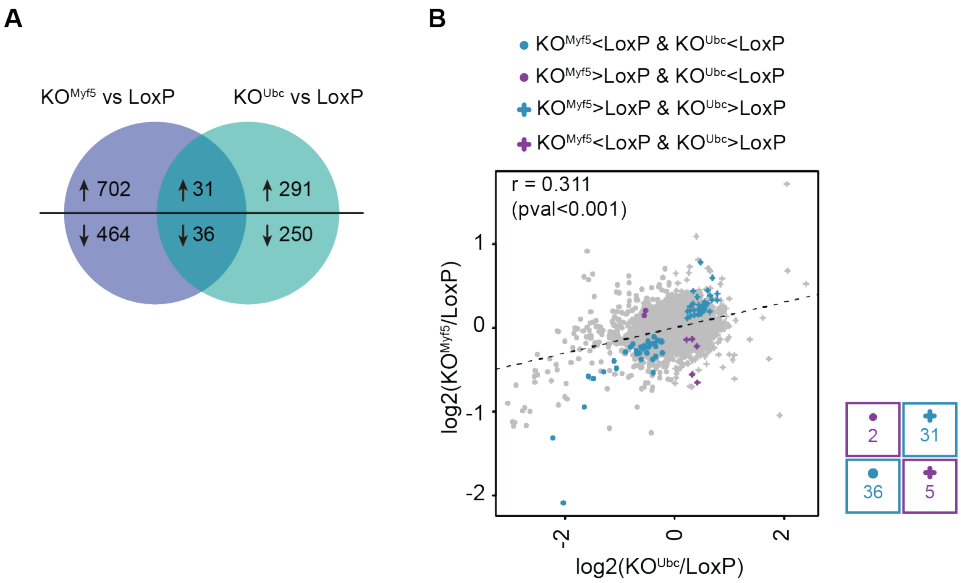

Figure 64. TP53INP2 ablation similarly modulates gene expression in KO^{Myf5} and KO^{Ubc} mice. Transcriptomic analysis performed in interscapular brown adipose tissue from control (LoxP) (n=4) or global-TP53INP2 knockout (KO^{Myf5}) mice (n=4) and compared to transcriptomic analysis from LoxP (n=4) and KO^{Myf5} mice housed at 22°C. (A) Number of genes upregulated or downregulated and (B) fold change correlation plot (KO^{Myf5}/LoxP and KO^{Ubc}/LoxP) between both transcriptomic studies.

Gene set enrichment analysis (KEGG) also revealed that among the top ten downregulated pathways with a higher significance, 4 of them were common with the ones observed in KO^{Myf5} mice. Fatty acid metabolism, peroxisome and oxidative phosphorylation gene sets were downregulated in both KO^{Myf5} and KO^{Ubc} brown adipose tissue samples (Figure 65).

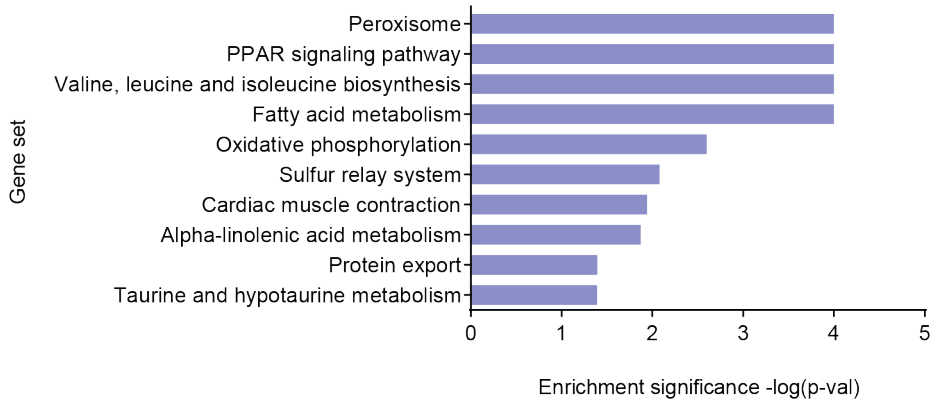

Figure 65. Gene sets downregulated in iBAT from KO^{Ubc} mice. Transcriptomic analysis and Gene Set Enrichment Analysis (GSEA) performed in interscapular brown adipose tissue from control (LoxP) (n=4) or global-TP53INP2 knockout (KO^{Ubc}) mice (n=4). Enrichment significance (-log(p-value)) of downregulated gene sets (KEGG).

Adipogenesis signaling pathway (Broad Hallmarks) and brown adipose tissue specific gene set (Alvarez-Dominguez et al., 2015) also followed the same trend, and were found downregulated in KO^{Ubc} mice (Figure 66). This supports a role of TP53INP2 in the maintenance of the differentiation state in brown adipocytes.

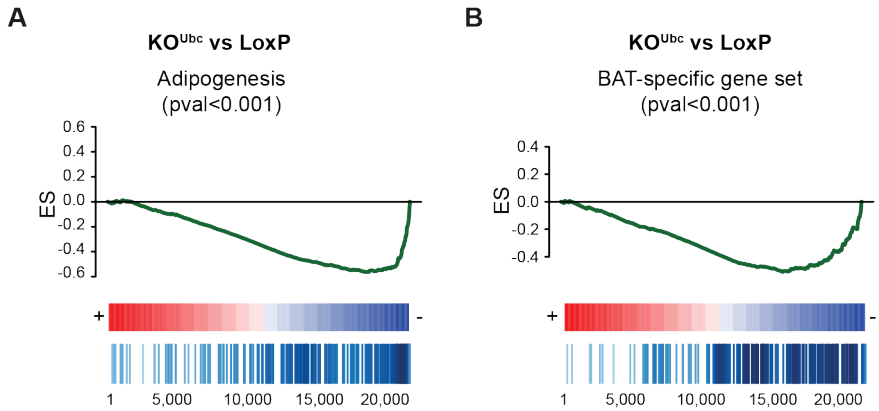

Figure 66. Enrichment plots of adipogenesis and brown adipose tissue specific genes. Transcriptomic analysis and Gene Set Enrichment Analysis (GSEA) performed in interscapular brown adipose tissue from control (LoxP) (n=4) or global-TP53INP2 knockout (KO^{Ubc}) mice (n=4). Enrichment plots of adipogenesis (Broad Hallmarks) and custom gene set for brown adipose tissue (BAT)-specific genes.

The expression of genes involved in adipogenesis as well as in thermogenesis was measured in brown adipose tissue samples. Our results confirmed the reduction of the adipogenic genes *PPARγ2* and *C/EBPβ* in KO^{Ubc} male mice compared to control littermates, while *Prdm16* showed a trend to be decreased but did not reach statistically significance (Figure 67). Furthermore, genes involved in thermogenesis were found downregulated by TP53INP2 ablation in adult mice, including *Ucp1*, *Pgc1α*, *Cox8b*, *Dio2* and *Elovl3* (Figure 67), all of them being also decreased in iBAT from KO^{Myf5} mice (Figure 34).

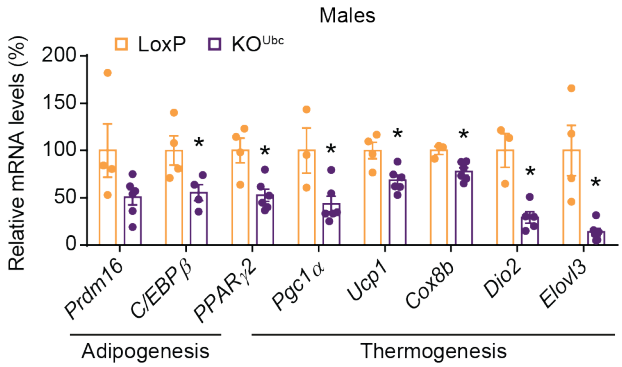

Figure 67. Downregulated expression of adipogenic and thermogenic genes by T53INP2 ablation. Expression of adipogenic and thermogenic genes in interscapular brown adipose tissue from control (LoxP) and global-TP53INP2 knockout male mice (KO^{Ubc}) at 4-months of age housed at 22°C and subjected to a chow diet (n=4-6). Data are mean ± SEM. *p<0.05 vs. control LoxP group.

When mRNA levels of the same genes were measured in female mice, an identical profile was observed (Figure 68A). This is in contrast with female KO^{Myf5} which showed milder gene expression modulation by TP53INP2 ablation (Figure 35). However, mRNA levels of *Pref1* were unchanged between groups in female mice (Figure 68B), which is coherent with the fact that TP53INP2 expression is not altered during brown adipose tissue development in KO^{Ubc} mice model.

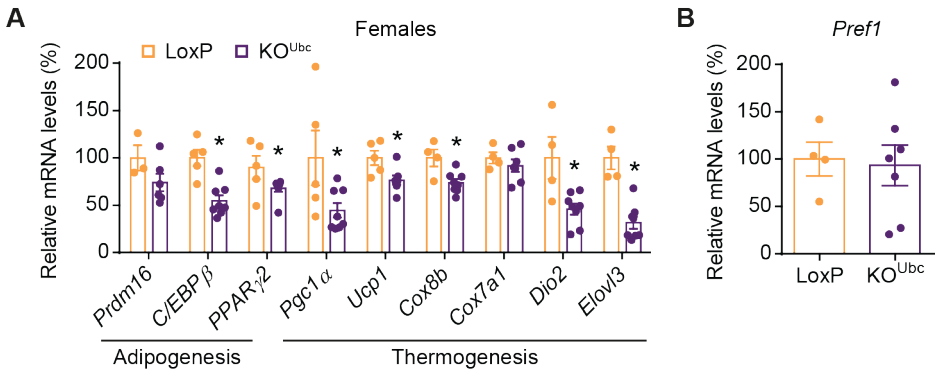

Figure 68. Global-TP53INP2 ablated mice present downregulated expression of adipogenic and thermogenic genes. Control (LoxP) and global-TP53INP2 knockout female mice (KO^{Ubc}) at 4-months of age housed at 22°C and subjected to a chow diet (n=4-7). Expression of (A) adipogenic and thermogenic genes, and (B) preadipocyte factor 1 (*Pref1*) in interscapular brown adipose tissue. Data are mean ± SEM. *p<0.05 vs. control LoxP group.

Thus, TP53INP2 ablation in brown preadipocytes or in mature brown adipose tissue seems to generate a similar pattern of metabolic changes. Based on these observations, we postulate that TP53INP2 is not only involved in brown adipogenesis, but also in the maintenance of brown adipocyte features.

4.5.4. TP53INP2 ablation in adult mice impairs the morphological characteristics of brown adipose tissue metabolism

Having determined that TP53INP2 ablation in mature brown adipose tissue reduces the expression of brown adipogenic and thermogenic genes, we analyzed whether the tissue functionality was compromised. To this end, iBAT sections from LoxP and KO^{Ubc} mice were stained with hematoxilyn-eosin, and LD number and size were measured both in male and female mice at 4-months of age. Under these conditions, an inactive morphology was specially found in male KO^{Ubc} mice (Figure 69A), which was characterized by reduced LD number and increased LD area (Figure 69B and C). No statistically significant differences were detected in control and KO^{Ubc} female mice, although a slight tendency of increased LD size

in knockout animals could be observed. These results are consistent with the fact that iBAT weight was increased only in male mice, due to increased lipid content.

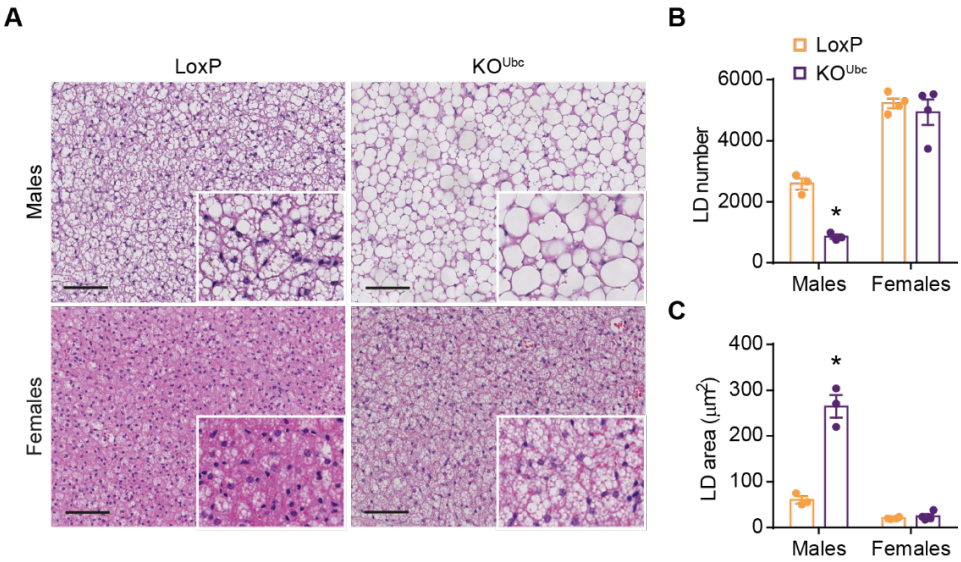

Figure 69. Global-TP53INP2 knockout mice have altered iBAT morphology. Control (LoxP) and global-TP53INP2 knockout male or female mice (KO^{Ubc}) at 4-months of age housed at 22°C and subjected to a chow diet (n=3-4). (A) Hematoxylin-eosin staining of interscapular brown adipose tissue sections, (B) lipid droplet (LD) number and LD average area measurements. Data are mean ± SEM. *p<0.05 vs. control LoxP group. Scale bar, 100μm.

To further confirm these observations, iBAT samples from older mice were also evaluated. Under these conditions, 8-months old KO^{Ubc} male and female mice presented enhanced lipid accumulation (Figure 70A), which caused a dramatic loss of multilocularity (Figure 70B and C).

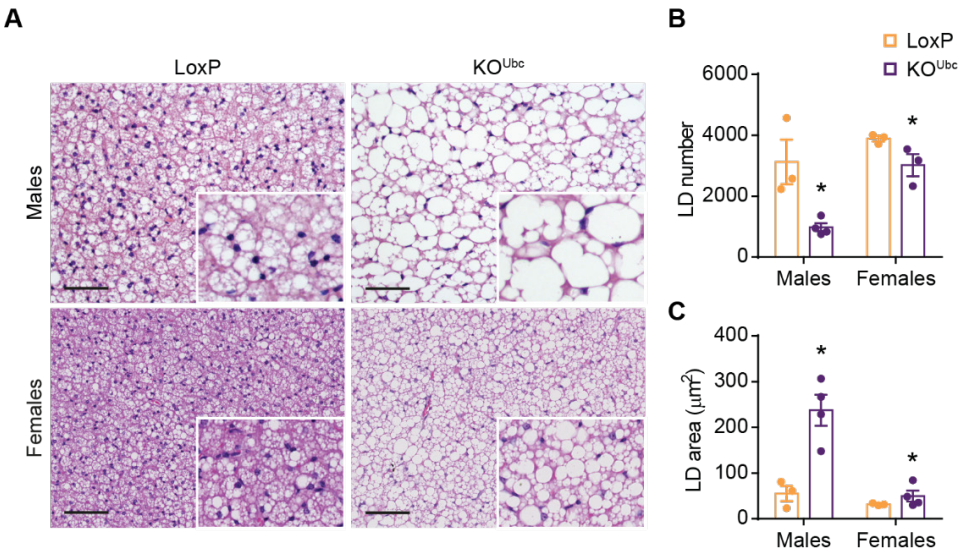

Figure 70. Older TP53INP2 knockout mice have a dramatic loss of iBAT multilocularity. Control (LoxP) and global-TP53INP2 knockout male or female mice (KO^{Ubc}) at 8-months of age housed at 22°C and subjected to a chow diet (n=3-4). (A) Hematoxylin-eosin staining of interscapular brown adipose tissue sections, (B) lipid droplet (LD) number and LD average area measurements. Data are mean ± SEM. *p<0.05 vs. control LoxP group. Scale bar, 100μm.

4.5.5. Global-TP53INP2 ablated mice show a decreased energy expenditure

Decreased energy expenditure was found in KO^{Myf5} which was a result of a decreased non-shivering thermogenic capacity, and gene expression and histological examination suggested that global-TP53INP2 ablation also resulted in brown adipose tissue dysfunction. That is why we next determined whether the lack of TP53INP2 in adult mice also impacted energy balance. Indirect calorimetry was performed in LoxP and KO^{Ubc} mice at 4-months of age. Given the fact that both sexes showed a similar phenotype, energy expenditure was assessed in male and in female mice. VO_2, VCO_2 and EE were corrected by an adjusted body weight of 27.0833g in the case of male mice or 24.8342g for female mice (determined using ANCOVA). Our results confirmed an impaired energy balance by the global-TP53INP2 depletion in both sexes. Male and female KO^{Ubc} mice presented

decreased VO_2, VCO_2 and EE when compared to control littermates (Figure 71A, D and G). Moreover, the representation of these parameters as a function of body weight confirmed that the relation between them (body weight to VO_2, VCO_2 or EE) was statistically different between genotypes (Figure 71B, C, E, F, H and I), which demonstrated that the differences between groups were not a consequence of increased body weight in the knockout group.

Locomotor activity or the respiratory exchange ratio (RER) were again unaltered by TP53INP2 deletion (Figure 72A, B and C). However, both female and male knockout mice presented a decreased glucose oxidation, while lipid oxidation remained the same in the two groups (Figure 72D and E).

Overall the metabolic data further supports the concept of a decreased metabolic rate due to TP53INP2 ablation as the responsible for the decreased energy expenditure profile.

Food and water intake and urine and faeces excretion were also measured in LoxP and KO^{Ubc} male mice, and showed no differences between genotypes (Figure 73).

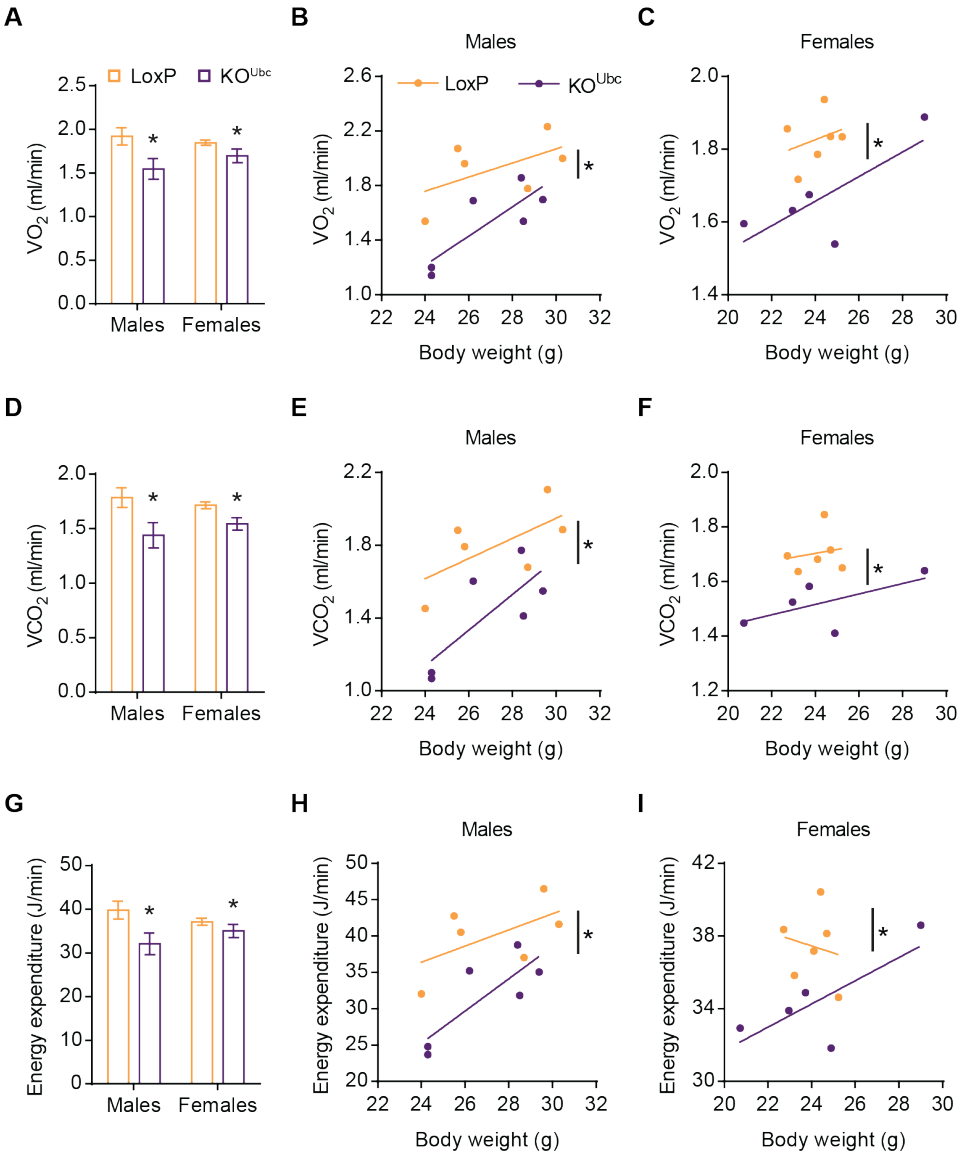

Figure 71. Decreased oxygen consumption, carbon dioxide production and energy expenditure in global-TP53INP2 knockout mice. Control (LoxP) and global-TP53INP2 knockout (KO^{Ubc}) male or female mice at 4-months of age housed at 22°C and subjected to a chow diet (n=5-6). (A), (B) and (C) oxygen consumption (VO_2); (D), (E) and (F) carbon dioxide production (VCO_2); (G), (H) and (I) energy expenditure (EE). Adjusted means (based on a normalized mouse weight of 27.0833g (male) or 24.8342g (female) determined using ANCOVA) or correlation with body weight. Data are mean ± SEM. *p<0.05 vs. control LoxP group.

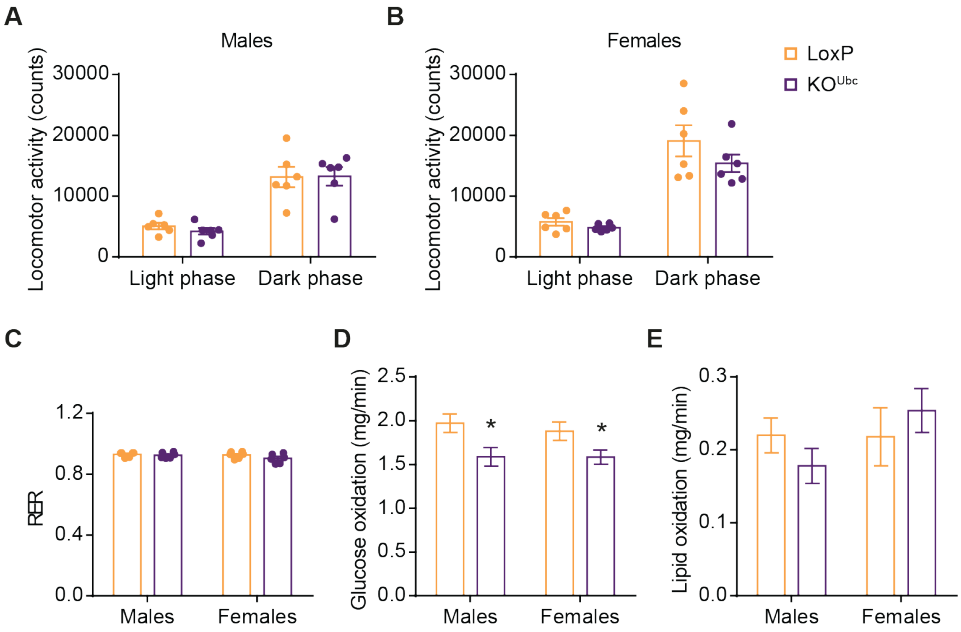

Figure 72. Metabolic parameters in control and global-TP53INP2 knockout mice. Control (LoxP) and global-TP53INP2 knockout (KO^{Ubc}) male or female mice at 4-months of age housed at 22°C and subjected to a chow diet (n=5-6). (A) And (B) locomotor activity during light (inactive) and dark (active) phase. (C) Respiratory exchange ratio (RER). (D) Glucose and (E) lipid oxidation adjusted means (based on a normalized mouse weight of 27.0833g (male) or 24.8342g (female) determined using ANCOVA). Data are mean ± SEM. *p<0.05 vs. control LoxP group.

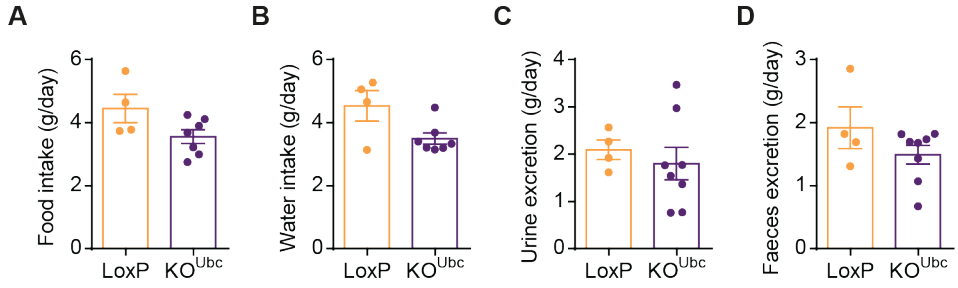

Figure 73. Food or water intake and urine or faeces excretion are not altered in global-TP53INP2 knockout mice. Control (LoxP) and global-TP53INP2 knockout (KO^{Ubc}) male mice at 4-months of age housed at 22°C and subjected to a chow diet (n=4-8). Daily (A) food and (B) water intake. Daily (C) urine and (D) faeces excretion. Data are mean ± SEM.

4.5.6. TP53INP2 is required for the maintenance of the differentiation state of brown adipocytes

In order to validate the role of TP53INP2 in mature brown adipocytes, and to further rule out the influence of non-cell-autonomous effects on the phenotype observed in brown adipose tissue, we used *in vitro* differentiated brown adipocytes. Brown preadipocytes from the TP53INP2$^{loxP/loxP}$ Cre-Ubc-ERT2 mice were isolated, immortalized and differentiated as previously described (section 4.2.1). At day 7 of differentiation we considered that cells were mature adipocytes, based on the expression of UCP1. Then, adipocytes were treated with DMSO as a vehicle or with 4-hydroxy-tamoxifen (TAM) for 3 days to activate Cre-expression and induce TP53INP2 repression. TAM treatment reduced to 60% *Tp53inp2* mRNA levels, but also significantly reduced the expression of *Prdm16*, *Ucp1* and *Pgc1α*, which are brown adipogenic and thermogenic genes, compared to vehicle treated adipocytes (Figure 74). Under these conditions, the expression of *Cox7a1*, *Cox8b* or *PPARγ2* was unchanged (Figure 74).

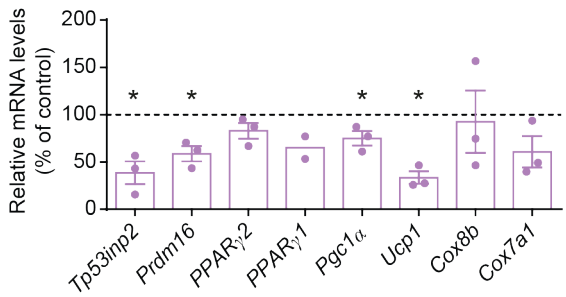

Figure 74. TP53INP2 loss-of-function in brown adipocytes decreases the expression of adipogenic and thermogenic genes. Expression of genes in TP53INP2$^{loxP/loxP}$ Cre-Ubc-ERT2 brown preadipocytes differentiated to day 7 and treated with 4-hydroxy-tamoxifen (TAM) **1μM** or with vehicle (DMSO) for 3 days (n=2-3). Values of TAM treated cells are represented relative to DMSO treated group. Data are mean ± SEM. *p<0.05 vs. control DMSO group.

Brown preadipocytes without Cre-recombinase expression were used in the same experimental conditions as a negative control for the TAM treatment. In these cells, no differences in *Tp53inp2* gene expression were found (Figure 75). Moreover,

the absence of changes in the expression of adipogenic and thermogenic genes validated that gene modulation in Cre-expressing adipocytes was specific to TP53INP2 downregulation (Figure 75).

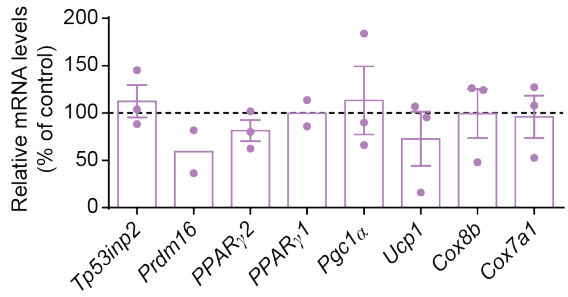

Figure 75. Downregulation of thermogenic and adipogenic genes is specific to TP53INP2 loss-of-function. Expression of genes in TP53INP2$^{loxP/loxP}$ brown preadipocytes differentiated to day 7 and treated with 4-hydroxy-tamoxifen (TAM) 1μM or with vehicle (DMSO) for 3 days (n=2-3). Values of TAM treated cells are represented relative to DMSO treated group. Data are mean ± SEM.

Altogether, these results indicate that TP53INP2, in addition to its role in stimulating brown adipogenesis, it also shows a key role in the maintenance of the differentiation state in mature brown adipocytes under *in vitro* and *in vivo* conditions.

4.6. Analysis of the mechanisms by which TP53INP2 regulates brown adipose tissue metabolism

The importance of TP53INP2 in the regulation of brown adipogenesis and in the maintenance of the differentiation state of brown adipocytes was examined in the previous chapters. In the present section the aim was to explore the molecular mechanisms by which TP53INP2 participates in these processes.

4.6.1. PPAR signaling pathway is downregulated by TP53INP2 ablation

To identify the mechanism by which TP53INP2 regulates brown adipogenesis, we turned into the gene expression profiling performed in TP53INP2-deficient brown adipose tissue. Gene set enrichment analysis revealed a significant downregulation of PPAR signaling pathway in brown adipose tissue upon loss of TP53INP2, both in KO^{Myf5} and in KO^{Ubc} mice (Figure 76).

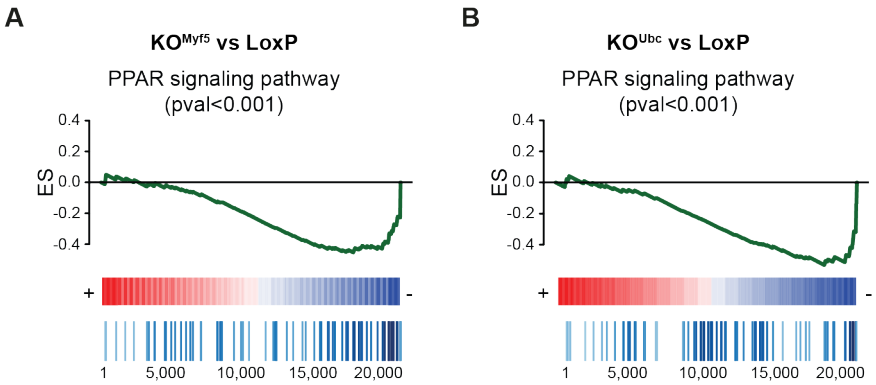

Figure 76. PPAR signaling pathway is altered by the absence of TP53INP2. Transcriptomic analysis and Gene Set Enrichment Analysis (GSEA) performed in interscapular brown adipose tissue from control (LoxP) (n=4), Myf5-specific TP53INP2 knockout (KO^{Myf5}) mice (n=4) or global-TP53INP2 knockout (KO^{Ubc}) mice. Enrichment plots of PPAR signaling pathway (KEEG) in (A) KO^{Myf5} and in (B) KO^{Ubc} mice.

This was of interest since it has been documented that TP53INP2 overexpression has the capacity of co-regulating the transcriptional activity of different nuclear receptors that includes peroxisome proliferator-activated receptor (Sancho et al., 2012), and in addition, PPARγ is an essential protein for brown adipogenesis and a key regulator of adipocyte metabolism (Barak et al., 1999; Koutnikova et al., 2003; Nedergaard et al., 2005).

4.6.2. Decreased PPRE activity in TP53INP2 depleted brown preadipocytes

Our laboratory has previously described that TP53INP2 transfection in HeLa or HEK-293T cells together with PPARγ was able to induce the transcriptional activity of the PPAR response element (PPRE), which was enhanced by treatment with PPARγ specific ligand rosiglitazone. Moreover, TP53INP2 mutations in its N-terminal part, including mutations of the NES motif, showed reduced ability to co-activate nuclear receptors (Sancho et al., 2012), showing that the N-terminal part of TP53INP2 is required for this action.

Thus, we next focused on the potential role of TP53INP2 to modulate PPAR transcriptional activity in mouse brown preadipocyte cell context. Transcriptional activity was measured by transfecting a construct containing the PPRE fused to the luciferase reporter gene in the absence or in the presence of the PPARγ-specific ligand. Control preadipocytes showed a marked stimulation of PPRE activity in the presence of rosiglitazone (Figure 77). In contrast, TP53INP2 deficient cells (KO) showed a reduced response upon rosiglitazone treatment, suggesting the existence of a disruption in PPAR transcriptional activity (Figure 77).

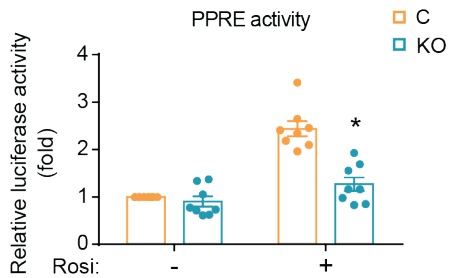

Figure 77. TP53INP2 ablated preadipocytes present decreased PPRE activity. Transcriptional activity of PPRE in control (C) or TP53INP2 knockout (KO) brown preadipocytes treated with vehicle (-) or with rosiglitazone (+) 10μM for 24 hours (n=8). Data are mean ± SEM. *p<0.05 vs. C.

However, *PPARγ1* and *PPARγ2* mRNA levels were found downregulated by TP53INP2 loss-of function compared with control cells (Figure 78A). Moreover,

protein levels of PPARγ1, which is the predominant isoform in preadipocytes, also showed decreased abundance in KO cells (Figure 78B). This could be explained by the fact that PPARγ activity can directly regulate its own transcription.

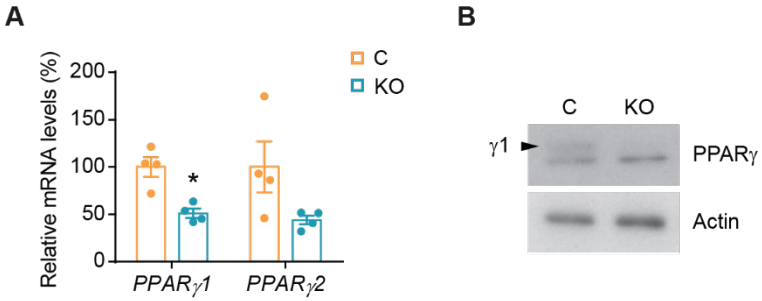

Figure 78. Downregulation of PPARγ expression by TP53INP2 deletion. Control (C) or TP53INP2 knockout (KO) brown preadipocytes. (A) Relative mRNA levels of PPARγ1 and PPARγ2 (n=4). (B) PPARγ1 protein abundance (n=3). Data are mean ± SEM. *p<0.05 vs. C.

In order to ensure that PPARγ protein was not a limiting factor for the transcriptional action, control or TP53INP2 ablated cells were co-transfected with PPARγ and the PPRE reporter construct. Again, the lack of TP53INP2 reduced PPARγ transcriptional activity, both in the presence or in the absence of the ligand (Figure 79).

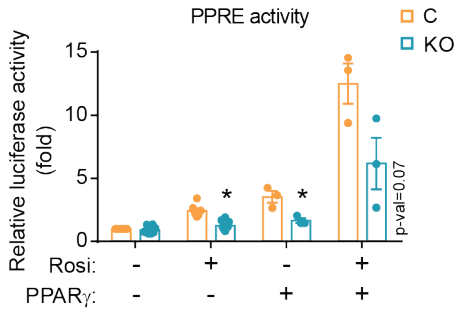

Figure 79. Decreased PPRE transcriptional activity is independent on PPARγ protein levels. Transcriptional activity of PPRE in control (C) or TP53INP2 knockout (KO) brown preadipocytes transfected with empty vector (-) or with PPARγ plasmid, and treated with vehicle (-) or with rosiglitazone (+) 10μM for 24 hours (n=3). Data are mean ± SEM. *p<0.05 vs. C.

Additionally, to further validate these results, a cell line stably-overexpressing PPARγ was generated through a retroviral infection. TP53INP2 ablation in this cellular context was induced using the same methodology described above (section 4.2.1). Cellular models were validated according to *PPARγ* and *Tp53inp2* expression (Figure 80A and B). PPARγ was significantly overexpressed both control and TP53INP2 KO preadipocytes, and PPARγ did not alter *Tp53inp2* mRNA levels.

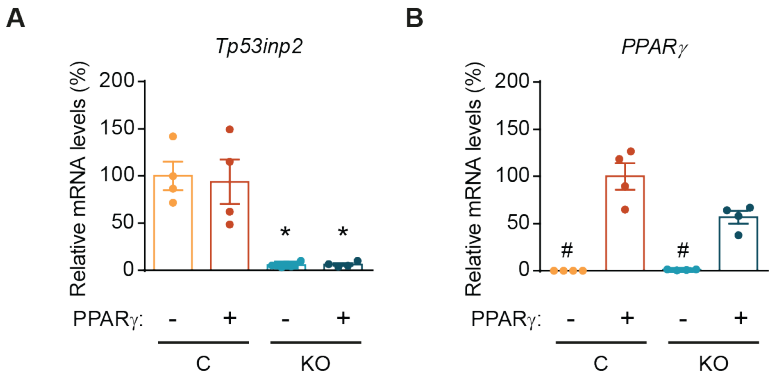

Figure 80. Validation of PPARγ stably overexpressing preadipocytes with or without TP53INP2. PPARγ stably overexpressing preadipocytes (+) or empty vector expressing cells (-) with endogenous (C) or TP53INP2 knockout (KO) levels. Relative mRNA levels of (A) *Tp53inp2* and (B) *PPARγ*. Data are mean ± SEM. *p<0.05 vs. C. #p<0.05 vs. PPARγ overexpressing cells group.

Thus, PPAR transcriptional activity was assessed in TP53INP2 control or deficient preadipocytes stably-expressing PPARγ. The transfection of PPRE reporter construct in PPARγ overexpressing cells in the presence of rosiglitazone showed increased transcriptional activity when compared with non-overexpressing cells. However this induction was completely blunted in TP53INP2 knockout cells (Figure 81).

Taking together, all these results document that TP53INP2 loss-of-function in preadipocytes results in a defective PPARγ activity, which is independent of the PPARγ protein levels.

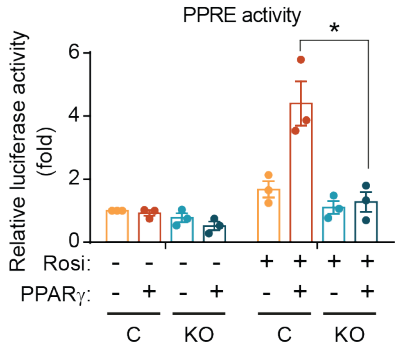

Figure 81. TP53INP2 is required for PPARγ transcriptional activity. Transcriptional activity of PPRE in PPARγ stably overexpressing preadipocytes (+) or empty vector expressing cells (-) with endogenous (C) or TP53INP2 knockout (KO) levels. Cells were treated with vehicle (-) or with rosiglitazone (+) 10μM for 24 hours (n=3). Data are mean ± SEM. *p<0.05 vs. C.

4.6.3. PPARγ overexpression does not recover adipogenic capacity in TP53INP2 deficient preadipocytes

Given the fact that TP53INP2 ablated brown adipose tissue and brown preadipocytes show a reduced PPAR transcriptional activity, our next aim was to determine whether TP53INP2 was involved in the regulation of adipogenesis through the modulation of this signaling pathway. Overexpression of PPARγ enhanced the adipogenic capacity of brown preadipocytes when compared with non-overexpressing cells as described (Zhang et al., 2004). This was evidenced by increased *Pgc1α*, *Ucp1*, *Cox7a1* and *Cox8b* mRNA levels at day 9 of differentiation (Figure 82), while *Prdm16* or *PPARγ1* remained unaffected.

Following this idea, PPARγ overexpressing cells with or without endogenous TP53INP2 were induced to differentiate. Surprisingly, PPARγ overexpression in the absence of TP53INP2 was characterized by reduced capacity to undergo differentiation, analyzed by the expression of adipogenic and thermogenic genes at the end of the differentiation process (Figure 83).

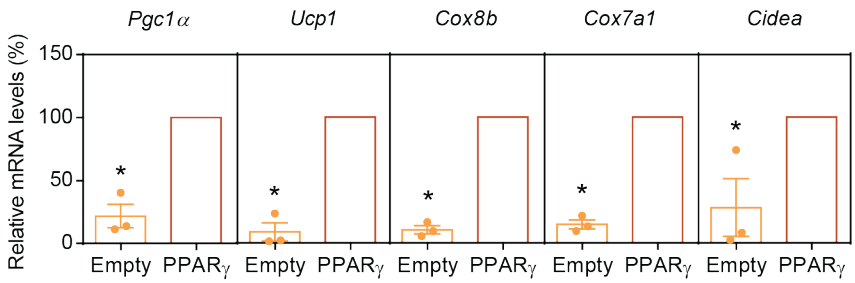

Figure 82. PPARγ overexpression increases adipogenic capacity. Expression of genes in PPARγ stably overexpressing brown preadipocytes or empty vector expressing cells differentiated to day 9 (n=3). Data are mean ± SEM. *p<0.05 vs. PPARγ overexpressing cells group.

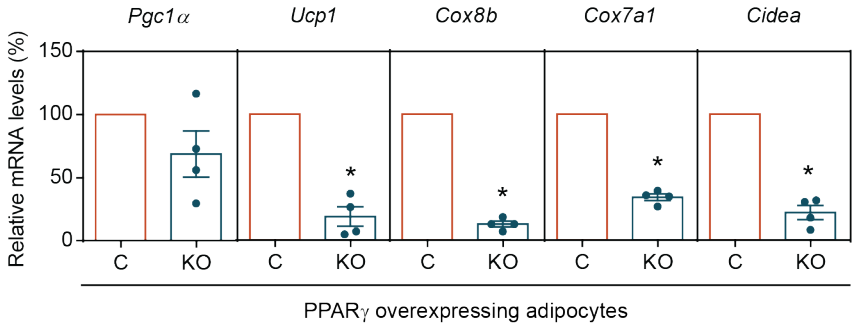

Figure 83. PPARγ overexpression in TP53INP2 ablated preadipocytes is not able to recover differentiation capacity. Expression of genes in PPARγ stably overexpressing brown preadipocytes with endogenous (C) or TP53INP2 knockout (KO) levels (n=4).Data are mean ± SEM. *p<0.05 vs. C cells group.

Again, these results manifest that the role of TP53INP2 in the regulation of brown adipogenesis is not dependent on PPARγ protein levels.

4.6.4. Chronic activation of PPARγ rescues the differentiation defect in TP53INP2 deficient cells

Chronic activation of PPARγ has been reported to enhance brown adipogenesis by triggering mitochondrial biogenesis and UCP1 expression (Petrovic et al., 2008). Based on this, we chronically incubated control and TP53INP2 KO preadipocytes with rosiglitazone during differentiation. In the absence of rosiglitazone, TP53INP2

KO cells showed a reduced expression of the brown adipogenic protein UCP1 or of the mitochondrial proteins TIM44 and MFN2 (Figure 84) as described above (Figure 23). However, when cells were differentiated in the presence of rosiglitazone the expression of all these proteins was rescued and achieved the same levels than control ones (Figure 84).

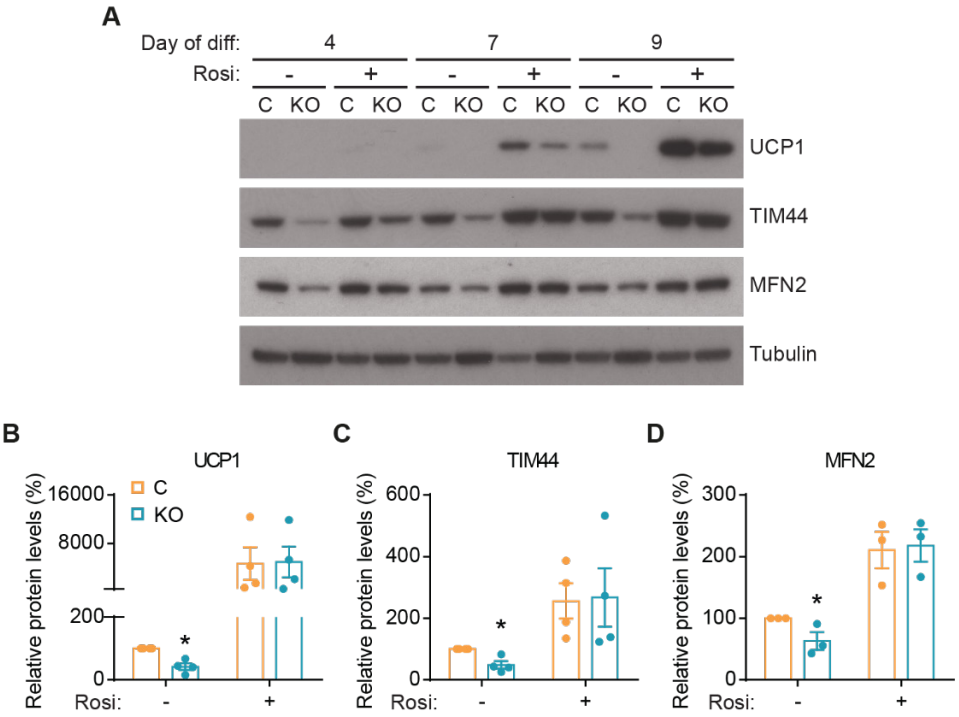

Figure 84. Chronic rosiglitazone treatment rescues adipogenic defect induced by TP53INP2 ablation. Differentiation of control (C) and TP53INP2 knockout (KO) mouse brown preadipocytes in the presence (+) or the absence (+) of rosiglitazone **1µM** during all the process. (A) UCP1, TIM44 and MFN2 protein abundance during differentiation and (B) western blot quantification at day 9 of differentiation (n=3-4). Data are mean ± SEM. *p<0.05 vs. C.

These data support the view that the effect of TP53INP2 on brown adipogenesis depend on PPARγ activity rather than on its protein abundance. Moreover, it also proves that the downregulation of PPAR signaling pathway is involved in the phenotype resulting from TP53INP2 ablation, and that TP53INP2 function is upstream of PPARγ activity.

4.6.5. PPARγ ubiquitination is diminished in TP53INP2 depleted cells

Previous studies in our laboratory have demonstrated that TP53INP2 binds to ubiquitin and enhances the degradation rate of ubiquitinated proteins (Sala et al., 2014). In addition, TP53INP2 binds to the E3 ubiquitin ligases TRAF6 (Ivanova et al., 2019) and Parkin (Yuliana Enciso, PhD thesis, 2018). PPARγ is a protein that undergoes post-translational regulation by phosphorylation, sumoylation, ubiquitination and acetylation events which directly impact on its transcriptional activity (Hu et al., 1996; Hauser et al., 2000; Floyd and Stephens, 2004; Ohshima et al., 2004; Kilroy et al., 2009; Qiang et al., 2012). Upon ligand activation, PPARγ undergoes ubiquitination, and this is required to activate transcription of targets genes (Kilroy et al., 2009). Consequently, after transcriptional activation, PPARγ is degraded by the proteasome (Hauser et al., 2000; Floyd and Stephens, 2002; Kilroy et al., 2009). Indeed, the rate of proteasomal degradation of PPARγ is considered to be directly proportional to its transcriptional activity in white adipocytes. In this regard, several proteins have been described as E3 ubiquitin ligases for PPARγ (Kilroy et al., 2012; Kim et al., 2014; Watanabe et al., 2015; Li et al., 2016; Lee et al., 2018). PPARγ ubiquitination has been studied in white adipose cells, and whether PPARγ is similarly regulated in brown adipocytes remains to be determined. Taking into account all this information, we speculated that TP53INP2 could regulate PPARγ transcriptional activity by facilitating its ubiquitination and subsequent activation.

Thus, PPARγ protein accumulation was measured upon proteasomal inhibition induced by the combination of MG132 and Epoxomicin (E) in brown preadipocytes stably expressing HA-PPARγ. In agreement with the studies performed in white adipose cells (Kilroy et al., 2009), PPARγ accumulated upon proteasomal inhibition under basal conditions and further increased by rosiglitazone in control brown preadipocytes (Figure 85). The decrease in PPARγ protein levels mediated by rosiglitazone treatment was not observed, probably due to the stable overexpression of PPARγ. In contrast, PPARγ protein levels were mostly unaffected

by proteasomal inhibition in TP53INP2 deficient cells (Figure 85), independently of the presence or the absence of rosiglitazone. These data go in parallel with the diminished PPAR transcriptional activity observed in TP53INP2 deficient cells.

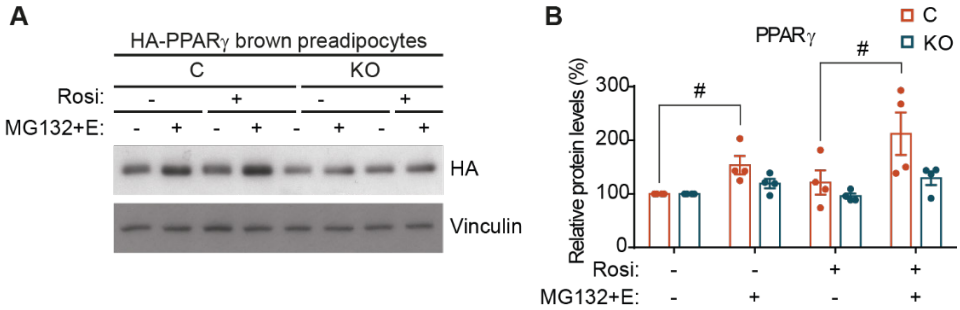

Figure 85. PPARγ protein degradation rate is decreased in TP53INP2 ablated preadipocytes. HA-PPARγ stably overexpressing brown preadipocytes with endogenous (C) or TP53INP2 knockout (KO) levels treated with vehicle (-) or rosiglitazone (+) 10μM for 4 hours and in the presence (+) or absence (-) of the proteasome inhibitors MG132 10μM and epoxomicin (E) 0.1μM for 5 hours (n=4). (A) HA-PPARγ protein abundance and (B) western blot quantification. Data are mean ± SEM. #p<0.05 vs. proteasome inhibitors treated group.

To further confirm whether a decreased level of PPARγ ubiquitination is responsible for its decreased transcriptional activity, PPARγ ubiquitination levels were analyzed. HA-PPARγ overexpressing were brown preadipocytes were treated or not with proteasomal inhibitors and rosiglitazone and they were further subjected to denaturing immunoprecipitation with an anti-HA antibody. PPARγ ubiquitination was detectable in control and KO cells treated with proteasome inhibitors, showing similar ubiquitination levels between genotypes under basal conditions (Figure 86). In addition, rosiglitazone treatment enhanced PPARγ ubiquitination in control cells, which is coherent with previous reports (Kilroy et al., 2009). However, in knockout cells ubiquitination was not induced by the treatment of PPARγ ligand (Figure 86). Immunoprecipitation with anti-IgG conjugated beads as a negative control showed that HA pull down was specific. Moreover, the increase in ubiquitinated proteins upon proteasome inhibition in input fraction confirmed the efficacy of the treatment.

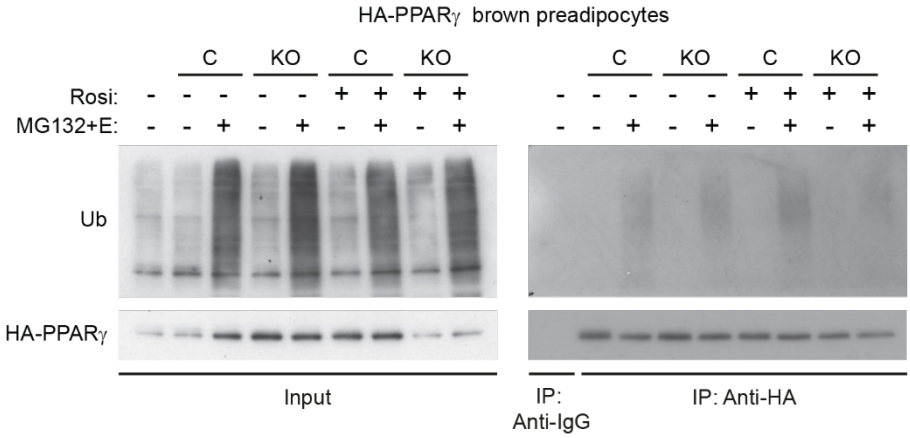

Figure 86. Decreased rosiglitazone induced PPARγ ubiquitination levels in TP53INP2 knockout cells. HA-PPARγ denaturing immunoprecipitation in HA-PPARγ stably overexpressing cells with endogenous (C) or TP53INP2 knockout (KO) levels. Whole cell extracts were harvested under denaturing conditions at the end of 5 hours of proteasome inhibitors (+) or vehicle treatment (-) in the presence (+) or the absence (-) of rosiglitazone 10μM for 4 hours (n=1). HA-PPARγ was pulled-down with anti-HA beads. Anti-IgG conjugated beads were used as negative control. Immunoblots showing PPARγ (HA) and ubiquitin (Ub) protein levels in input and pull down fractions (IP).

In order to validate these results, PPARγ ubiquitination levels were also evaluated after ubiquitin overexpression which increases the flux through the proteasome. Transfection of ubiquitin was associated with increased poly-ubiquitinated proteins in total lysates (input fraction). Under these conditions, PPARγ ubiquitination was markedly detected in cells subjected to proteasome inhibition (Figure 87). Furthermore, PPARγ ubiquitination was markedly reduced in KO cells (Figure 87). Rosiglitazone treatment did not enhance ubiquitination, probably because ubiquitin overexpression enhances PPARγ turnover and the endogenous regulation is lost (Figure 87).

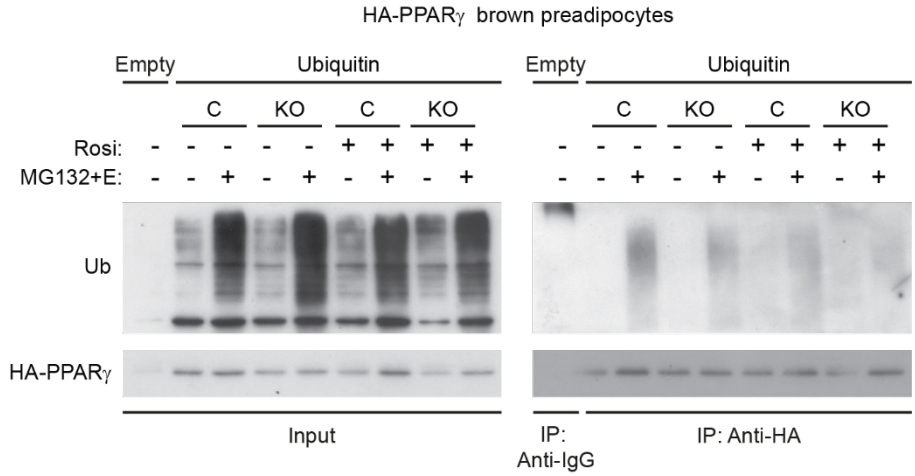

Figure 87. TP53INP2 ablation reduces PPARγ ubiquitination levels. HA-PPARγ denaturing immunoprecipitation in HA-PPARγ stably overexpressing cells with endogenous (C) or TP53INP2 knockout (KO) levels transfected with ubiquitin or empty vector. Whole cell extracts were harvested under denaturing conditions at the end of 5 hours of proteasome inhibitors (+) or vehicle treatment (-) in the presence (+) or the absence (-) of rosiglitazone 10μM for 4 hours (n=3). HA-PPARγ was pulled-down with anti-HA beads. Anti-IgG conjugated beads were used as negative control. Immunoblots showing PPARγ (HA) and ubiquitin (Ub) protein levels in input and pull down fractions (IP).

These data provide additional support to the view that TP53INP2 deficiency is linked to reduced PPARγ ubiquitination, which is coherent with its low transcriptional activity.

DISCUSSION

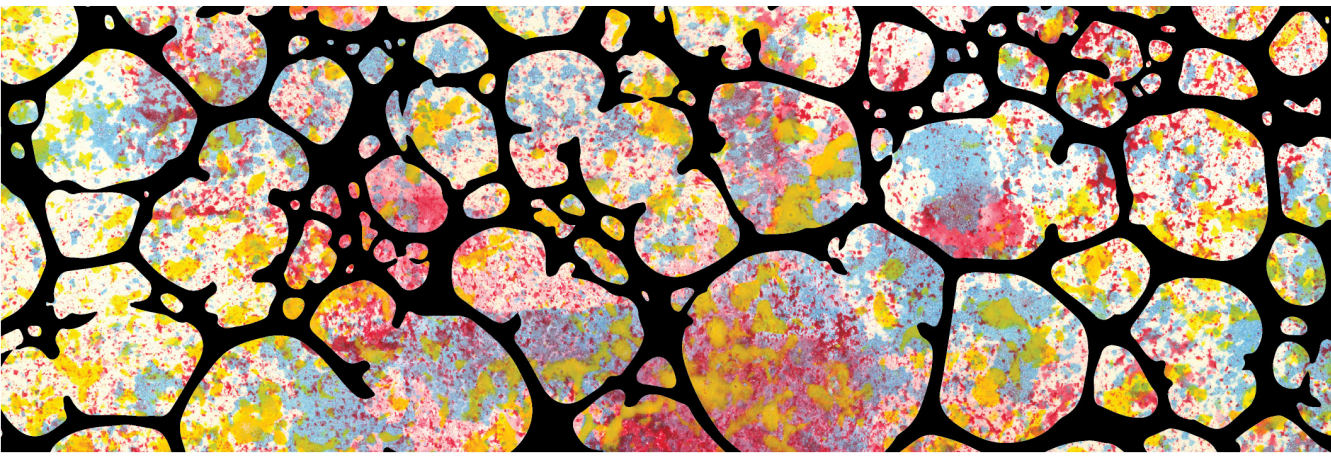

5.1. Thermogenesis modulates TP53INP2 expression in brown adipose tissue

TP53INP2 has been reported to be expressed in metabolically active tissues, from which the skeletal muscle showed the higher levels of expression in rodents and in humans (Baumgartner et al., 2007; Sala et al., 2014). Moreover, the expression of TP53INP2 is repressed in the skeletal muscle from obese or type 2 diabetic rats or human patients. Taking into account that brown adipose tissue is a highly metabolically active tissue and that its function can impact on the regulation of insulin sensitivity (Cannon and Nedergaard, 2004), we evaluated TP53INP2 expression and modulation in the tissue. Our results demonstrate that TP53INP2 is highly expressed in brown adipose tissue and its expression is regulated by thermogenic activity.

As explained in the introduction, brown adipose tissue activity responds to ambient temperature. Thermogenesis is induced under low temperature environment in order to maintain body temperature (Smith and Roberts, 1964; Thomas and Palmiter, 1997), and is inhibited when temperature is equal or higher than the thermoneutral zone, which is defined as the temperature in which an animal does not have to expend energy for thermoregulation (Donhoffer and Szelényi, 1967; Gordon, 1990). Brown adipose tissue also increases its thermogenic capacity as a protective mechanism to prevent excessive lipid accumulation after feeding (Mercer and Trayhurn, 1984; Divakaruni et al., 2012; Fedorenko et al., 2012; García-Ruiz et al., 2015).

Based on the results presented in this dissertation, we concluded that TP53INP2 expression is high in brown adipose tissue, and it is modulated in parallel to thermogenesis. In this regard, TP53INP2 expression levels in mouse brown adipose tissue are comparable to the ones from the skeletal muscle, which is coherent with the fact that both tissues originate from a common precursor cell (Timmons et al., 2007). In addition, TP53INP2 expression is induced under situations of

acute thermogenic activation, such as cold exposure, or under circumstances of prolonged brown adipose tissue recruitment, like extended feeding periods with lipid overload. In contrast, thermogenesis inhibition by thermoneutral environment results in a downregulation of *Tp53inp2* mRNA levels.

The main regulation of brown adipose tissue thermogenesis is mediated by the SNS and the adrenergic signaling pathway. The release of catecholamines induced by the SNS, enhances the intracellular cAMP levels in brown adipocytes, which results in the expression of thermogenic genes and in a lipolytic signal, culminating in the uncoupled β-oxidation of the generated FFA (Thomas and Palmiter, 1997; Cannon and Nedergaard, 2004). Our results suggest that the adrenergic signaling is responsible for the upregulation of TP53INP2 expression specifically in brown adipocytes, and in addition that TP53INP2 is relevant for brown adipose tissue activation and recruitment.

TP53INP2 protein levels are also positively regulated by thermogenesis activation, as HFD fed mice showed increased protein abundance in brown adipose tissue. However, thermoneutrality does not decrease TP53INP2 protein expression. This opens the possibility that TP53INP2 expression under thermoneutral environment may be sustained by other pathways than the adrenergic signaling, or that TP53INP2 has additional functions in the tissue.

Even though we have unraveled that the adrenergic signaling is involved in the regulation of TP53INP2 expression, the factors implicated in this process remain unknown. It would be really interesting to deeply characterize the molecular mechanisms involved in the regulation of TP53INP2 expression, however this molecular view was out of the focus of this PhD thesis. Taking into account that the adrenergic signaling involves PKA activation, its downstream transcription factors CREB or ATF-2 may be involved in the modulation of TP53INP2 expression. Brown adipose tissue recruitment also drives PPAR and thyroid hormone signaling, thus, it can be speculated that TP53INP2 promoter may contain PPRE

or thyroid hormone receptor elements (TRE) motifs that will allow its regulation upon thermogenic activation.

The already described functions of TP53INP2 could explain why it is required for brown adipose tissue function. On the one hand, TP53INP2 is a coactivator of nuclear receptors, and upon overexpression can co-activate the transcriptional activity of the PPARγ and TR (Baumgartner et al., 2007; Sancho et al., 2012). The transcriptional activity of this two receptors is of crucial importance for brown adipose thermogenesis. For instance, *Pgc1α* and *Ucp1* gene promoters contain PPRE and/or TRE motifs (Cassard-Doulcier et al., 1994; Sears et al., 1996; Cao et al., 2004; Hondares et al., 2006). Thus, TP53INP2 could facilitate the transcription of these thermogenic genes by increasing PPRE and TRE transcriptional activity. On the other hand, TP53INP2 is a positive regulator of autophagy (Nowak et al., 2009; Francis et al., 2010; Mauvezin et al., 2010; Sancho et al., 2012; Sala et al., 2014; Romero et al., 2018). Although controversial, some studies have also implicated a role of autophagy in the regulation of brown adipose tissue activity. Acute cold exposure for one hour has been described to induce autophagy (Martinez-Lopez et al., 2016), while sustained activation of thermogenesis is characterized by decreased brown and beige adipocytes autophagy and mitophagy (Altshuler-Keylin et al., 2016; Cairó et al., 2016, 2019). These studies suggest the existence of a time-dependent relation between autophagy and thermogenesis. One possible interpretation is that, upon thermogenesis activation, TP53INP2 expression is increased to rapidly activate autophagy in brown adipocytes to immediately obtain FFA for β-oxidation. Then, as the stimulus persists, brown adipose tissue recruitment is induced and results in the differentiation of new adipocytes and in mitochondria development. When the classical thermogenic machinery is already maximized to burn FFA, mitophagy downregulation would be aimed at preserving mitochondrial mass. In this regard, TP53INP2 expression upon prolonged thermogenic activation conditions would be directed to inhibit mitophagy. This idea is coherent with previous results from our laboratory that demonstrated a role

of T53INP2 in inhibiting mitophagy (Yuliana Enciso, PhD Thesis, 2017).

5.2. TP53INP2 induces brown adipogenesis through PPARγ activity

Brown adipose recruitment, in addition to thermogenesis activation in brown adipocytes, also entails proliferation and differentiation of brown preadipocytes (Géloën et al., 1990). In a recent article, our laboratory has demonstrated that TP53INP2 is a negative regulator of white adipogenesis (Romero et al., 2018). Cellular studies also revealed that TP53INP2 induces differentiation of myoblasts and osteoclasts (Baumgartner et al., 2007; Linares et al., 2011). Results obtained in this thesis indicate that TP53INP2 expression was higher in mouse brown adipocytes than in brown preadipocytes. All these evidences suggested that TP53INP2 could participate in brown adipocyte differentiation.

Lineage tracing experiments have demonstrated that classical brown preadipocytes and skeletal muscle precursor cells originate from a common precursor mesenchymal stem cell that express Myf5, Pax7 and EN1 (Atit et al., 2006; Timmons et al., 2007; Lepper and Fan, 2010; Sanchez-Gurmaches and Guertin, 2014). In spite of different developmental origins, PPARγ and C/EBPs transcription factors are the main regulators of white and brown adipocyte differentiation (Barak et al., 1999; Rosen et al., 1999; Karamitri et al., 2009). However, overexpression of C/EBPβ and PPARγ does not result in the induction of brown fat-specific gene program (Tapia et al., 2018). This implies the existence of cell-specific regulators that cause the fat accumulation or fat dissipation features in white or brown adipose depots respectively. PRDM16 and PGC1α are mayor players in the regulation of this divergence.

The transcriptional co-activator PRDM16 participates in the early determination of brown fat precursor cells by repressing muscle and white adipose specific

gene programs (Seale et al., 2007; Kajimura et al., 2008, 2009). PRDM16 binds to C/EBPβ and PPARγ to direct these transcription factors to activate brown fat specific genes (Seale et al., 2008; Hondares et al., 2011a; Harms et al., 2015). For instance, PRDM16 interaction with C/EBPβ induces the expression of the master mitochondrial biogenesis regulator PGC1α (Kajimura et al., 2009). Moreover, PRDM16 also binds to the complex PGC1α-PPARγ to directly induce the expression of UCP1 (Iida et al., 2015). In this regard, ectopic expression of PRDM16 into white adipocytes induces the brown fat gene program, including PGC1α and UCP1, and represses white adipocyte specific gene expression (Seale et al., 2011).

Albeit PGC1α is dispensable for brown adipogenesis, it is essential to activate the thermogenic gene program upon adrenergic stimulation (Uldry et al., 2006). PGC1α transcriptional coactivator induces thermogenic characteristics by enhancing the expression of genes involved in mitochondrial biogenesis, peroxisome metabolism and fatty acid β-oxidation (Wu et al., 1999a; Puigserver and Spiegelman, 2003; Bagattin et al., 2010). In addition, it co-activates PPARγ, and their interaction drives the expression of the thermogenic protein UCP1 (Puigserver et al., 1998; Tiraby et al., 2003).

Taking into account all this information, we evaluated the relevance of TP53INP2 expression in the process of brown fat differentiation. To do so, brown preadipocyte cell line was generated through the immortalization of brown preadipocytes primary cultures from the TP53INP2$^{loxP/loxP}$ mice. Then, TP53INP2 knockout was induced by using an adenoviral-mediated expression of the Cre-recombinase.

Our results support a role of TP53INP2 in the induction of brown adipogenesis. Upon TP53INP2 ablation, *in vitro* differentiated brown adipocytes showed less morphological characteristics of mature adipocytes. Moreover, the absence of TP53INP2 during differentiation drives downregulated expression of PPARγ1 and PPARγ2, diminished mitochondrial biogenesis (assessed by lower mitochondrial

protein abundance), and a dramatic reduced UCP1 expression in mature brown adipocytes. As a consequence, the decreased brown adipogenic capacity induced by TP53INP2 loss-of-function results in non-functional adipocytes. Thus, TP53INP2 KO adipocytes show a decreased capacity to respond to the β3-adrenergic agonist CL by inducing *Ucp1* or *Prdm16*, and a blunted ability to increase oxygen consumption when treated with NE. It is important to note that these alterations do not emanate from decreased β3AR expression, but to a defective intracellular signaling.

Surprisingly, TP53INP2 shows opposite effects on adipose differentiation of white and brown preadipocytes. Thus, it has been reported that TP53INP2 blocks white adipose differentiation by enhancing WNT/TCF activity (Romero et al., 2018), whereas here we document a stimulatory effect of TP53INP2 in brown preadipocytes. In this respect, WNT signaling pathway has been described to inhibit both white and brown adipogenesis through the repression of PPARγ and C/EBPβ, but also PGC1α expression (Kang et al., 2005; Christodoulides et al., 2009; Wang et al., 2010), which implies that TP53INP2 action on brown adipogenesis may be independent on WNT/TCF activity.

As mentioned above, PPARγ activity is required for adipogenesis (Barak et al., 1999; Rosen et al., 1999; Koutnikova et al., 2003), although it is dispensable for brown fat cell commitment (Barak et al., 1999). Our laboratory has previously described that TP53INP2 co-activates nuclear receptors, including PPARγ (Sancho et al., 2012). Consistent with this report, TP53INP2 ablated brown preadipocytes show decreased PPAR transcriptional activity either in the absence or in the presence of PPARγ protein overexpression, which demonstrates that TP53INP2 modulates PPAR transcriptional activity independently on PPARγ protein levels. Reduced PPARγ activity by genetic mutations is associated to decreased brown adipose tissue development and thermogenic activity (Gray et al., 2006). Thus it was speculated that downregulation of PPAR signaling pathway by TP53INP2 ablation may be the cause of the defective brown fat differentiation. Furthermore,

as PPARγ activation results in the induction of its own transcription through a positive feedback loop in MEF cells (Wu et al., 1999b; Rosen et al., 2002), we attribute to the decreased transcriptional activity the decreased PPARγ1 mRNA and protein expression in TP53INP2 ablated preadipocytes.

In accordance with the reporter assays results, PPARγ overexpression in brown preadipocytes is not sufficient to rescue differentiation capacity in TP53INP2 deficient cells. This again demonstrates that the action of TP53INP2 in the regulation of PPAR transcriptional activity is independent on PPARγ protein abundance. By contrast, chronic PPARγ activation with its specific synthetic ligand rosiglitazone overcomes brown adipogenic defect due to the lack of TP53INP2. Differentiation of TP53INP2 KO brown preadipocytes in the presence of rosiglitazone induces adipogenesis and mitochondrial biogenesis to the same extent than control cells, proving the involvement of PPAR signaling pathway in TP53INP2 action on brown fat differentiation.

In addition to the role of TP53INP2 in stimulating brown adipogenesis through the induction of PPARγ activity, we do not discard that other mechanisms may be involved in this regulation. For instance, TP53INP2 enhances autophagy, and this process is required for brown fat differentiation (Martinez-Lopez et al., 2013). Thyroid hormone signaling is also important for adipocyte differentiation and UCP1 expression (Darimont et al., 1993; Marrif et al., 2005), and TP53INP2 has been described to physically interact with TRα1. Thus, it would be really interesting to evaluate whether this two processes are involved in the regulation of brown adipogenesis mediated by TP53INP2.

5.3. TP53INP2 is required for brown adipose tissue differentiation and thermogenesis

The results obtained placing TP53INP2 as a positive regulator of brown adipogenesis

encouraged us to investigate the functional role of TP53INP2 in brown adipose tissue *in vivo*. With that aim, a Myf5-specific TP53INP2 knockout mouse model (KO^{Myf5}) was generated. Myf5 is expressed in a subset of mesenchymal precursor cells that will give rise to myoblasts and brown preadipocytes, depending on lineage determination mediated by EBF2, EHMT1 and PRDM16 (Seale et al., 2007; Timmons et al., 2007; Kajimura et al., 2008, 2009; Ohno et al., 2013; Wang et al., 2014). Hence, in the generated mouse model TP53INP2 expression is ablated both in skeletal muscle and in brown adipose tissue. This system was chosen because a Myf5-Cre expressing mouse was the only available mouse with Cre-expression in brown adipose tissue precursor cells. As an example, Cre-expressing mice under the control of the brown fat specific UCP1 promoter could be used to generate brown fat specific-knockout mouse models. However, UCP1 is expressed in mature adipocytes and not at preadipocyte level.

Previous *in vitro* studies of our laboratory have demonstrated that TP53INP2 induces myogenesis (Baumgartner et al., 2007). However, some years later, a skeletal muscle-specific TP53INP2 knockout mice model was generated (SKM-KO) (Sala et al., 2014). The phenotyping of these mice showed that TP53INP2 was not required for myogenesis *in vivo*, as both control and SKM-KO mice presented the same differentiation markers and myogenic capacity to regenerate upon an injury (David Sala, PhD thesis, 2013). In fact, SKM-KO mice showed muscle hypertrophy as a result of increased fiber size (Sala et al., 2014). Moreover, SKM-KO mice did not show any alteration in energy balance nor in glucose tolerance, which demonstrated that TP53INP2 expression in skeletal muscle does not directly participate in whole body metabolic homeostasis. With these evidences, we were quite confident with the use of the KO^{Myf5}, especially because one of our main interests was to evaluate whether TP53INP2 ablation in brown adipose tissue impacts on energy balance, and we already know that TP53INP2 deletion in skeletal muscle would not participate in this process.

Data obtained in this PhD thesis strongly indicates that TP53INP2 is required

for the *in vitro* and *in vivo* differentiation of brown adipose cells. In this regard, TP53INP2 ablation in brown adipose precursor cells reduces the expression of adipogenic and thermogenic genes, enhances lipid accumulation in brown adipose tissue, decreases thermogenic capacity and energy expenditure, induces insulin resistance, and facilitates the development of diet or age-induced obesity.

Inhibition of physiological thermogenesis is achieved by thermoneutral environment. Previous studies have reported gene expression modulation in brown adipose tissue by thermoneutrality. It decreases the expression brown fat-specific genes, reduces post-transcriptional functions as RNA process and translation, and downregulates lipolytic, thermogenic and adipogenic gene expression (Bai et al., 2017). In order to determine whether TP53INP2 ablation results in brown adipose tissue dysfunction, we performed transcriptomic analysis by microarray in brown adipose tissue samples from control and KO^{Myf5} mice. GSEA showed that TP53INP2 ablation significantly downregulated pathways involved in the oxidative capacity of the tissue, including TCA cycle, fatty acid peroxisome metabolism. These alterations pointed to an inactive brown adipose tissue condition by TP53INP2 deletion. To validate this idea, we compared our transcriptomic data with the gene modulation induced by thermoneutrality already published (Bai et al., 2017). Surprisingly, almost 40% of the genes that showed significant differential expression by the absence of TP53INP2 were also modulated under thermoneutral environment. Moreover, a positive correlation of the gene expression modulation was detected between the two transcriptomic studies, further proving that the lack of TP53INP2 results in a metabolic condition similar to thermogenesis inhibition. In spite of that, there was an important amount of genes that were modulated differentially by TP53INP2 ablation or by thermoneutrality. Thus, TP53INP2 could be also involved in functions other than the regulation of thermogenesis. An important difference between both studies that could impact the results is the fact that TP53INP2 ablation was directed in brown preadipocytes, and that at the age analyzed, knockout mice had been 3 months without TP53INP2. Under these

conditions, brown adipose tissue development may be affected, and compensatory mechanisms may have been activated. By contrast, thermoneutrality environment was performed in adult mice for 7 days, without disturbing brown fat development, and during a period short enough to directly detect acute gene modulation induced by the absence of cold-induced thermogenesis. It is also important to highlight that the two transcriptomic analysis compared had used a different methodology. While our study was performed measuring mRNA expression using microarrays, the published transcriptomic data corresponded to RNAseq, which means that other types of RNA than mRNA were present among the list of probes that were significantly regulated.

Transcriptomic data obtained from LoxP and KO^{My5} mice also revealed that knockout animals displayed significantly reduced brown fat-specific gene expression and decreased adipogenic signaling pathway. PPAR signaling pathway was also significantly downregulated in TP53INP2 ablated brown adipose tissue. This is in keeping with our previous *in vitro* observations demonstrating a role of TP53INP2 in brown adipose cell differentiation through the activation of PPAR signaling. More importantly, TP53INP2 depletion in brown adipose tissue did not significantly modify WNT signaling pathway, further supporting our idea that the role of TP53INP2 in brown adipogenesis is independent on WNT/TCF activity. Gene expression was also validated by qPCR, which confirmed that KO^{My5} mice showed decreased adipogenic and thermogenic genes. Interestingly, TP53INP2 ablation enhanced the expression *Pref1*, which is known to be expressed in preadipocytes, and to inhibit adipogenesis and thermogenesis gene expression (Lee et al., 2003; Armengol et al., 2012). At least two different possibilities could explain this result: TP53INP2 depleted brown adipocytes may be in a "less differentiated" state, or in the tissue there is increased presence of precursor cells that have not been able to differentiate. It would have been really interesting to demonstrate this hypothesis, for example, by counting the amount of preadipocytes in adult brown adipose tissue, or by comparing *Pref1* expression in adipocytes versus

preadipocytes. Overall these data support the idea that TP53INP2 is required for brown adipogenesis *in vitro* and *in vivo*.

Brown adipose tissue protect mammals against cold exposure or to lipid overload by inducing thermogenesis, in order to maintain body temperature or to prevent an excessive fat accumulation. The thermogenic capacity of brown adipose tissue can have an impact on energy balance. In this regard, functional data obtained in this PhD thesis demonstrate that TP53INP2 induces thermogenesis in brown adipose tissue.

Using indirect calorimetry approaches, we detected that T53INP2 ablated mice showed decreased energy expenditure and diminished brown adipose tissue specific thermogenic capacity, which was independent on locomotor activity and on food intake. Normal skeletal muscle mitochondrial respiration was detected in KO^{Myf5} mice, which is in keeping with previous observations (Sala et al., 2014), and further demonstrates that TP53INP2 ablation in skeletal muscle does not directly impact energy balance. By contrast, brown adipose tissue exhibited mitochondrial dysfunction, and presented decreased complex II mitochondrial respiration upon succinate administration. Actually, brown adipocytes are known to rapidly metabolize succinate. Its oxidation through succinate dehydrogenase initiates production of reactive oxygen species and drives thermogenic respiration. Contrary, succinate dehydrogenase inhibition suppresses thermogenesis (Mills et al., 2018). These results are coherent with transcriptomic data obtained and are most likely contributing to the decreased thermogenic capacity detected in brown adipose tissue. Therefore, these metabolic alterations had consequences in brown adipose tissue. A decreased mitochondrial function resulted in enhanced lipid content and greater brown adipose tissue mass. Brown adipocytes displayed a thermogenic inactive morphology, characterized by decreased LD number and increased LD size. This is in keeping with our gene expression results that pointed to a decreased thermogenic phenotype, and with previous studies demonstrating brown adipose lipid accumulation as a result of thermogenesis dysfunction

(Inokuma et al., 2006; Ahmadian et al., 2011).

Measurement of maximal thermogenic capacity is an accepted tool for the assessment of brown adipose tissue functionality (Virtue and Vidal-Puig, 2013). Instead of measuring the energy that a mouse is expending under free-living conditions, it refers to the greatest quantity of heat that a mouse can produce. The group of Cannon and Nedergaard have clearly demonstrated that the difference between maximal thermogenic capacities measured at two different thermogenic conditions is directly dependent on the quantity of UCP1 (Golozoubova et al., 2006). Thus, we measured maximal thermogenic capacity in mice that were acclimated either to 22°C or to 30°C. We could observe that the difference in oxygen consumption between 30°C and 22°C was much lower in KO^{Myf5} mice compared to control animals, which suggests that total UCP1 content in KO^{Myf5} mice is decreased. Consequently, with these results we can conclude that brown adipose tissue thermogenesis is impaired by TP53INP2 ablation. Nevertheless, body temperature was not different between genotypes, which revealed that adaptive mechanisms aimed at preserving body temperature are induced in KO^{Myf5} mice.

As already mentioned above, brown adipose tissue thermogenesis directly impacts on energy balance. Alterations in brown adipose tissue functionality are associated to decreased energy expenditure and development of obesity (Trayhurn, 1979; Lowell et al., 1993; Bachman et al., 2002), while pharmacological activation of brown fat thermogenesis protects against this disorder (Kopecky et al., 1995; Guerra et al., 1998; Cederberg et al., 2001). In this line, our next aim was to study whether the thermogenic defect associated to the *in vivo* TP53INP2 deletion results in weight gain. We analyzed two parameters that are positively correlated with the development of obesity: age and diet. Our results demonstrate that as KO^{Myf5} were getting older, their body weight was enhanced in a higher extent than in control ones. This was a consequence of an expansion of the white adipose depots and the total fat mass, demonstrating that TP53INP2 ablation in brown adipose

tissue sensitizes to age-induced obesity. Brown adipose tissue mass was also enhanced in older mice, with a dramatic loss of brown adipocyte multilocularity. Under this condition, KO^{Myf5} mice showed decreased brown adipose tissue UCP1 protein content. These data reinforce the idea that the development of obesity by TP53INP2 ablation in brown adipose tissue is derived from decreased UCP1-thermogenesis. Furthermore, HFD administration also resulted in a higher effect in KO^{Myf5} mice than in LoxPs animals. After 16 weeks of HFD treatment, knockout animals showed 4-fold increase in their total body fat amount compared to control mice. More importantly, KO^{Myf5} displayed increased liver weight, which probably results from an increased fat content. Overall these results demonstrate that the thermogenic role of TP53INP2 prevents the development of age- and diet-induced obesity.

Human beings live under thermoneutral conditions and usually display an average metabolic rate of about 1.6 times of the basal metabolic rate. Calorimetry studies in mice performed under thermoneutral conditions demonstrated that mice display mean diurnal energy expenditure about 1.8 times higher than their resting metabolic rate, closely resembling the human situation. Thus, results obtained from metabolic studies under thermoneutral conditions are more likely to be translated to humans (Fischer et al., 2018). Importantly, living at 22°C, which is below the thermoneutral zone of mice, induces a chronic need for thermogenesis to defend body temperature. Under these conditions, mice have to increase their metabolism, and thus their food intake, to 50-60% above basal for thermoregulation (Golozoubova et al., 2004). Hence, in case of non-shivering thermogenesis dysfunction, other heat generation processes are activated to maintain body temperature. Increased skeletal muscle shivering or white adipose tissue browning are two of the most common adaptations occurring in conditions of brown adipose tissue dysfunction (Feldmann et al., 2009; Martinez-Lopez et al., 2013; Blondin et al., 2017). These phenomena are going to influence the overall phenotype and can result in misleading interpretations. The importance of

performing experiments in the absence of cold-stress arise from the studies using the UCP1 knockout mice. The expected phenotype of the UCP1-ablated mice was that they were cold intolerant, that they depended on shivering thermogenesis to maintain body temperature, and that failed to recruit adrenergic thermogenesis during acclimation to cold, all of them already demonstrated (Enerbäck et al., 1997; Golozoubova et al., 2001, 2006). In addition, it was expected that UCP1 knockout mice would be susceptible to become obese, as a result of absent non-shivering thermogenesis and consequent fat accumulation. However, the first studies using this animal model failed to demonstrate an obesogenic effect due to the lack of UCP1 (Enerbäck et al., 1997; Liu et al., 2003; Kontani et al., 2005). In fact, UCP1 mutants showed increased body temperature, which was sustained through muscle shivering. This thermogenic process is less efficient than non-shivering thermogenesis and was preventing the development of obesity (Golozoubova et al., 2006). Some years later, it was demonstrated that ambient temperature is a determinant factor that can influence the final outcome of metabolic studies. In this study, the authors found that by housing UCP1 knockout mice in the absence of cold-stress they were developing obesity, even when they were receiving a normal diet, and further enhanced by HFD administration (Feldmann et al., 2009). From this study it was also concluded that no other protein or mechanism can substitute UCP1 mediated diet-induced adrenergic thermogenesis, and that modulating UCP1 activity could be a relevant tool to counteract human obesity.

The fact that KO^{Myf5} mice showed unaltered body temperature in spite of defective non-shivering thermogenesis unraveled that some adaptive mechanisms directed to body thermoregulation may be induced. Taking into account the importance of environment temperature on the metabolic rate and aiming to directly determine the impact of TP53INP2 ablation in the overall phenotype, we analyzed LoxP and KO^{Myf5} mice that were maintained at thermoneutrality. In the absence of cold-stress body weight differences between genotypes were diminished. More importantly, brown adipose tissue weight and morphology was indistinguishable

between groups. Then, we induced thermogenesis activation in thermoneutral housed mice by feeding them with a HFD. While diet-induced thermogenesis was induced in control animals, assessed by the presence of multilocular adipocytes, this effect was clearly blunted in TP53INP2 knockout mice. Additionally, HFD restored body weight differences between genotypes, and it induced a higher increase in fat mass in the knockout group. These results were corroborated by the measurement of maximal thermogenic capacity. In this case, we evaluated this metabolic parameter in thermoneutral housed mice that received either a CD or a HFD, as a low or high thermogenic condition respectively. Under this scenario, NE induced a significant increase in control and knockout mice when fed a HFD compared with a CD. However, the difference in ΔVO_2 between the two diets was decreased in KO^{Myf5}. This experiment confirms that TP53INP2 ablated mice have decreased diet-induced thermogenesis, and as a result, they develop an obese phenotype.

Notably, TP53INP2 expression is repressed in conditions of thermoneutrality. This could indicate that this physiological mechanism contributes to the development of obesity, at least in mice. We propose that the activation of TP53INP2 in brown adipose tissue in conditions of thermoneutrality through a stimulus other than a HFD (which activates thermogenesis but also have negative impacts on the organism) could be an efficient tool to increase the thermogenic capacity at the whole body level, and to prevent metabolic disorders.

Brown adipose thermogenesis utilizes FFA as a main substrate, but it also uses glucose, especially in conditions of SNS stimulation (Cannon and Nedergaard, 2004). FFA and glucose can be taken from circulation by brown adipocytes, which places them as a perfect target for the treatment of type 2 diabetes and other metabolic disorders. However, the potential of brown adipocytes to mediate insulin sensitivity does not only rely on its capacity to take up glucose from circulation, but also from the capacity to secrete batokines to regulate whole body glucose homeostasis (Silva and Larsen, 1985). This was demonstrated with brown adipose

tissue transplant experiments in 2013, and further characterized later (Stanford et al., 2013; Villarroya et al., 2017a, 2017b).

After the determination that TP53INP2 deletion in brown adipose precursor cells results in brown adipose tissue dysfunction, we wondered whether it leads to systemic effects. To this end, glucose tolerance and insulin sensitivity was evaluated at different conditions. 3 months old KO^{Myf5} showed severe glucose intolerance that was consequence of insulin resistance, and was not associated to defective insulin secretion. It is important to highlight that at this age, there were no differences in body weight nor in fat mass between genotypes. Thus, insulin resistance is not derived from increased adiposity, but from a brown fat-autonomous effect due to the lack of TP53INP2. Thermoneutrality housing experiments were again really useful in further characterizing this phenotype. Insulin sensitivity was restored in KO^{Myf5} mice that were maintained at 30°C and received a CD, which presented the same decreased brown adipose thermogenic activity than control mice. In spite of that, they still presented glucose intolerance. HFD administration induced a profound glucose intolerance both in control and knockout mice, and KO^{Myf5} animals displayed an exacerbated phenotype. Again, this effect was a result of insulin resistance.

Globally, these data reveals that TP53INP2-dependent brown adipose tissue activity mediates glucose metabolism. Under conditions thermoneutrality and with a CD, non-shivering thermogenesis is mainly inactive. Under these conditions, TP53INP2 knockout mice displayed glucose intolerance. This suggests that glucose intolerance is not a direct result from impaired thermogenesis induced-glucose uptake in brown adipose tissue by the lack of TP53INP2. Our interpretation is that, at least one part of the phenotype is mediated by the interruption of endocrine signals from brown adipose tissue in the absence of TP53INP2. Under thermogenic active conditions, as it is at 22°C or at 30°C with HFD, control animals increase its thermogenic capacity, and consequently, enhance glucose uptake. This enhances metabolic differences between genotypes, and thus, glucose intolerance and insulin

resistance is higher evidenced in KO^{Myf5} mice. These results most probably indicate that thermogenic-induced glucose uptake is blunted in knockout mice. Again, we can discard that TP53INP2 ablation in skeletal muscle per se is participating in the phenotype, as previous studies demonstrated normal glucose metabolism in SKM-KO mice (David Sala, PhD thesis, 2013). It would be really exciting to elucidate the signals implicated in the development of insulin resistance. Decreased brown adipose tissue FGF21 secretion could be impairing glucose sensitivity into target tissues. It is well established that, upon thermogenic activation, brown adipose tissue releases FGF21. This adipokine induces browning of white adipose tissue and mediates insulin sensitivity through the induction of PGC1α protein levels in this tissue, and lipid and glucose uptake liver (Fisher et al., 2012; Muise et al., 2013; Hondares et al., 2011b). Cold exposure also results in IL-6 release by brown adipose tissue (Burýšek and Houštěk, 1997). IL-6 is nowadays considered distinct from standard proinflammatory cytokine. For instance, it is known to be released by skeletal muscle after exercise to promote insulin sensitivity (Ikeda et al., 2016). In adipose tissue, IL-6 signaling promotes M2 macrophage activation and sensitizes these cells to interleukin 4 action, which contributes to insulin sensitization (Mauer et al., 2014). Browning of white adipose tissue also depends on IL-6, determined by the lack of cold-induced UCP1 expression in mice with targeted deletion of IL-6 (Knudsen et al., 2014).

Although TP53INP2 shows contrary effects in adipose tissues, TP53INP2 seems to favor energy wasting over energy accumulation in fat depots. In all, the maintenance of a high activity of TP53INP2 protein in white and brown adipose depots prevents the development of obesity in the mouse. It may be speculated that TP53INP2 is involved in the brown fat versus white preadipocyte cell determination. An open question is whether TP53INP2 induces browning of white adipose depots. Results obtained in our laboratory demonstrate that TP53INP2 ablation in white adipose tissue results in adipose hyperplasia and hypertrophy (Romero et al., 2018). Thus, these results would be coherent with a role of TP53INP2 in beige

adipocyte induction. However, detailed studies should be performed to address this hypothesis.

5.4. Mature adipocytes require TP53INP2 to maintain the differentiation state

Based on the results demonstrating a role of TP53INP2 into the positive regulation of brown adipogenesis, our next aim was to study whether TP53INP2 exerts a function in differentiated brown adipocytes. To do so, we needed a different animal model than the KO^{Myf5} to avoid the effects of TP53INP2 in differentiation. We took profit from the inducible global-TP53INP2 knockout mice (KO^{Ubc}) already generated in the laboratory (Romero et al., 2018). The use of this animal model allowed the normal development of brown adipose tissue with endogenous TP53INP2 expression. Then, at 2 months of age Cre-recombinase is induced by tamoxifen diet administration to adult mice to direct TP53INP2 ablation in mature brown adipose tissue.

In order to have a broader view of the effects of TP53INP2 depletion in gene expression modulation in mature brown adipose tissue, microarrays were performed in brown adipose samples from LoxP and KO^{Ubc} mice. Transcriptomic results were also compared with the data obtained with the KO^{Myf5} mouse model. Surprisingly, from the top ten significantly downregulated gene sets, 4 of them were in common in both transcriptomic studies. These included fatty acid metabolism, peroxisome, oxidative phosphorylation, and more importantly, PPAR signaling pathway. This suggested that the phenotype of KO^{Ubc} brown adipose tissue would be really similar to the one from KO^{Myf5}, showing a diminished oxidative gene expression profile. However, when individual gene expression was compared, a decreased total number of significantly modulated genes were found in the KO^{Ubc} mice. Moreover, only a 10% of the genes that were altered in KO^{Ubc} mice were also modified in KO^{Myf5} mice. In spite of that, all the genes that were modulated in

common in the two mouse models were doing so in the same direction, with the exception of 7 genes. That means that exists a strong positive correlation between gene modulation between the two analyses. Our interpretation is that TP53INP2 impacts a higher number of genes in KO^{Myf5} brown adipose tissue because of its role in brown fat development. Strikingly, adipogenesis signaling pathway and brown-fat specific gene sets were also downregulated in adult TP53INP2 ablated brown adipose tissue. Gene expression modulation was confirmed by qPCR in brown adipose samples, confirming a decreased expression of adipogenic and thermogenic genes, such as *C/EBPβ*, *PPARγ2*, *Pgc1α* and *Ucp1*. By contrast, the expression of *Pref1* was unaltered between genotypes when TP53INP2 was deleted in adult brown adipose tissue. One possible explanation for this result is that TP53INP2 does not induce increased number of precursor cells in the tissue, but it is required to sustain the expression of adipogenic and thermogenic genes. Thus, TP53INP2 ablation in brown adipocytes would not direct the de-differentiation to precursor cells, but would reduce their identity as mature brown adipocytes. Another explication could be that *Pref1* is not downregulated upon differentiation in the absence of TP53INP2 in precursor cells. Thus, as in the KO^{Ubc} mouse model TP53INP2 is eliminated in mature brown adipose tissue, in which the principal cell type are brown adipocytes, *Pref1* expression in preadipocytes might be unaltered.

Next, we tested the hypothesis that TP53INP2 is a factor required for the maintenance of the differentiation state in brown adipocytes. To do so, we used brown preadipocytes isolated from Cre-recombinase-inducible $TP53INP2^{loxP/loxP}$ mice. When preadipocytes were differentiated (day 7 of differentiation protocol) were treated for 3 days with TAM which efficiently reduced to 60% *Tp53inp2* mRNA levels. TAM treatment also downregulated the expression of *Prdm16*, *Pgc1α* and *Ucp1*, which are brown adipogenic and thermogenic genes, compared to vehicle treated adipocytes. Under these conditions however, the expression of *Cox7a1*, *Cox8b* or *PPARγ2* was unchanged. No difference in gene expression was found when using *in vitro* differentiated brown adipocytes without Cre-

recombinase expression under the same experimental conditions, validating that the downregulation of these genes was a specific effect due to the modulation of TP53INP2 expression and not to side effects from the TAM treatment. Altogether, our data indicate that TP53INP2 shows a key role in the maintenance of the differentiation state of mature brown adipocytes under *in vitro* and *in vivo* conditions.

Calorimetry experiments in LoxP and KO^{Ubc} mice demonstrated that TP53INP2 ablation in adult mice results in decreased energy expenditure. Again this was not a consequence of differences in locomotor activity or food intake. Brown adipose tissue from KO^{Ubc} mice also displayed enhanced weight and lipid contend compared with control ones, which was exacerbated with age. Under these conditions, body weight and adiposity were also incremented in KO^{Ubc} mice, in keeping with reported data (Romero et al., 2018). Although we did not assess maximal thermogenic capacity in this animal model, the similarities with the KO^{Myf5} phenotype indicate that TP53INP2 ablation in adult mice reduces brown adipose tissue thermogenesis and contributes to the development of the obesity.

To sum up, the results obtained in this section indicate that TP53INP2 is necessary for the maintenance of the differentiation state of brown adipocytes. Thus, ablation of TP53INP2 in adult mice causes brown adipose dysfunction, altered expression of metabolic genes, decreased energy expenditure and obesity. In line with these data, we have also documented that TP53INP2 deficiency in mature brown adipocytes reduces the expression of key brown adipose differentiation genes such as *Ucp1* or *Pgc1α*. Our interpretation is that TP53INP2 sustains the transcriptional activity of PPARγ in the differentiated adipocytes so its depletion reduces PPARγ activity and decreases the expression of target genes.

One interesting observation from the KO^{Ubc} mice is that, in spite of brown adipose dysfunction, they present unaltered glucose tolerance and insulin sensitivity when compared to control animals. Even though we did not get into further details in

the mechanisms involved, this shows that KO^{Ubc} mice present some metabolic advantage compared to KO^{Myf5}. One possible explanation is that TP53INP2 ablation in precursor cells or in mature brown adipocytes could result in different metabolic profile of brown adipocytes, or that TP53INP2 ablation in mature adipocytes does not impair the endocrine signals involved in glucose homeostasis as it occurs in KO^{Myf5}. Nonetheless, the fact that KO^{Ubc} mice present enhanced capacity of white adipose tissue expandability due to a specific role of TP53INP2 could also be participating in this phenomenon. We propose that the global lack of TP53INP2 reduces fat oxidation in brown adipose tissue, which directs fatty acids into white adipose depots and thus prevents ectopic lipid accumulation and consequent lipotoxicity, a hallmark of insulin resistance.

5.5. Regulation of PPARγ transcriptional activity by TP53INP2

As already mentioned above, PPARγ expression is high in adipose tissue and is an essential protein for both white and brown adipogenesis (Barak et al., 1999; Rosen et al., 1999; Karamitri et al., 2009). In this regard, PPARγ-deficient mouse models showed no formation of white or brown adipose tissues (Barak et al., 1999; Rosen et al., 1999; Koutnikova et al., 2003), and specific ablation of PPARγ in mature adipocytes tissue results in progressive lipodystrophy (He et al., 2003; Imai et al., 2004; Jones et al., 2005). Despite being required for brown adipogenesis, PPARγ overexpression into non adipose cells drives them to a white fat phenotype, indicating that other factors cooperate with PPARγ in order to induce brown fat features, such as UCP1 expression (Tontonoz et al., 1994; Kajimura et al., 2010). One candidate that mediates the activation of brown fat characteristics by PPARγ is PRDM16. This was evidenced by the fact that treatment with PPARγ ligands induces thermogenic machinery in brown adipose tissue and enhances browning of white adipose depots through the stabilization of PRDM16 protein (Petrovic et al., 2008; Ohno et al., 2012).

Transcriptomic data from KO^{Myf5} and KO^{Ubc} mice showed downregulation of PPAR signaling pathway in brown adipose tissue in the absence of TP53INP2. Moreover, studies using mouse brown preadipocytes have revealed that TP53INP2 is required for the maintenance of PPARγ activity. Thus, TP53INP2 deficiency is linked to reduced PPARγ transcriptional activity, and chronic activation with the ligand rosiglitazone rescues the PPARγ deficit on brown adipogenesis, indicating that TP53INP2 is upstream of PPARγ. This phenotype is coherent with a reported study in which the effect of a dominant-negative PPARγ mutation (P465L) in adipose tissue was evaluated (Gray et al., 2006). This mutation impairs PPARγ interaction with coactivators, enhances corepressor recruitment and impairs ligand-dependent corepressor release (Barroso et al., 1999; Gurnell et al., 2000; Agostini et al., 2004). In the article the authors demonstrated that reduced PPARγ activity results in enhanced lipid accumulation in brown adipose tissue, defective white and brown adipose tissue recruitment and UCP1 induction upon cold exposure, and reduced thermogenic capacity (Gray et al., 2006). These observations clearly show that *in vivo* PPARγ is required for full activation and recruitment of brown adipocytes when increased thermogenic capacity is required.

Thiazolidinediones are used as antidiabetic drugs due to their insulin sensitizer effects through their binding with PPARγ in adipocytes. Rosiglitazone, a PPARγ specific agonist, reduces glucose, fatty acids and insulin blood glucose levels (Olefsky, 2000; Punthakee et al., 2014; Li et al., 2018). PPARγ stimulation by synthetic ligands also enhance the differentiation and function of brown adipocytes, and induces browning of white adipose tissue (Tai et al., 1996; Fukui et al., 2000; Sell et al., 2004; Wilson-Fritch et al., 2004; Rong et al., 2007; Vernochet et al., 2009; Petrovic et al., 2010). These evidences place PPARγ as a candidate target that if could be selectively activated in brown adipose tissue to regulate thermogenesis may contribute to facilitate weight loss and improve carbohydrate metabolism (Thurlby et al., 1987; Digby et al., 1998; Sell et al., 2004). Our results suggest that TP53INP2 expression activation in brown adipose tissue could have

beneficial metabolic effects similar to the ones produced by PPARγ agonists. Most likely, TP53INP2 overexpression in brown preadipocytes will induce PPARγ activation, brown fat adipogenesis and non-shivering thermogenesis. This could result in negative energy balance and body weight reduction. Also, maintaining TP53INP2 expression in brown adipose tissue is of crucial importance for insulin sensitivity. Thus, induction of T53INP2 activity in models of type 2 diabetes could help in lowering blood glucose levels. In addition, it would be really interesting to evaluate the capacity of TP53INP2 in inducing browning of white adipose tissue, which probably would contribute to weight loss and insulin sensitivity. In summary, we propose TP53INP2 expression in brown adipose tissue as a potential therapeutic target for counteracting the development of obesity and its pathological consequences though the regulation of PPARγ activity.

Taking into account these evidences, we considered of importance to study the regulation of PPARγ activity by TP53INP2. The transcriptional activity of PPARγ is regulated through several post-translational modifications (PTM), including phosphorylation, sumoylation, acetylation and ubiquitination (Hu et al., 1996; Hauser et al., 2000; Floyd and Stephens, 2004; Ohshima et al., 2004; Kilroy et al., 2009; Qiang et al., 2012). Most of these PTMs have been identified in the context of the proadipogenic role of PPARγ in white adipose tissue, and whether PPARγ is similarly regulated by PTMs in brown adipocytes remains to be determined.

Upon ligand activation, PPARγ undergoes ubiquitination, which is required to activate transcription of targets genes. Consequently, after transcriptional activation, PPARγ is degraded by the proteasome (Kilroy et al., 2009). Indeed, the rate of proteasomal-mediated degradation of PPARγ is directly proportional to its transcriptional activity in white adipocytes. Moreover, the ubiquitination of a transcription factor is necessary to reduce its binding to corepressors in response to a ligand (Perissi et al., 2004). Thus, PPARγ protein accumulation was measured upon proteasomal inhibition induced by the combination of MG132 and Epoxomicin in brown preadipocytes stably expressing HA-PPARγ. In agreement with other

studies (Kilroy et al., 2009), PPARγ accumulated upon proteasomal inhibition under basal conditions and further increased by rosiglitazone. In contrast, PPARγ protein levels were mostly unaffected by proteasomal inhibition in TP53INP2 deficient cells, independently of the presence or absence of rosiglitazone, which goes in parallel with the diminished PPAR transcriptional activity observed in these cells. To further confirm whether a decreased level of PPARγ ubiquitination is responsible for its decreased transcriptional activity, PPARγ ubiquitination levels were analysed. PPARγ ubiquitination was detectable in control cells treated with proteasome inhibitors. However, TP53INP2 ablation caused a marked reduction in PPARγ ubiquitination levels. These data provide further validation to the view that PPARγ activity is also regulated by the ubiquitin-proteasome system in brown preadipocyte cells, and that TP53INP2 deficiency is linked to reduced PPARγ ubiquitination and consequent low PPARγ activity. We propose that TP53INP2 is required for the ubiquitination of PPARγ in brown adipose cells. Although we did not identify the specific mechanism involved in PPARγ regulation through TP53INP2, our data are consistent with the view that TP53INP2 deficiency interrupts the sequence of steps necessary for the cycle of activation-degradation of PPARγ.

The process of ubiquitination, meaning the conjugation of ubiquitin molecules to a substrate protein, is achieved through an enzymatic sequential mechanism involving distinct classes of enzymes (Finley, 2009). The first step involves the ubiquitin-activating enzyme (E1), which activates the C-terminal glycine residue of an ubiquitin in an ATP-dependent manner. Then, the activated ubiquitin is transferred to an ubiquitin-conjugation enzyme (E2), that will bound to a member of the ubiquitin ligase family (E3) enzyme. In the last step, the E3 catalyzes the covalent attachment of ubiquitin to the substrate (Pickart, 2001). The contrary process, named deubiquitination, is controlled by deubiquitinating enzymes and removes ubiquitin from ubiquitinated substrates (Ventii and Wilkinson, 2008; Dambacher et al., 2016). From these enzymes, the E3 are the ones responsible for

the selectivity of the ubiquitination process (Pickart, 2001). Moreover, different types of ubiquitin chains can be generated, each of them associated to different biological signaling, including proteasomal degradation, signal transduction or cell cycle regulation, among others (Peng et al., 2003). At least 8 different types of E3 have been described to direct PPARγ ubiquitination, affecting its transcriptional activity and protein stability in different ways: SIAH2, MKRN1, TRIM23, NEDD4, FBXO9, CHIP, CUL4B and TRIM25 (Kilroy et al., 2012; Kim et al., 2014; Watanabe et al., 2015; Li et al., 2016; Lee et al., 2016; Kim et al., 2017; Lee et al., 2018). Nevertheless, all these studies were performed in the context of white adipose cells, and whether these E3 can also mediate PPARγ ubiquitination in brown adipocytes remain to be elucidated.

We think that, with the data obtained from this thesis, it would be important to perform future studies oriented to the identification of the molecular mechanisms implicated in the regulation of PPARγ by TP53INP2. For that reason, we believe that major points that would need to be addressed in future research are: 1) determine whether the described E3 for PPARγ are also involved in this process in brown fat cell context; 2) evaluate whether TP53INP2 binds to some of the E3 of PPARγ to mediate its activation; 3) analyze the phenotype of TP53INP2 ablated mice after the treatment with PPARγ agonists; 4) investigate which other processes could TP53INP2 mediate that result in an impairment of PPARγ ubiquitination.

Unfortunately, we did not have enough time to proceed with this investigation, but we have yet some hypotheses to proceed future investigations. From our microarray data obtained in brown adipose tissue from control mice, we have selected all the E3 that were detected and sorted them by levels of expression. Interestingly, the E3 that showed higher expression in brown adipose tissue was NEDD4, a known PPARγ E3 (Li et al., 2016). More importantly, we analyzed NEDD4 expression in microarray data from ingWAT of WT mice that our laboratory generated, and found that it presented really low expression levels when compared to brown adipose tissue. This was of our interest, because TP53INP2 shows opposite effects

in brown and white adipose tissue PPARγ regulation. Thus, a tissue-specific process would be required to determine the two different functions of TP53INP2.

Recently, it has also been reported that autophagy inhibition in liver results in the accumulation of repressors of the peroxisome proliferator-activated receptor-α (PPARα) as a result of decreased autophagic degradation. Mechanistically, the increase in the levels of repressors histone deacetylase 3 (HDAC3) and nuclear receptor co-repressor 1 (NCoR1) reduced PPARα transcriptional activity and decreased the fatty acid oxidation capacity of the liver (Iershov et al., 2019). In fact, NCoR1 and HDAC3 are not PPARα-specific repressors, but also repress the transcriptional activity of PPARγ (Guan et al., 2005; Yu et al., 2005; Jiang et al., 2014). Even though previous studies indicated that these repressors are degraded through the ubiquitin-proteasome system (Zhang et al., 1998; Frasor et al., 2005; Zhao et al., 2010; Kim et al., 2015), it would be really interesting to validate these results in the context of PPARγ in brown adipose cells. Most likely, the reduction of autophagy flux by TP53INP2 ablation will result in increased abundance of PPARγ corepressors that will prevent its ligand-induced ubiquitination and consequent PPARγ activation.

Overall, the results obtained and discussed in the present study can be summarized in these 4 concepts graphically illustrated in Figure 88:

1. TP53INP2 expression is induced during adipogenesis and is positively regulated by thermogenesis in brown adipose tissue through the adrenergic signaling pathway.

2. TP53INP2 is required for *in vitro* and *in vivo* brown adipogenesis and maintenance of differentiation state.

3. Brown adipose tissue TP53INP2 ablation reduces non-shivering thermogenic capacity and predisposes to weight gain and insulin resistance.

4. The action of TP53INP2 on brown fat regulation involves a mechanism dependent on PPARγ ubiquitination and activation.

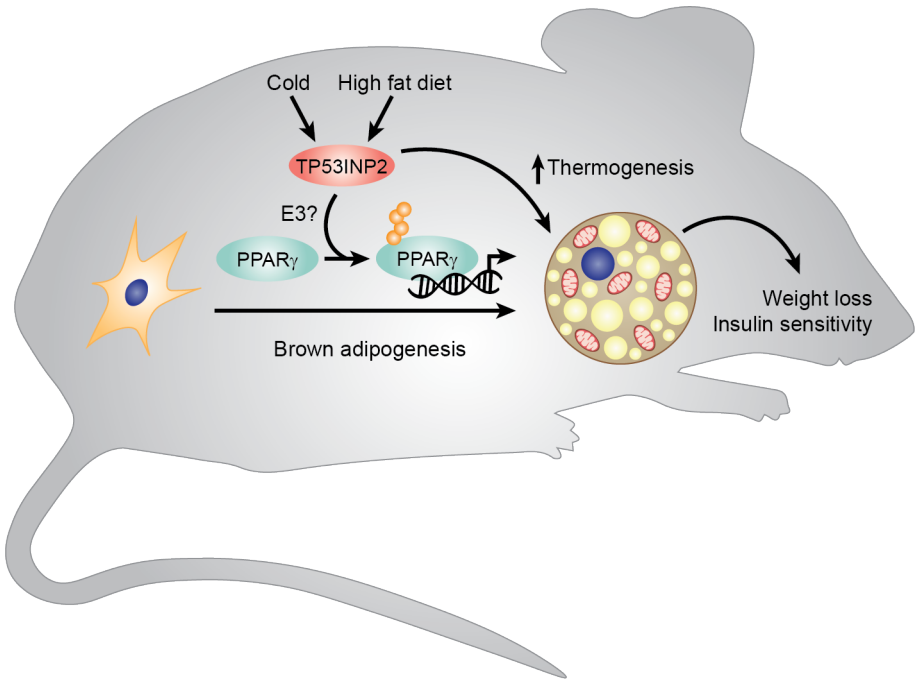

Figure 88. Proposed model of the mechanisms involved in TP53INP2 mediated regulation of brown adipogenesis and thermogenesis.

CONCLUSIONS

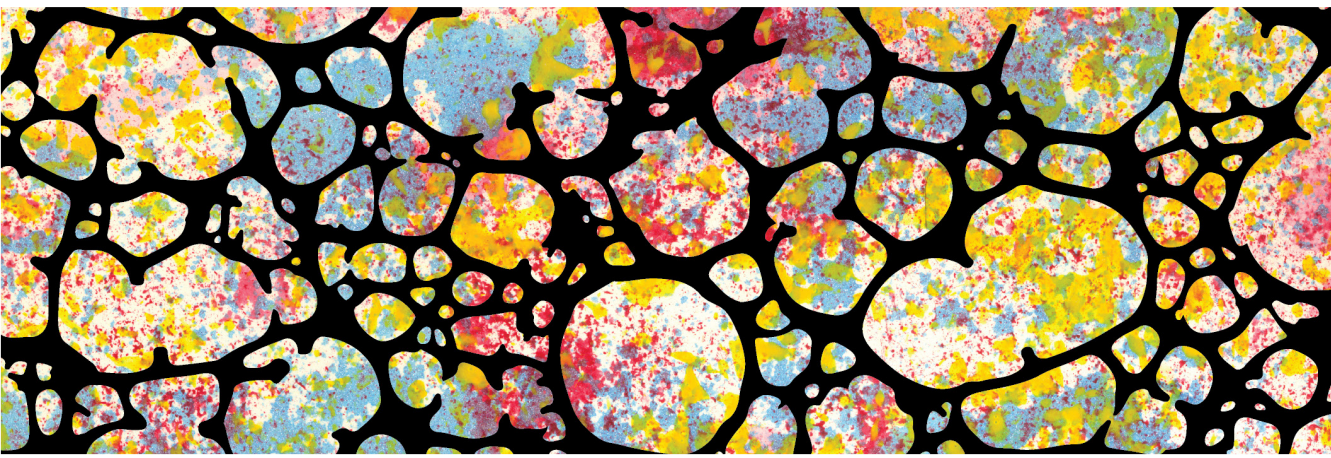

The results obtained in this PhD thesis permit us to propose the following conclusions:

1. TP53INP2 expression is enhanced during brown adipogenesis and is positively regulated by thermogenic activity in mouse brown adipose tissue. The adrenergic signaling pathway induces TP53INP2 expression in brown adipocytes.

2. Brown adipogenesis is stimulated by TP53INP2. TP53INP2 loss-of-function in mouse brown preadipocytes decreases PPARγ transcriptional activity and as a consequence reduces brown adipogenic capacity.

3. TP53INP2 induces cold and diet-induced non-shivering thermogenesis. Brown adipose tissue TP53INP2 ablation induces thermogenic dysfunction which triggers positive energy balance, development of obesity, glucose intolerance and insulin resistance.

4. TP53INP2 maintains the differentiation state of brown adipocytes. Depletion of TP53INP2 in adult mouse brown adipose tissue reduces thermogenic gene expression and energy expenditure, which favors the development of an obese phenotype.

5. PPARγ activity is linked to the ubiquitin proteasome system in brown adipose cells. TP53INP2 deficiency reduces PPARγ activity, PPARγ ubiquitination and its proteasomal degradation. We propose a model in which TP53INP2 regulates brown adipogenesis and thermogenesis by promoting PPARγ activation through ubiquitination.

MATERIALS AND METHODS

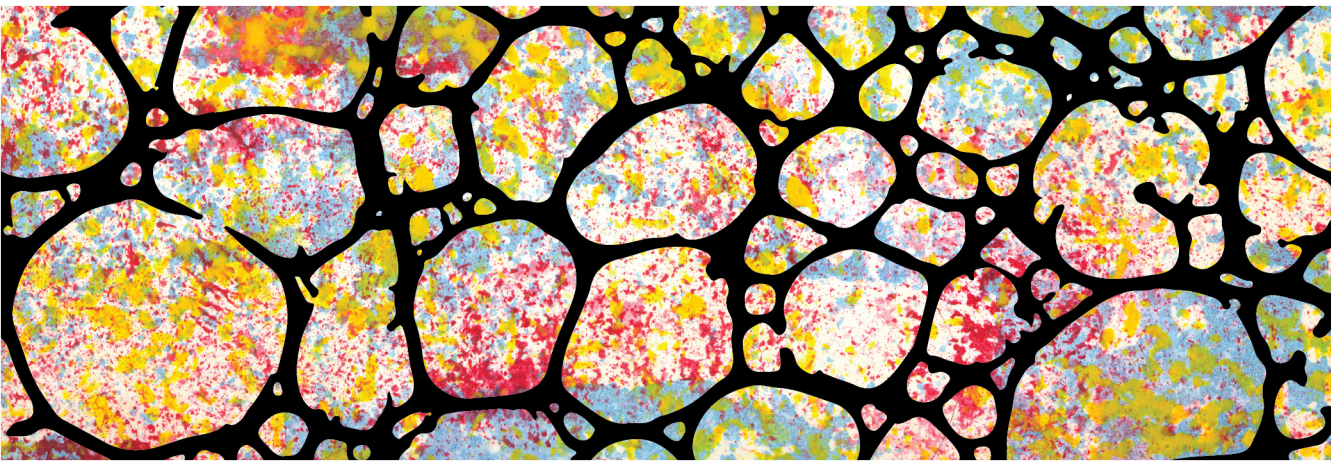

7.1. Materials

In this section are presented the materials used for the development of this thesis. Materials are classified into four different categories and are listed in the following tables accompanied with useful information. The first table presents the plasmids used for retrovirus production and DNA transfection. The second contains all the primers used, both Sybr Green primers for real time PCR and primers used for PCR genotyping. Third table incorporates primary and secondary antibodies used. Finally, in the fourth table are listed the reagents used.

Table 1. Plasmids for virus production and DNA transfection.

Retroviral plasmids			
Name	**Vector**	**Bacterial selection**	**Supplier**
SV40-LT	pBABE-Puro	Ampicillin	Addgene #13970
SV40-LT	pBABE-Neo	Ampicillin	Addgene #8581
pBABE-Empty	pBABE-Puro	Ampicillin	Addgene #1764
PPARγ2	pBABE-Puro	Ampicillin	Addgene #8859
Plasmids for DNA transfection			
Name	**Vector**	**Bacterial selection**	**Supplier**
PPRE-TK-Luc	ptkLUC	Ampicillin	Addgene #1015
Renilla	pRL-CMV	Ampicillin	Promega E2261
PPARγ2	pSV-Sport	Ampicillin	Addgene #8862
Ubiquitin	pCI	Ampicillin	Addgene #31815

Table 2. Primers used in this thesis.

Sybr Green primers for real time PCR		
Gene name	**Forward**	**Reverse**
Arp	AAGCGCGTCCTGGCATTGTCT	CCGCAGGGGCAGCAGTGGT
C/EBPβ	GGCCAAGAAGACGGTGGAC	GTCAGCTCCAGCACCTTGTG
Cox7a1	CAGCGTCATGGTCAGTCTGT	AGAAAACCGTGTGGCAGAG
Cox8b	GAACCATGAAGCCAACGACT	GCGAAGTTCACAGTGGTTCC
Dio2	CAGTGTGGTGCACGTCTCCAATC	TGAACCAAAGTTGACCACCAG
Tp53inp2	AACCACAGCCTGCTTCTAATACCTT	TCAGCCAGTCTCAACACAAAACAC
Elovl3	GCCTCTCATCCTCTGGTCCT	TGCCATAAACTTCCACATCCT
Pgc1a	AGCCGTGACCACTGACAAC	GCTGCATGGTTCTGAGTGC
PPARγ1	GGACTGTGTGACAGACAAGATTTGA	CTGAATATCAGTGGTTCACCGC
PPARγ2	CTCTGTTTTATGCTGTTATGGGTGA	GGTCAACAGGAGAATCTCCCAG
Prdm16	CAGCACGGTGAAGCCATTC	GCGTGCATCCGCTTGTG
Pref1	CTGTGTCAATGGAGTCTGCAAG	CTACGATCTCACAGAAGTTGC
Ucp1	GGAAAGGGACGACCCCTAATC	CCGGCAACAAGAGCTGACA
Genotyping PCR primers		
Gene name	**Forward**	**Reverse**
Tp53inp2	CTGTGAGACTTTAGGTAGTTATCTTATTTC	CCTGTCAAAGGGACTGAAAAGGAGTGG
Cre	CGGTCGATGCAACGAGTGATGAGG	CCAGAGACGGAAATCCATCGCTCG

Table 3. Antibodies used.

Primary antibodies				
Target	**Host**	**WB dilution**	**Cat. Number**	**Supplier**
α-tubulin	Mouse	1/10,000	T5168	Sigma-Aldrich
β-actin	Mouse	1/10,000	A1978	Sigma-Aldrich
HA	Rabbit	1/1,000	3724	Cell Signaling
MFN2	Mouse	1/1,000	ab56889	Abcam
PGC1α	Rabbit	1/500	NBP1-04676	Novus Biologicals
PPARγ	Rabbit	1/1,000	sc-7196	Santa Cruz
TBP	Mouse	1/2,000	ab818	Abcam
TIM44	Mouse	1/1,000	612582	BD Biosciences
TP53INP2	Mouse	1/5	DOR 3.15	Generated in the Lab
Ubiquitin	Rabbit	1/1,000	3933	Cell Signaling
UCP1	Rabbit	1/1,000	ab10983	Abcam
Vinculin	Mouse	1/5,000	ab18058	Abcam
Secondary antibodies				
Target	**Conjugated**	**WB dilution**	**Cat. Number**	**Supplier**
Mouse	HRP	1/10,000	715-035-150	Jackson Immuno Research
Rabbit	HRP	1/10,000	711-035-152	Jackson Immuno Research

Table 4. Details of reagents used.

Reagents				
Name	**Working conditions**	**Application**	**Cat. Number**	**Supplier**
4-hydroxy-tamoxifen	1μM	Cre-recombinase induction	H7904	Sigma-Aldrich
ADP	BAT: 1mM SKM: 2.5mM	Complex V substrate	A5285	Sigma-Aldrich
Antimycin A	2.5μM	Complex III inhibitor	A8674	Sigma-Aldrich
BSA fraction V	4%	Isolation of brown preadipocytes	A9647	Sigma-Aldrich
CCCP	0.25μM	Mitochondria depolarization	C2759	Sigma-Aldrich
CL-316,243	1μM	β3-adrenergic agonist	C5976	Sigma-Aldrich
Collagenase A	1mg/ml	Isolation of brown preadipocytes	10103578001	Roche
Cytochrome c	10μM	High resolution respirometry	C2037	Sigma-Aldrich
Dexamethasone	0.5μM	Cell differentiation	D2915	Sigma-Aldrich
Epoxomicin	0.1μM	Proteasome inhibitor	I-110-200	R&D Systems
Funguizone mix	1x	Isolation of brown preadipocytes	15240	Life Technologies
Glutamic acid	10mM	Complex I substrate	sc211703	Santa Cruz
IBMX	0.5mM	Cell differentiation	I7018	Sigma-Aldrich
Indomethacin	0.125mM	Cell differentiation	I8280	Sigma-Aldrich
Insulin	20nM	Cell differentiation	T6397	Sigma-Aldrich
Malic acid	2mM	Complex I substrate	M1000	Sigma-Aldrich
MG132	10μM	Proteasome inhibitor	474790	Merck
Neomycin	50μg/ml	Stable cell line selection	10131-027	Life Technologies
Norepinephrine	Cells: 1μM Mice: 1mg/kg	Adrenergic stimulation	A0937	Sigma-Aldrich
Oligomycin A	1μM	Complex V inhibitor	75351	Sigma-Aldrich
Puromycin	3μg/ml	Stable cell line selection	sc108071	Santa Cruz
Rosiglitazone	Chronic: 1μM Acute: 10μM	PPARγ ligand	R2408	Sigma-Aldrich
Rotenone	2.5μM	Complex I inhibitor	R8875	Sigma-Aldrich
Succinate	10mM	Complex II substrate	S2378	Sigma-Aldrich
T3	1nM	Cell differentiation	I1882	Sigma-Aldrich

7.2. Methods

7.2.1. Animal studies

7.2.1.1. Animal care, housing conditions and diets

Mice were breaded in a C57BL/6J genetic background, were kept under a 12-h dark-light period, and provided with a standard chow-diet and water ad libitum. Environment temperature was set around 22°C. When indicated, animal cages were placed inside a thermostated chamber at 30°C starting after weaning.

Tamoxifen diet was used during one month to induce Cre-recombinase expression and to induce TP53INP2 ablation (Envigo RMS Division). When indicated, mice were fed a high-fat diet (60 kcal% Fat, Research Diets Inc.).

Animal studies were approved and conducted according to guidelines established. This project has been assessed favorably by the Institutional Animal Care and Use Committee from Parc Científic de Barcelona (IACUC-PCB) and the IACUC considers that the above-mentioned project complies with standard ethical regulations and meets the requirements of current applicable legislation (RD 53/2013 Council Directive; 2010/63/UE; Order 214/1997/GC).

7.2.1.2. Generation of mouse models

For the development of this PhD thesis we have used two animal models: a knockout model with global TP53INP2 ablation and a mouse model that presented TP53INP2 deletion in brown adipose tissue and skeletal muscle precursor cells.

The KO^{Myf5} mouse line was generated by crossing homozygous $TP53INP2^{loxP/loxP}$ mice (Sala et al., 2014) with a Cre-recombinase expressing mouse strain under the control of the myogenic factor 5 (Myf5) promoter (B6.129S4-Myf5(tm3(cre)

Sor)/J, stock number 007893, The Jackson Laboratory). Experimental groups contained TP53INP2$^{loxP/loxP}$ Cre negative (LoxP) and TP53INP2$^{loxP/loxP}$ Cre positive mice (KO^{Myf5}). This mouse model was generated during this PhD thesis with the purpose of studying the physiological role of TP53INP2 in a tissue specific context.

The global-TP53INP2 (KO^{Ubc}) mouse line was obtained by crossing homozygous TP53INP2$^{loxP/loxP}$ mice with a mouse strain expressing the Cre-recombinase under the control of the ubiquitin promoter (UBC-Cre-ERT2) as described (Romero et al., 2018). Experimental groups contained TP53INP2$^{loxP/loxP}$ Cre negative (LoxP) and TP53INP2$^{loxP/loxP}$ Cre positive mice (KO^{Ubc}). At two months of age, both LoxP and KO^{Ubc} mice received a tamoxifen diet for one month to induce global TP53INP2 ablation. KO^{Ubc} mouse model was already generated in the laboratory by Dr. Montserrat Romero.

7.2.1.3. Measurement of body composition

Mice body composition was measured using magnetic resonance with the EchoMRI™ Body Composition Analyzer. During the measurement (10 seconds), mice were restrained but not anesthetized. Total fat and lean mass was determined.

7.2.1.4. Metabolic cages

Metabolic cages were used to measure food and water intake, as well as urine and feces excretion. Mice were placed individually in metabolic cages and let to acclimate to the new environment for 48 hours. Measurements were collected every 24h during two consecutive days.

7.2.1.5. Indirect calorimetry

Evaluation of oxygen consumption (VO_2), carbon dioxide production (VCO_2) and locomotor activity were performed using an indirect calorimetry system (Oxymax,

Columbus Instrument). This system consisted of 8 individual cages connected to a calorimetry system which allowed for the detection of oxygen and carbon dioxide concentration. Oxygen and carbon dioxide sensors were calibrated at the beginning of the experiment using a gas with a determined composition (79% N_2, 20.5% O_2 and 0.5% CO_2). Mice were housed individually in calorimetry cages and had free access to food and water ad libitum. They were acclimated to the new environment for 3 days, and measurements were collected during 24 hours on intervals of 20 min during the 4th day.

EE, VO_2, VCO_2, glucose oxidation and lipid oxidation were calculated with respective formulas and adjusted to an average mice body weight determined using ANCOVA. This correction has been reported as a good method to eliminate variance in metabolic parameters derived from differences in body weight between animals, as a bigger animal will expend more energy than a smaller one (Tschöp et al., 2012). Thus, an idealized body weight is calculated, and the metabolic parameter of each group (LoxP or KO) is referred to this body weight. By doing this correction we ensure that significant differences emerge from a genotype effect and not from differences in body weight between groups. The respiratory exchange ratio was calculated with its respective formula. The following formulas were used:

$$VO_2 = O_{2\ initial} - O_{2\ final}$$
$$VCO_2 = CO_{2\ initial} - CO_{2\ final}$$
$$EE = (3.815 \times VO_2) + (1.232 \times VCO_2)$$
$$RER = VCO_2/VO_2$$
$$Glucose\ oxidation = (4.545 \times VCO_2) - (3.205 \times VO_2)$$
$$Lipid\ oxidation = 1.672 \times (VO_2 - VCO_2)$$

7.2.1.6. Assessment of maximal thermogenic capacity

A better measure than whole body energy expenditure to directly assess brown adipose tissue function is to evaluate its maximal thermogenic capacity. It represents

the maximal quantity of heat than a mouse can produce after the administration of a supramaximal dose of an adrenergic stimulant (Virtue and Vidal-Puig, 2013). This treatment will activate adrenergic signaling in several tissues other than brown adipose tissue, as skeletal muscle or liver. Thus, brown adipose tissue thermogenesis represents the difference of the maximal thermogenic capacity between two conditions characterized by different brown adipose tissue recruitment. In this regard, thermogenesis was assessed in the following conditions:

1. Cold-induced thermogenesis: in mice that had been acclimated either to 22°C or to 30°C as a high and low brown adipose tissue thermogenic activity respectively.
2. Diet-induced thermogenesis: in mice that had been acclimated to 30°C and fed a chow or a high fat diet for three months, as a low and high brown adipose tissue thermogenic activity respectively.

Maximal thermogenic capacity was evaluated in anesthetized mice, as it has been described that it reduces energy expenditure increase due to the stress induced by mice manipulation, reduce noise related to physical activity associated energy expenditure, and minimizes endogenous SNS. While the majority of anesthetics reduce endogenous SNS, it is important that the anesthetic of choice does not impair sympathetic signaling, as for example does isoflurane (Ohlson et al., 1994). The best anesthetic to perform this experiment is pentobarbital (Virtue and Vidal-Puig, 2013). Moreover, as the anesthetic reduces endogenous SNS, to avoid hypothermia it is important to maintain mice body temperature. To do so, calorimetry cages are placed inside a chamber maintained at 30-32°C.

The protocol used for the maximal thermogenic capacity assessment was the following:

1. Anesthetize mice by an intraperitoneal injection of pentobarbital (80mg/kg), and place them inside the 30°C chamber to prevent hypothermia.
2. After the ascertainment of deep anesthesia by the absence of reflexes, place

mice inside the calorimetry cage. Record basal oxygen consumption (VO_2) in intervals of 4 min during 20-30 min, when it gets stabilized.

3. Then, open the cage and inject mice with a subcutaneous dose of norepinephrine (1mg/kg) to measure NE-induced VO_2.
4. Record VO_2 during 2 additional hours. NE induces a rapid increase in VO_2, and this return to basal levels after the maximal stimulation.
5. Stop the measurements and maintain mice inside the 30°C chamber until they are completely recovered from anesthesia.

Those animals that were awaken during the experiment were removed from data analysis. Observing the decrease in VO_2 after the maximal NE-induced stimulation was used to determine that mice were still anesthetized. Thus, mice in which a decrease in VO_2 was not detected after reaching the maximal NE-response were also removed, as we were unable to determine whether VO_2 increase was a result of NE or of the anesthesia recovery.

Basal VO_2 was defined as the average of the las 5 measurements before NE injection. Data was represented as oxygen consumption increase (ΔVO_2) from the basal VO_2.

The experimental setup allowed the simultaneous measurement of 2 cages, thus, one control and one knockout mice were used at the same time.

7.2.1.7. Rectal temperature measurement

Rectal thermometry is a common method of measuring body temperature in rodents. To do so, a rectal prove coupled to a digital lector was used. To facilitate the prove insertion to the rectum, it was lubricated. In adult mice, an insertion depth of >2 cm will yield colonic temperatures (Meyer et al., 2017). Thus, the rectal prove was marked at this distance to ensure the same insertion in each mice. This invasive procedure induces significant stress to mice that directly alters temperature measurements. Because of that, mice were familiarized to the rectal

prove daily during one weak. Then, body temperature was measured the following day.

7.2.1.8. Glucose and insulin tolerance tests

Glucose tolerance test (GTT) is a technique used to evaluate the glucose uptake capacity. It is based in the following of blood glucose levels upon administration of a glucose bolus. Thus, a delay in blood glucose clearance is associated to insulin resistance. In this regard, insulin tolerance test (ITT) consists of the tracing of glucose levels upon an injection of insulin. This technique is an approximation to evaluate insulin sensitivity.

We have used these two techniques in LoxP and KO^{Myf5} male and female mice at 3 months of age when housed at 22°C. Mice housed at thermoneutrality fed either a CD or a HFD were subjected to the GTT and the ITT at 6 months of age.

GTT protocol:

1. The day before the experiment, remove food from mice cages to subject them to 16 hours of fasting.
2. Perform a small cut at the end of the tail to extract blood and measure fasting glycaemia with a glucometer.
3. Inject mice intraperitoneally with a glucose dose of 2g/kg.
4. Measure glucose levels 5, 15, 30, 60, 90, 120 and 150 min after glucose injection.
5. Collect 50µl of blood at these time points using Microvette® tubes (Starstedt) for the posterior determination of plasma insulin levels.
6. Centrifuge extracted blood 10 min at 3,000rpm and at 4°C. Collect plasma (supernatant fraction) to either use directly for insulin detection, or store at -80°C.
7. Determine plasma insulin levels using *Ultra Sensitive Mouse Insulin ELISA*

kit (CristalChem) following manufacturer instructions.

ITT protocol is similar to the GTT with the differences:

1. Mice are fasted 4 hours before the experiment
2. Insulin (Humalog) is injected intraperitoneally in spite of glucose. Insulin doses used were:
    a. 0.7U/kg in male or female mice housed at 22°C.
    b. 1U/kg in male mice housed at 30°C and fed with a CD.
    c. 1.5U/kg in male mice housed at 30°C and fed with a HFD.

7.2.1.9. Histological analysis

iBAT samples were fixed overnight in 4% PBS-buffered formalin. Fixed samples were dehydrated and embedded in paraffin. iBAT sections were stained with hematoxylin and eosin. Lipid droplet (LD) area and LD number were quantified with Ilastik software. 10 different images per animal were quantified, and the average per mouse was used for calculations.

7.2.2. Cell culture

7.2.2.1. Cell maintenance and preservation

During the development of this PhD thesis we have used immortalized brown preadipocytes as a cellular model, which has been studied at preadipocyte level or upon differentiation. Phoenix-ECO (ATCC CRL-3214) cells were used as retroviral producing cells. Cells were grown in culture media containing DMEM high glucose (Life Technologies) with 10% FBS, 20mM HEPES (Sigma-Aldrich) and 100 U/ml of penicillin/streptomycin (Life Technologies) at 37°C in a humidified atmosphere of 5% CO_2 and 95% O_2. Mycoplasma detection test was performed once every two weeks to ensure no contamination of the cells. When mycoplasma

was detected, cells were decontaminated with 25µg/ml Plasmocin treatment (Ibian Technologies).

Proliferating cells were maintained sub-confluent by regular splitting in 75cm^2 flasks. Growth medium was removed, cells were washed with PBS and 3mL of trypsin was added to detach cells from surface. Trypsin was incubated 5 min at 37°C and was subsequently inhibited by the addition of 3mL of culture medium. Usually, a 1:20 to 1:30 dilution was done to maintain cells sub-confluent for 3-4 days. In the case that a specific number of cells was needed, cells were counted using a Neubauer chamber. Brown preadipocytes used were of less than 20 passages.

Cellular stocks were kept at -80°C. In order to preserve cells, trypsinized suspension was centrifuged at 500g for 5 min and resuspended in freezing media (10% DMSO in FBS). Cell vials were placed in stratacooler at -80°C during 24 hours, and then stored in boxes. Contrary, to thaw aliquots, cryovials were rapidly transferred from -80°C to a 37°C water-bath to ensure rapid thawing. Freezing media was removed by centrifuging cells at 500g for 5 min. Finally cells were resuspended in complete medium and were plated in culture flasks.

7.2.2.2. Brown preadipocyte isolation and immortalization

Primary brown preadipocytes were isolated from 6-8 iBAT depots from 1 month old TP53INP2$^{loxP/loxP}$ or TP53INP2$^{loxP/loxP}$ UBC-Cre-ERT2 mice, following a protocol previously described (Fasshauer et al., 2001). Subsequently, when an enough amount of cells had proliferated (50% of confluence minimum), cells were immortalized with SV40-LT retrovirus produced in HEK293-Ecotropic cells. As it is difficult do exactly determine how many days will take for the preadipocytes to proliferate, retrovirus suspension can be produced with anticipation, filtered and conserved at 4°C for few days or to -80°C for longer periods.

Table 5. Composition of buffers used for primary brown preadipocyte isolation.

Preservation buffer	
HBSS medium	
BSA frac. V	4%
Antibiotic-antimycotic	1x

Digestion buffer	
HBSS medium	
BSA frac. V	4%
Pen/Strep	100U/ml
Collagenase A*	1mg/ml

*Add collagenase just before using and then filter with a 0.2µm filter.

Primary culture medium	
DMEM:Ham's F12 (1:1)	
NCS	10%
HEPES	20mM
Pen/Strep	100U/ml

Brown preadipocyte isolation:

1. Drain anesthetized mouse by cardiac puncture and sacrifice.
2. Clean mouse back and surgical material with 70% ethanol to sterilize.
3. Dissect iBAT depot avoiding pieces of white adipose tissue or skeletal muscle. Place dissected iBAT depots in ice-cooled preservation buffer while processing all mice.
4. Mince iBAT depots very finely with surgical scissors and scalpels on top of a cell culture plate maintained on ice. Foie-grass texture is required.
5. Collect all minced tissue into a sterile 50mL corning tube and add 15mL of digestion buffer.
6. Digest suspension at 37°C in a water-bath with agitation for 30-40 min (we did not have an automatic water-bath shaker, so manual shaking was performed every 2 minutes). This is the critical step. Under-digestion will result in a low efficiency and over-digestion will release lipid droplets from adipocytes and will difficult isolation.
7. Filter digestion using a 100µm dispensable cell strainer (BD #352360) into a sterile 15mL corning tube.
8. Maintain filtered suspension 20 min on ice. Mature adipocytes will float and will go into the top fraction.

9. Remove upper white fat layer containing mature adipocytes. Take the next 2/3 and leave the bottom 1/3 into the tube (preadipocytes seem to be slightly less dense than other parts of the stroma vascular fraction).
10. Mix the suspension 1:1 with primary culture medium.
11. Centrifuge at 700g for 10 min at room temperature.
12. Discard supernatant and resuspend cell pellet with 10mL of primary culture medium.
13. Centrifuge again at 700g for 10 min at room temperature.
14. Discard supernatant and resuspend cell pellet with 10mL of primary culture medium. A lot of pipetting up and down is required and there may be still some debris. Let them settle and avoid plating.
15. Seed cell suspension into one 10cm cell culture plate to immortalize them. A small amount of cell suspension is seeded in a 3.5cm cell plate to use as a control for antibiotic selection.
16. After 24 hours, wash generously twice with PBS to remove as much as blood cells that won't be attached, and add fresh primary culture medium.
17. During the first days preadipocytes may be difficult to see with the optical microscope. After 2-3 day they will be easily observed. When the cell plate is about 50% confluence immortalization can be performed.

Production of SV40-LT retrovirus:

To generate retrovirus we used Phoenix-ECO cells that stably express ecotropic envelope virus protein (pCL-Eco). All the work involving retrovirus was performed in a cell culture room with a biosafety level of 2 and a hood with biosafety category IIA.

1. Seed $7x10^6$ cells in a 10cm cell culture plate with complete medium. One plate of Phoenix-ECO cells is needed per plate of primary preadipocytes to be immortalized.
2. When cells are attached, remove growth medium and add 10mL of

OptiMEM (Life Technologies) per plate. A confluence of 80% is required to proceed.

3. Transfect 10µg of pBABE-SV40-LT plasmid as follows (quantities are per one plate of cells):
    a. Mix in a 2mL Eppendorf tube the volume of plasmid with 1560µl of 150mM NaCl (filtered solution). Incubate 5 min.
    b. Add 78µl of PEI 1mg/ml pH=7 to the mixture. Incubate 20 min.
    c. Add all the mixture to the Phoenix-ECO cell plate.
4. Incubate transfection medium a minimum of 6 and a maximum of 16 hours at 37°C.
5. The following day, remove transfection medium and add 10mL of complete medium per cell plate. Incubate cells at 33°C (at this temperature viral particles are more stable).
6. Approximately 30 hours later, collect cell medium and filter with a 0.45µm sterile filter. This medium that contains viral particles can be directly used to perform the first infection if target cells are ready, or can be kept until they are ready.
7. Add 8mL of complete medium per cell plate. Incubate cells at 33°C for additional 24 hours.
8. Collect cell medium and filter with a 0.45µm sterile filter. This medium that contains viral particles can be directly used to perform the second infection if target cells are ready, or can be kept until they are ready.
9. Generally, two infections are enough and at this point Phoenix-ECO cells can be discarded. If a third infection is desired, repeat steps 7 and 8.

<u>Immortalization of primary brown preadipocytes with SV40-LT retrovirus:</u>

Proliferate primary brown preadipocytes at 37°C until enough cells are obtained (aprox. 50% confluence) before proceeding with immortalization. Replace primary cell culture medium every 2-3 days. Immortalization is performed as follows:

1. Remove primary cell culture media from preadipocytes.
2. Add all the first viral suspension (10mL) already filtered with 4µg/mL Polybrene. Add viral suspension only to 10cm cell plate containing preadipocytes that are going to be immortalized, the 3.5cm cell plate will be used as a control for antibiotic selection.
3. Incubate 24 hours at 37°C.
4. The following day do not remove culture medium from the preadipocyte cell plate. Add the second viral suspension (8mL) directly on top of the first viral suspension with 4µg/mL Polybrene. Add viral suspension only to 10cm cell plate containing preadipocytes that are going to be immortalized, the 3.5cm cell plate will be used as a control for antibiotic selection.
5. Incubate 24 hours at 37°C.
6. The following day aspirate the virus containing medium and add cell culture medium with the appropriate antibiotic to start selection. Add cell culture medium with antibiotic to the 3.5cm cell plate used as control. Antibiotics used are 3µg/ml puromycin or 50µg/ml neomycin (geneticin).
7. Replace cell culture medium with antibiotic each 2-3 days until the cells from the 3.5cm cell plate are all dead. Usually, one week is enough to perform selection of infected cells, but sometimes it may take longer. If required, the concentration of antibiotic can be incremented progressively until the death of non-infected cells is achieved.
8. When selection is finished, maintain cells in cell culture medium without antibiotic.

7.2.2.3. Brown preadipocyte differentiation

Differentiation of immortalized brown preadipocytes was performed seeding a density of 5,000cells/cm^2. Cells were seeded and grown until confluence for 3 days in differentiation medium. Subsequently, differentiation was induced by switching

cells to induction medium (day 0) for 48 hours. Then cells were maintained again in differentiation medium for 7 additional days.

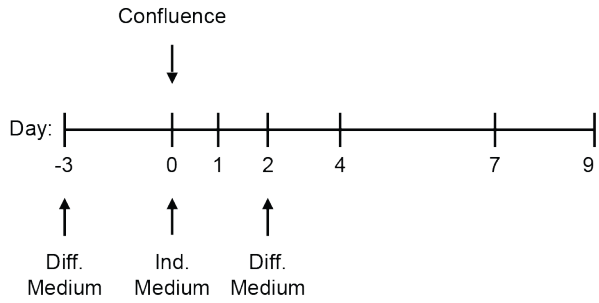

Figure 89. Brown preadipocyte differentiation protocol.

Table 6. Composition of cell culture media used for brown preadipocyte differentiation.

Differentiation medium	
Proliferation media	
Insulin	20nM
T3	1nM

Induction medium	
Proliferation media	
Insulin	20nM
T3	1nM
Dexamethasone	0.5μM
Indomethacin	0.125mM
IBMX	0.5mM

7.2.2.4. Generation of TP53INP2 knockout brown preadipocyte cell line

Control (C) and TP53INP2 knockout (KO) brown preadipocyte cell lines were generated by adenoviral infection and posterior sorting. C cells were generated using a GFP adenovirus (pAdenoCMV-V5-GFP, generated in lab (Pich et al., 2005) while KO cells using a Cre-recombinase-GFP adenovirus (Ad5CMVCre from University of Iowa Viral Vector Core Facility). Adenovirus were amplified infecting HEK293A cells with 20μl of the viral crude stock. After 48 hours, culture

media and cells were collected and centrifuged at 1,300rpm for 5 min. Cell pellet was resuspended in 10mL of culture medium, and then cells were lysed with 3 freeze/thaw cycles by placing them at -80°C for 30 min and then at 37°C for 15 min. Finally, lysed cells were centrifuged at 3,000rpm for 5 min. Supernatant containing virus was filtered with 0.45µm sterile filters and aliquoted in 1mL cryovials. Adenovirus titration was performed with the Adeno-X Rapid Titer kit (631028 Clontech) using manufacturer recommendations. Adenoviral infection of brown preadipocytes was performed as follows:

1. Seed 300,000 brown preadipocytes in a 10cm cell plate. At least one plate per condition is required because infection efficiency is very low.
2. After 6 hours, when they are already attached, infect them with 1000MOI of Ad-GFP or Ad-Cre-GFP.
3. 48 hours after infection, wash cells several times to completely remove viral particles.
4. Trypsinize cells, centrifuge at 500g for 5 min and resuspended in 500µL of culture medium.
5. Sort infected cells against GFP fluorescence (BD FACS Aria Fusion II from the Cytometry Facility of the Barcelona Scientific Park).

7.2.2.5. Generation of PPARγ overexpressing brown preadipocyte cell line

Brown preadipocytes stably expressing HA-PPARγ were generated by retroviral infection into WT immortalized brown preadipocytes. In this case, the SV40-LT used for immortalization was with neomycin resistance, because HA-PPARγ retrovirus expressed puromycin resistance. HA-PPARγ retrovirus were generated using the same protocol than for the SV40-LT retrovirus (section 7.2.2.2). Once PPARγ overexpressing cell line was generated, TP53INP2 C or KO was induced by adenoviral infection as described above (section 7.2.2.4).

7.2.2.6. Cell treatments

In order to activate adrenergic signaling pathway, brown adipocytes were treated with the 1μM CL-316,243 (C5976, Sigma-Aldrich). To induce TP53INP2 knockdown in TP53INP2$^{loxP/loxP}$ UBC-Cre-ERT2 brown preadipocytes, they were treated with 1μM 4-hydroxy-tamoxifen (H7904, Sigma-Aldrich). Chronic PPARγ activation during differentiation was performed including 1μM rosiglitazone during the whole process of differentiation.

7.2.3. Mitochondrial respiration

7.2.3.1. Oxygen consumption measurements in brown adipocytes

Control and TP53INP2 KO brown preadipocytes were plated in SeaHorse Bioscience XF24 plates (3,000 cells/well) and induced to differentiate as described above (section 7.2.2.3). Mitochondrial respiration was evaluated at day 9 of differentiation. Cells were switched to respirometry medium containing DMEM (D5030) supplemented with 1mM glutamine, 2mM pyruvate and 5mM glucose.

Mitochondrial respiration profile was evaluated by measuring oxygen consumption rates (OCR) following these sequential steps:

1. Basal conditions
2. Addition of 1μM oligomycin A to inhibit complex V respiration
3. Addition of two titrations of 0.25μM CCCP each to induce mitochondrial depolarization
4. Addition of 2.5μM antimycin A and 2.5μM rotenone to inhibit complex I and III respiration

Basal respiration is mitochondrial respiration measurement under basal conditions. Proton leak is oligomycin A induced mitochondrial respiration. Maximal respiration is induced upon CCCP addition. ATP production is calculated by the difference

between basal and maximal respiration. Oxygen consumption rates obtained after antimycin A and rotenone addition correspond to non-mitochondrial processes, and thus these values are subtracted to the anterior mentioned. Data are shown as average OCR.

In order to measure NE-induced mitochondrial respiration, OCR was detected under basal and NE-stimulated conditions (1μM). Non-mitochondrial derived OCR was subtracted and measured by adding rotenone and antimycin A. Data are shown as NE-induced OCR increase (ΔOCR).

7.2.3.2. Mitochondrial enriched fractions from brown adipose tissue

In order to measure mitochondrial function in brown adipose tissue, mitochondrial enriched fractions were obtained as follows:

1. Sacrifice mice and dissect iBAT.
2. Homogenize iBAT in ice-cold sucrose buffer using a motor-driven Teflon potter homogenizer, by performing 10 strokes at 1,800 rpm.
3. Centrifuge homogenized iBAT at 740g for 5 min at 4°C.
4. Collect the supernatant and centrifuge again at 740g for 5 min at 4°C. The pellet contain non homogenized material.
5. Collect the supernatant and centrifuge at 9,000g for 15 min at 4°C. Discard the supernatant.
6. Resuspend the mitochondrial pellet in 500μl of sucrose buffer and centrifuge again at 10,000g for 15 min at 4°C. Discard the supernatant.
7. Resuspend the mitochondrial pellet in 200μl of sucrose buffer. This corresponds to the brown adipose tissue mitochondrial enriched fraction.
8. Quantify mitochondrial protein with BCA protein assay.

Table 7. Composition of sucrose buffer to obtain brown adipose tissue mitochondrial enriched fractions. Protease inhibitors are cOmplete EDTA-free (05056489001, Roche).

Sucrose buffer pH 7.4	
Sucrose	250mM
KCl	50mM
EDTA	5mM
$MgCl_2 \cdot 6H_2O$	5mM
$Na_4P_2O_7$	1mM
Protease inhibitors	1tablet/50mL buffer

7.2.3.3. Isolation and permeabilization of muscle fibers

Mitochondrial respiration in skeletal muscle was performed in fibers from tibialis muscle, as it represents a mixed muscle of glycolytic and oxidative fibers. The isolation and permeabilization of the fibers was performed as follows:

1. Sacrifice mice and dissect tibialis muscle. Place it in a tube containing 1ml of ice-cold biopsy preservation solution (BIOPS) buffer.
2. Mechanically separate individual fiber bundles using two pairs of sharp tweezers and permeabilize them for 30 min in 2mL of ice-cold BIOPS buffer containing 50µg/ml saponin.
3. Then wash fiber bundles for 10 min twice with mitochondrial respiration buffer (MiR05 buffer) to remove excess saponin.
4. Finally, dry and weigh individual fibers before transferring them to the oxygraph.

Table 8. BIOPS buffer composition to preserve muscle biopsies.

BIOPS buffer pH 7.1	
CaK_2EGTA	2.77mM
K_2EGTA	7.23mM
Imidazole	20mM
Taurine	20mM
MES	50mM
K_2HPO_4	3mM
$MgCl_2 \cdot 6H_2O$	6.56mM
Na_2ATP	5.77mM
Na_2-phosphocreatine	15mM
DTT	0.5mM

7.2.3.4. High resolution respirometry

Respiration of permeabilized muscle fibers or brown adipose tissue mitochondria was measured at 37°C in MiR05 buffer by high-resolution respirometry with the Oxygraph-2k (Oroboros Instruments, Innsbruck, Austria). Chambers were hyperoxygenated and closed at an O_2 concentration of approximately 500µM. Oxygen limitation of respiration was prevented by maintaining the oxygen levels in the chamber above air saturation in the range of 500 to 200µM, and when required, chamber was re-oxygenated. 250µg of mitochondrial protein was used in the case of brown adipose tissue mitochondria, and 2 to 4mg of fibers for tibialis muscle. All respiration measurements were made on fresh tissues immediately following dissection, and each sample was assayed in duplicate.

Oxygen flux (shown as "Leak" in figures) was measured with 2mM malate and 10mM glutamate, in the absence of ADP. Complex I derived mitochondrial respiration (denoted as "C I" in figures) was evaluated with the addition of ADP

(1mM for iBAT mitochondria and 2.5mM for permeabilized fibers). Finally succinate was added to a final concentration of 10mM to measure electron flow through both complex I and II (denoted as "C I+II" in figures). Complex V inhibition was induced with 0.5µM oligomycin A, uncoupling was induced with 0.1µM FCCP titrations, and complex I inhibition with 0.5µM rotenone. However this treatments were inducing almost negligible effects in oxygen consumption, and because of that they were not considered for calculations. Non mitochondrial respiration levels were subtracted and determined by the addition of 2.5µM antimycin A. In order to ensure the integrity of the outer mitochondrial membrane, 10µM cytochrome c was added before succinate injection to ensure that was not inducing a stimulation in respiration.

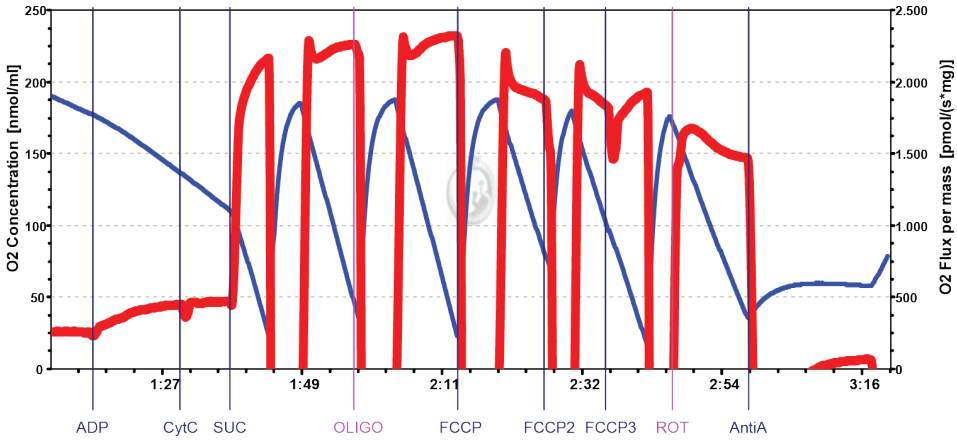

Figure 90. Representative experiment of brown adipose tissue mitochondrial respiration profile. O_2 flux in red shows mitochondrial respiration upon successive addition of ADP, cytochrome C, succinate, oligomycin, FCCP, rotenone and antimycin A. O_2 concentration is in blue. High mitochondrial respiration rates after succinate addition induced a rapid decay in O_2 concentration, and because of that the chamber was re-oxygenated several times.

Table 9. Composition of buffer MiR05 to measure mitochondrial respiration.

MiR05 buffer pH 7.1	
EGTA	0.5mM
$MgCl_2 \cdot 6H_2O$	3mM
K-lactobionate	60mM
Taurine	20mM
KH_2PO_4	10mM
HEPES	20mM
Sucrose	110mM
BSA	1mg/ml

7.2.4. Manipulation and detection of nucleic acids protocols

7.2.4.1. Transformation of competent cells

Competent bacteria heat-shock transformation was used for plasmid amplification. Top10 competent Escherichia coli bacteria were prepared by the laboratory technician. Transformation was performed following this protocol:

1. Mix 100µl of bacteria with 20-40ng of plasmid.
2. Place the tube on ice for 30 min to induce plasmid-bacterial wall contact.
3. Incubate 60-90s at 42°C. The heat-shock is the critical step for efficient transformation.
4. Place the tube again on ice for 2 min.
5. Add 900µl of LB buffer without antibiotic to the tube.
6. Incubate at 37°C for 1 hour to allow bacteria recuperate from the heat-shock.
7. Seed 100µl of the transformation reaction mix in a LB-agar dish

containing the appropriate antibiotic (the most commonly used is 100µg/ml ampicillin).

8. Incubate the plate O/N at 37°C to grow single-cell colonies.

7.2.4.2. Plasmid DNA purification

Maxi-prep was performed to purify high amount of plasmids:

1. Select one individual bacteria colony and picke it with a tip. Place the tip in a starter tube containing 5ml of LB buffer and the appropriate antibiotic.
2. Incubate the starter culture at 37°C with mild shaking for 6 hours.
3. Then, transfer the starter culture to a 2L Erlenmeyer containing 200ml of LB buffer and antibiotic. Grow bacteria at 37°C with mild shaking for 16 hours.
4. Pellet bacteria and purify DNA (MaxiPrep) using the NucleoBond Xtra Maxi Kit (Macherey-Nagel) following manufacturer recommendations.
5. Measure plasmid concentration with the Nanodrop™ 2000/2000c spectrometer (Thermo Scientific) and the ND1000 software (Thermo Scientific).

7.2.4.3. RNA extraction

Total RNA was extracted by homogenization of mouse tissues or cell cultures with TRIzol reagent (Thermo Fisher Scientific) or with Lysis Buffer (PureLink™ RNA Mini Kit) respectively.

Mouse tissues: tissues were placed in a tube with TRizol reagent maintaining a proportion of 20-50mg tissue with 500µl or 50-100mg with 1000µl. Mechanic tissue disruption was induced with a Mini Bead Beater, placing three beads per tube, and performing 2 rounds of 30s each at maximal speed. In the case of white adipose tissue, homogenate was centrifuged at 3,000rpm for 5 min at 4°C. The

infranatant (organic phase) was kept (a lipid layer will stay on the top of the tube, and debris on the bottom). 100µl of chloroform were added per 500µl of TRizol, and the tubes were mixed during 2-3 min and centrifuged at 12,000rpm for 15 min at 4°C. The aqueous phase was transferred to a new tube and was mixed with an equal volume of 70% ethanol (diluted in RNAse-free water).

Cell cultures: cells were homogenized in Lysis buffer supplemented with 1%DTT 2M. A volume of 300µl was used for a well of a 6-well plate or 900µl for a 10cm cell plate. Cells were scraped and cell lysate was passed through a 25G syringe 10 times. The lysate was transferred to an Eppendorf tube and was mixed with an equal volume of 70% ethanol (diluted in RNase-free water).

Once homogenized, RNA from tissues or cells was purified with the PureLink™ RNA Mini Kit columns (Thermo Fisher Scientific) following manufacturer instructions. All the steps can be performed at room temperature:

1. Transfer up to 700µl of the sample to the spin cartridge with a collection tube.
2. Centrifuge 12,000g for 30s and discard the flow-through. Repeat step 1 and 2 until all the sample is loaded into the column.
3. Add 700µl of Wash Buffer I to the spin cartridge.
4. Centrifuge 12,000g for 30s and discard the flow-through.
5. DNase solution is prepared mixing 8µl of Pure Link 10x DNase Buffer (Thermo Scientific) with 10µl of DNase stock solution and 62µl of RNase-free water. Add 80µl of DNase solution per column.
6. Incubate 15 min.
7. Add 500µl of Wash Buffer II to the spin cartridge.
8. Centrifuge 12,000g for 30s and discard the flow-through.
9. Repeat steps 7 and 8 once.
10. Dry the membrane with bound RNA by centrifuging the spin cartridge at 12,000g for 2 min.

11. Add 30µl of RNase-free water warmed at 70°C and incubate 1 min.
12. Elute in an RNase-free collection tube by centrifugation at 12,000g for 2 min.
13. Directly use RNA or store at -80°C.

7.2.4.4. RNA reverse transcription

RNA samples were maintained always on ice and were preserved at -80°C. RNA concentration was measured with Nanodrop™ 2000/2000c spectrometer (Thermo Scientific) and the ND1000 software (Thermo Scientific). Sample purity was ensured when an >1.8 A260/A280 absorbance ratio was detected.

An amount of 2µg of RNA was reverse-transcribed with the SuperScript™ II RT kit (Thermo Fisher Scientific) with a 2720™ Thermal Cycler (applied Biosystems):

1. Mix the volume corresponding to 2µg of RNA with 1µl of oligodT (500µg/ml) and RNase-free water to a volume of 11µl in PCR tubes.
2. Incubate 5 min at 65°C.
3. Prepare a master mix containing: 4µl 5x First-Strand Buffer, 2µl 0.1M DTT, 1µl RNase OUT™ (40U/µl) and 1µl of 10mM dNTPs (dATP, dCTP, dGTP and dTTP 1:1:1:1).
4. Place the PCR tubes on ice and add 8µl of the master mix per sample.
5. Incubate 2 min at 42°C.
6. Add 1µl of SuperScript™ II reverse transcriptase (200U/µl) per sample.
7. Incubate 50 min at 42°C.
8. Denaturalize retrotranscriptase 15 min at 70°C.
9. Generated cDNA is cooled to 4°C, diluted 1/40 to 2.5ng/µl with Milli-Q H_2O and stored at -20°C.

7.2.4.5. Quantitative real-time PCR

Gene expression was analyzed by quantitative real-time PCR using Power SYBR™ Green PCR Master Mix (Life Technologies) and ABI Prism 7900 HT real-time PCR system (Applied Biosystems). ARP was used as internal control for normalization. Primers used for qPCR are listed on Table 2. Each reaction was performed in 10µl of a 384-wells plate and contained 4µl of cDNA 2.5ng/µl, 0.6µl of 10µM primers (forward and reverse), 5µl of Power SYBR™ Green PCR Master Mix and 0.4µl of Milli-Q H_2O. Melting curve was analyzed to verify primer specificity.

7.2.4.6. Transcriptomic analysis

Microarray services were provided by the IRB Barcelona Functional Genomics Core Facility, including quality control tests of total RNA using an Agilent Bioanalyzer and nanodrop spectrophotometry. Briefly, complementary DNA library preparation and amplification were performed from 25ng total RNA using WTA2 (Sigma-Aldrich) with 17 cycles of amplification. cDNA (8µg) was subsequently fragmented by DNaseI and biotinylated by terminal transferase obtained from the GeneChip Mapping 250K Nsp Assay Kit (Affymetrix). The hybridization mixture was prepared following Affymetrix's protocol. Each sample was hybridized to a Mouse Genome 430 PM strip (Affymetrix). Arrays were washed and stained in a Fluidics Station 450 (Fluidics protocol FS450_002) and scanned in a GeneChip Scanner 3000 (both Affymetrix) following the manufacturer's recommendations. CEL files were generated from DAT files using GCOS software (Affymetrix).

Processing of microarray samples was carried out using packages affy (Gautier et al., 2004) and affyplm (Bolstad et al., 2005) from Bioconductor (Gentleman et al., 2004). Raw cel files were normalized using RMA background correction and summarization (Irizarry et al., 2003). Technical metrics PM MED, PM IQR, RMA IQR and RNA DEG described in (Eklund and Szallasi, 2008) were computed and recorded as additional features for each sample.

Differential expression between TP53INP2-KO vs LoxP conditions was performed using the moderated t-statistics by empirical Bayes shrinkage method (Ritchie et al., 2015). Batch representing the strip and Eklund metric RNA DEG were both included as adjusting variables in the model to correct for technical variability.

The moderated t-statistic information (positive change when TP53INP2-KO was higher than LoxP and negative change when TP53INP2-KO was lower than LoxP) was considered to rank all genes in the genome and Gene set enrichment analysis (GSEA) was performed using the Broad Institute's implementation (Subramanian et al., 2005) on the KEGG (Kyoto Encyclopedia of Genes and Genomes) collection (Kanehisa and Goto, 2000).

In order to compare transcriptomic analysis from LoxP and KO^{Myf5} with the transcriptomic study aimed at studying the physiological gene expression modulation by thermoneutrality, we downloaded paired-end RNA-seq data from the GSE86338 study (Bai et al., 2017). Only samples GSM 2300503 (control 1), GSM 2300504 (control 2), GSM 2300505 (30oC7days 1), GSM 2300506 (30oC7days 2) were considered for normalization and data analysis. Files were aligned against the mm10 genome with STAR 2.3.0e in strand-specific paired-end mode with default parameters (Dobin et al., 2013). Alignments were sorted and indexed with sambamba v0.5.1 (Tarasov et al., 2015). Counts per genomic feature were computed with the R package casper (Rossell et al., 2014), function wrapKnown. A quantile normalization was applied to the resulting rpkm expression matrix.

Differential expression between 30°C7days vs Control conditions was performed on the normalized data using the moderated t-statistics by empirical Bayes shrinkage method (Ritchie et al., 2015). A size factor that measured the total number of reads per sample was included as adjusting variable in the model.

7.2.5. Protein detection protocols

7.2.5.1. Protein extraction

Total cellular protein extracts were prepared for western blot analysis.

Cell culture protein extracts:

Cells were rinsed twice with PBS while being maintained on a cold surface. Cells were lysed by scraping in a lysis buffer (250µl per 10cm cell dish) containing 50mM Tris-HCl pH 8.0, 150mM NaCl, 1% NP-40, 0.1% SDS and 1mM EDTA and freshly supplemented with phosphatase inhibitors 1mM Na_3VO_4, 5mM $Na_4P_2O_7$ and 50mM NaF, and protease inhibitor cocktail (11836153001 Complete-Mini, Roche). Lysates were passed through a 25g syringe 10 times and were centrifuged at 16,000g for 30 min at 4°C. Supernatant containing soluble proteins was stored at -20°C.

Brown adipose tissue protein extracts:

20-40mg of tissue was weighted and placed inside an Eppendorf tube. Tissue was homogenized with a Polytron PT 2500E homogenizer (Kinematica) in a lysis buffer (300µl/20mg tissue) containing 50mM Tris-HCl pH 7.5, 150mM NaCl, 1% Triton x-100 and 1mM EDTA and freshly supplemented with phosphatase inhibitors 1mM Na_3VO_4, 5mM $Na_4P_2O_7$ and 50mM NaF, and protease inhibitor cocktail (11836153001 Complete-Mini, Roche). Lysates were incubated for 1 hour at 4°C on an orbital rotor and centrifuged at 16,000g for 20 min at -4°C. This temperature helps in the solidification of intracellular lipids that will form a layer on the top of the tube. Soluble protein fraction was took avoiding the lipid fraction and was placed in a clean Eppendorf tube. Protein extracts were stored at -80°C.

7.2.5.2. Protein quantification and sample preparation

Protein lysates were quantified with the Pierce BCA Protein assay kit (Thermo Fisher Scientific). A standard curve between 0 mg/ml to 8mg/ml using the 2mg/ml BSA solution from the kit was used to determine the relation between absorbance and protein concentration. 1µl of protein standard or protein lysate was placed in a well from a 96-well plate in triplicate, and then 200µl of the reaction mixture (solutions A+B at 50:1) was added to each well using a multichannel pipette to avoid differential time of incubation between samples. The plate was incubated 30 min at 37°C and then the absorbance at 562nm was measured with a plate reader *Sunrise* (Tecan). Protein concentration was calculated by interpolation from the standard curve.

Samples for western blot contained 40µg of protein and loading sample buffer with 10mM DTT. They were adjusted to the same final volume with Milli-Q H_2O. Samples were boiled 5 min at 95°C before loading into the SDS-PAGE gel.

7.2.5.3. Western blot

Proteins were resolved on SDS-PAGE gels of different acrylamide concentration depending on the molecular weight of the protein of interest (usually 7.5%, 10%, 12.5% or 15%). Samples were run at 80-120V in running buffer (25mM Tris-base, 200mM glycine, 0.1% w/v SDS) in parallel with the molecular weight marker Spectra™ Multicolor Broad Range Protein Ladder (Thermo Fisher Scientific). When the blue colour front of the loading buffer escaped the gel, the electrophoresis was stopped. Then, resolved proteins were transferred onto Immobilon PVDF membranes (Milipore) at 250mA for 1.5h in transfer buffer (25mM Tris-HCl pH 8.3, 200mM glycine and 20% v/v methanol). Membranes were blocked in 5% milk in TBS-Tween20 (10mM Tris-HCl pH 7.5, 100mM NaCl and 0.1% Tween20) for 1 hour at room temperature. Primary antibodies diluted in 5% milk TBS-Tween solution were incubated O/N at 4°C with rotation. The following day, membranes

were washed three times during 5 min each with TBS-Tween20 and then incubated with the secondary HRP-conjugated antibody diluted in 5% milk TBS-Tween solution during 1 hour at room temperature. Then, membranes were washed three times during 10 min each with TBS-Tween20. Protein detection was performed by incubating membranes 5 min with the chemiluminiscence solution Amersham™ ECL Western Blotting Detection Reagents (GE Healthcare). Finally membranes were transferred to a developing cassette and in the dark room were exposed to hypersensitive films. Some membranes were stripped to reuse with other primary antibodies with the RestoreTM Western Blot Stripping Buffer (Thermo Fisher Scientific).

7.2.5.4. Luciferase reporter assay

PPARγ transcriptional activity was assayed in brown preadipocytes with a luciferase reporter plasmid encoding the PPAR response element (PPRE). 50,000 cells/well were plated on a 6-well plate and the following day were transfected with PEI MAX 40K (Polysciences Inc.). Transfections included 1μg of the reporter plasmid PPRE-TK-Luc and, when indicated, 500ng of PPARγ. To normalize for transfection efficiency, 100ng of Renilla plasmid was used. Transfection medium was incubated for 24 hours. Then, cells were treated with vehicle or with 10μM rosiglitazone for 24 hours. Cells were scraped with 100μl/well Luciferase Cell Culture Lysis Reagent (Promega) and incubated with mild shaking 15 min at room temperature. 20μl of the cell lysate was placed in a luminometer tube and luciferase and Renilla activity were assayed with 10μl of Dual-Glo® Luciferase and 10μl of Dual-Glo Stop&Glo® reagent (buffer:substrate 100:1) respectively from the Dual-Glo® Luciferasa Assay System (E2920, Promega). Chemiluminiscence was detected during 5s just after the addition of the corresponding reagent with a luminometer Lumat LB 9507 (Berthold Technologies).

Transfection was performed as follows (conditions per one well):

1. Dilute 1µg of DNA in 150µl OptiMEM and incubate 5 min.
2. Dilute 3µl of 1mg/ml PEI MAX 40K in 150µl OptiMEM and incubate 5 min.
3. Mix DNA and PEI containing solutions and incubate 30 min.
4. Add transfection mix to cells.

7.2.5.5. Detecting PPARγ turnover

To determine PPARγ2 protein turnover, brown preadipocytes stably overexpressing HA-PPARγ2 were pre-treated for 1 hour with proteasome inhibitors 10µM MG-132 (Merck) and 0.1µM Epoxomicin (R&D Systems), followed by treatment with 10µM rosiglitazone (R2408, Sigma-Aldrich) for 4 hours. Total cell lysates were collected at the end of 5 hours of proteasome inhibition, and were obtained as described in section 7.2.5.1.

7.2.5.6. Detecting PPARγ ubiquitination

In order to detect PPARγ ubiquitination we used brown preadipocytes with stable overexpression of HA-PPARγ. HA-PPARγ was pulled down with HA-antibody conjugated beads under denaturing conditions, to ensure that PPARγ was not bound to ubiquitinated proteins. One 150mm cell dish was used per condition to have enough sensibility. When indicated, cells were transfected with His-ubiquitin plasmid by Lipofectamine 3000 (Thermo Fisher Scientific) to increase ubiquitin-proteasome flux. Transfection was performed as follows (per 150mm cell dish):

1. Tube 1: mix 750µl OptiMEM + 40µl P3000 reagent + 35µg plasmid
2. Tube 2: mix 750µl OptiMEM + 29.6µl Lipofectamine3000
3. Add tube 1 onto tube 2 and incubate 5 min
4. Add transfection mix to cells.

Transfection medium was incubated for 48 hours, and then cells were let to recover for 24 hours in complete medium. When indicated, cells were treated with vehicle or proteasome inhibitors 10μM MG-132 and 0.1μM Epoxomicin for 5 hours. One hour after the initiation of proteasome inhibitor treatment, cells were treated with vehicle or with 10μM rosiglitazone for 4 hours. Denaturing lysis buffer was prepared freshly and contained 50mM Tris-HCl pH 7.4, 150mM NaCl, 1mM EDTA, 1% Igepal, 0.5% sodium deoxycholate and 0.1% sodium dodecyl sulphate, supplemented with freshly added 10 mM N-Ethylmaleimide (Sigma-Aldrich), protease (Complete-EDTA free, Roche) and phosphatase (Set IV, Merck) inhibitor cocktails. Then cells were lysed and processed as follows:

1. Wash cell plates with PBS twice
2. Scrap cells in denaturing lysis buffer (200μl per 150mm cell dish), and collect lysate into a clean Eppendorf tube.
3. Incubate on ice for 10 min.
4. Sonicate 5 pulses of 5 seconds each while maintaining the tube on ice.
5. Centrifuge at 16,000g for 20 min at 4°C.
6. Collect supernatant and determine protein concentration by BCA Protein assay.
7. Prepare samples with at least 500μg of protein (use the maxim amount possible). Fill up all samples with denaturing lysis buffer to the same final volume.
8. Take the input fraction from each sample (IN) (a minimum of 80μg of protein to run 2 SDS-PAGE gels).
9. Take 20μl anti-HA-antibody agarose beads suspension (A2095, Sigma Aldrich) per sample. The suspension contains beads:buffer 1:1 (20μl of suspension will result in a volume of 10μl beads).
10. Wash the beads x3: add 500μl denaturing lysis buffer and centrifuge at 2,000g for 1 min at 4°C.
11. Resuspend the beads with 10μl denaturing lysis buffer. Add 20μl of beads

suspension per sample. Cut the end of the tip to facilitate pipetting.

12. Incubate O/N at 4°C on an orbital rotor.
13. The following day, centrifuge samples at 2,000g for 1 min at 4°C. Collect the supernatant that contains unbound protein (SN).
14. Wash the beads x5: add 500µl denaturing lysis buffer and centrifuge at 2,000g for 1 min at 4°C.
15. Remove supernatant as much as possible. Add 40µl LSB+DTT 2x per sample to elute pulled down proteins.
16. Boil samples at 95°C for 3 min and centrifuge at 2,000g for 1 min at 4°C.
17. The supernatant contains the pulled down fraction (IP).
18. Load IN (40µg), SN (40µg) and IP (all) fractions to 10% SDS-PAGE gels and detect HA-PPARγ and ubiquitin levels with the corresponding antibodies.

7.2.6. Data representation and statistics

In bar dot plots, each individual value is represented together with the average ± standard error per group. Data from XY plots are represented with the average ± standard error per group. Statistical analysis of the data presented was performed using the Student t-test. Statistical analysis was conducted only to data sets with an n≥3 independent experiments.

Calorimetry data was normalized with an average mouse weight determined using ANCOVA with IBM SPSS Statistics program, taking into account genotype, body weight and VO_2, VCO_2 or EE per animal. The statistical analysis compared the relation of this two magnitudes between control and KO group, to detect whether the difference in VO_2, VCO_2 or EE was dependent on the body weight (p-val>0.05) or on the genotype (p-val<0.05).

For the statistical comparison of the ΔVO_2 curves (NE-induced thermogenic capacity), we fitted a random slope mixed effects model separately for 22°C

measures and 30°C measures that take into consideration the longitudinal structure of the data. We considered the ΔVO_2 as the dependent variable. The time, the genotype (LoxP or KO^{Myf5}) and the interaction of the two were taken as independent variables. The time linear effect difference between KO^{Myf5} and LoxP was estimated by a REML procedure using the lme function from the nlme R package. Although only time points between 56 min to 100 min were considered for this analysis, obtained results were consistent for other starting times.

RESUM EN CATALÀ

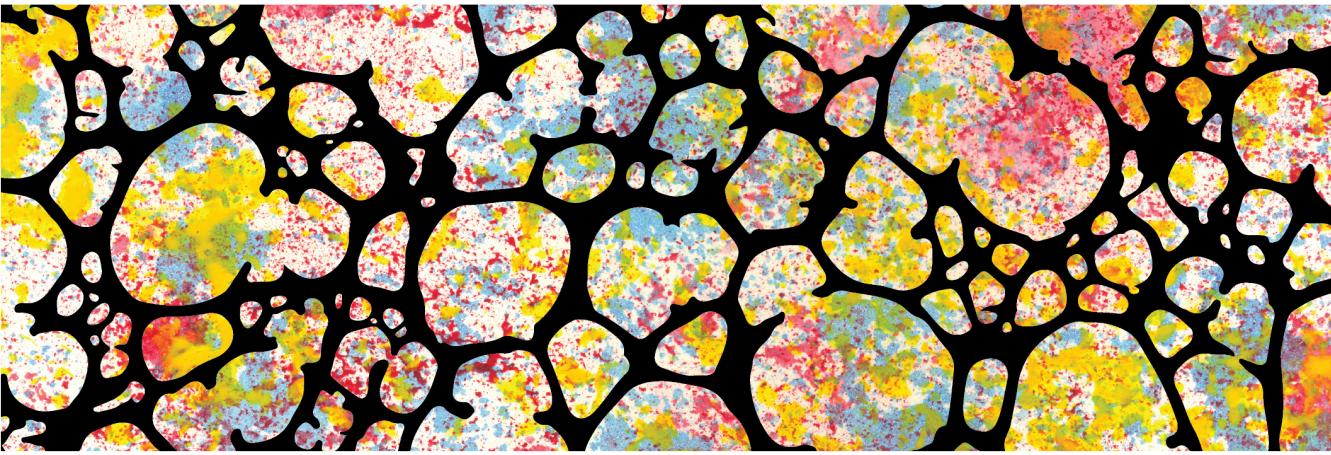

8.1. Introducció

El teixit adipós va ser considerat durant molt de temps com un òrgan passiu involucrat únicament en l'acumulació de greix. En canvi, avui en dia es coneix que aquest teixit és dinàmic i està involucrat en moltes d'altres funcions que afecten l'homeòstasi d'un organisme. El teixit adipós està distribuït en diferents dipòsits i tradicionalment s'ha classificat en dos tipus. Per una banda, el teixit adipós blanc es caracteritza per la seva alta capacitat d'emmagatzematge d'energia en forma de lípids, però també allibera citocines involucrades en la regulació del metabolisme global i la sensibilitat a la insulina (Kershaw and Flier, 2004). Per altre banda, el teixit adipós marró té una capacitat menor d'acumular greixos i està implicat en la dissipació d'energia gràcies a la seva funció termogènica. Així doncs, tot i que tenen funcions oposades, un adequat equilibri entre les funcions del teixit adipós blanc i marró és necessari per a mantenir el balanç energètic d'un organisme. Aquesta tesi s'ha centrat en l'estudi del teixit adipós marró.

Tot i que l'existència del teixit adipós marró es coneix des del 1551, no va ser fins la dècada passada quan es va descriure la presència de teixit adipós marró funcional en humans adults sans (Nedergaard et al., 2007; Cypess et al., 2009; van Marken Lichtenbelt et al., 2009; Virtanen et al., 2009; Zingaretti et al., 2009). En rosegadors i hibernadors el teixit adipós marró hi és present durant tota la vida, mentre que en d'altres mamífers, com és el cas dels humans, la seva funció disminueix amb l'edat. El principal dipòsit de teixit adipós marró en ratolins es troba en la zona interescapular, i d'altres més petits es localitzen en la zona cervical, axil·lar, perirenal i periaòrtica. En humans, en canvi, el dipòsit que presenta major activitat és el localitzat en la zona supraclavicular. Altres dipòsits menors es situen en la zona cervical, axil·lar i paravertebral. El teixit adipós marró està format principalment per adipòcits marrons, però també s'hi troben cèl·lules precursores, o preadipòcits, cèl·lules vasculars i un gran nombre de nervis del sistema nerviós simpàtic (SNS) (Fawcett, 1952; Géloën et al., 1990; Cinti, 2005).

El paper fisiològic del teixit adipós marró és el de protegir l'organisme de canvis ambientals, com ara l'exposició al fred o l'exposició prolongada a una dieta hiperlipídica. En aquestes condicions, la termogènesi no associada a tremolor, o també anomenada termogènesi adaptativa, s'activa en els adipòcits marrons per tal de mantenir la temperatura corporal o per prevenir una acumulació excessiva de lípids (Himms-Hagen, 1990). Aquests dos processos es coneixen com a termogènesi adaptativa induïda pel fred o per la dieta, respectivament. La capacitat termogènica d'aquest teixit ve conferida per la proteïna desacoblant 1 (UCP1). La proteïna UCP1 és un transportador de protons transmembrana que es localitza a la membrana mitocondrial interna. Gràcies a la seva capacitat transportadora desacobla la cadena transportadora d'electrons de la síntesi d'ATP, alliberant finalment l'energia en forma de calor (Lin and Klingenberg, 1980; Cannon et al., 1982; Lowell and Spiegelman, 2000; Cannon and Nedergaard, 2004).

La funció termogènica del teixit adipós marró està regulada principalment per l'acció del SNS el qual allibera catecolamines en resposta al fred o a la dieta. La norepinefrina (NE), la catecolamina amb major capacitat d'activar la termogènesi, interacciona amb els receptors adrenèrgics situats a la membrana plasmàtica dels adipòcits marrons i dona lloc a l'augment dels nivells intracel·lulars de AMP cíclic (cAMP) (Zhao et al., 1997). L'acumulació de cAMP activa la funció de la proteïna quinasa A (PKA), la qual fosforila i indueix la lipasa sensible a hormones (HSL) per començar la hidròlisi dels triglicèrids (TGA) acumulats (Holm, 2003; Souza et al., 2007). Al mateix temps, la PKA també fosforila molècules senyalitzadores com ara el factor de transcripció CREB i la proteïna quinasa p38. D'aquesta manera s'incrementa l'expressió del co-activador del receptor activador de la proliferació de peroxisomes (PGC1α), el qual controla la biogènesi mitocondrial. A més a més, l'acció de CREB i PGC1α incrementen l'expressió de UCP1. Així doncs, els àcids grassos generats seran oxidats en els mitocondris i gràcies a la funció de la proteïna UCP1, s'allibera l'energia en forma de calor. El fet d'estimular la lipòlisi també dona lloc a una activació de la funció de UCP1, la qual es veu positivament regulada per

àcids grassos (Prusiner et al., 1968).

El teixit adipós marró es desenvolupa en l'etapa fetal ja que en el moment del naixement els nounats requereixen un mecanisme termogènic actiu per tal de sobreviure. Els preadipòcits marrons originen d'una cèl·lula precursora mesenquimàtica que expressa Myf5, Pax7 i EN1, i és comú amb la del múscul esquelètic (Atit et al., 2006; Timmons et al., 2007; Lepper and Fan, 2010; Sanchez-Gurmaches and Guertin, 2014). La determinació cap al llinatge de preadipòcit està regulada pels gens EBF2, EHMT1, BMP7 i PRDM16, els quals no només indueixen l'expressió dels gens característics dels adipòcits marrons, sinó també bloquegen l'expressió dels gens musculars (Seale et al., 2007, 2008; Tseng et al., 2008; Kajimura et al., 2009; Ohno et al., 2013; Schulz et al., 2013; Wang et al., 2014). Tot i que el teixit adipós blanc i el marró tenen orígens diferents, la seva adipogènesi està principalment controlada pels factors de transcripció PPARγ i C/EBPβ (Barak et al., 1999; Rosen et al., 1999; Karamitri et al., 2009). En el cas del teixit adipós marró, la interacció d'aquests dos factors de transcripció amb els co-reguladors específics del teixit PRDM16 i PGC1α, són els que donaran lloc a l'activació dels gens característics del teixit i que el diferencien del teixit adipós blanc (Kajimura et al., 2009). A més, la proteïna PGC1α coactiva l'activitat de PPARγ per tal d'induir l'expressió de UCP1, proteïna característica del teixit adipós marró.

La proteïna PPARγ juga un paper essencial en l'adipogènesi. En aquest sentit, s'ha descrit que la seva absència impedeix la formació del teixit adipós, mentre que l'augment de la seva quantitat mitjançant manipulació genètica és capaç de donar caràcter adipogènic a cèl·lules no adiposes (Barak et al., 1999; Rosen et al., 1999; Koutnikova et al., 2003). De la mateixa manera, la disminució de l'activitat PPARγ per mutació s'associa a una menor capacitat termogènica del teixit adipós marró (Gray et al., 2006). Pel contrari, l'activació de PPARγ amb lligands sintètics dona lloc a l'augment de la maquinària termogènica del teixit adipós marró (Petrovic et al., 2008; Ohno et al., 2012).

El balanç energètic és el resultant de l'energia ingerida i de l'energia dissipada mitjançant el metabolisme basal, l'activitat física i la termogènesi. D'aquesta manera, la funció termogènica del teixit adipós marró té un impacte directe en el balanç energètic i per això té la capacitat de modular el guany de pes corporal. En aquesta direcció, la disfunció del teixit adipós marró s'associa al desenvolupament d'obesitat com a conseqüència de la disminució de la despesa energètica (Lowell et al., 1993). De manera oposada, també s'ha descrit que l'augment de la funció del teixit adipós marró protegeix contra el sobrepès (Kopecky et al., 1995; Guerra et al., 1998; Cederberg et al., 2001).

Els àcids grassos són el principal substrat per a la termogènesi, tot i això, en condicions d'activació del SNS, els adipòcits marrons també capten gran quantitat de glucosa de la circulació (Cannon and Nedergaard, 2004). En els adipòcits marrons la glucosa es converteix o bé en piruvat, per tal de mantenir els nivells ATP cel·lulars, o en àcids grassos, per tal de reomplir les reserves de lípids intracel·lulars (Ma and Foster, 1986). Això situa al teixit adipós marró com a un component actiu en la regulació del metabolisme de la glucosa i la sensibilitat a la insulina. De fet, estudis utilitzant trasplantaments de teixit adipós marró han demostrat que aquest és capaç de revertir la resistència a la insulina induïda per la dieta (Stanford et al., 2013).

Amb el descobriment de que els humans tenen dipòsits funcionals de teixit adipós marró, el camp va atraure un gran interès científic i actualment, la informació disponible sobre la biologia de la cèl·lula adiposa marró ha augmentat exponencialment. De la mateixa manera que amb ratolins, la funció del teixit adipós marró humà es correlaciona negativament amb la quantitat total de greix o amb l'índex de massa corporal (van Marken Lichtenbelt et al., 2009; Saito et al., 2009; Vijgen et al., 2011), i positivament amb la tolerància t a la glucosa (Lee et al., 2010; Jacene et al., 2011; Ouellet et al., 2011; Blondin et al., 2015; Iwen et al., 2017). També s'ha detectat que les persones amb obesitat tenen menys quantitat i activitat de teixit adipós marró (Orava et al., 2013).

Totes aquestes evidencies situen al teixit adipós marró com a una diana potencial per al tractament de l'obesitat i la diabetis de tipus 2. Per tant, el coneixement del seu desenvolupament així com de la seva activació termogènica és de gran rellevància per al disseny de tractaments eficients contra aquests trastorns metabòlics.

El gen *Tp53inp2* va ser identificat a partir d'un estudi genètic en múscul esquelètic orientat a descobrir gens amb expressió disminuïda en condicions d'obesitat i diabetis de tipus 2. La proteïna TP53INP2 s'expressa abundantment en el múscul esquelètic humà i de rosegadors, i en menor quantitat en d'altres teixits metabòlicament actius com ara el cor, el fetge, el cervell i el teixit adipós blanc. Els primers estudis funcionals de TP53INP2 van demostrar que és una proteïna localitzada principalment al nucli en condicions basals, i que en resposta a estrès, com ara la privació d'aminoàcids, surt al citoplasma (Baumgartner et al., 2007). A nivell molecular, TP53INP2 és capaç d'estimular el procés d'autofàgia (Mauvezin et al., 2010; Sala et al., 2014; Romero et al., 2018), d'induir apoptosi (Ivanova et al., 2019) i de co-activar l'activitat transcripcional de receptors nuclears d'hormones, com ara el receptor activador de la proliferació de peroxisomes (PPAR) i el receptor d'hormona tiroïdal (TR) (Baumgartner et al., 2007; Francis et al., 2010; Sancho et al., 2012). A més a més, TP53INP2 facilita la degradació de proteïnes ubiqüitinades mitjançant la seva interacció amb cadenes de poli-ubiqüitina i amb E3 ubiqüitines lligases, com ara TRAF6 (Sala et al., 2014; Ivanova et al., 2019). Des d'un punt de vista fisiològic, s'ha descrit que TP53INP2 regula la massa muscular (Sala et al., 2014) i bloqueja l'adipogènesi del teixit adipós blanc (Romero et al., 2018).

8.2. Objectius

Les evidencies obtingudes prèviament a l'inici d'aquesta tesi doctoral situaven a TP53INP2 com a un regulador de la massa muscular i del pes corporal a través de la repressió de l'adipositat. Donat que el teixit adipós marró té un precursor comú amb el múscul esquelètic, i que és un teixit amb una funció dissipadora

d'energia capaç d'impactar el balanç energètic, el principal objectiu postulat en aquesta tesi doctoral va ser el de determinar si TP53INP2 té un paper regulador en el metabolisme del teixit adipós marró. Per això es van plantejar els següents objectius específics:

1. Estudiar la regulació de l'expressió de TP53INP2 en el teixit adipós marró i caracteritzar la seva funció en preadipòcits marrons en cultiu.

2. Avaluar l'impacte de l'ablació genètica de TP53INP2 en teixit adipós marró en models de ratolí.

3. Determinar els mecanismes moleculars implicats en la regulació de les cèl·lules adiposes marrons a través de TP53INP2.

8.3. Resultats i discussió

8.3.1. L'activitat termogènica modula l'expressió de TP53INP2 en teixit adipós marró

L'activitat del teixit adipós marró respon a canvis en la temperatura ambient: s'indueix quan un organisme s'exposa a baixes temperatures per tal de mantenir la temperatura corporal, i s'inhibeix quan la temperatura ambient és igual o superior a la temperatura termoneutral (Smith and Roberts, 1964; Donhoffer and Szelényi, 1967; Gordon, 1990; Thomas and Palmiter, 1997). La dieta també té un paper activador de la termogènesi, amb l'objectiu de prevenir una acumulació excessiva de lípids (Mercer and Trayhurn, 1984; Divakaruni et al., 2012; Fedorenko et al., 2012; García-Ruiz et al., 2015).

Els resultats obtinguts en aquesta tesi doctoral demostren que l'expressió de *Tp53inp2* és elevada en teixit adipós marró interescapular (iBAT). La seva expressió en aquest teixit és comparable amb la del múscul esquelètic (Figura 1.

Els nivells d'expressió de Tp53inp2 en iBAT i múscul esquelètic són comparables. Nivells relatius de ARNm de Tp53inp2 en quàdriceps (Quadri), teixit adipós blanc inguinal (ingWAT) i teixit adipós marró interescapular (iBAT) de ratolí (n=4-8). Les dades estan representades com a mitjana ± error estàndard. *p<0.05 vs. ingWAT.), la qual cosa és coherent amb el fet que ambdós teixits provenen d'una mateixa cèl·lula precursora (Timmons et al., 2007).

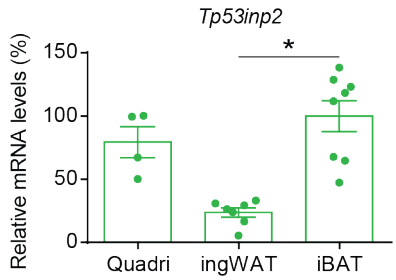

Figura 1. Els nivells d'expressió de *Tp53inp2* en iBAT i múscul esquelètic són comparables. Nivells relatius de ARNm de *Tp53inp2* en quàdriceps (Quadri), teixit adipós blanc inguinal (ingWAT) i teixit adipós marró interescapular (iBAT) de ratolí (n=4-8). Les dades estan representades com a mitjana ± error estàndard. *p<0.05 vs. ingWAT.

Pel que fa a la regulació de l'expressió de TP53INP2 hem determinat que els seus nivells de ARNm s'indueixen en situacions d'activació termogènica aguda, com ara l'exposició al fred (Figura 2A), o en circumstàncies de reclutament prolongat, com per exemple períodes continuats amb dieta rica en greixos (HFD) (Figura 2B). Contràriament, l'expressió de *Tp53inp2* es veu disminuïda en condicions en que l'activitat termogènica és mínima, com ho és en un ambient termoneutral (Figura 2C). Els gens termogènics *Ucp1, Pgc1α* i *Prdm16* van ser usats per tal de comprovar que la termogènesi es veia augmentada o disminuïda en les condicions experimentals utilitzades.

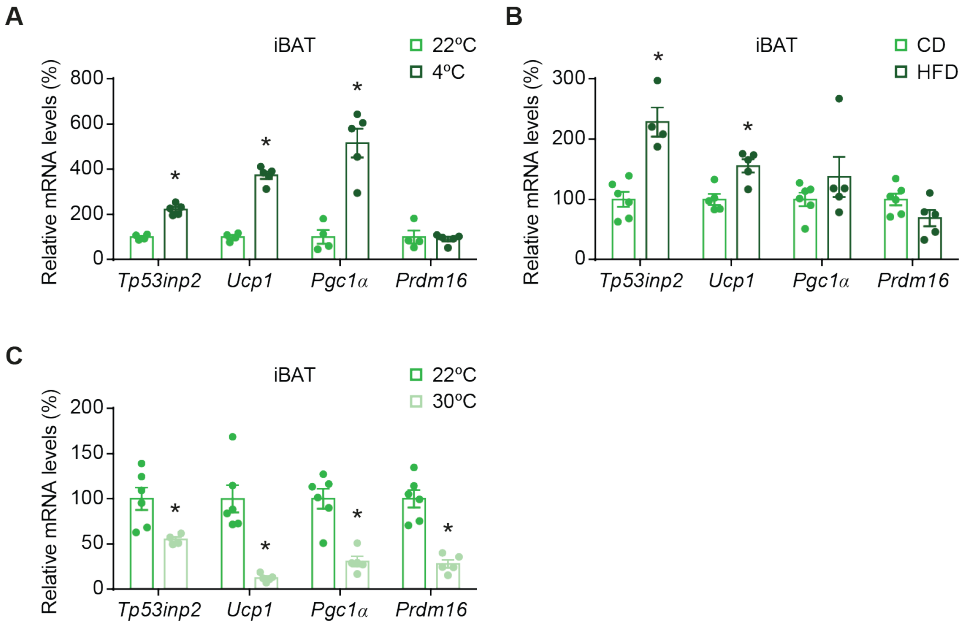

Figura 2. L'expressió de *Tp53inp2* es modula en funció de l'activitat termogènica. Nivells relatius de *Tp53inp2*, *Ucp1*, *Pgc1α* i *Prdm16* en teixit adipós marró interescapular de ratolí. (A) Ratolins estabulats a 22°C o a 4°C durant 10 hores (n=4-5). (B) Ratolins estabulats a 22°C alimentats amb una dieta normal (CD) o amb una dieta rica en greixos (HFD) (n=5-6). (C) Ratolins estabulats a 22°C o a 30°C durant 5 mesos (n=5-6). Les dades estan representades com a mitjana ± error estàndard. *p<0.05 vs. 22°C o CD.

El SNS és el principal regulador de la senyalització adrenèrgica en els adipòcits marrons per tal d'activar la termogènesi. La norepinefrina interacciona amb els receptors β3-adrenergics, la qual dona lloc a una acumulació dels nivells intracel·lulars de cAMP. Això indueix una resposta lipolítica, i els àcids grassos alliberats finalment es degraden de forma desacoblada en els mitocondris (Thomas and Palmiter, 1997; Cannon and Nedergaard, 2004). Així doncs, vam voler estudiar si la via adrenèrgica estava involucrada en la regulació de l'expressió de TP53INP2. Amb aquest objectiu, adipòcits marrons en cultiu van ser tractats amb un agonista β3-adrenergic (CL) durant 4 hores i es van analitzar els nivells de ARNm. Els resultats obtinguts demostren que *Tp53inp2* es veu modulat per la via adrenèrgica, tot i que amb menor intensitat que *Ucp1* i *Pgc1α* (Figura 3).

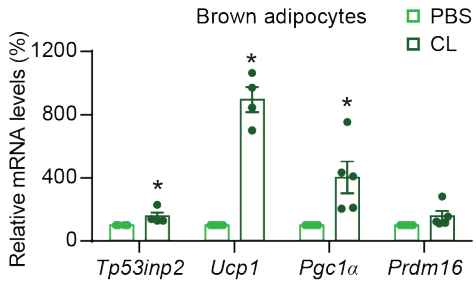

Figura 3. L'expressió de *Tp53inp2* es veu augmentada per estimulació adrenèrgica. Nivells relatius de *Tp53inp2*, *Ucp1*, *Pgc1α* i *Prdm16* en adipòcits marrons tractats amb solvent (PBS) o amb l'agonista β3-adrenèrgic CL-316,243 (CL) durant 4 hores (n=4). Les dades estan representades com a mitjana ± error estàndard. *p<0.05 vs. PBS.

Els nivells de la proteïna TP53INP2 també augmenten en condicions de termogènesi induïda per la dieta (Figura 4). En canvi, els nivells de proteïna TP53INP2 no es veuen alterats en condicions de baixa activitat termogènica. Això significa que en condicions de termoneutralitat, l'expressió de TP53INP2 es manté per una via diferent a l'adrenèrgica, o que TP53INP2 té d'altres funcions en el teixit adipós marró.

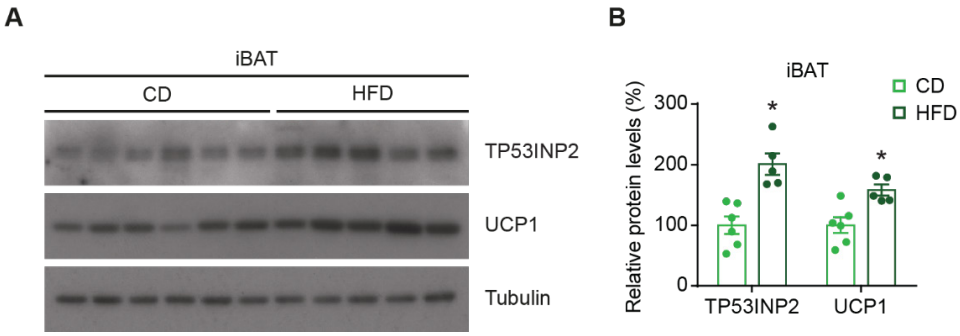

Figura 4. La proteïna TP53INP2 es modula per HFD. (A) Anàlisi per Western blot i (B) quantificació del contingut de TP53INP2 i UCP1 en teixit adipós interescapular (iBAT) de ratolins estabulats a 22°C alimentats amb una dieta normal (CD) o amb dieta rica en greixos (HFD) durant 16 setmanes (n=5-6). Les dades estan representades com a mitjana ± error estàndard. *p<0.05 vs. CD.

Aquestes dades suggereixen que TP53INP2 és necessari per a l'activitat termogènica del teixit adipós marró. Algunes de les funcions de TP53INP2 fins ara descrites podrien explicar el seu requeriment. Per una banda, sabem que TP53INP2 és un co-activador de l'activitat transcripcional de PPARγ i de TR (Baumgartner et al., 2007; Sancho et al., 2012), les quals són molt importants per la regulació termogènica (Cassard-Doulcier et al., 1994; Sears et al., 1996; Cao et al., 2004; Hondares et al., 2006). Per tant, podria ser que TP53INP2 estigués facilitant l'activitat transcripcional d'aquests dos factors. I per altre banda, TP53INP2 també és necessari per a induir autofàgia (Nowak et al., 2009; Francis et al., 2010; Mauvezin et al., 2010; Sancho et al., 2012; Sala et al., 2014; Romero et al., 2018). En aquest sentit, s'ha descrit que l'activació de la termogènesi requereix d'autofàgia (Martinez-Lopez et al., 2016), mentre que en processos d'activitat termogènica continuada l'autofàgia disminueix per tal de mantenir la massa mitocondrial (Altshuler-Keylin et al., 2016; Cairó et al., 2016, 2019). Això ens indicaria que TP53INP2 podria estar activant l'autofàgia en processos de termogènesi aguda, mentre que en condicions de reclutament de teixit adipós marró, TP53INP2 estaria bloquejant la mitofàgia. Pel que respecta a aquest segon concepte, això seria coherent amb observacions del nostre laboratori que han demostrat que TP53INP2 pot disminuir la mitofàgia (Yuliana Enciso, Tesi doctoral, 2017).

8.3.2. TP53INP2 indueix l'adipogènesi marró a través de la regulació de l'activitat de PPARγ

Un estudi del nostre laboratori ha descrit que TP53INP2 és un regulador negatiu de l'adipogènesi blanca (Romero et al., 2018). Les dades obtingudes en aquesta tesi doctoral han demostrat que l'expressió de TP53INP2 s'indueix en condicions de reclutament de teixit adipós, el qual comporta un augment de la diferenciació dels preadipòcits marrons (Géloën et al., 1990). Aquestes dades ens van suggerir que TP53INP2 podria estar jugant un paper regulador en l'adipogènesi marró. Per això, vam decidir estudiar si l'expressió de TP53INP2 es veia modulada pel procés

de diferenciació. Els resultats obtinguts demostren que l'expressió de TP53INP2 es veu augmentada durant la diferenciació, sent així més elevada en adipòcits madurs que en cèl·lules precursores (Figura 5). Aquest resultat va reforçar la idea de que TP53INP2 pot ser important per l'adipogènesi marró.

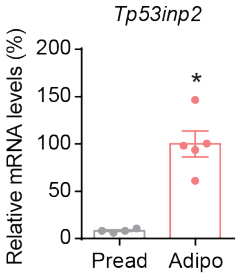

Figura 5. Els adipòcits marrons tenen major expressió de *Tp53inp2* que els preadipòcits. Nivells relatius de *Tp53inp2* en preadipòcits marrons (Pread) o en adipòcits marrons (Adipo) (n=4). Les dades estan representades com a mitjana ± error estàndard. *p<0.05 vs. Pread.

Amb aquest objectiu, vam generar un model cel·lular de preadipòcits marrons a partir del qual vam obtenir una línia cel·lular amb expressió endògena de TP53INP2 (C) i una altre en la qual es va eliminar l'expressió de TP53INP2 (KO). La diferenciació dels preadipòcits marrons va mostrar que les cèl·lules KO tenien menys capacitat adipogènica (Figura 6A). A més, els adipòcits KO tenien menys expressió de proteïnes involucrades en adipogènesi, com ara PPARγ1 i PPARγ2, menys biogènesi mitocondrial, determinat per una menor inducció de proteïnes mitocondrials com MFN2 i TIM44, i el més rellevant, una expressió disminuïda de UCP1, el marcador per excel·lència dels adipòcits marrons (Figura 6B).

Des d'un punt de vista funcional, l'eliminació de TP53INP2 també redueix la resposta adrenèrgica en els adipòcits madurs. D'aquesta manera, les cèl·lules KO tenien menys resposta a l'hora d'induir l'expressió de *Ucp1* al ser tractats amb un agonista β3-adrenergic (Figura 7A), i una deficiència en augmentar la respiració mitocondrial al ser tractats amb NE (Figura 7B). Aquests resultats demostren que TP53INP2 és necessari per al correcte desenvolupament de l'adipogènesi marró.

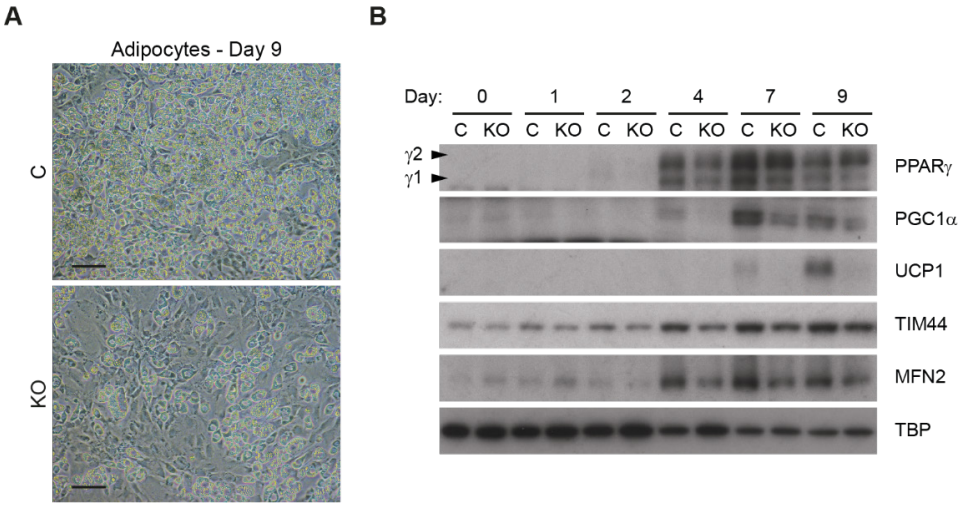

Figura 6. L'ablació genètica de TP53INP2 redueix l'adipogènesi marró. (A) Imatges de microscòpia òptica d'adipòcits marrons control (C) o TP53INP2 genoanul·lats (KO) a dia 9 de diferenciació. (B) Anàlisi per Western blot del contingut de les proteïnes PPARγ, PGC1α, UCP1, TIM44 i MFN2 durant la diferenciació de preadipòcits marrons C o KO (n=2-6). Barra d'escala, 100μm.

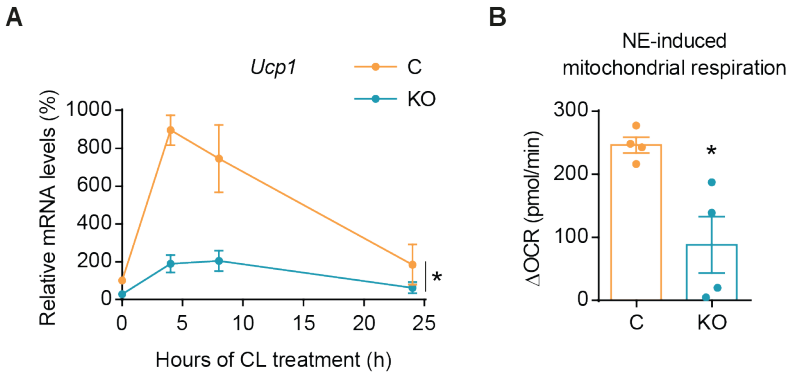

Figura 7. La manca de TP53INP2 redueix la senyalització adrenèrgica en adipòcits marrons. Adipòcits marrons control (C) o TP53INP2 genoanul·lats (KO). (A) Nivells relatius de ARNm de *Ucp1* en adipòcits marrons tractats amb CL-316,243 (CL) a diferents temps (n=4) i (B) increment del consum d'oxigen (ΔOCR) induït per norepinefrina (NE) en adipòcits marrons (n=4). Les dades estan representades com a mitjana ± error estàndard. *p<0.05 vs. C.

Sorprenentment, TP53INP2 mostra efectes oposats en l'adipogènesi blanca i en la marró. S'ha descrit que TP53INP2 bloqueja l'adipogènesi blanca a través de

l'activació de la via de senyalització de WNT/TCF, la qual té un paper inhibitori en la diferenciació (Romero et al., 2018). En canvi, TP53INP2 té un paper estimulador de l'adipogènesi marró. Donat que s'ha descrit que la via de WNT/TCF també inhibeix la diferenciació dels preadipòcits marrons (Kang et al., 2005; Christodoulides et al., 2009; Wang et al., 2010), l'acció de TP53INP2 en aquest procés ha de ser independent a aquesta via de senyalització.

Tal i com s'ha mencionat, l'activitat de PPARγ és necessària per a l'adipogènesi marró (Barak et al., 1999; Rosen et al., 1999; Koutnikova et al., 2003). Conseqüentment, una menor activitat PPARγ s'associa a un menor desenvolupament del teixit adipós marró i a una capacitat termogènica disminuïda (Gray et al., 2006). Com que TP53INP2 s'ha descrit com un co-activador de l'activitat transcripcional de PPARγ, vam voler estudiar si TP53INP2 estava duent a terme la seva acció en la diferenciació de preadipòcits marrons a través de la regulació de l'activitat de PPARγ. Perseguint aquest objectiu, es va mesurar l'activitat transcripcional de PPARγ en cèl·lules C i KO a través d'assajos luciferasa. Els nostres resultats demostren que l'activitat PPARγ no s'activa en resposta al lligand rosiglitazona en les cèl·lules KO (Figura 8). A més a més, aquest efecte és independent de la quantitat de proteïna PPARγ, ja que inclús quan es va sobreexpressar la proteïna, les cèl·lules KO presentaven una resposta al lligand disminuïda (Figura 8).

Per tal de comprovar si la deficiència d'activitat PPARγ era la responsable de la capacitat adipogènica defectiva en les cèl·lules TP53INP2 genoanul·lades, es va generar un model cel·lular de sobreexpressió estable de PPARγ mitjançant una infecció retroviral. A continuació, es va eliminar TP53INP2 de la mateixa manera que anteriorment. Així doncs, es va avaluar la capacitat adipogènica de les cèl·lules que presentaven sobreexpressió de PPARγ amb o sense TP53INP2 (C i KO respectivament). L'augment de PPARγ va demostrar ser capaç d'augmentar la capacitat adipogènica de les cèl·lules control, de forma coherent amb estudis prèviament publicats (Zhang et al., 2004). En canvi, la sobreexpressió de PPARγ en el context cel·lular de deficiència de TP53INP2 va demostrar ser menys eficient

a l'hora d'induir l'expressió de gens marcadors de diferenciació com *Ucp1* i *Cidea*, i de gens mitocondrials com *Cox8b* i *Cox7a1* (Figura 9).

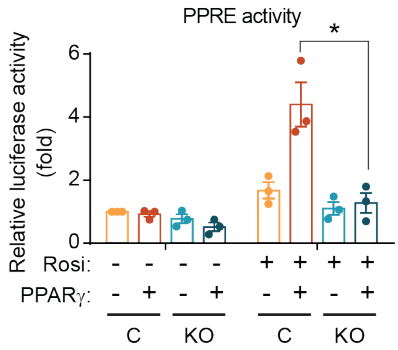

Figura 8. L'activitat transcripcional de PPARγ es veu disminuïda en absència de TP53INP2. Activitat transcripcional PPRE en preadipòcits marrons que sobreexpressen un vector buit (-) o PPARγ (+) controls (C) o TP53INP2 genoanul·lats (KO). Les cèl·lules van ser tractades amb solvent (-) o amb rosiglitazona (+) 10μM durant 24 hores (n=3). Les dades estan representades com a mitjana ± error estàndard. *p<0.05 vs. C.

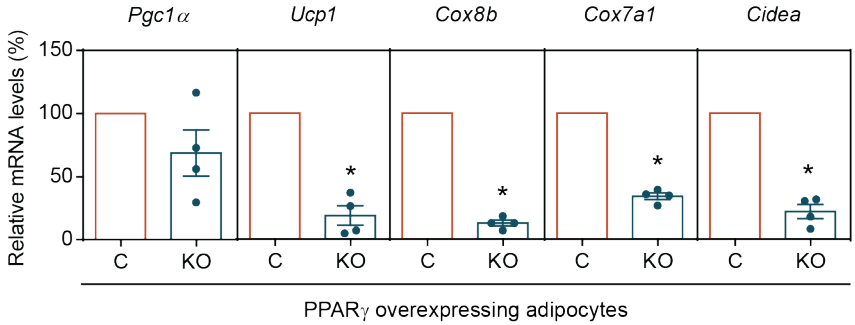

Figura 9. La sobreexpressió de PPARγ no és capaç de rescatar la deficiència adipogènica induïda per la pèrdua de funció de TP53INP2. Nivells relatius de ARNm dels gens indicats en adipòcits marrons diferenciats fins a dia 9 que sobreexpressen PPARγ controls (C) o TP53INP2 genoanul·lats (KO) (n=4). Les dades estan representades com a mitjana ± error estàndard. *p<0.05 vs. C.

Aquestes dades són coherents amb els resultats obtinguts de l'estudi de l'activitat transcripcional, que demostren que l'acció de TP53INP2 en la regulació de PPARγ és independent dels seus nivells de proteïna. Per altre banda, també s'ha descrit que la diferenciació de preadipòcits marrons en presència crònica del lligand sintètic de PPARγ rosiglitazona augmenta la seva diferenciació i biogènesi

mitocondrial (Petrovic et al., 2008). Per tant, es va decidir estudiar si la presència de rosiglitazona durant el procés de diferenciació era capaç de rescatar la deficiència induïda per la manca de TP53INP2. Els resultats obtinguts indiquen que l'augment de l'activitat PPARγ per presència de rosiglitazona és capaç d'augmentar la diferenciació marró en les cèl·lules KO fins al mateix nivell que en les cèl·lules control (Figura 10).

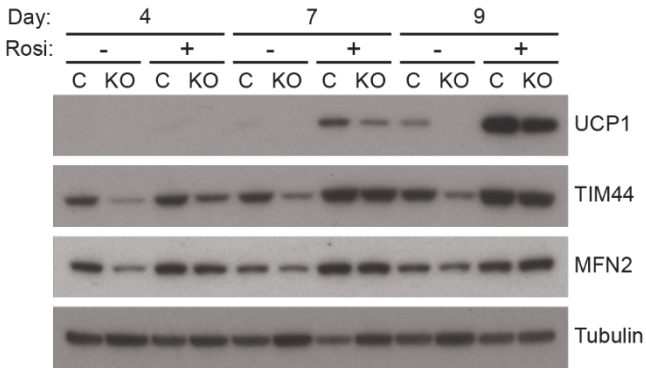

Figura 10. El tractament crònic amb rosiglitzona rescata la deficiència adipogènica induïda per la pèrdua de funció de TP53INP2. Anàlisi per Western blot del contingut de les proteïnes UCP1, TIM44 i MFN2 durant la diferenciació de preadipòcits marrons controls (C) o TP53INP2 genoanul·lats (KO) tractats de manera crònica amb solvent (-) o amb rosiglitazona 1μM (+) (n=3-4).

Aquestes dades demostren que TP53INP2 estimula l'adipogènesi marró a través de la regulació de l'activitat de PPARγ. Tot i això, no descartem que TP53INP2 pugui estar també implicat en d'altres processos a través dels quals estigui modulant la diferenciació. Per exemple, s'ha descrit que l'autofàgia és necessària per a la diferenciació del teixit adipós marró (Martinez-Lopez et al., 2013), i per tant, TP53INP2 podria estar implicat també en aquesta regulació. Una altre possibilitat seria que TP53INP2 estigués induint l'expressió de *Ucp1* a través de la seva unió amb el receptor d'hormones tiroïdals TRα1 (Darimont et al., 1993; Marrif et al., 2005). Tot i que seria molt interessant poder estudiar la implicació d'aquests dos mecanismes en el fenotip observat, per qüestions de temps no s'ha pogut avaluar durant el desenvolupament d'aquesta tesi doctoral.

8.3.3. La proteïna TP53INP2 és necessària per a la diferenciació i la termogènesi del teixit adipós marró

Després de determinar que TP53INP2 és un regulador de la diferenciació de preadipòcits marrons en cultiu, vam voler estudiar si la seva funció també era necessària pel teixit adipós marró *in vivo.* D'aquesta manera, es va generar un model animal de ratolí amb ablació genètica específica en les cèl·lules precursores que expressen Myf5. Es va escollir aquest model ja que era l'única possibilitat d'eliminar TP53INP2 en l'estadi de cèl·lula precursora del teixit adipós marró. Per contra, My5 també s'expressa en les cèl·lules precursores de múscul esquelètic, per tant l'eliminació de TP53INP2 es durà a terme en ambdós teixits. Tot i això, es coneixen els efectes de la repressió de TP53INP2 en múscul esquelètic. Estudis previs del nostre laboratori utilitzant models amb modulació genètica de TP53INP2 específicament en el múscul esquelètic van demostrar que TP53INP2 no afecta al balanç energètic ni al metabolisme de la glucosa per mitjà d'aquest òrgan (Sala et al., 2014).

La caracterització del model d'ablació genètica de TP53INP2 específicament en cèl·lules Myf5 (KO^{Myf5}) va demostrar que l'eliminació de TP53INP2 dona lloc a una disminució de l'expressió de gens involucrats en adipogènesi i termogènesi (Figura 11). Per tal de comprovar si l'ablació de TP53INP2 resulta en una disfunció del teixit adipós marró, es va dur a terme un anàlisi transcriptòmic en mostres de teixit adipós marró de ratolins control (LoxP) i d'animals KO^{Myf5}. Els resultats obtinguts es van comparar amb un estudi publicat en que s'avaluava la modulació genètica per la inhibició fisiològica de la termogènesi per exposició a temperatura termoneutral. Sorprenentment, un 40% dels gens que es veien alterats per l'eliminació de TP53INP2 també es veien modulats de manera natural al disminuir l'activitat termogènica. A més a més, la regulació d'aquests gens tenia lloc en el mateix sentit en ambdós estudis, per la qual cosa es va determinar que existeix una correlació positiva entre ells. La modulació d'alguns d'aquests gens es va validar per PCR quantitativa (Figura 11).

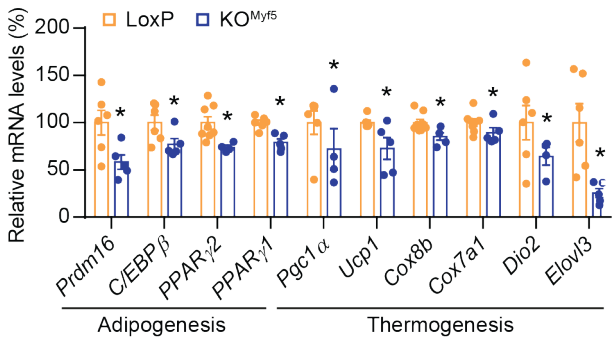

Figura 11. L'eliminació de TP53INP2 en teixit adipós marró redueix l'expressió de gens adipogènics i termogènics. Nivells relatius de ARNm dels gens indicats en teixit adipós marró interescapular de ratolins mascles control (LoxP) o TP53INP2 genoanul·lats específicament en cèl·lules Myf5 positives (KO^{Myf5}) a 3 mesos d'edat, estabulats a 22°C i alimentats amb una dieta normal (n=7-9). Les dades estan representades com a mitjana ± error estàndard. *p<0.05 vs. LoxP.

Mitjançant anàlisi d'enriquiment de conjunt de gens es va detectar que l'eliminació de TP53INP2 en teixit adipós també donava lloc a una disminució en la via de senyalització de PPAR. De la mateixa manera, la pèrdua de funció de TP53INP2 també redueix el grup de gens expressats específicament en teixit adipós marró i la via d'adipogènesi. Aquestes dades van en la mateixa direcció que les observades en cèl·lules en cultiu, i per tant reforcen la idea de que TP53INP2 és necessari per a la diferenciació i l'activitat PPARγ del teixit adipós marró *in vivo.*

Donat que les dades d'expressió genètica apuntaven que l'eliminació de TP53INP2 condueix a una menor activitat termogènica, el nostre següent objectiu va ser el d'estudiar aquesta hipòtesi. Utilitzant experiments de calorimetria indirecta vam poder determinar que els ratolins KO^{Myf5} presentaven menys consum d'oxigen, menys producció de diòxid de carboni i per tant menor despesa energètica (Figura 12). Aquestes alteracions es van detectar en absència de diferències en l'activitat motora ni en la ingesta.

Per tal d'identificar quins eren els teixits implicats en la disminució de la despesa energètica, es van realitzar experiments de respirometria d'alta resolució en fraccions enriquides de mitocondris de teixit adipós marró i en fibres permeabilitzades de

múscul esquelètic. La respiració mitocondrial del múscul esquelètic no estava alterada per la manca de TP53INP2, en canvi, la respiració mitocondrial associada al complex II dels mitocondris de teixit adipós marró estava disminuïda per la pèrdua de funció de TP53INP2 (Figura 13).

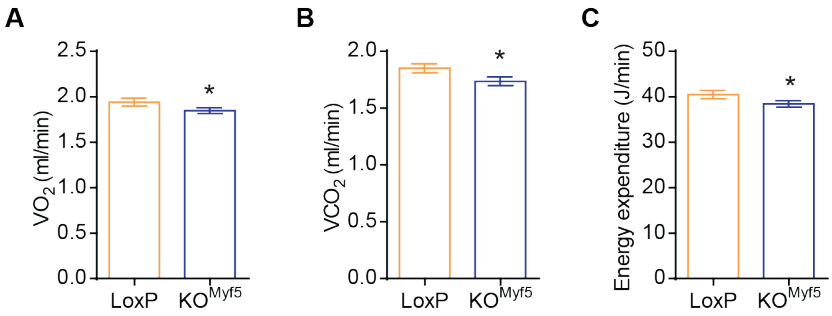

Figura 12. Els ratolins genoanul·lats de TP53INP2 tenen menys despesa energètica. Calorimetria indirecta en ratolins mascles control (LoxP) o TP53INP2 genoanul·lats específicament en cèl·lules Myf5 positives (KO^{Myf5}) a 3 mesos d'edat, estabulats a 22°C i alimentats amb una dieta normal. (A) Consum d'oxigen; (B) producció de diòxid de carboni i (C) despesa energètica (n=7). Les dades es mostren com a mitjana ajustada (basat amb un pes de ratolí normalitzat de 29.4714g determinat mitjançant ANCOVA) ± error estàndard. *p<0.05 vs. LoxP.

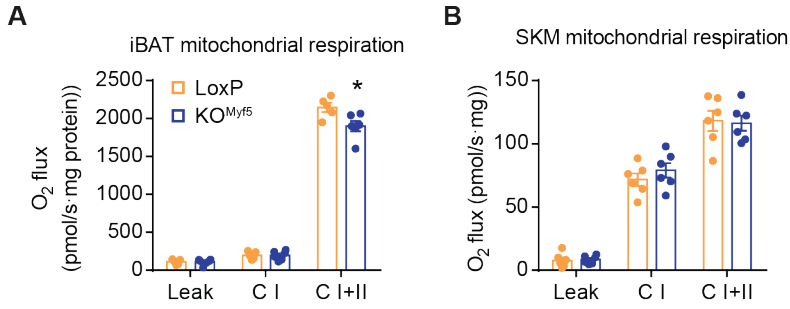

Figura 13. La respiració mitocondrial del teixit adipós marró es veu alterada en els ratolins genoanul·lats de TP53INP2. Respirometria d'alta resolució en (A) mitocondris aïllats de teixit adipós marró interescapular (iBAT) o (B) en fibres permeabilitzades del múscul tibial anterior (SKM) de ratolins mascles control (LoxP) o TP53INP2 genoanul·lats específicament en cèl·lules Myf5 positives (KO^{Myf5}) a 3 mesos d'edat, estabulats a 22°C i alimentats amb una dieta normal (n=5-6). Les dades estan representades com a mitjana ± error estàndard. *p<0.05 vs. LoxP.

Aquestes dades estarien indicant que la disfunció del teixit adipós marró degut a l'absència de TP53INP2 és la responsable de l'alteració del balanç energètic. A més a més, l'alteració mitocondrial va resultar tenir conseqüències en el teixit adipós marró. Estudis histològics van demostrar que l'eliminació de TP53INP2 conduïa a un augment de la mida de les gotes lipídiques, i conseqüentment a una disminució en el seu número per superfície (Figura 14A, B i C). Això va donar lloc a un augment del pes del teixit en els animals KO^{Myf5} de 3 mesos d'edat en comparació amb els ratolins control (Figura 14D). Aquesta morfologia del teixit s'associa a una menor activitat termogènica del teixit adipós marró, i per tant reforça la idea de que TP53INP2 és necessari per a la termogènesi. Tot i això, en aquestes condicions el pes corporal o la quantitat total de greix no estava afectada per l'absència de TP53INP2 (Figura 14E i F).

Els resultats obtinguts fins al moment suggerien que l'eliminació de TP53INP2 estava donant lloc a una menor capacitat termogènica del teixit adipós, tot i això vam creure rellevant mesurar directament aquesta propietat. Amb aquesta idea, es va mesurar la capacitat d'incrementar el consum d'oxigen en resposta a una injecció de NE en animals aclimatats a dues temperatures diferents. S'ha descrit que la diferència d'inducció màxima a NE entre dues condicions d'activitat termogènica diferent és directament a proporcional a la quantitat de UCP1 (Golozoubova et al., 2006). Així doncs, es va mesurar la capacitat d'augmentar el consum d'oxigen en un grup d'animals aclimatats a 22°C i un altre a 30°C, com a condició d'alta i baixa activitat termogènica respectivament. Els resultats mostren clarament que la resposta a NE és molt més alta en els animals aclimatats a 22°C en comparació amb els estabulats a 30°C, coherent amb el fet que a 22°C hi ha més activitat termogènica. Addicionalment, també vam poder observar que la diferència entre ambdues temperatures era major en els animals control en comparació amb els ratolins KO^{Myf5} (Figura 15). Aquestes dades demostren que la deficiència de TP53INP2 redueix la funció termogènica del teixit adipós marró.

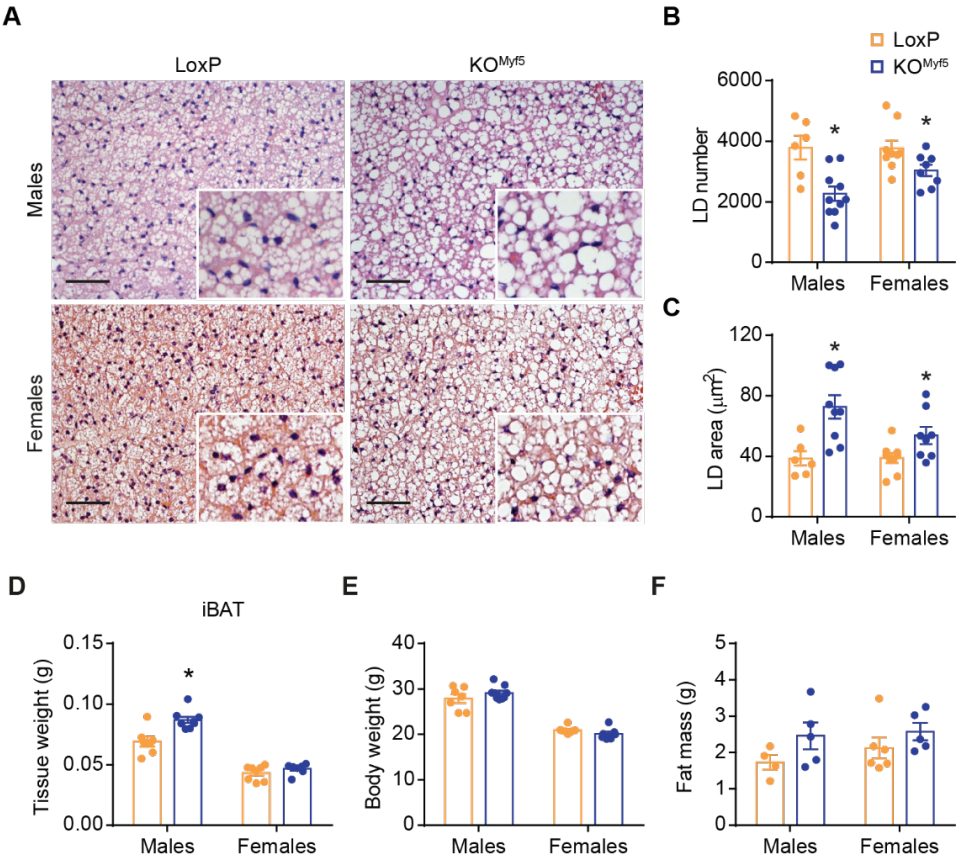

Figura 14. La pèrdua de funció de TP53INP2 indueix una morfologia d'inactivitat en el teixit adipós marró. Ratolins mascles o femelles control (LoxP) o TP53INP2 genoanul·lats específicament en cèl·lules Myf5 positives (KO^{Myf5}) a 3 mesos d'edat, estabulats a 22°C i alimentats amb una dieta normal. (A) Tinció hematoxilina-eosina en seccions de teixit adipós marró interescapular (iBAT), (B) quantificació del nombre de gotes lipídiques (LD) i (C) de l'àrea mitjana de les LD (n=6-9). (D) Pes del iBAT, (E) pes corporal i (F) quantitat total de greix (n=5-9). Les dades estan representades com a mitjana ± error estàndard. *p<0.05 vs. LoxP. Barra d'escala, 100μm.

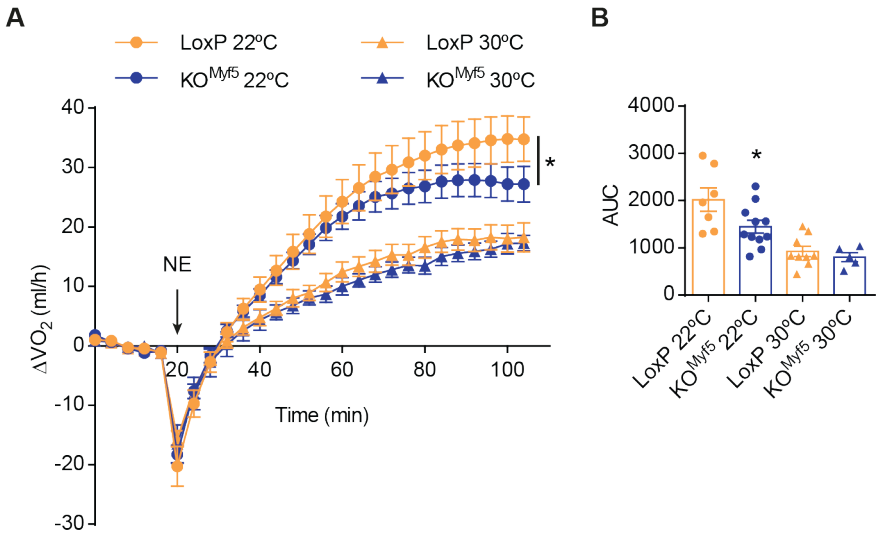

Figura 15. TP53INP2 indueix la termogènesi adaptativa. (A) Augment del consum d'oxigen (ΔVO_2) induït per norepinefrina (NE) i (B) quantificació de l'àrea sota la corba en ratolins mascles control (LoxP) o TP53INP2 genoanul·lats específicament en cèl·lules Myf5 positives (KO^{Myf5}) a 4 mesos d'edat, estabulats a 22°C o a 30°C durant 2 mesos i alimentats amb una dieta normal (n=5-11). Les dades estan representades com a mitjana ± error estàndard. *p<0.05 vs. LoxP.

Tal i com ja s'ha comentat, la capacitat dissipadora d'energia del teixit adipós marró pot tenir un impacte en el balanç energètic i regular el guany de pes. Després d'haver determinat que la termogènesi esta disminuïda en els animals KO^{Myf5}, vam voler estudiar si això tenia un impacte en el desenvolupament d'obesitat. Amb aquesta idea vam estudiar animals control i TP53INP2 deficients a 6 mesos d'edat. En aquestes condicions, es va trobar que els ratolins KO^{Myf5} presentaven major pes corporal (Figura 16A). L'estudi detallat dels teixits va mostrar que l'augment del pes corporal es devia a un augment a la quantitat total de greix de l'animal, i a més, en aquestes condicions el pes del teixit adipós marró en els animals amb ablació de TP53INP2 pesava el doble que en els ratolins control (Figura 16B i C). A aquesta edat, la morfologia del teixit adipós marró encara estava més alterada, i presentava una major pèrdua de multilocularitat (Figura 16D, E i F).

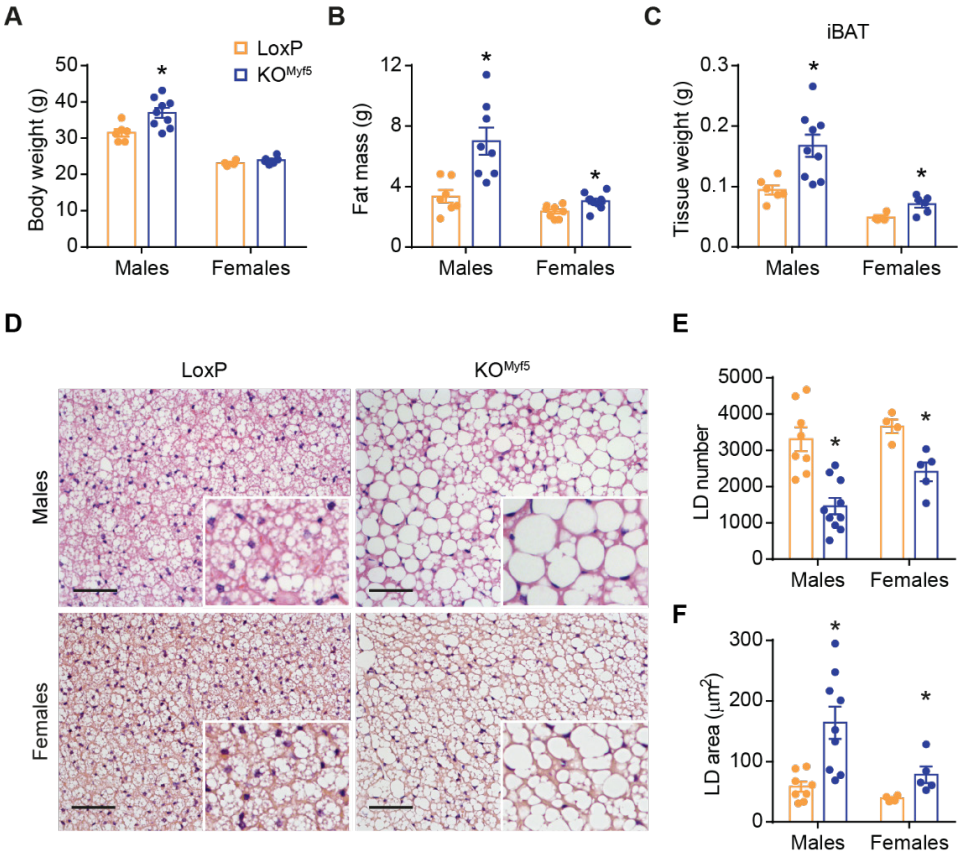

Figura 16. Els ratolins genoanul·lats de TP53INP2 tenen major adipositat. Ratolins mascles o femelles control (LoxP) o TP53INP2 genoanul·lats específicament en cèl·lules Myf5 positives (KO^{Myf5}) a 6 mesos d'edat, estabulats a 22°C i alimentats amb una dieta normal. (A) Pes corporal, (B) quantitat total de greix i (C) pes del teixit adipós marró interescapular (iBAT) (n=6-9). (D) Tinció hematoxilina-eosina en seccions de iBAT, (E) quantificació del nombre de gotes lipídiques (LD) i (F) de l'àrea mitjana de les LD (n=4-10). Les dades estan representades com a mitjana ± error estàndard. *p<0.05 vs. LoxP. Barra d'escala, 100µm.

De manera global, podem concloure que l'absència de TP53INP2 en teixit adipós marró disminueix la seva capacitat adipogènica. Conseqüentment, la seva despesa energètica i activitat termogènica també es veuen alterades, i amb l'edat, l'acumulació de l'energia no dissipada dona lloc al desenvolupament d'obesitat.

El fet d'estabular els ratolins a 22°C, temperatura per sota de la seva zona termoneutral, provoca l'activació crònica de la termogènesi per tal de mantenir

la temperatura corporal. Així doncs, en cas de que hi hagi algun defecte en la termogènesi adaptativa, s'induiran d'altres mecanismes termogènics per tal de mantenir la temperatura corporal. Un d'aquests mecanismes adaptatius és per exemple la termogènesi associada a tremolor que té lloc en el múscul esquelètic (Feldmann et al., 2009; Martinez-Lopez et al., 2013; Blondin et al., 2017). Tenint en compte aquesta informació, vam pensar que aquest podria ser el cas en el nostre model animal. Per tant, vam decidir caracteritzar l'impacte de l'eliminació de TP53INP2 en condicions termoneutrals. En aquestes condicions, les diferències de pes corporal entre genotips es van veure disminuïdes (Figura 17A). De forma important, el pes del teixit adipós marró era el mateix en els dos grups (Figura 17B). Després, vam induir l'increment de la termogènesi induïda per la dieta administrant una HFD. Mentre que la termogènesi induïda per la dieta es va veure augmentada en els animals controls, determinat per l'aparició d'adipòcits marrons multiloculars, aquest efecte es va veure clarament disminuït en els ratolins KO^{Myf5} (Figura 17D, E i F). A més, la HFD va restaurar les diferències de pes corporal i de teixit adipós marró entre genotips (Figura 17A, B i C).

Aquestes dades indiquen que en absència de TP53INP2 la termogènesi induïda per la dieta està disminuïda. Per tal de corroborar-ho, es va mesurar la capacitat termogènica en resposta a NE. En aquest cas, es van utilitzar animals estabulats a 30°C, un grup alimentat amb dieta normal (CD) i l'altre amb HFD. Els resultats obtinguts confirmen el requeriment de TP53INP2 per a la termogènesi induïda per la dieta (Figura 18).

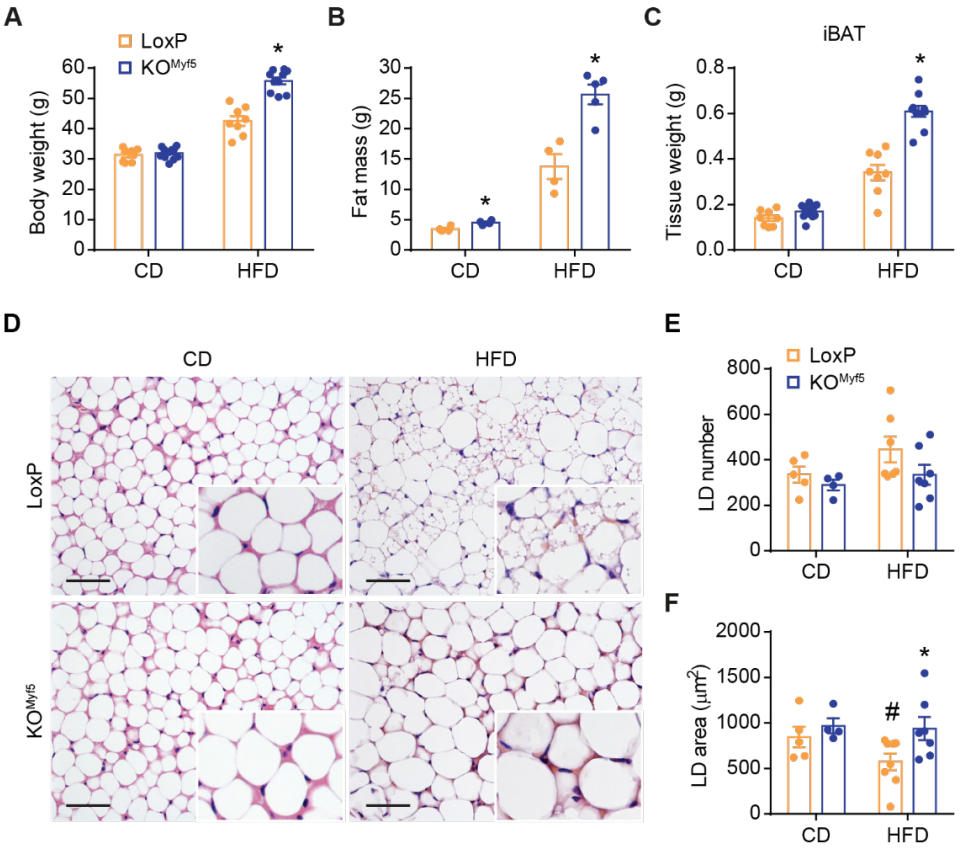

Figura 17. Els ratolins genoanul·lats de TP53INP2 tenen menor capacitat d'activar la termogènesi induïda per la dieta. Ratolins mascles control (LoxP) o TP53INP2 genoanul·lats específicament en cèl·lules Myf5 positives (KO^{Myf5}) a 6 mesos d'edat, estabulats a 30°C i alimentats amb una dieta normal (CD) o amb una dieta rica en greixos (HFD). (A) Pes corporal, (B) quantitat total de greix i (C) pes del teixit adipós marró interescapular (iBAT) (n=8-12). (D) Tinció hematoxilina-eosina en seccions de iBAT, (E) quantificació del nombre de gotes lipídiques (LD) i (F) de l'àrea mitjana de les LD (n=4-7). Les dades estan representades com a mitjana ± error estàndard. *p<0.05 vs. LoxP. #p<0.1 vs CD. Barra d'escala, 100µm.

Donat que el teixit adipós marró també està involucrat en la regulació del metabolisme de la glucosa, i que hem determinat que l'eliminació de TP53INP2 dona lloc a disfunció termogènica, vam voler estudiar si la homeòstasi de la glucosa estava alterada (Figura 19). Experiments de tolerància a la glucosa i a la insulina van demostrar que els animals KO^{Myf5} eren intolerants a la glucosa com a conseqüència de resistència a la insulina (Figura 19A i B). Sorprenentment, la

sensibilitat a la insulina no estava alterada en animals estabulats a 30°C i alimentats amb una CD (Figura 19C), però reapareixia al alimentar-los amb HFD (Figura 19F). Aquests resultats indiquen que, al menys una part del fenotip s'origina per la disfunció del teixit adipós marró degut a la manca de TP53INP2. Tot i això, també podem veure intolerància a la glucosa en condicions en que l'activitat termogènica és mínima (termoneutralitat i CD). Això vol dir que, aparentment el teixit adipós marró està enviant senyals endocrines a altres teixits per a captar glucosa, i que quan eliminem TP53INP2 aquesta senyal probablement està alterada.

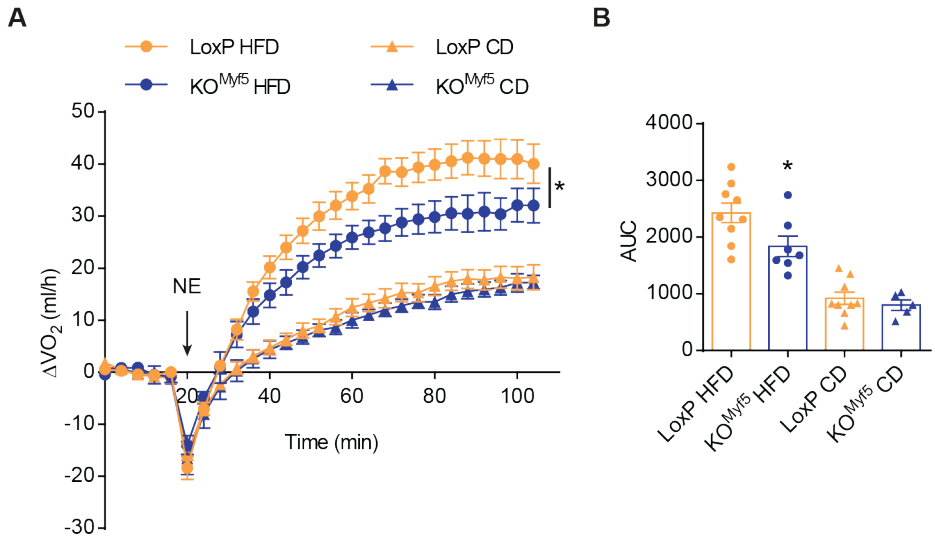

Figura 18. TP53INP2 indueix la termogènesi induïda per la dieta. (A) Augment del consum d'oxigen (ΔVO_2) induït per norepinefrina (NE) i (B) quantificació de l'àrea sota la corba en ratolins mascles control (LoxP) o TP53INP2 genoanul·lats específicament en cèl·lules Myf5 positives (KO^{Myf5}) a 4 mesos d'edat, estabulats a 30°C i alimentats amb una dieta normal (CD) o amb una dieta rica en greixos (HFD) (n=5-9). Les dades estan representades com a mitjana ± error estàndard. *p<0.05 vs. LoxP.

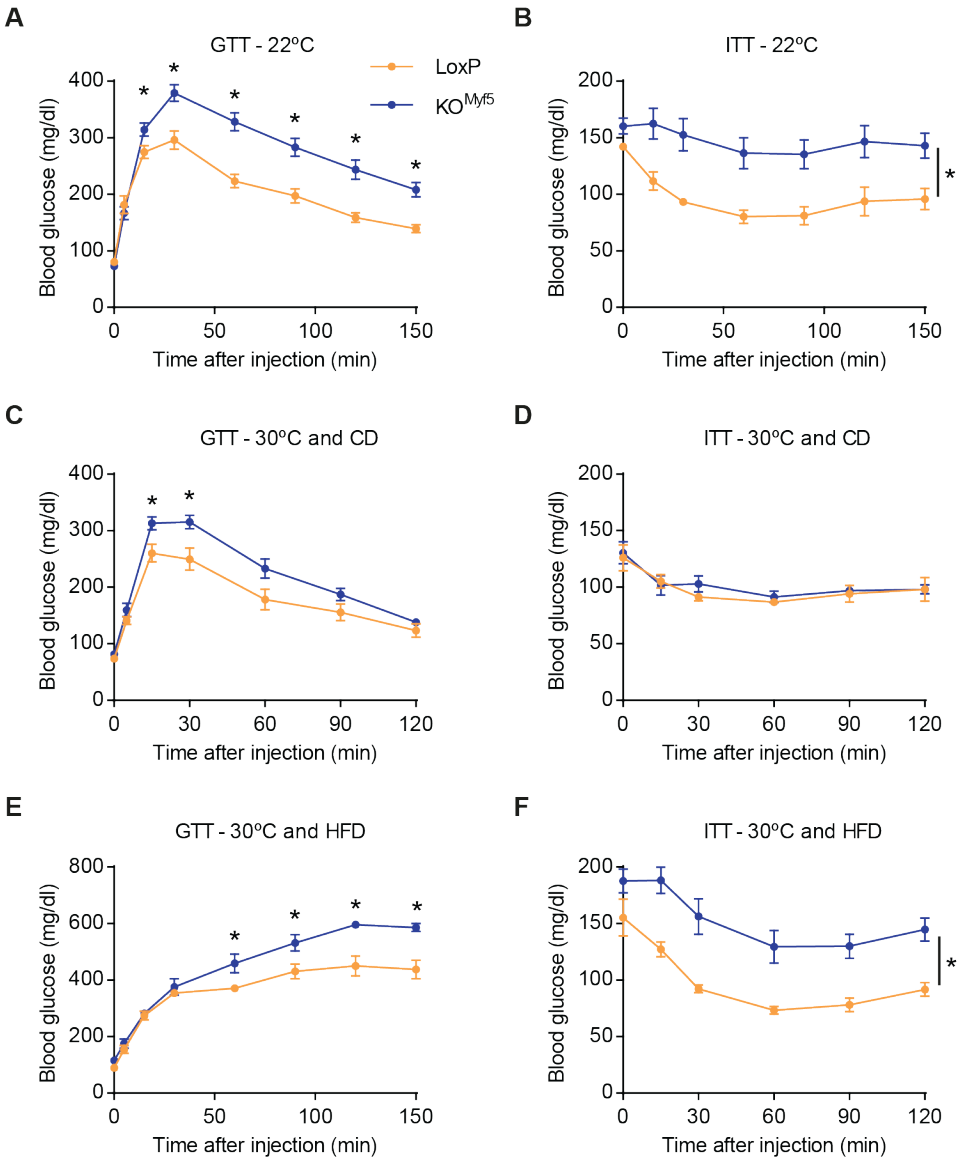

Figura 19. TP53INP2 modula la tolerància a la glucosa i la sensibilitat a la insulina. Nivells de glucosa en sang durant test de tolerància a la glucosa (GTT) o a la insulina (ITT) en ratolins mascles control (LoxP) o TP53INP2 genoanul·lats específicament en cèl·lules Myf5 positives (KO^{Myf5}) estabulats a 22**°C** o a 30°C i alimentats amb una dieta normal (CD) o amb una dieta rica en greixos (HFD) (n=4-9). Les dades estan representades com a mitjana ± error estàndard. *p<0.05 vs. LoxP.

8.3.4. Els adipòcits marrons requereixen TP53INP2 per al manteniment de l'estat diferenciat

Amb la idea d'estudiar si TP53INP2, a més a més de la seva funció en la regulació de l'adipogènesi, té un rol en la regulació de l'adipòcit madur, vam generar un model animal de ratolí genoanul·lat de TP53NP2 a nivell global de forma induïble (KO^{Ubc}). D'aquesta manera, la formació del teixit adipós marró no es veu alterada, i quan els animals són adults, s'indueix l'eliminació de TP53INP2 mitjançant una dieta amb tamoxifè. La caracterització d'aquest model animal va demostrar ser molt similar al model KO^{Myf5}. El teixit adipós marró dels ratolins KO^{Ubc} presentava menys expressió de gens adipogènics i termogènics en comparació amb els seus germans controls (Figura 20). A més, estudis de transcriptòmica en mostres de teixit adipós marró van revelar que l'eliminació de TP53INP2 en etapa adulta dona lloc a una disminució en la via de senyalització de PPAR, en la via d'adipogènesi i en l'expressió de gens característics de teixit adipós marró.

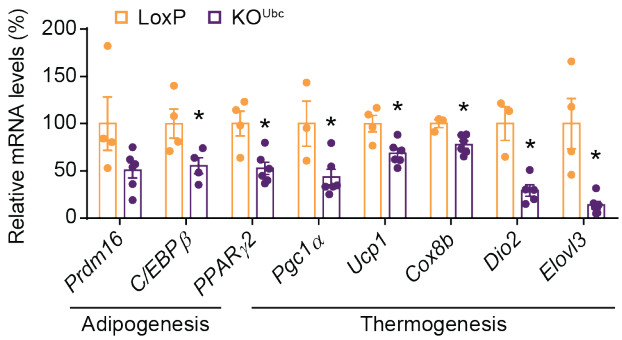

Figura 20. L'eliminació de TP53INP2 en teixit adipós marró adult redueix l'expressió de gens adipogènics i termogènics. Nivells relatius de ARNm dels gens indicats en teixit adipós marró interescapular de ratolins mascles control (LoxP) o TP53INP2 genoanul·lats a nivell global (KO^{Ubc}) a 4 mesos d'edat, estabulats a 22°C i alimentats amb una dieta normal (n=4-6). Les dades estan representades com a mitjana ± error estàndard. *p<0.05 vs. LoxP.

També es van realitzar experiments de calorimetria per avaluar si l'eliminació de TP53INP2 en el teixit adipós marró madur disminueix la seva activitat termogènica. Els resultats van demostrar que els ratolins KO^{Ubc} presentaven menys despesa

energètica en comparació als controls (Figura 21), i això tenia lloc en absència de canvis en l'activitat motora o en la ingesta.

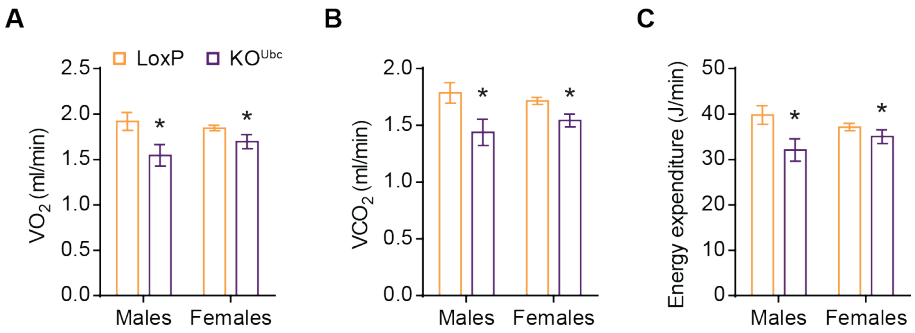

Figura 21. La pèrdua de funció de TP53INP2 redueix la despesa energètica. Calorimetria indirecta en ratolins mascles o femelles control (LoxP) o TP53INP2 genoanul·lats a nivell global (KO^{Ubc}) a 4 mesos d'edat, estabulats a 22°C i alimentats amb una dieta normal. (A) Consum d'oxigen; (B) producció de diòxid de carboni i (C) despesa energètica (n=5-6). Les dades es mostren com a mitjana ajustada (basat amb un pes de ratolí normalitzat de 27.0833g (mascles) o 24.8342g (femelles) determinat mitjançant ANCOVA) ± error estàndard. *p<0.05 vs. LoxP.

Conseqüentment, el pes del teixit adipós marró dels animals KO^{Ubc} estava augmentat com a resultat d'un increment del contingut lipídic (Figura 22). De la mateixa manera que amb el model KO^{Myf5}, la capacitat termogènica disminuïda per la manca de TP53INP2 propiciava el desenvolupament d'obesitat.

De manera conjunta, els resultats obtinguts en aquesta secció indiquen que TP53INP2 és necessari per a mantenir l'estat de diferenciació dels adipòcits marrons. Així, l'ablació genètica de TP53INP2 en ratolins adults provoca disfunció adiposa marró, expressió alterada de gens metabòlics, disminució de la despesa energètica i obesitat.

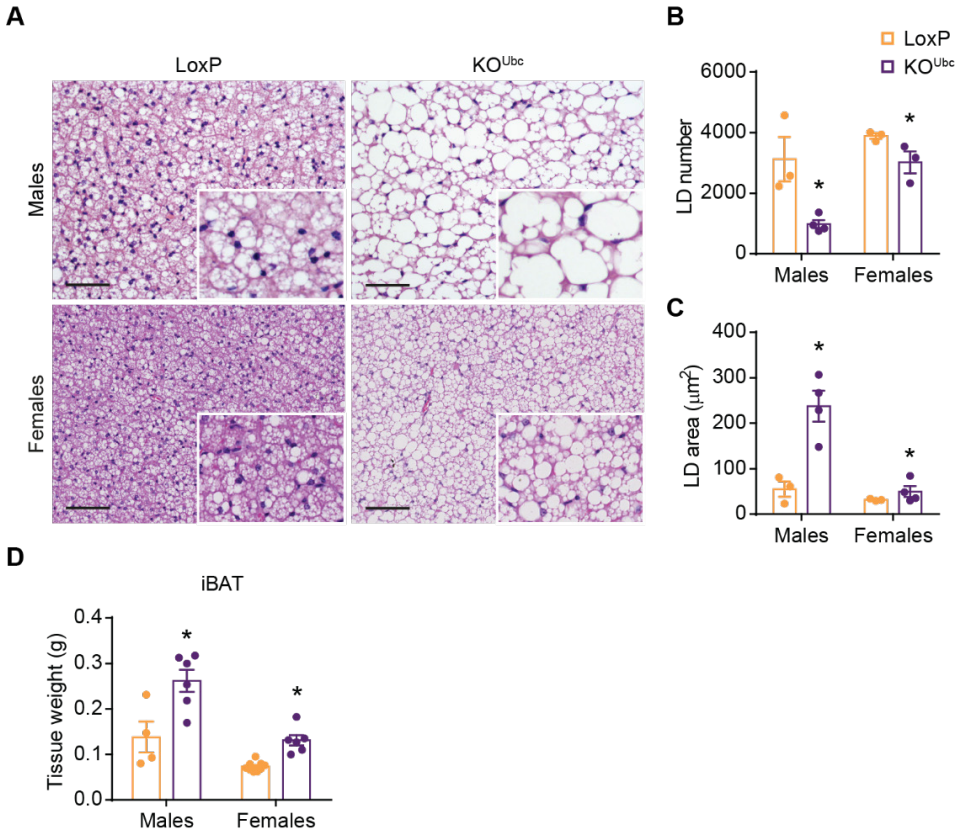

Figura 22. Els animals genoanul·lats de TP53INP2 a nivell global tenen un teixit adipós marró inactiu. Ratolins mascles o femelles control (LoxP) o TP53INP2 genoanul·lats a nivell global (KO^{Ubc}) a 8 mesos d'edat, estabulats a 22°C i alimentats amb una dieta normal. (A) Tinció hematoxilina-eosina en seccions de teixit adipós marró interescapular (iBAT), (B) quantificació del nombre de gotes lipídiques (LD) i (C) de l'àrea mitjana de les LD (n=3-4). (D) Pes del iBAT (n=4-9). Les dades estan representades com a mitjana ± error estàndard. *p<0.05 vs. LoxP. Barra d'escala, 100µm.

8.3.5. L'activitat PPARγ es veu regulada per TP53INP2

Les dades obtingudes posen de manifest que TP53INP2 és un regulador de la via de senyalització de PPARγ, tant en cèl·lules en cultiu com en teixit adipós marró. A través d'aquesta funció, TP53INP2 regula la diferenciació de preadipòcits marrons i indueix l'activitat termogènica en adipòcits marrons. Per això es va considerar important estudiar el mecanisme a través del qual tenia a lloc aquesta regulació.

L'activitat transcripcional de la proteïna PPARγ està regulada per diferents

modificacions postranscripcionals, incloent fosforilació, sumoilació, ubiqüitinació i acetilació (Hu et al., 1996; Hauser et al., 2000; Floyd and Stephens, 2004; Ohshima et al., 2004; Kilroy et al., 2009; Qiang et al., 2012). La majoria d'aquestes modificacions, però, s'han descrit en el context del rol adipogènic de PPARγ en la cèl·lula adiposa blanca, i es desconeix si la proteïna es regula de la mateixa manera en adipòcits marrons. Després de l'activació per lligand, s'indueix la ubiqüitinació de PPARγ, la qual és necessària per la seva activitat transcripcional. En conseqüència, després de la seva activació, la proteïna PPARγ és degradada a través del proteasoma. De fet, la taxa de degradació proteasomal de PPARγ és considerada proporcional a la seva activitat en adipòcits blancs. A més, la ubiqüitinació d'un factor de transcripció és necessària per reduir la seva unió als corepressors en resposta al lligand.

Tenint en compte aquesta informació, i donat que s'ha descrit que TP53INP2 és capaç d'unir-se a proteïnes ubiqüitinades per tal de regular la seva degradació (Sala et al., 2014; Ivanova et al., 2019), vam estudiar si TP53INP2 regula l'activació de PPARγ mitjançant el sistema ubiqüitina-proteasoma. Com a model cel·lular es van utilitzar preadipòcits marrons amb sobreexpressió estable de PPARγ amb o sense TP53INP2 endogen (C i KO respectivament). Al tractar els preadipòcits amb inhibidors del proteasoma, les cèl·lules control mostraren una acumulació de proteïna PPARγ, la qual es va veure augmentada per la presència de rosiglitazona (Figura 23). En canvi, els nivells de PPARγ van romandre pràcticament constants en les cèl·lules KO (Figura 23). Aquestes dades són coherents amb una menor activitat transcripcional de PPARγ per la manca de TP53INP2.

Per tal de confirmar si el fet responsable de la menor activitat era una ubiqüitinació disminuïda, es va immunoprecipitar la proteïna PPARγ en condicions de desnaturalització, i en presència de sobreexpressió d'ubiqüitina per tal d'augmentar el flux de degradació. La imunodeteció utilitzant un anticòs contra ubiqüitina va mostrar que en presència d'inhibidors de proteasoma les cèl·lules C presentaven major grau d'ubiqüitinació de PPARγ en comparació amb les cèl·lules KO (Figura 24).

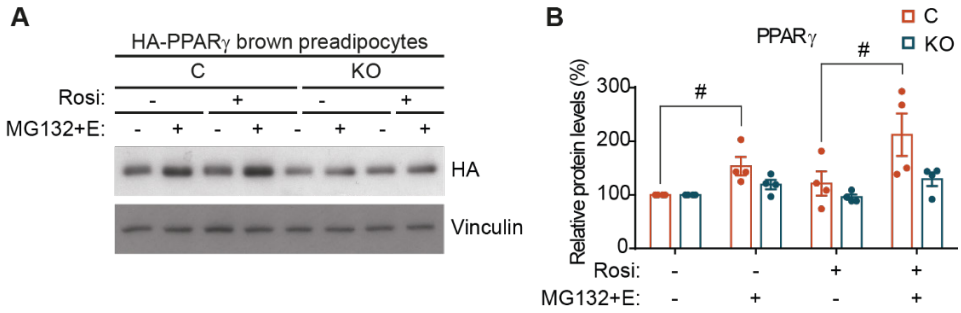

Figura 23. La degradació de PPARγ està reduïda per l'absència de TP53INP2. (A) Anàlisi per Western blot del contingut de PPARγ (HA) i (B) quantificació en preadipòcits marrons que sobreexpressen PPARγ controls (C) o TP53INP2 genoanul·lats (KO). Les cèl·lules van ser tractades amb solvent (-) o amb rosiglitazona (+) 10μM durant 4 hores i amb els inhibidors del proteasoma MG132 10μM i epoxomicina (E) 0.1μM (+) durant 5 hores (n=4). Les dades estan representades com a mitjana ± error estàndard. #p<0.05 vs. grup no tractat amb MG132+E.

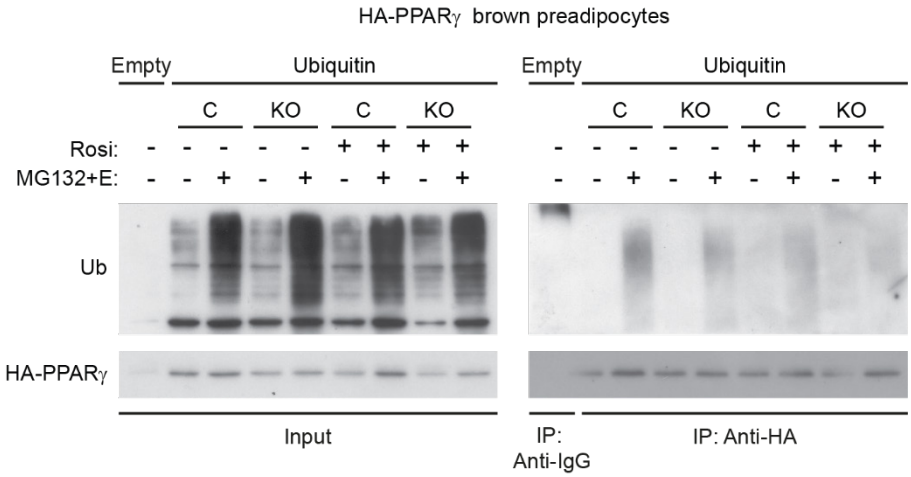

Figura 24. TP53INP2 augmenta la ubiqüitinació de PPARγ. Immunoprecipitació en condicions desnaturalitzants de PPARγ en preadipòcits marrons que sobreexpressen PPARγ controls (C) o TP53INP2 genoanul·lats (KO) i transfectats amb un vector buit (empty) o amb ubiqüitina. Les cèl·lules van ser tractades amb solvent (-) o amb rosiglitazona (+) 10μM durant 4 hores i amb els inhibidors del proteasoma MG132 10μM i epoxomicina (E) 0.1μM (+) durant 5 hores. Anàlisi per Western blot del contingut de PPARγ (HA) i ubiqüitina (Ub) en homogenats totals (input) o en la fracció immunoprecipitada (IP) (n=3).

Aquestes dades proporcionen una validació addicional al fet que l'activitat PPARγ també està regulada pel sistema ubiqüitina-proteasoma en preadipòcits marrons, i que la deficiència de TP53INP2 està relacionada amb la reducció de la ubiqüitinació i de l'activitat de PPARγ. D'aquesta manera, proposem que TP53INP2 és necessari per a la ubiqüitinació de PPARγ en cèl·lules adiposes marrons per tal de regular la seva diferenciació i activitat termogènica.

8.4. Conclusions

Les dades recopilades en aquesta tesi doctoral permeten concloure:

1. L'expressió de TP53INP2 augmenta durant l'adipogènesi marró i està regulada positivament per l'activitat termogènica en teixit adipós marró de ratolí. La via de senyalització adrenèrgica indueix l'expressió de TP53INP2 en adipòcits marrons.

2. L'adipogènesi marró es veu estimulada per TP53INP2. La pèrdua de funció de TP53INP2 en preadipòcits marrons de ratolí disminueix l'activitat transcripcional de PPARγ i, com a conseqüència, redueix la seva capacitat adipogènica.

3. La proteïna TP53INP2 promou la termogènesi adaptativa induïda pel fred o per la dieta. L'ablació genètica de TP53INP2 en teixit adipós marró indueix una disfunció termogènica que dona lloc a un balanç energètic positiu, al desenvolupament d'obesitat, a la intolerància a la glucosa i a la resistència a la insulina.

4. TP53INP2 manté l'estat de diferenciació dels adipòcits marrons. La manca de TP53INP2 en el teixit adipós marró de ratolins adults redueix l'expressió de gens termogènics i la despesa energètica, cosa que afavoreix el desenvolupament d'un fenotip d'obesitat.

5. L'activitat de PPARγ està relacionada amb el sistema d'ubiqüitina-proteasoma en cèl·lules adiposes marrons. La deficiència de TP53INP2 redueix l'activitat de PPARγ, la seva ubiqüitinació i la seva degradació proteasomal. Proposem un model en el qual TP53INP2 regula l'adipogènesi marró i la termogènesi mitjançant l'activació de PPARγ per ubiqüitinació.

REFERENCES

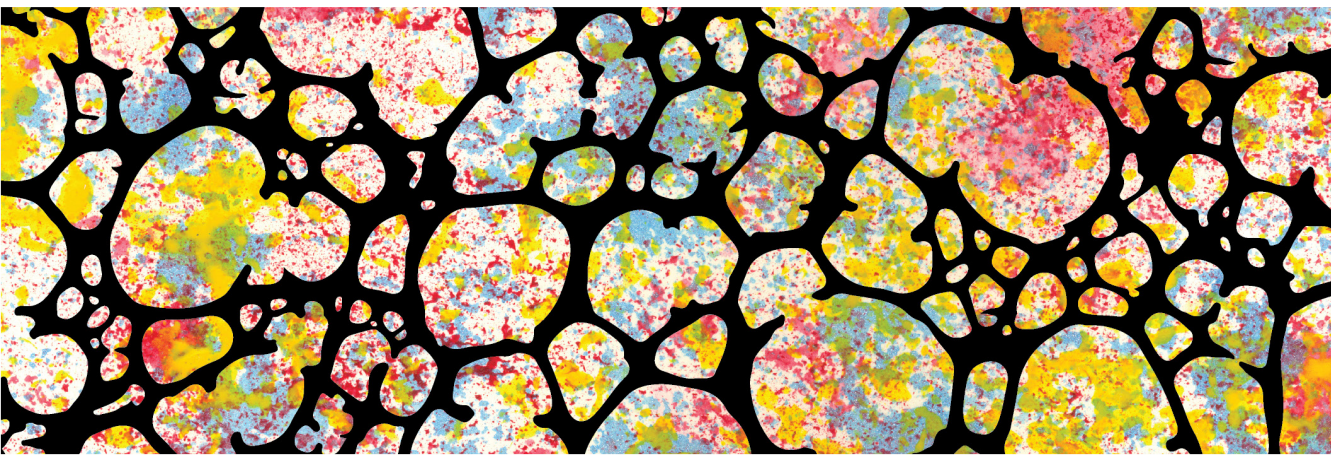

Agostini, M., Gurnell, M., Savage, D.B., Wood, E.M., Smith, A.G., Rajanayagam, O., Garnes, K.T., Levinson, S.H., Xu, H.E., Schwabe, J.W.R., et al. (2004). Tyrosine Agonists Reverse the Molecular Defects Associated with Dominant-Negative Mutations in Human Peroxisome Proliferator-Activated Receptor γ. Endocrinology *145*, 1527–1538.

Aherne, W., and Hull, D. (1966). Brown adipose tissue and heat production in the newborn infant. J Pathol Bacteriol *91*, 223–234.

Ahmadian, M., Abbott, M.J., Tang, T., Hudak, C.S.S., Kim, Y., Bruss, M., Hellerstein, M.K., Lee, H.-Y., Samuel, V.T., Shulman, G.I., et al. (2011). Desnutrin/ATGL Is Regulated by AMPK and Is Required for a Brown Adipose Phenotype. Cell Metabolism *13*, 739–748.

Altshuler-Keylin, S., Shinoda, K., Hasegawa, Y., Ikeda, K., Hong, H., Kang, Q., Yang, Y., Perera, R.M., Debnath, J., and Kajimura, S. (2016). Beige Adipocyte Maintenance Is Regulated by Autophagy-Induced Mitochondrial Clearance. Cell Metabolism *24*, 402–419.

Alvarez-Dominguez, J.R., Bai, Z., Xu, D., Yuan, B., Lo, K.A., Yoon, M.J., Lim, Y.C., Knoll, M., Slavov, N., Chen, S., et al. (2015). De Novo Reconstruction of Adipose Tissue Transcriptomes Reveals Long Non-coding RNA Regulators of Brown Adipocyte Development. Cell Metabolism *21*, 764–776.

Anderson, C.M., Kazantzis, M., Wang, J., Venkatraman, S., Goncalves, R.L.S., Quinlan, C.L., Ng, R., Jastroch, M., Benjamin, D.I., Nie, B., et al. (2015). Dependence of Brown Adipose Tissue Function on CD36-Mediated Coenzyme Q Uptake. Cell Reports *10*, 505–515.

Armengol, J., Villena, J.A., Hondares, E., Carmona, M.C., Sul, H.S., Iglesias, R., Giralt, M., and Villarroya, F. (2012). Pref-1 in brown adipose tissue: specific involvement in brown adipocyte differentiation and regulatory role of C/EBPδ. Biochem. J. *443*, 799–810.

Atit, R., Sgaier, S.K., Mohamed, O.A., Taketo, M.M., Dufort, D., Joyner, A.L., Niswander, L., and Conlon, R.A. (2006). β-catenin activation is necessary and sufficient to specify the dorsal dermal fate in the mouse. Developmental Biology *296*, 164–176.

Bachman, E.S., Dhillon, H., Zhang, C.-Y., Cinti, S., Bianco, A.C., Kobilka, B.K., and Lowell, B.B. (2002). Beta-AR Signaling Required for Diet-Induced Thermogenesis and Obesity Resistance. Science *297*, 843.

Bagattin, A., Hugendubler, L., and Mueller, E. (2010). Transcriptional coactivator PGC-1α promotes peroxisomal remodeling and biogenesis. PNAS *107*, 20376–20381.

Bai, Z., Chai, X., Yoon, M.J., Kim, H.-J., Lo, K.A., Zhang, Z., Xu, D., Siang, D.T.C., Walet, A.C.E., Xu, S., et al. (2017). Dynamic transcriptome changes during adipose tissue energy expenditure reveal critical roles for long noncoding RNA regulators. PLoS Biol *15*, e2002176.

Barak, Y., Nelson, M.C., Ong, E.S., Jones, Y.Z., Ruiz-Lozano, P., Chien, K.R., Koder, A., and Evans, R.M. (1999). PPARγ Is Required for Placental, Cardiac, and Adipose Tissue Development. Molecular Cell 11.

Barroso, I., Gurnell, M., Crowley, V.E.F., Agostini, M., Schwabe, J.W., Soos, M.A., Maslen, G.L., Williams, T.D.M., Lewis, H., Schafer, A.J., et al. (1999). Dominant negative mutations in human PPARγ associated with severe insulin resistance, diabetes mellitus and hypertension. Nature *402*, 880.

Baumgartner, B.G., Orpinell, M., Duran, J., Ribas, V., Burghardt, H.E., Bach, D., Villar, A.V., Paz, J.C., González, M., Camps, M., et al. (2007). Identification of a Novel Modulator of Thyroid Hormone Receptor-Mediated Action. PLoS ONE *2*, e1183.

Bengtsson, T., Cannon, B., and Nedergaard, J. (2000). Differential adrenergic regulation of the gene expression of the β-adrenoceptor subtypes β1, β2 and β3 in brown adipocytes. Biochemical Journal *347*, 643–651.

Blondin, D.P., Labbé, S.M., Tingelstad, H.C., Noll, C., Kunach, M., Phoenix, S., Guérin, B., Turcotte, É.E., Carpentier, A.C., Richard, D., et al. (2014). Increased Brown Adipose Tissue Oxidative Capacity in Cold-Acclimated Humans. J Clin Endocrinol Metab *99*, E438–E446.

Blondin, D.P., Labbé, S.M., Noll, C., Kunach, M., Phoenix, S., Guérin, B., Turcotte, É.E., Haman, F., Richard, D., and Carpentier, A.C. (2015). Selective Impairment of Glucose but Not Fatty Acid or Oxidative Metabolism in Brown Adipose Tissue of Subjects With Type 2 Diabetes. Diabetes *64*, 2388–2397.

Blondin, D.P., Frisch, F., Phoenix, S., Guérin, B., Turcotte, É.E., Haman, F., Richard, D., and Carpentier, A.C. (2017). Inhibition of Intracellular Triglyceride Lipolysis Suppresses Cold-Induced Brown Adipose Tissue Metabolism and Increases Shivering in Humans. Cell Metabolism *25*, 438–447.

Bolstad, B.M., Collin, F., Brettschneider, J., Simpson, K., Cope, L., Irizarry, R.A., and Speed, T.P. (2005). Quality Assessment of Affymetrix GeneChip Data. In Bioinformatics and Computational Biology Solutions Using R and Bioconductor, R. Gentleman, V.J. Carey, W. Huber, R.A. Irizarry, and S. Dudoit, eds. (New York, NY: Springer New York), pp. 33–47.

Bronnikov, G., Bengtsson, T., Kramarova, L., Golozoubova, V., Cannon, B., and Nedergaard, J. (1999). β1 to β3 Switch in Control of Cyclic Adenosine Monophosphate during Brown Adipocyte Development Explains Distinct β-Adrenoceptor Subtype Mediation of Proliferation and Differentiation. Endocrinology *140*, 4185–4197.

Burýšek, L., and Houštěk, J. (1997). β-Adrenergic stimulation of interleukin-1α and interleukin-6 expression in mouse brown adipocytes. FEBS Letters *411*, 83–86.

Cairó, M., Villarroya, J., Cereijo, R., Campderrós, L., Giralt, M., and Villarroya, F. (2016). Thermogenic activation represses autophagy in brown adipose tissue. Int J Obes *40*, 1591–1599.

Cairó, M., Campderrós, L., Gavaldà-Navarro, A., Cereijo, R., Delgado-Anglés, A., Quesada-López, T., Giralt, M., Villarroya, J., and Villarroya, F. (2019). Parkin controls brown adipose tissue plasticity in response to adaptive thermogenesis. EMBO Reports *20*, e46832.

Cannon, B., and Nedergaard, J. (2004). Brown Adipose Tissue: Function and Physiological Significance. Physiological Reviews *84*, 277–359.

Cannon, B., and Nedergaard, J. (2011). Nonshivering thermogenesis and its adequate measurement in metabolic studies. Journal of Experimental Biology *214*, 242–253.

Cannon, B., Hedin, A., and Nedergaard, J. (1982). Exclusive occurrence of thermogenin antigen in brown adipose tissue. FEBS Lett. *150*, 129–132.

Cao, W., Medvedev, A.V., Daniel, K.W., and Collins, S. (2001). β-Adrenergic Activation of p38 MAP Kinase in Adipocytes: cAMP INDUCTION OF THE UNCOUPLING PROTEIN 1 (UCP1) GENE REQUIRES p38 MAP KINASE. J. Biol. Chem. *276*, 27077–27082.

Cao, W., Daniel, K.W., Robidoux, J., Puigserver, P., Medvedev, A.V., Bai, X., Floering, L.M., Spiegelman, B.M., and Collins, S. (2004). p38 Mitogen-Activated Protein Kinase Is the Central Regulator of Cyclic AMP-Dependent Transcription of the Brown Fat Uncoupling Protein 1 Gene. Molecular and Cellular Biology *24*, 3057–3067.

Carmona, M.C., Hondares, E., Rodríguez De La Concepción, M.L., Rodríguez-Sureda, V., Peinado-Onsurbe, J., Poli, V., Iglesias, R., Villarroya, F., and Giralt, M. (2005). Defective thermoregulation, impaired lipid metabolism, but preserved adrenergic induction of gene expression in brown fat of mice lacking C/EBPβ. Biochem. J. *389*, 47–56.

Cassard-Doulcier, A.M., Larose, M., Matamala, J.C., Champigny, O., Bouillaud, F., and Ricquier, D. (1994). In vitro interactions between nuclear proteins and uncoupling protein gene promoter reveal several putative transactivating factors including Ets1, retinoid X receptor, thyroid hormone receptor, and a CACCC box-binding protein. J. Biol. Chem. *269*, 24335–24342.

Cederberg, A., Grønning, L.M., Ahrén, B., Taskén, K., Carlsson, P., and Enerbäck, S. (2001). FOXC2 Is a Winged Helix Gene that Counteracts Obesity, Hypertriglyceridemia, and Diet-Induced Insulin Resistance. Cell *106*, 563–573.

Chondronikola, M., Volpi, E., Børsheim, E., Porter, C., Annamalai, P., Enerbäck, S., Lidell, M.E., Saraf, M.K., Labbe, S.M., Hurren, N.M., et al. (2014). Brown Adipose Tissue Improves Whole-Body Glucose Homeostasis and Insulin Sensitivity in Humans. Diabetes *63*, 4089–4099.

Christodoulides, C., Lagathu, C., Sethi, J.K., and Vidal-Puig, A. (2009). Adipogenesis and WNT signalling. Trends Endocrinol. Metab. *20*, 16–24.

Cinti, S. (2005). The adipose organ. Prostaglandins, Leukotrienes and Essential Fatty Acids *73*, 9–15.

Cousin, B., Cinti, S., Morroni, M., Raimbault, S., Ricquier, D., Pénicaud, L., and Casteilla, L. (1992). Occurrence of brown adipocytes in rat white adipose tissue: molecular and morphological characterization. J. Cell. Sci. *103 (Pt 4)*, 931–942.

Cui, X., Nguyen, N.L.T., Zarebidaki, E., Cao, Q., Li, F., Zha, L., Bartness, T., Shi, H., and Xue, B. (2016). Thermoneutrality decreases thermogenic program and promotes adiposity in high-fat diet-fed mice. Physiol Rep *4*, e12799.

Cypess, A.M., Williams, G., Goldfine, A.B., Tseng, Y.-H., and Kolodny, G.M. (2009). Identification and Importance of Brown Adipose Tissue in Adult Humans. The New England Journal of Medicine 9.

Cypess, A.M., White, A.P., Vernochet, C., Schulz, T.J., Xue, R., Sass, C.A., Huang, T.L., Roberts-Toler, C., Weiner, L.S., Sze, C., et al. (2013). Anatomical localization, gene expression profiling and functional characterization of adult human neck brown fat. Nat Med *19*, 635–639.

Dambacher, C.M., Worden, E.J., Herzik, M.A., Martin, A., and Lander, G.C. (2016). Atomic structure of the 26S proteasome lid reveals the mechanism of deubiquitinase inhibition. ELife *5*.

Darimont, C., Gaillard, D., Ailhaud, G., and Negrel, R. (1993). Terminal differentiation of mouse preadipocyte cells: adipogenic and antimitogenic role of triiodothyronine. Mol. Cell. Endocrinol. *98*, 67–73.

Digby, J.E., Montague, C.T., Sewter, C.P., Sanders, L., Wilkison, W.O., O'Rahilly, S., and Prins, J.B. (1998). Thiazolidinedione Exposure Increases the Expression of Uncoupling Protein 1 in Cultured Human Preadipocytes. Diabetes *47*, 138–141.

Divakaruni, A.S., Humphrey, D.M., and Brand, M.D. (2012). Fatty Acids Change the Conformation of Uncoupling Protein 1 (UCP1). J. Biol. Chem. *287*, 36845–36853.

Dobin, A., Davis, C.A., Schlesinger, F., Drenkow, J., Zaleski, C., Jha, S., Batut, P., Chaisson, M., and Gingeras, T.R. (2013). STAR: ultrafast universal RNA-seq aligner. Bioinformatics *29*, 15–21.

Donhoffer, S., and Szelényi, Z. (1967). The role of brown adipose tissue in thermoregulatory heat production in the warm- and cold-adapted adult rat. Acta Physiol Acad Sci Hung *32*, 53–60.

Eklund, A.C., and Szallasi, Z. (2008). Correction of technical bias in clinical microarray data improves concordance with known biological information. Genome Biol. *9*, R26.

Enerbäck, S., Jacobsson, A., Simpson, E.M., Guerra, C., Yamashita, H., Harper, M.E., and Kozak, L.P. (1997). Mice lacking mitochondrial uncoupling protein are cold-sensitive but not obese. Nature *387*, 90–94.

Entringer, S., Rasmussen, J., Cooper, D.M., Ikenoue, S., Waffarn, F., Wadhwa, P.D., and Buss, C. (2017). Association between supraclavicular brown adipose tissue composition at birth and adiposity gain from birth to 6 months of age. Pediatric Research *82*, 1017–1021.

von Essen, G., Lindsund, E., Cannon, B., and Nedergaard, J. (2017). Adaptive facultative diet-induced thermogenesis in wild-type but not in UCP1-ablated mice. American Journal of Physiology-Endocrinology and Metabolism *313*, E515–E527.

Farmer, S.R. (2006). Transcriptional control of adipocyte formation. Cell Metabolism *4*, 263–273.

Fasshauer, M., Klein, J., Kriauciunas, K.M., Ueki, K., Benito, M., and Kahn, C.R. (2001). Essential Role of Insulin Receptor Substrate 1 in Differentiation of Brown Adipocytes. Molecular and Cellular Biology *21*, 319–329.

Fawcett, D.W. (1952). A comparison of the histological organization and cytochemical reactions of brown and white adipose tissues. Journal of Morphology *90*, 363–405.

Fedorenko, A., Lishko, P.V., and Kirichok, Y. (2012). Mechanism of Fatty-Acid-Dependent UCP1 Uncoupling in Brown Fat Mitochondria. Cell *151*, 400–413.

Feldmann, H.M., Golozoubova, V., Cannon, B., and Nedergaard, J. (2009). UCP1 Ablation Induces Obesity and Abolishes Diet-Induced Thermogenesis in Mice Exempt from Thermal Stress by Living at Thermoneutrality. Cell Metabolism *9*, 203–209.

Ferri, K.F., and Kroemer, G. (2001). Mitochondria--the suicide organelles. Bioessays *23*, 111–115.

Finley, D. (2009). Recognition and Processing of Ubiquitin-Protein Conjugates by the Proteasome. Annual Review of Biochemistry *78*, 477–513.

Fischer, A.W., Cannon, B., and Nedergaard, J. (2018). Optimal housing temperatures for mice to mimic the thermal environment of humans: An experimental study. Molecular Metabolism *7*, 161–170.

Fisher, f. M., Kleiner, S., Douris, N., Fox, E.C., Mepani, R.J., Verdeguer, F., Wu, J., Kharitonenkov, A., Flier, J.S., Maratos-Flier, E., et al. (2012). FGF21 regulates PGC-1 and browning of white adipose tissues in adaptive thermogenesis. Genes & Development *26*, 271–281.

Fleury, C., Neverova, M., Collins, S., Raimbault, S., Champigny, O., Levi-Meyrueis, C., Bouillaud, F., Seldin, M.F., Surwit, R.S., Ricquier, D., et al. (1997). Uncoupling protein-2: a novel gene linked to obesity and hyperinsulinemia. Nature Genetics *15*, 269.

Floyd, Z.E., and Stephens, J.M. (2002). Interferon-γ-mediated Activation and Ubiquitin-Proteasome-dependent Degradation of PPARγ in Adipocytes. J. Biol. Chem. *277*, 4062–4068.

Floyd, Z.E., and Stephens, J.M. (2004). Control of Peroxisome Proliferator-Activated Receptor γ2 Stability and Activity by SUMOylation. Obesity Research *12*, 921–928.

Forest, C., Doglio, A., Ricquier, D., and Ailhaud, G. (1987). A preadipocyte clonal line from mouse brown adipose tissue: Short- and long-term responses to insulin and β-adrenergics. Experimental Cell Research *168*, 218–232.

Francis, V.A., Zorzano, A., and Teleman, A.A. (2010). dDOR Is an EcR Coactivator that Forms a Feed-Forward Loop Connecting Insulin and Ecdysone Signaling. Current Biology *20*, 1799–1808.

Frasor, J., Danes, J.M., Funk, C.C., and Katzenellenbogen, B.S. (2005). Estrogen down-regulation of the corepressor N-CoR: Mechanism and implications for estrogen derepression of N-CoR-regulated genes. PNAS *102*, 13153–13157.

Fukui, Y., Masui, S., Osada, S., Umesono, K., and Motojima, K. (2000). A new thiazolidinedione, NC-2100, which is a weak PPAR-gamma activator, exhibits potent antidiabetic effects and induces uncoupling protein 1 in white adipose tissue of KKAy obese mice. Diabetes *49*, 759–767.

Fulda, S., and Debatin, K.-M. (2006). Extrinsic versus intrinsic apoptosis pathways in anticancer chemotherapy. Oncogene *25*, 4798.

García-Ruiz, E., Reynés, B., Díaz-Rúa, R., Ceresi, E., Oliver, P., and Palou, A. (2015). The intake of high-fat diets induces the acquisition of brown adipocyte gene expression features in white adipose tissue. Int J Obes *39*, 1619–1629.

Gautier, L., Cope, L., Bolstad, B.M., and Irizarry, R.A. (2004). affy--analysis of Affymetrix GeneChip data at the probe level. Bioinformatics *20*, 307–315.

Géloën, A., Collet, A.J., Guay, G., and Bukowiecki, L.J. (1990). In vivo differentiation of brown adipocytes in adult mice: an electron microscopic study. Am. J. Anat. *188*, 366–372.

Gentleman, R.C., Carey, V.J., Bates, D.M., Bolstad, B., Dettling, M., Dudoit, S., Ellis, B., Gautier, L., Ge, Y., Gentry, J., et al. (2004). Bioconductor: open software development for computational biology and bioinformatics. Genome Biol. *5*, R80.

Goldgof, M., Xiao, C., Chanturiya, T., Jou, W., Gavrilova, O., and Reitman, M.L. (2014). The Chemical Uncoupler 2,4-Dinitrophenol (DNP) Protects against Diet-induced Obesity and Improves Energy Homeostasis in Mice at Thermoneutrality. J. Biol. Chem. *289*, 19341–19350.

Golozoubova, V., Hohtola, E., Matthias, A., Jacobsson, A., Cannon, B., and Nedergaard, J. (2001). Only UCP1 can mediate adaptive nonshivering thermogenesis in the cold. The FASEB Journal *15*, 2048–2050.

Golozoubova, V., Gullberg, H., Matthias, A., Cannon, B., Vennström, B., and Nedergaard, J. (2004). Depressed Thermogenesis but Competent Brown Adipose Tissue Recruitment in Mice Devoid of All Hormone-Binding Thyroid Hormone Receptors. Mol Endocrinol *18*, 384–401.

Golozoubova, V., Cannon, B., and Nedergaard, J. (2006). UCP1 is essential for adaptive adrenergic nonshivering thermogenesis. American Journal of Physiology-Endocrinology and Metabolism *291*, E350–E357.

Gordon, C.J. (1990). Thermal biology of the laboratory rat. Physiol. Behav. *47*, 963–991.

Granneman, J.G., and Lahners, K.N. (1995). Regulation of mouse beta 3-adrenergic receptor gene expression and mRNA splice variants in adipocytes. American Journal of Physiology-Cell Physiology *268*, C1040–C1044.

Gray, S.L., Dalla Nora, E., Backlund, E.C., Manieri, M., Virtue, S., Noland, R.C., O'Rahilly, S., Cortright, R.N., Cinti, S., Cannon, B., et al. (2006). Decreased Brown Adipocyte Recruitment and Thermogenic Capacity in Mice with Impaired Peroxisome Proliferator-Activated Receptor (P465L PPARγ) Function. Endocrinology *147*, 5708–5714.

Guan, H.-P., Ishizuka, T., Chui, P.C., Lehrke, M., and Lazar, M.A. (2005). Corepressors selectively control the transcriptional activity of PPARγ in adipocytes. Genes Dev. *19*, 453–461.

Guerra, C., Koza, R.A., Yamashita, H., Walsh, K., and Kozak, L.P. (1998). Emergence of brown adipocytes in white fat in mice is under genetic control. Effects on body weight and adiposity. J Clin Invest *102*, 412–420.

Guerra, C., Navarro, P., Valverde, A.M., Arribas, M., Brüning, J., Kozak, L.P., Kahn, C.R., and Benito, M. (2001). Brown adipose tissue–specific insulin receptor knockout shows diabetic phenotype without insulin resistance. J. Clin. Invest. *108*, 1205–1213.

Gunawardana, S.C., and Piston, D.W. (2012). Reversal of Type 1 Diabetes in Mice by Brown Adipose Tissue Transplant. Diabetes *61*, 674–682.

Gunawardana, S.C., and Piston, D.W. (2015). Insulin-independent reversal of type 1 diabetes in nonobese diabetic mice with brown adipose tissue transplant. American Journal of Physiology-Endocrinology and Metabolism *308*, E1043–E1055.

Gurnell, M., Wentworth, J.M., Agostini, M., Adams, M., Collingwood, T.N., Provenzano, C., Browne, P.O., Rajanayagam, O., Burris, T.P., Schwabe, J.W., et al. (2000). A Dominant-negative Peroxisome Proliferator-activated Receptor γ (PPARγ) Mutant Is a Constitutive Repressor and Inhibits PPARγ-mediated Adipogenesis. J. Biol. Chem. *275*, 5754–5759.

Haemmerle, G. (2006). Defective Lipolysis and Altered Energy Metabolism in Mice Lacking Adipose Triglyceride Lipase. Science *312*, 734–737.

Harms, M.J., Ishibashi, J., Wang, W., Lim, H.-W., Goyama, S., Sato, T., Kurokawa, M., Won, K.-J., and Seale, P. (2014). Prdm16 Is Required for the Maintenance of Brown Adipocyte Identity and Function in Adult Mice. Cell Metabolism *19*, 593–604.

Harms, M.J., Lim, H.-W., Ho, Y., Shapira, S.N., Ishibashi, J., Rajakumari, S., Steger, D.J., Lazar, M.A., Won, K.-J., and Seale, P. (2015). PRDM16 binds MED1 and controls chromatin architecture to determine a brown fat transcriptional program. Genes Dev. *29*, 298–307.

Hauser, S., Adelmant, G., Sarraf, P., Wright, H.M., Mueller, E., and Spiegelman, B.M. (2000). Degradation of the Peroxisome Proliferator-activated Receptor γ Is Linked to Ligand-dependent Activation. J. Biol. Chem. *275*, 18527–18533.

He, W., Barak, Y., Hevener, A., Olson, P., Liao, D., Le, J., Nelson, M., Ong, E., Olefsky, J.M., and Evans, R.M. (2003). Adipose-specific peroxisome proliferator-activated receptor knockout causes insulin resistance in fat and liver but not in muscle. Proceedings of the National Academy of Sciences *100*, 15712–15717.

Himms-Hagen, J. (1990). Brown adipose tissue thermogenesis: interdisciplinary studies. FASEB J. *4*, 2890–2898.

Holm, C. (2003). Molecular mechanisms regulating hormone-sensitive lipase and lipolysis. Biochemical Society Transactions *31*, 1120–1124.

Hondares, E., Mora, O., Yubero, P., de la Concepción, M.R., Iglesias, R., Giralt, M., and Villarroya, F. (2006). Thiazolidinediones and Rexinoids Induce Peroxisome Proliferator-Activated Receptor-Coactivator (PGC)-1α Gene Transcription: An Autoregulatory Loop Controls PGC-1α Expression in Adipocytes via Peroxisome Proliferator-Activated Receptor-γ Coactivation. Endocrinology *147*, 2829–2838.

Hondares, E., Rosell, M., Gonzalez, F.J., Giralt, M., Iglesias, R., and Villarroya, F. (2010). Hepatic FGF21 Expression Is Induced at Birth via PPARα in Response to Milk Intake and Contributes to Thermogenic Activation of Neonatal Brown Fat. Cell Metabolism *11*, 206–212.

Hondares, E., Rosell, M., Díaz-Delfín, J., Olmos, Y., Monsalve, M., Iglesias, R., Villarroya, F., and Giralt, M. (2011a). Peroxisome Proliferator-activated Receptor α (PPARα) Induces PPARγ Coactivator 1α (PGC-1α) Gene Expression and Contributes to Thermogenic Activation of Brown Fat: INVOLVEMENT OF PRDM16. J. Biol. Chem. *286*, 43112–43122.

Hondares, E., Iglesias, R., Giralt, A., Gonzalez, F.J., Giralt, M., Mampel, T., and Villarroya, F. (2011b). Thermogenic Activation Induces FGF21 Expression and Release in Brown Adipose Tissue. J. Biol. Chem. *286*, 12983–12990.

Hu, E., Kim, J.B., Sarraf, P., and Spiegelman, B.M. (1996). Inhibition of Adipogenesis Through MAP Kinase–Mediated Phosphorylation of PPARγ. *274*, 5.

Huang, R., Xu, Y., Wan, W., Shou, X., Qian, J., You, Z., Liu, B., Chang, C., Zhou, T., Lippincott-Schwartz, J., et al. (2015). Deacetylation of Nuclear LC3 Drives Autophagy Initiation under Starvation. Molecular Cell *57*, 456–466.

Hull, D. (1966). The structure and function of brown adipose tissue. Br. Med. Bull. *22*, 92–96.

Iershov, A., Nemazanyy, I., Alkhoury, C., Girard, M., Barth, E., Cagnard, N., Montagner, A., Chretien, D., Rugarli, E.I., Guillou, H., et al. (2019). The class 3 PI3K coordinates autophagy and mitochondrial lipid catabolism by controlling nuclear receptor PPARα. Nature Communications *10*, 1566.

Iida, S., Chen, W., Nakadai, T., Ohkuma, Y., and Roeder, R.G. (2015). PRDM16 enhances nuclear receptor-dependent transcription of the brown fat-specific Ucp1 gene through interactions with Mediator subunit MED1. Genes Dev. *29*, 308–321.

Ikeda, S.-I., Tamura, Y., Kakehi, S., Sanada, H., Kawamori, R., and Watada, H. (2016). Exercise-induced increase in IL-6 level enhances GLUT4 expression and insulin sensitivity in mouse skeletal muscle. Biochem. Biophys. Res. Commun. *473*, 947–952.

Imai, T., Takakuwa, R., Marchand, S., Dentz, E., Bornert, J.-M., Messaddeq, N., Wendling, O., Mark, M., Desvergne, B., Wahli, W., et al. (2004). Peroxisome proliferator-activated receptor is required in mature white and brown adipocytes for their survival in the mouse. Proceedings of the National Academy of Sciences *101*, 4543–4547.

Inokuma, K., Okamatsu-Ogura, Y., Omachi, A., Matsushita, Y., Kimura, K., Yamashita, H., and Saito, M. (2006). Indispensable role of mitochondrial UCP1 for antiobesity effect of Beta3-adrenergic stimulation. Endocrinol Metab *290*, 8.

Irizarry, R.A., Hobbs, B., Collin, F., Beazer-Barclay, Y.D., Antonellis, K.J., Scherf, U., and Speed, T.P. (2003). Exploration, normalization, and summaries of high density oligonucleotide array probe level data. Biostatistics *4*, 249–264.

Ivanova, S., Polajnar, M., Narbona-Perez, A.J., Hernandez-Alvarez, M.I., Frager, P., Slobodnyuk, K., Plana, N., Nebreda, A.R., Palacin, M., Gomis, R.R., et al. (2019). Regulation of death receptor signaling by the autophagy protein TP53INP2. EMBO J. e99300.

Iwen, K.A., Backhaus, J., Cassens, M., Waltl, M., Hedesan, O.C., Merkel, M., Heeren, J., Sina, C., Rademacher, L., Windjäger, A., et al. (2017). Cold-Induced Brown Adipose Tissue Activity Alters Plasma Fatty Acids and Improves Glucose Metabolism in Men. J Clin Endocrinol Metab *102*, 4226–4234.

Jacene, H.A., Cohade, C.C., Zhang, Z., and Wahl, R.L. (2011). The Relationship between Patients' Serum Glucose Levels and Metabolically Active Brown Adipose Tissue Detected by PET/CT. Mol Imaging Biol *13*, 1278–1283.

Jacobson, M.D., Weil, M., and Raff, M.C. (1997). Programmed Cell Death in Animal Development. Cell *88*, 347–354.

Jespersen, N.Z., Larsen, T.J., Peijs, L., Daugaard, S., Homøe, P., Loft, A., de Jong, J., Mathur, N., Cannon, B., Nedergaard, J., et al. (2013). A Classical Brown Adipose Tissue mRNA Signature Partly Overlaps with Brite in the Supraclavicular Region of Adult Humans. Cell Metabolism *17*, 798–805.

de Jesus, L.A., Carvalho, S.D., Ribeiro, M.O., Schneider, M., Kim, S.-W., Harney, J.W., Larsen, P.R., and Bianco, A.C. (2001). The type 2 iodothyronine deiodinase is essential for adaptive thermogenesis in brown adipose tissue. The Journal of Clinical Investigation *108*, 7.

Jiang, X., Ye, X., Guo, W., Lu, H., and Gao, Z. (2014). Inhibition of HDAC3 promotes ligand-independent PPARγ activation by protein acetylation. Journal of Molecular Endocrinology *53*, 191–200.

Jones, J.R., Barrick, C., Kim, K.-A., Lindner, J., Blondeau, B., Fujimoto, Y., Shiota, M., Kesterson, R.A., Kahn, B.B., and Magnuson, M.A. (2005). Deletion of PPARγ in adipose tissues of mice protects against high fat diet-induced obesity and insulin resistance. PNAS *102*, 6207–6212.

Kajimura, S., Seale, P., Tomaru, T., Erdjument-Bromage, H., Cooper, M.P., Ruas, J.L., Chin, S., Tempst, P., Lazar, M.A., and Spiegelman, B.M. (2008). Regulation of the brown and white fat gene programs through a PRDM16/CtBP transcriptional complex. Genes Dev. *22*, 1397–1409.

Kajimura, S., Seale, P., Kubota, K., Lunsford, E., Frangioni, J.V., Gygi, S.P., and Spiegelman, B.M. (2009). Initiation of myoblast to brown fat switch by a PRDM16-C/EBP-beta transcriptional complex. Nature *460*, 1154–1158.

Kajimura, S., Seale, P., and Spiegelman, B.M. (2010). Transcriptional Control of Brown Fat Development. Cell Metabolism *11*, 257–262.

Kalinovich, A.V., de Jong, J.M.A., Cannon, B., and Nedergaard, J. (2017). UCP1 in adipose tissues: two steps to full browning. Biochimie *134*, 127–137.

Kanehisa, M., and Goto, S. (2000). KEGG: kyoto encyclopedia of genes and genomes. Nucleic Acids Res. *28*, 27–30.

Kang, S., Bajnok, L., Longo, K.A., Petersen, R.K., Hansen, J.B., Kristiansen, K., and MacDougald, O.A. (2005). Effects of Wnt Signaling on Brown Adipocyte Differentiation and Metabolism Mediated by PGC-1α. Molecular and Cellular Biology *25*, 1272–1282.

Karamitri, A., Shore, A.M., Docherty, K., Speakman, J.R., and Lomax, M.A. (2009). Combinatorial Transcription Factor Regulation of the Cyclic AMP-response Element on the Pgc-1α Promoter in White 3T3-L1 and Brown HIB-1B Preadipocytes. J. Biol. Chem. *284*, 20738–20752.

Kershaw, E.E., and Flier, J.S. (2004). Adipose Tissue as an Endocrine Organ. J Clin Endocrinol Metab *89*, 2548–2556.

Khedoe, P.P.S.J., Hoeke, G., Kooijman, S., Dijk, W., Buijs, J.T., Kersten, S., Havekes, L.M., Hiemstra, P.S., Berbée, J.F.P., Boon, M.R., et al. (2015). Brown adipose tissue takes up plasma triglycerides mostly after lipolysis. J. Lipid Res. *56*, 51–59.

Kilroy, G., Kirk-Ballard, H., Carter, L.E., and Floyd, Z.E. (2012). The Ubiquitin Ligase Siah2 Regulates PPARγ Activity in Adipocytes. Endocrinology *153*, 1206–1218.

Kilroy, G.E., Zhang, X., and Floyd, Z.E. (2009). PPAR-γ AF-2 Domain Functions as a Component of a Ubiquitin-dependent Degradation Signal. Obesity *17*, 665–673.

Kim, J.-H., Park, K.W., Lee, E.-W., Jang, W.-S., Seo, J., Shin, S., Hwang, K.-A., and Song, J. (2014). Suppression of PPARγ through MKRN1-mediated ubiquitination and degradation prevents adipocyte differentiation. Cell Death Differ *21*, 594–603.

Kim, J.-H., Shin, S., Seo, J., Lee, E.-W., Jeong, M., Lee, M., Han, H.-J., and Song, J. (2017). C-terminus of HSC70-Interacting Protein (CHIP) Inhibits Adipocyte Differentiation via Ubiquitin- and Proteasome-Mediated Degradation of PPARγ. Scientific Reports *7*, 40023.

Kim, Y., Kim, H., Park, D., and Jeoung, and D. (2015). miR-335 Targets SIAH2 and Confers Sensitivity to Anti-Cancer Drugs by Increasing the Expression of HDAC3. Molecules and Cells *38*, 562–572.

Klein, J., Fasshauer, M., Ito, M., Lowell, B.B., Benito, M., and Kahn, C.R. (1999). β3-Adrenergic Stimulation Differentially Inhibits Insulin Signaling and Decreases Insulin-induced Glucose Uptake in Brown Adipocytes. J. Biol. Chem. *274*, 34795–34802.

Klingenberg, M., and Echtay, K.S. (2001). Uncoupling proteins: the issues from a biochemist point of view. Biochimica et Biophysica Acta (BBA) - Bioenergetics *1504*, 128–143.

Knudsen, J.G., Murholm, M., Carey, A.L., Biensø, R.S., Basse, A.L., Allen, T.L., Hidalgo, J., Kingwell, B.A., Febbraio, M.A., Hansen, J.B., et al. (2014). Role of IL-6 in exercise training- and cold-induced UCP1 expression in subcutaneous white adipose tissue. PLoS ONE *9*, e84910.

Kontani, Y., Wang, Y., Kimura, K., Inokuma, K.-I., Saito, M., Suzuki-Miura, T., Wang, Z., Sato, Y., Mori, N., and Yamashita, H. (2005). UCP1 deficiency increases susceptibility to diet-induced obesity with age. Aging Cell *4*, 147–155.

Kopecky, J., Clarke, G., Enerbäck, S., Spiegelman, B., and Kozak, L.P. (1995). Expression of the mitochondrial uncoupling protein gene from the aP2 gene promoter prevents genetic obesity. J Clin Invest *96*, 2914–2923.

Koutnikova, H., Cock, T.-A., Watanabe, M., Houten, S.M., Champy, M.-F., Dierich, A., and Auwerx, J. (2003). Compensation by the muscle limits the metabolic consequences of lipodystrophy in PPAR gamma hypomorphic mice. Proc. Natl. Acad. Sci. U.S.A. *100*, 14457–14462.

Kozak, L.P. (2010). Brown Fat and the Myth of Diet-Induced Thermogenesis. Cell Metabolism *11*, 263–267.

Lans, A.A.J.J. van der, Hoeks, J., Brans, B., Vijgen, G.H.E.J., Visser, M.G.W., Vosselman, M.J., Hansen, J., Jörgensen, J.A., Wu, J., Mottaghy, F.M., et al. (2013). Cold acclimation recruits human brown fat and increases nonshivering thermogenesis. J Clin Invest *123*, 3395–3403.

Lean, M.E., James, W.P., Jennings, G., and Trayhurn, P. (1986). Brown adipose tissue in patients with phaeochromocytoma. Int J Obes *10*, 219–227.

Lee, J.M., Choi, S.S., Lee, Y.H., Khim, K.W., Yoon, S., Kim, B., Nam, D., Suh, P.-G., Myung, K., and Choi, J.H. (2018). The E3 ubiquitin ligase TRIM25 regulates adipocyte differentiation via proteasome-mediated degradation of PPARγ. Exp Mol Med *50*, 135.

Lee, K., Villena, J.A., Moon, Y.S., Kim, K.-H., Lee, S., Kang, C., and Sul, H.S. (2003). Inhibition of adipogenesis and development of glucose intolerance by soluble preadipocyte factor–1 (Pref-1). J. Clin. Invest. *111*, 453–461.

Lee, K.W., Kwak, S.H., Koo, Y.D., Cho, Y.-K., Lee, H.M., Jung, H.S., Cho, Y.M., Park, Y.J., Chung, S.S., and Park, K.S. (2016). F-box only protein 9 is an E3 ubiquitin ligase of PPARγ. Exp. Mol. Med. *48*, e234.

Lee, P., Greenfield, J.R., Ho, K.K.Y., and Fulham, M.J. (2010). A critical appraisal of the prevalence and metabolic significance of brown adipose tissue in adult humans. American Journal of Physiology-Endocrinology and Metabolism *299*, E601–E606.

Lee, P., Werner, C.D., Kebebew, E., and Celi, F.S. (2014). Functional thermogenic beige adipogenesis is inducible in human neck fat. International Journal of Obesity *38*, 170–176.

Lepper, C., and Fan, C.-M. (2010). Inducible lineage tracing of Pax7-descendant cells reveals embryonic origin of adult satellite cells. Genesis *48*, 424–436.

Li, H., Zhu, H., Xu, C., and Yuan, J. (1998). Cleavage of BID by Caspase 8 Mediates the Mitochondrial Damage in the Fas Pathway of Apoptosis. Cell *94*, 491–501.

Li, J., Xue, Y.-M., Zhu, B., Pan, Y.-H., Zhang, Y., Wang, C., and Li, Y. (2018). Rosiglitazone Elicits an Adiponectin-Mediated Insulin-Sensitizing Action at the Adipose Tissue-Liver Axis in Otsuka Long-Evans Tokushima Fatty Rats.

Li, J.J., Wang, R., Lama, R., Wang, X., Floyd, Z.E., Park, E.A., and Liao, F.-F. (2016). Ubiquitin Ligase NEDD4 Regulates PPARγ Stability and Adipocyte Differentiation in 3T3-L1 Cells. Sci Rep *6*, 38550.

Lidell, M.E., Betz, M.J., Leinhard, O.D., Heglind, M., Elander, L., Slawik, M., Mussack, T., Nilsson, D., Romu, T., Nuutila, P., et al. (2013). Evidence for two types of brown adipose tissue in humans. Nat Med *19*, 631–634.

Lin, C.S., and Klingenberg, M. (1980). Isolation of the uncoupling protein from brown adipose tissue mitochondria. FEBS Lett. *113*, 299–303.

Linares, G.R., Xing, W., Burghardt, H., Baumgartner, B., Chen, S.-T., Ricart, W., Fernández-Real, J.M., Zorzano, A., and Mohan, S. (2011). Role of diabetes- and obesity-related protein in the regulation of osteoblast differentiation. American Journal of Physiology-Endocrinology and Metabolism *301*, E40–E48.

Liu, X., Rossmeisl, M., McClaine, J., and Kozak, L.P. (2003). Paradoxical resistance to diet-induced obesity in UCP1-deficient mice. J Clin Invest *111*, 399–407.

Lowell, B.B., and Spiegelman, B.M. (2000). Towards a molecular understanding of adaptive thermogenesis. Nature *404*, 652.

Lowell, B.B., S-Susulic, V., Hamann, A., Lawitts, J.A., Himms-Hagen, J., Boyer, B.B., Kozak, L.P., and Flier, J.S. (1993). Development of obesity in transgenic mice after genetic ablation of brown adipose tissue. Nature *366*, 740.

Luo, X., Budihardjo, I., Zou, H., Slaughter, C., and Wang, X. (1998). Bid, a Bcl2 Interacting Protein, Mediates Cytochrome c Release from Mitochondria in Response to Activation of Cell Surface Death Receptors. Cell *94*, 481–490.

Ma, S.W., and Foster, D.O. (1986). Uptake of glucose and release of fatty acids and glycerol by rat brown adipose tissue in vivo. Can. J. Physiol. Pharmacol. *64*, 609–614.

van Marken Lichtenbelt, W.D., Vanhommerig, J.W., Smulders, N.M., Drossaerts, J.M.A.F.L., Kemerink, G.J., Bouvy, N.D., Schrauwen, P., and Teule, G.J.J. (2009). Cold-activated brown adipose tissue in healthy men. N. Engl. J. Med. *360*, 1500–1508.

Marrif, H., Schifman, A., Stepanyan, Z., Gillis, M.-A., Calderone, A., Weiss, R.E., Samarut, J., and Silva, J.E. (2005). Temperature homeostasis in transgenic mice lacking thyroid hormone receptor-alpha gene products. Endocrinology *146*, 2872–2884.

Martinez-Lopez, N., Athonvarangkul, D., Sahu, S., Coletto, L., Zong, H., Bastie, C.C., Pessin, J.E., Schwartz, G.J., and Singh, R. (2013). Autophagy in Myf5+ progenitors regulates energy and glucose homeostasis through control of brown fat and skeletal muscle development. EMBO Rep *14*, 795–803.

Martinez-Lopez, N., Garcia-Macia, M., Sahu, S., Athonvarangkul, D., Liebling, E., Merlo, P., Cecconi, F., Schwartz, G.J., and Singh, R. (2016). Autophagy in the CNS and Periphery Coordinate Lipophagy and Lipolysis in the Brown Adipose Tissue and Liver. Cell Metabolism *23*, 113–127.

Martinez-Vicente, M., and Cuervo, A.M. (2007). Autophagy and neurodegeneration: when the cleaning crew goes on strike. The Lancet Neurology *6*, 352–361.

Matthias, A., Ohlson, K.B.E., Fredriksson, J.M., Jacobsson, A., Nedergaard, J., and Cannon, B. (2000). Thermogenic Responses in Brown Fat Cells Are Fully UCP1-dependent UCP2 OR UCP3 DO NOT SUBSTITUTE FOR UCP1 IN ADRENERGICALLY OR FATTY ACID-INDUCED THERMOGENESIS. J. Biol. Chem. *275*, 25073–25081.

Mauer, J., Chaurasia, B., Goldau, J., Vogt, M.C., Ruud, J., Nguyen, K.D., Theurich, S., Hausen, A.C., Schmitz, J., Brönneke, H.S., et al. (2014). Signaling by IL-6 promotes alternative activation of macrophages to limit endotoxemia and obesity-associated resistance to insulin. Nat. Immunol. *15*, 423–430.

Mauvezin, C., Orpinell, M., Francis, V.A., Mansilla, F., Duran, J., Ribas, V., Palacín, M., Boya, P., Teleman, A.A., and Zorzano, A. (2010). The nuclear cofactor DOR regulates autophagy in mammalian and Drosophila cells. EMBO Rep *11*, 37–44.

Mauvezin, C., Sancho, A., Ivanova, S., Palacin, M., and Zorzano, A. (2012). DOR undergoes nucleo-cytoplasmic shuttling, which involves passage through the nucleolus. FEBS Letters *586*, 3179–3186.

Maxwell, G.M., Nobbs, S., and Bates, D.J. (1987). Diet-induced thermogenesis in cafeteria-fed rats: a myth? American Journal of Physiology-Endocrinology and Metabolism *253*, E264–E270.

McCormack, J.G. (1982). The regulation of fatty acid synthesis in brown adipose tissue by insulin. Progress in Lipid Research *21*, 195–223.

Medema, J.P., Scaffidi, C., Kischkel, F.C., Shevchenko, A., Mann, M., Krammer, P.H., and Peter, M.E. (1997). FLICE is activated by association with the CD95 death-inducing signaling complex (DISC). EMBO J. *16*, 2794–2804.

Mercer, S.W., and Trayhurn, P. (1984). Effect of high fat diets on the thermogenic activity of brown adipose tissue in cold-acclimated mice. J. Nutr. *114*, 1151–1158.

Mercer, S.W., and Trayhurn, P. (1987). Effect of High Fat Diets on Energy Balance and Thermogenesis in Brown Adipose Tissue of Lean and Genetically Obese ob/ob Mice. The Journal of Nutrition *117*, 2147–2153.

Meyer, C.W., Ootsuka, Y., and Romanovsky, A.A. (2017). Body Temperature Measurements for Metabolic Phenotyping in Mice. Front Physiol *8*.

Mills, E.L., Pierce, K.A., Jedrychowski, M.P., Garrity, R., Winther, S., Vidoni, S., Yoneshiro, T., Spinelli, J.B., Lu, G.Z., Kazak, L., et al. (2018). Accumulation of succinate controls activation of adipose tissue thermogenesis. Nature *560*, 102.

Muise, E.S., Souza, S., Chi, A., Tan, Y., Zhao, X., Liu, F., Dallas-Yang, Q., Wu, M., Sarr, T., Zhu, L., et al. (2013). Downstream signaling pathways in mouse adipose tissues following acute in vivo administration of fibroblast growth factor 21. PLoS ONE *8*, e73011.

Nagano, G., Ohno, H., Oki, K., Kobuke, K., Shiwa, T., Yoneda, M., and Kohno, N. (2015). Activation of Classical Brown Adipocytes in the Adult Human Perirenal Depot Is Highly Correlated with PRDM16–EHMT1 Complex Expression. PLOS ONE *10*, e0122584.

Nedergaard, J., Petrovic, N., Lindgren, E.M., Jacobsson, A., and Cannon, B. (2005). PPARγ in the control of brown adipocyte differentiation. Biochimica et Biophysica Acta (BBA) - Molecular Basis of Disease *1740*, 293–304.

Nedergaard, J., Bengtsson, T., and Cannon, B. (2007). Unexpected evidence for active brown adipose tissue in adult humans. American Journal of Physiology-Endocrinology and Metabolism *293*, E444–E452.

Nicholls, D.G. (1974). Hamster Brown-Adipose-Tissue Mitochondria. European Journal of Biochemistry *49*, 573–583.

Nicholls, D.G., and Locke, R.M. (1984). Thermogenic mechanisms in brown fat. Physiological Reviews *64*, 1–64.

Nowak, J., Archange, C., Tardivel-Lacombe, J., Pontarotti, P., Pébusque, M.-J., Vaccaro, M.I., Velasco, G., Dagorn, J.-C., and Iovanna, J.L. (2009). The TP53INP2 Protein Is Required for Autophagy in Mammalian Cells. MBoC *20*, 870–881.

Ohlson, K.B., Mohell, N., Cannon, B., Lindahl, S.G., and Nedergaard, J. (1994). Thermogenesis in brown adipocytes is inhibited by volatile anesthetic agents. A factor contributing to hypothermia in infants? Anesthesiology *81*, 176–183.

Ohno, H., Shinoda, K., Spiegelman, B.M., and Kajimura, S. (2012). PPARγ agonists Induce a White-to-Brown Fat Conversion through Stabilization of PRDM16 Protein. Cell Metabolism *15*, 395–404.

Ohno, H., Shinoda, K., Ohyama, K., Sharp, L.Z., and Kajimura, S. (2013). EHMT1 controls brown adipose cell fate and thermogenesis through the PRDM16 complex. Nature *504*, 163–167.

Ohshima, T., Koga, H., and Shimotohno, K. (2004). Transcriptional Activity of Peroxisome Proliferator-activated Receptor γ Is Modulated by SUMO-1 Modification. J. Biol. Chem. *279*, 29551–29557.

Olefsky, J.M. (2000). Treatment of insulin resistance with peroxisome proliferator–activated receptor γ agonists. J Clin Invest *106*, 467–472.

Omatsu-Kanbe, M., Zarnowski, M.J., and Cushman, S.W. (1996). Hormonal regulation of glucose transport in a brown adipose cell preparation isolated from rats that shows a large response to insulin. Biochemical Journal *315*, 25–31.

Orava, J., Nuutila, P., Lidell, M.E., Oikonen, V., Noponen, T., Viljanen, T., Scheinin, M., Taittonen, M., Niemi, T., Enerbäck, S., et al. (2011). Different Metabolic Responses of Human Brown Adipose Tissue to Activation by Cold and Insulin. Cell Metabolism *14*, 272–279.

Orava, J., Nuutila, P., Noponen, T., Parkkola, R., Viljanen, T., Enerbäck, S., Rissanen, A., Pietiläinen, K.H., and Virtanen, K.A. (2013). Blunted metabolic responses to cold and insulin stimulation in brown adipose tissue of obese humans. Obesity *21*, 2279–2287.

Ouellet, V., Routhier-Labadie, A., Bellemare, W., Lakhal-Chaieb, L., Turcotte, E., Carpentier, A.C., and Richard, D. (2011). Outdoor Temperature, Age, Sex, Body Mass Index, and Diabetic Status Determine the Prevalence, Mass, and Glucose-Uptake Activity of 18F-FDG-Detected BAT in Humans. J Clin Endocrinol Metab *96*, 192–199.

Ouellet, V., Labbé, S.M., Blondin, D.P., Phoenix, S., Guérin, B., Haman, F., Turcotte, E.E., Richard, D., and Carpentier, A.C. (2012). Brown adipose tissue oxidative metabolism contributes to energy expenditure during acute cold exposure in humans. J Clin Invest *122*, 545–552.

Owen, B.M., Ding, X., Morgan, D.A., Coate, K.C., Bookout, A.L., Rahmouni, K., Kliewer, S.A., and Mangelsdorf, D.J. (2014). FGF21 Acts Centrally to Induce Sympathetic Nerve Activity, Energy Expenditure, and Weight Loss. Cell Metabolism *20*, 670–677.

Peirce, V., and Vidal-Puig, A. (2013). Regulation of glucose homoeostasis by brown adipose tissue. The Lancet Diabetes & Endocrinology *1*, 353–360.

Peng, J., Schwartz, D., Elias, J.E., Thoreen, C.C., Cheng, D., Marsischky, G., Roelofs, J., Finley, D., and Gygi, S.P. (2003). A proteomics approach to understanding protein ubiquitination. Nature Biotechnology *21*, 921.

Perissi, V., Aggarwal, A., Glass, C.K., Rose, D.W., and Rosenfeld, M.G. (2004). A Corepressor/Coactivator Exchange Complex Required for Transcriptional Activation by Nuclear Receptors and Other Regulated Transcription Factors. Cell *116*, 511–526.

Petrovic, N., Shabalina, I.G., Timmons, J.A., Cannon, B., and Nedergaard, J. (2008). Thermogenically competent nonadrenergic recruitment in brown preadipocytes by a PPARγ agonist. American Journal of Physiology-Endocrinology and Metabolism *295*, E287–E296.

Petrovic, N., Walden, T.B., Shabalina, I.G., Timmons, J.A., Cannon, B., and Nedergaard, J. (2010). Chronic Peroxisome Proliferator-activated Receptor γ (PPARγ) Activation of Epididymally Derived White Adipocyte Cultures Reveals a Population of Thermogenically Competent, UCP1-containing Adipocytes Molecularly Distinct from Classic Brown Adipocytes. J. Biol. Chem. *285*, 7153–7164.

Pfannenberg, C., Werner, M.K., Ripkens, S., Stef, I., Deckert, A., Schmadl, M., Reimold, M., Häring, H.-U., Claussen, C.D., and Stefan, N. (2010). Impact of Age on the Relationships of Brown Adipose Tissue With Sex and Adiposity in Humans. Diabetes *59*, 1789–1793.

Pich, S., Bach, D., Briones, P., Liesa, M., Camps, M., Testar, X., Palacín, M., and Zorzano, A. (2005). The Charcot–Marie–Tooth type 2A gene product, Mfn2, up-regulates fuel oxidation through expression of OXPHOS system. Hum Mol Genet *14*, 1405–1415.

Pickart, C.M. (2001). Mechanisms Underlying Ubiquitination. Annual Review of Biochemistry *70*, 503–533.

Prusiner, S.B., Cannon, B., and Lindberg, O. (1968). Oxidative Metabolism in Cells Isolated from Brown Adipose Tissue. European Journal of Biochemistry *6*, 15–22.

Puigserver, P., and Spiegelman, B.M. (2003). Peroxisome Proliferator-Activated Receptor-γ Coactivator 1α (PGC-1α): Transcriptional Coactivator and Metabolic Regulator. Endocrine Reviews *24*, 78–90.

Puigserver, P., Wu, Z., Park, C.W., Graves, R., Wright, M., and Spiegelman, B.M. (1998). A Cold-Inducible Coactivator of Nuclear Receptors Linked to Adaptive Thermogenesis. Cell *92*, 829–839.

Punthakee, Z., Alméras, N., Després, J.-P., Dagenais, G.R., Anand, S.S., Hunt, D.L., Sharma, A.M., Jung, H., Yusuf, S., and Gerstein, H.C. (2014). Impact of rosiglitazone on body composition, hepatic fat, fatty acids, adipokines and glucose in persons with impaired fasting glucose or impaired glucose tolerance: a sub-study of the DREAM trial. Diabetic Medicine *31*, 1086–1092.

Qiang, L., Wang, L., Kon, N., Zhao, W., Lee, S., Zhang, Y., Rosenbaum, M., Zhao, Y., Gu, W., Farmer, S.R., et al. (2012). Brown Remodeling of White Adipose Tissue by SirT1-Dependent Deacetylation of Pparγ. Cell *150*, 620–632.

Ritchie, M.E., Phipson, B., Wu, D., Hu, Y., Law, C.W., Shi, W., and Smyth, G.K. (2015). limma powers differential expression analyses for RNA-sequencing and microarray studies. Nucleic Acids Res. *43*, e47.

Romero, M., Sabaté-Pérez, A., Francis, V.A., Castrillón-Rodriguez, I., Díaz-Ramos, Á., Sánchez-Feutrie, M., Durán, X., Palacín, M., Moreno-Navarrete, J.M., Gustafson, B., et al. (2018). TP53INP2 regulates adiposity by activating β-catenin through autophagy-dependent sequestration of GSK3β. Nat Cell Biol *20*, 443–454.

Rong, J.X., Qiu, Y., Hansen, M.K., Zhu, L., Zhang, V., Xie, M., Okamoto, Y., Mattie, M.D., Higashiyama, H., Asano, S., et al. (2007). Adipose Mitochondrial Biogenesis Is Suppressed in db/db and High-Fat Diet-Fed Mice and Improved by Rosiglitazone. Diabetes *56*, 1751–1760.

Rosen, E.D., Sarraf, P., Troy, A.E., Bradwin, G., Moore, K., Milstone, D.S., Spiegelman, B.M., and Mortensen, R.M. (1999). PPARγ Is Required for the Differentiation of Adipose Tissue In Vivo and In Vitro. Molecular Cell *4*, 611–617.

Rosen, E.D., Hsu, C.-H., Wang, X., Sakai, S., Freeman, M.W., Gonzalez, F.J., and Spiegelman, B.M. (2002). C/EBPα induces adipogenesis through PPARγ: a unified pathway. Genes Dev *16*, 22–26.

Rossell, D., Stephan-Otto Attolini, C., Kroiss, M., and Stöcker, A. (2014). QUANTIFYING ALTERNATIVE SPLICING FROM PAIRED-END RNA-SEQUENCING DATA. Ann Appl Stat *8*, 309–330.

Rothwell, N.J., Stock, M.J., and Sudera, D.K. (1985). Beta-adrenoreceptors in rat brown adipose tissue: proportions of beta 1- and beta 2-subtypes. American Journal of Physiology-Endocrinology and Metabolism *248*, E397–E402.

Ruzankina, Y., Pinzon-Guzman, C., Asare, A., Ong, T., Pontano, L., Cotsarelis, G., Zediak, V.P., Velez, M., Bhandoola, A., and Brown, E.J. (2007). Deletion of the Developmentally Essential Gene ATR in Adult Mice Leads to Age-Related Phenotypes and Stem Cell Loss. Cell Stem Cell *1*, 113–126.

Saito, M., Okamatsu-Ogura, Y., Matsushita, M., Watanabe, K., Yoneshiro, T., Nio-Kobayashi, J., Iwanaga, T., Miyagawa, M., Kameya, T., Nakada, K., et al. (2009). High Incidence of Metabolically Active Brown Adipose Tissue in Healthy Adult Humans: Effects of Cold Exposure and Adiposity. Diabetes *58*, 1526–1531.

Sala, D., Ivanova, S., Plana, N., Ribas, V., Duran, J., Bach, D., Turkseven, S., Laville, M., Vidal, H., Karczewska-Kupczewska, M., et al. (2014). Autophagy-regulating TP53INP2 mediates muscle wasting and is repressed in diabetes. J. Clin. Invest. *124*, 1914–1927.

Sanchez-Gurmaches, J., and Guertin, D.A. (2014). Adipocytes arise from multiple lineages that are heterogeneously and dynamically distributed. Nat Commun *5*, 4099.

Sancho, A., Duran, J., García-España, A., Mauvezin, C., Alemu, E.A., Lamark, T., Macias, M.J., DeSalle, R., Royo, M., Sala, D., et al. (2012). DOR/Tp53inp2 and Tp53inp1 Constitute a Metazoan Gene Family Encoding Dual Regulators of Autophagy and Transcription. PLoS ONE *7*, e34034.

Schulz, T.J., Huang, P., Huang, T.L., Xue, R., McDougall, L.E., Townsend, K.L., Cypess, A.M., Mishina, Y., Gussoni, E., and Tseng, Y.-H. (2013). Brown-fat paucity due to impaired BMP signalling induces compensatory browning of white fat. Nature *495*, 379–383.

Seale, P., Kajimura, S., Yang, W., Chin, S., Rohas, L.M., Uldry, M., Tavernier, G., Langin, D., and Spiegelman, B.M. (2007). Transcriptional control of brown fat determination by PRDM16. Cell Metab. *6*, 38–54.

Seale, P., Bjork, B., Yang, W., Kajimura, S., Chin, S., Kuang, S., Scimè, A., Devarakonda, S., Conroe, H.M., Erdjument-Bromage, H., et al. (2008). PRDM16 controls a brown fat/skeletal muscle switch. Nature *454*, 961–967.

Seale, P., Conroe, H.M., Estall, J., Kajimura, S., Frontini, A., Ishibashi, J., Cohen, P., Cinti, S., and Spiegelman, B.M. (2011). Prdm16 determines the thermogenic program of subcutaneous white adipose tissue in mice. J. Clin. Invest. *121*, 96–105.

Sears, I.B., MacGinnitie, M.A., Kovacs, L.G., and Graves, R.A. (1996). Differentiation-dependent expression of the brown adipocyte uncoupling protein gene: regulation by peroxisome proliferator-activated receptor gamma. Mol. Cell. Biol. *16*, 3410–3419.

Sell, H., Berger, J.P., Samson, P., Castriota, G., Lalonde, J., Deshaies, Y., and Richard, D. (2004). Peroxisome Proliferator-Activated Receptor γ Agonism Increases the Capacity for Sympathetically Mediated Thermogenesis in Lean and *ob/ob* Mice. Endocrinology *145*, 3925–3934.

Sharp, L.Z., Shinoda, K., Ohno, H., Scheel, D.W., Tomoda, E., Ruiz, L., Hu, H., Wang, L., Pavlova, Z., Gilsanz, V., et al. (2012). Human BAT Possesses Molecular Signatures That Resemble Beige/Brite Cells. PLoS ONE *7*, e49452.

Shechtman, O., Papanek, P.E., and Fregly, M.J. (1990). Reversibility of cold-induced hypertension after removal of rats from cold. Can. J. Physiol. Pharmacol. *68*, 830–835.

Shibata, H., Perusse, F., Vallerand, A., and Bukowiecki, L.J. (1989). Cold exposure reverses inhibitory effects of fasting on peripheral glucose uptake in rats. American Journal of Physiology-Regulatory, Integrative and Comparative Physiology *257*, R96–R101.

Shimizu, Y., Nikami, H., Tsukazaki, K., Machado, U.F., Yano, H., Seino, Y., and Saito, M. (1993). Increased expression of glucose transporter GLUT-4 in brown adipose tissue of fasted rats after cold exposure. American Journal of Physiology-Endocrinology and Metabolism *264*, E890–E895.

Shimizu, Y., Satoh, S., Yano, H., Minokoshi, Y., Cushman, W.S., and Shimazu, T. (1998). Effects of noradrenaline on the cell-surface glucose transporters in cultured brown adipocytes: novel mechanism for selective activation of GLUT1 glucose transporters. Biochemical Journal *330*, 397–403.

Silva, J.E., and Larsen, P.R. (1985). Potential of brown adipose tissue type II thyroxine 5'-deiodinase as a local and systemic source of triiodothyronine in rats. J. Clin. Invest. *76*, 2296–2305.

Slot, J.W., Geuze, H.J., Gigengack, S., Lienhard, G.E., and James, D.E. (1991). Immuno-localization of the insulin regulatable glucose transporter in brown adipose tissue of the rat. The Journal of Cell Biology *113*, 123–135.

Small, L., Gong, H., Yassmin, C., Cooney, G.J., and Brandon, A.E. (2018). Thermoneutral housing does not influence fat mass or glucose homeostasis in C57BL/6 mice. Journal of Endocrinology *239*, 313–324.

Smith, R.E., and Roberts, J.C. (1964). THERMOGENESIS OF BROWN ADIPOSE TISSUE IN COLD-ACCLIMATED RATS. Am. J. Physiol. *206*, 143–148.

Smith, D.M., Bloom, S.R., Sugden, M.C., and Holness, M.J. (1992). Glucose transporter expression and glucose utilization in skeletal muscle and brown adipose tissue during starvation and re-feeding. Biochemical Journal *282*, 231–235.

Souza, S.C., Christoffolete, M.A., Ribeiro, M.O., Miyoshi, H., Strissel, K.J., Stancheva, Z.S., Rogers, N.H., D'Eon, T.M., Perfield, J.W., Imachi, H., et al. (2007). Perilipin regulates the thermogenic actions of norepinephrine in brown adipose tissue. J. Lipid Res. *48*, 1273–1279.

Stanford, K.I., Middelbeek, R.J.W., Townsend, K.L., An, D., Nygaard, E.B., Hitchcox, K.M., Markan, K.R., Nakano, K., Hirshman, M.F., Tseng, Y.-H., et al. (2013). Brown adipose tissue regulates glucose homeostasis and insulin sensitivity. J. Clin. Invest. *123*, 215–223.

Storlien, L.H., James, D.E., Burleigh, K.M., Chisholm, D.J., and Kraegen, E.W. (1986). Fat feeding causes widespread in vivo insulin resistance, decreased energy expenditure, and obesity in rats. American Journal of Physiology-Endocrinology and Metabolism *251*, E576–E583.

Subramanian, A., Tamayo, P., Mootha, V.K., Mukherjee, S., Ebert, B.L., Gillette, M.A., Paulovich, A., Pomeroy, S.L., Golub, T.R., Lander, E.S., et al. (2005). Gene set enrichment analysis: a knowledge-based approach for interpreting genome-wide expression profiles. Proc. Natl. Acad. Sci. U.S.A. *102*, 15545–15550.

Sugden, M.C., and Holness, M.J. (1993). Physiological modulation of the uptake and fate of glucose in brown adipose tissue. Biochemical Journal *295*, 171–176.

Susulic, V.S., Frederich, R.C., Lawitts, J., Tozzo, E., Kahn, B.B., Harper, M.-E., Himms-Hagen, J., Flier, J.S., and Lowell, B.B. (1995). Targeted Disruption of the β_3-Adrenergic Receptor Gene. J. Biol. Chem. *270*, 29483–29492.

Sutherland, J.C., Callahan, W.P., and Campbell, G.L. (1952). Hibernoma: a tumor of brown fat. Cancer *5*, 364–368.

Tai, T.-A.C., Jennermann, C., Brown, K.K., Oliver, B.B., MacGinnitie, M.A., Wilkison, W.O., Brown, H.R., Lehmann, J.M., Kliewer, S.A., Morris, D.C., et al. (1996). Activation of the Nuclear Receptor Peroxisome Proliferator-activated Receptor γ Promotes Brown Adipocyte Differentiation. J. Biol. Chem. *271*, 29909–29914.

Tapia, P., Fernández-Galilea, M., Robledo, F., Mardones, P., Galgani, J.E., and Cortés, V.A. (2018). Biology and pathological implications of brown adipose tissue: promises and caveats for the control of obesity and its associated complications. Biological Reviews *93*, 1145–1164.

Tarasov, A., Vilella, A.J., Cuppen, E., Nijman, I.J., and Prins, P. (2015). Sambamba: fast processing of NGS alignment formats. Bioinformatics *31*, 2032–2034.

Thomas, S.A., and Palmiter, R.D. (1997). Thermoregulatory and metabolic phenotypes of mice lacking noradrenaline and adrenaline. Nature *387*, 94–97.

Thonberg, H., Fredriksson, J.M., Nedergaard, J., and Cannon, B. (2002). A novel pathway for adrenergic stimulation of cAMP-response-element-binding protein (CREB) phosphorylation: mediation via α1-adrenoceptors and protein kinase C activation. Biochemical Journal *364*, 73–79.

Thurlby, P.L., Wilson, S., and Arch, J.R.S. (1987). Ciglitazone is not itself thermogenic but increases the potential for thermogenesis in lean mice. Bioscience Reports *7*, 573–577.

Tian, X.Y., Ganeshan, K., Hong, C., Nguyen, K.D., Qiu, Y., Kim, J., Tangirala, R.K., Tontonoz, P., and Chawla, A. (2016). Thermoneutral Housing Accelerates Metabolic Inflammation to Potentiate Atherosclerosis but Not Insulin Resistance. Cell Metabolism *23*, 165–178.

Timmons, J.A., Wennmalm, K., Larsson, O., Walden, T.B., Lassmann, T., Petrovic, N., Hamilton, D.L., Gimeno, R.E., Wahlestedt, C., Baar, K., et al. (2007). Myogenic gene expression signature establishes that brown and white adipocytes originate from distinct cell lineages. Proceedings of the National Academy of Sciences *104*, 4401–4406.

Tiraby, C., Tavernier, G., Lefort, C., Larrouy, D., Bouillaud, F., Ricquier, D., and Langin, D. (2003). Acquirement of Brown Fat Cell Features by Human White Adipocytes. J. Biol. Chem. *278*, 33370–33376.

Tontonoz, P., Hu, E., and Spiegelman, B.M. (1994). Stimulation of adipogenesis in fibroblasts by PPARγ2, a lipid-activated transcription factor. Cell *79*, 1147–1156.

Trayhurn, P. (1979). Thermoregulation in the diabetic-obese (db/db) mouse. The role of non-shivering thermogenesis in energy balance. Pflugers Arch. *380*, 227–232.

Tschöp, M.H., Speakman, J.R., Arch, J.R.S., Auwerx, J., Brüning, J.C., Chan, L., Eckel, R.H., Jr, R.V.F., Galgani, J.E., Hambly, C., et al. (2012). A guide to analysis of mouse energy metabolism. 7.

Tseng, Y.-H., Kokkotou, E., Schulz, T.J., Huang, T.L., Winnay, J.N., Taniguchi, C.M., Tran, T.T., Suzuki, R., Espinoza, D.O., Yamamoto, Y., et al. (2008). New role of bone morphogenetic protein 7 in brown adipogenesis and energy expenditure. Nature *454*, 1000–1004.

Uchida, K., Shiuchi, T., Inada, H., Minokoshi, Y., and Tominaga, M. (2010). Metabolic adaptation of mice in a cool environment. Pflugers Arch - Eur J Physiol *459*, 765–774.

Uldry, M., Yang, W., St-Pierre, J., Lin, J., Seale, P., and Spiegelman, B.M. (2006). Complementary action of the PGC-1 coactivators in mitochondrial biogenesis and brown fat differentiation. Cell Metabolism *3*, 333–341.

Vaux, D.L., and Korsmeyer, S.J. (1999). Cell Death in Development. Cell *96*, 245–254.

Ventii, K.H., and Wilkinson, K.D. (2008). Protein partners of deubiquitinating enzymes. Biochemical Journal *414*, 161–175.

Vernochet, C., Peres, S.B., Davis, K.E., McDonald, M.E., Qiang, L., Wang, H., Scherer, P.E., and Farmer, S.R. (2009). C/EBP and the Corepressors CtBP1 and CtBP2 Regulate Repression of Select Visceral White Adipose Genes during Induction of the Brown Phenotype in White Adipocytes by Peroxisome Proliferator-Activated Receptor Agonists. Molecular and Cellular Biology *29*, 4714–4728.

Vidal-Puig, A., Solanes, G., Grujic, D., Flier, J.S., and Lowell, B.B. (1997). UCP3: An Uncoupling Protein Homologue Expressed Preferentially and Abundantly in Skeletal Muscle and Brown Adipose Tissue. Biochemical and Biophysical Research Communications *235*, 79–82.

Vijgen, G.H.E.J., Bouvy, N.D., Teule, G.J.J., Brans, B., Schrauwen, P., and van Marken Lichtenbelt, W.D. (2011). Brown Adipose Tissue in Morbidly Obese Subjects. PLoS ONE *6*, e17247.

Villarroya, F., Cereijo, R., Villarroya, J., and Giralt, M. (2017a). Brown adipose tissue as a secretory organ. Nature Reviews Endocrinology *13*, 26–35.

Villarroya, F., Gavaldà-Navarro, A., Peyrou, M., Villarroya, J., and Giralt, M. (2017b). The Lives and Times of Brown Adipokines. Trends in Endocrinology & Metabolism *28*, 855–867.

Virtanen, K.A., Lidell, M.E., Orava, J., Heglind, M., Westergren, R., Niemi, T., Taittonen, M., Laine, J., Savisto, N.-J., Enerbäck, S., et al. (2009). Functional Brown Adipose Tissue in Healthy Adults. N Engl J Med *360*, 1518–1525.

Virtue, S., and Vidal-Puig, A. (2013). Assessment of brown adipose tissue function. Front. Physiol. *4*.

Waldén, T.B., Hansen, I.R., Timmons, J.A., Cannon, B., and Nedergaard, J. (2012). Recruited vs. nonrecruited molecular signatures of brown, "brite," and white adipose tissues. American Journal of Physiology-Endocrinology and Metabolism *302*, E19–E31.

Wang, L., Jin, Q., Lee, J.-E., Su, I. -h., and Ge, K. (2010). Histone H3K27 methyltransferase Ezh2 represses Wnt genes to facilitate adipogenesis. Proceedings of the National Academy of Sciences *107*, 7317–7322.

Wang, W., Kissig, M., Rajakumari, S., Huang, L., Lim, H., Won, K.-J., and Seale, P. (2014). Ebf2 is a selective marker of brown and beige adipogenic precursor cells. Proc Natl Acad Sci USA *111*, 14466–14471.

Watanabe, M., Takahashi, H., Saeki, Y., Ozaki, T., Itoh, S., Suzuki, M., Mizushima, W., Tanaka, K., and Hatakeyama, S. (2015). The E3 ubiquitin ligase TRIM23 regulates adipocyte differentiation via stabilization of the adipogenic activator PPARγ. ELife *4*, e05615.

Whittle, A.J., Carobbio, S., Martins, L., Slawik, M., Hondares, E., Vázquez, M.J., Morgan, D., Csikasz, R.I., Gallego, R., Rodriguez-Cuenca, S., et al. (2012). BMP8B Increases Brown Adipose Tissue Thermogenesis through Both Central and Peripheral Actions. Cell *149*, 871–885.

Wijers, S.L.J., Saris, W.H.M., and Lichtenbelt, W.D.V.M. (2009). Recent advances in adaptive thermogenesis: potential implications for the treatment of obesity. Obesity Reviews *10*, 218–226.

Wilson-Fritch, L., Nicoloro, S., Chouinard, M., Lazar, M.A., Chui, P.C., Leszyk, J., Straubhaar, J., Czech, M.P., and Corvera, S. (2004). Mitochondrial remodeling in adipose tissue associated with obesity and treatment with rosiglitazone. J. Clin. Invest. *114*, 1281–1289.

Wu, J., Boström, P., Sparks, L.M., Ye, L., Choi, J.H., Giang, A.-H., Khandekar, M., Virtanen, K.A., Nuutila, P., Schaart, G., et al. (2012). Beige Adipocytes Are a Distinct Type of Thermogenic Fat Cell in Mouse and Human. Cell *150*, 366–376.

Wu, Z., Puigserver, P., Andersson, U., Zhang, C., Adelmant, G., Mootha, V., Troy, A., Cinti, S., Lowell, B., Scarpulla, R.C., et al. (1999a). Mechanisms Controlling Mitochondrial Biogenesis and Respiration through the Thermogenic Coactivator PGC-1. Cell *98*, 115–124.

Wu, Z., Rosen, E.D., Brun, R., Hauser, S., Adelmant, G., Troy, A.E., McKeon, C., Darlington, G.J., and Spiegelman, B.M. (1999b). Cross-regulation of C/EBP alpha and PPAR gamma controls the transcriptional pathway of adipogenesis and insulin sensitivity. Mol. Cell *3*, 151–158.

Xiao, C., Goldgof, M., Gavrilova, O., and Reitman, M.L. (2015). Anti-obesity and metabolic efficacy of the β3-adrenergic agonist, CL316243, in mice at thermoneutrality compared to 22°C: Effect of Cl316243 at Thermoneutrality. Obesity *23*, 1450–1459.

Xu, Y., and Wan, W. (2019). TP53INP2 mediates autophagic degradation of ubiquitinated proteins through its ubiquitin-interacting motif. FEBS Letters.

Xu, Y., Wan, W., Shou, X., Huang, R., You, Z., Shou, Y., Wang, L., Zhou, T., and Liu, W. (2016). TP53INP2/DOR, a mediator of cell autophagy, promotes rDNA transcription via facilitating the assembly of the POLR1/RNA polymerase I preinitiation complex at rDNA promoters. Autophagy *12*, 1118–1128.

Xue, Y., Petrovic, N., Cao, R., Larsson, O., Lim, S., Chen, S., Feldmann, H.M., Liang, Z., Zhu, Z., Nedergaard, J., et al. (2009). Hypoxia-Independent Angiogenesis in Adipose Tissues during Cold Acclimation. Cell Metabolism *9*, 99–109.

Yoneshiro, T., Aita, S., Matsushita, M., Okamatsu-Ogura, Y., Kameya, T., Kawai, Y., Miyagawa, M., Tsujisaki, M., and Saito, M. (2011). Age-Related Decrease in Cold-Activated Brown Adipose Tissue and Accumulation of Body Fat in Healthy Humans. Obesity *19*, 1755–1760.

Yoneshiro, T., Aita, S., Matsushita, M., Kayahara, T., Kameya, T., Kawai, Y., Iwanaga, T., and Saito, M. (2013). Recruited brown adipose tissue as an antiobesity agent in humans. J. Clin. Invest. *123*, 3404–3408.

Young, P., Arch, J.R.S., and Ashwell, M. (1984). Brown adipose tissue in the parametrial fat pad of the mouse. FEBS Letters *167*, 10–14.

Yu, C., Markan, K., Temple, K.A., Deplewski, D., Brady, M.J., and Cohen, R.N. (2005). The Nuclear Receptor Corepressors NCoR and SMRT Decrease Peroxisome Proliferator-activated Receptor γ Transcriptional Activity and Repress 3T3-L1 Adipogenesis. J. Biol. Chem. *280*, 13600–13605.

Zhang, W., and Bi, S. (2015). Hypothalamic Regulation of Brown Adipose Tissue Thermogenesis and Energy Homeostasis. Front. Endocrinol. *6*.

Zhang, J., Guenther, M.G., Carthew, R.W., and Lazar, M.A. (1998). Proteasomal regulation of nuclear receptor corepressor-mediated repression. Genes Dev. *12*, 1775–1780.

Zhang, J., Fu, M., Cui, T., Xiong, C., Xu, K., Zhong, W., Xiao, Y., Floyd, D., Liang, J., Li, E., et al. (2004). Selective disruption of PPAR 2 impairs the development of adipose tissue and insulin sensitivity. Proceedings of the National Academy of Sciences *101*, 10703–10708.

Zhang, Q., Ye, H., Miao, Q., Zhang, Z., Wang, Y., Zhu, X., Zhang, S., Zuo, C., Zhang, Z., Huang, Z., et al. (2013). Differences in the metabolic status of healthy adults with and without active brown adipose tissue. Wien Klin Wochenschr *125*, 687–695.

Zhao, H.-L., Ueki, N., and Hayman, M.J. (2010). The Ski protein negatively regulates Siah2-mediated HDAC3 degradation. Biochemical and Biophysical Research Communications *399*, 623–628.

Zhao, J., Cannon, B., and Nedergaard, J. (1997). α1-Adrenergic Stimulation Potentiates the Thermogenic Action of β3-Adrenoreceptor-generated cAMP in Brown Fat Cells. J. Biol. Chem. *272*, 32847–32856.

Zimmermann, R. (2004). Fat Mobilization in Adipose Tissue Is Promoted by Adipose Triglyceride Lipase. Science *306*, 1383–1386.

Zingaretti, M.C., Crosta, F., Vitali, A., Guerrieri, M., Frontini, A., Cannon, B., Nedergaard, J., and Cinti, S. (2009). The presence of UCP1 demonstrates that metabolically active adipose tissue in the neck of adult humans truly represents brown adipose tissue. The FASEB Journal *23*, 3113–3120.

APPENDIX

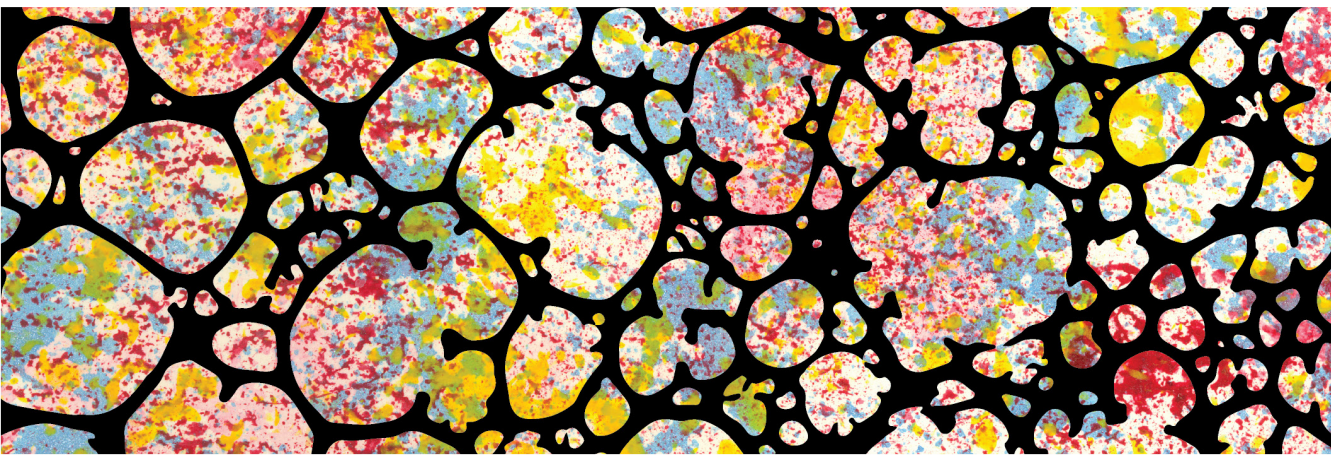

ARTICLE:

TP53INP2 regulates adiposity by activating β-catenin through autophagy-dependent sequestration of GSK3β

Montserrat Romero, Alba Sabaté-Pérez, Víctor A. Francis, Ignacio Castrillón-Rodriguez, Ángels Díaz-Ramos, Manuela Sánchez-Feutrie, Xavier Durán, Manuel Palacín, José María Moreno-Navarrete, Birgit Gustafson, Ann Hammarstedt, José Manuel Fernández-Real, Joan Vendrell, Ulf Smith and Antonio Zorzano

Nature Cell Biology, Vol. 20, pp. 443–454, April 2018.

nature cell biology

ARTICLES

https://doi.org/10.1038/s41556-018-0072-9

TP53INP2 regulates adiposity by activating β-catenin through autophagy-dependent sequestration of GSK3β

Montserrat Romero[1,2,3], Alba Sabaté-Pérez[1,2,3], Víctor A. Francis[1,2,3], Ignacio Castrillón-Rodriguez[1,2,3], Ángels Díaz-Ramos[1,2,3], Manuela Sánchez-Feutrie[1,2,3], Xavier Durán[3,4,5], Manuel Palacín[1,2,6], José María Moreno-Navarrete[7,8], Birgit Gustafson[9], Ann Hammarstedt[9], José Manuel Fernández-Real[7,8], Joan Vendrell[3,4,5], Ulf Smith[9] and Antonio Zorzano[1,2,3]*

Excessive fat accumulation is a major risk factor for the development of type 2 diabetes mellitus and other common conditions, including cardiovascular disease and certain types of cancer. Here, we identify a mechanism that regulates adiposity based on the activator of autophagy TP53INP2. We report that TP53INP2 is a negative regulator of adipogenesis in human and mouse preadipocytes. In keeping with this, TP53INP2 ablation in mice caused enhanced adiposity, which was characterized by greater cellularity of subcutaneous adipose tissue and increased expression of master adipogenic genes. TP53INP2 modulates adipogenesis through autophagy-dependent sequestration of GSK3β into late endosomes. GSK3β sequestration was also dependent on ESCRT activity. As a result, TP53INP2 promotes greater β-catenin levels and induces the transcriptional activity of TCF/LEF transcription factors. These results demonstrate a link between autophagy, sequestration of GSK3β into late endosomes and inhibition of adipogenesis in vivo.

Obesity, and its comorbidities, most notably type 2 diabetes mellitus, atherosclerosis, hypertension and hyperlipidaemia, have become major public health concerns[1,2]. Adipocyte hypertrophy prevails in obesity[3], and enlarged adipocytes in patients with type 2 diabetes mellitus are an independent marker of insulin resistance in subcutaneous white adipose tissue (WAT)[4,5]. Hypertrophic obesity may be explained by dysregulated generation of new adipocytes, and in this connection, preadipocytes from individuals with type 2 diabetes mellitus display a gene expression profile of decreased differentiation capacity[6]. Adipogenesis is also inhibited in subcutaneous WAT in insulin-resistant obese subjects[7,8]. In all, current information suggests that, in an obesogenic context, WAT homeostasis is disrupted mainly due to dysregulated adipogenesis[9,10].

Although the regulation of adipocyte metabolism and differentiation have been studied extensively[11,12], further understanding of the molecular mechanisms influencing adipocyte biology is critical for advances in the treatment of obesity and associated metabolic diseases. It is well established that locally secreted and circulating factors regulate adipogenesis[13]. One of the most important regulators of adipogenesis is the WNT/β-catenin signalling pathway[14]. The canonical WNT signalling cascade converges on the transcriptional regulator β-catenin[15]. In the absence of WNTs, cytoplasmic β-catenin is recruited to a degradation complex, which facilitates its phosphorylation by casein kinase I and glycogen synthase kinase 3β (GSK3β). This phosphorylation process primes β-catenin for ubiquitination and proteasomal degradation. WNT activation in 3T3-L1 preadipocytes through overexpression of WNT1 or a GSK3β phosphorylation-defective β-catenin mutant has been shown to inhibit adipogenesis[16,17] by blocking peroxisome proliferator-activated receptor-γ (PPAR-γ) and CCAAT/enhancer-binding protein-α (C/EBP-α) induction. Endogenous inhibitors of preadipocyte differentiation include WNT6, WNT10a and WNT10b[16–19], which are expressed in precursor cells and decline during differentiation. Transgenic mice expressing WNT10b in fat are lean, resistant to diet-induced and genetic obesity and have improved glucose homeostasis[20–22]. In all, WNT signalling is a molecular switch that, when activated, represses adipogenesis.

Deficiency of essential autophagy proteins causes a major impairment in the adipogenic differentiation of mouse embryo fibroblasts and in preadipocytes[23–26]. Moreover, adipose tissue-specific ablation of autophagy-related protein 7 (Atg7) reduces fat mass and adipose cell size. Overall, these studies demonstrate a key role for autophagy in WAT differentiation[27]. In the present study, we have addressed the contribution of the protein tumour protein p53-inducible nuclear protein 2 (TP53INP2), a regulator of autophagy, to adipose cell differentiation. Surprisingly, we found that TP53INP2 represses adipogenesis by promoting the sequestering

[1]Department of Biochemistry and Molecular Biomedicine, Faculty of Biology, University of Barcelona, Barcelona, Spain. [2]Institute for Research in Biomedicine (IRB Barcelona), The Barcelona Institute of Science and Technology, Barcelona, Spain. [3]Centro de Investigación Biomédica en Red de Diabetes y Enfermedades Metabólicas Asociadas (CIBERDEM), Instituto de Salud Carlos III (ISCIII), Madrid, Spain. [4]Department of Endocrinology, Hospital Joan XXIII, Rovira i Virgili University, Tarragona, Spain. [5]Institut d'Investigació Sanitaria Pere Virgili (IISPV), Tarragona, Spain. [6]Centro de Investigación Biomédica en Red de Enfermedades Raras (CIBERER), ISCIII, Madrid, Spain. [7]Department of Diabetes, Endocrinology and Nutrition, Institut d'Investigació Biomèdica de Girona (IdIBGi), Hospital of Girona 'Dr Josep Trueta', Girona, Spain. [8]Centro de Investigación Biomédica en Red de Fisiopatología de la Obesidad y Nutrición (CIBEROBN), ISCIII, Madrid, Spain. [9]Department of Molecular and Clinical Medicine, The Lundberg Laboratory for Diabetes Research, Sahlgrenska Academy at the University of Gothenburg, Gothenburg, Sweden. *e-mail: antonio.zorzano@irbbarcelona.org

of GSK3β via an autophagy-dependent and endosomal sorting complexes required for transport (ESCRT)-dependent mechanism.

Results

TP53INP2 regulates adipogenesis in human and murine cells. TP53INP2, an activator of autophagy[28–31], is expressed similarly both in adipocytes and in the stromal vascular fraction from human subcutaneous fat (Fig. 1a), thereby supporting the notion that this protein has a potential role in adipose precursor cells. To address the participation of TP53INP2 in adipogenesis, we studied the effects of TP53INP2 loss of function in 3T3-L1 preadipocytes by infection with lentiviruses encoding short interfering RNA (siRNA; knockdown (KD)) (Supplementary Fig. 1a). TP53INP2-KD adipocytes were larger (Supplementary Fig. 1b) and accumulated more triglycerides than control cells (Fig. 1b and Supplementary Fig. 1c). In addition, TP53INP2-deficient adipocytes showed increased expression

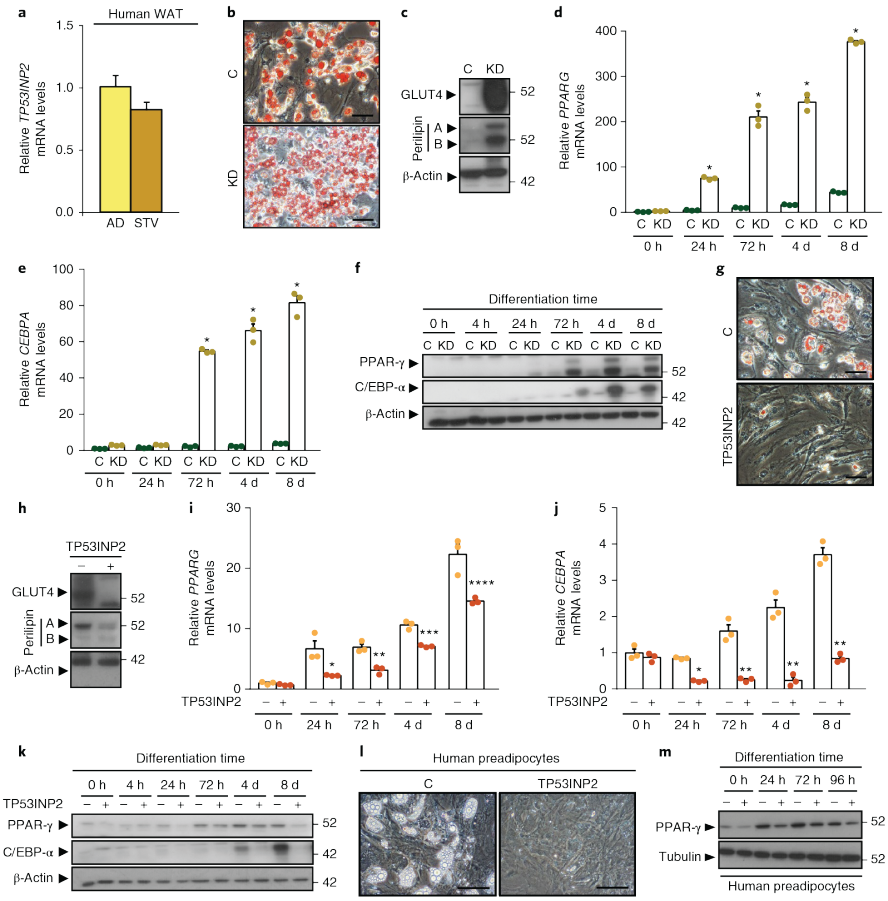

Fig. 1 | TP53INP2 regulates adipogenesis. a, *TP53INP2* mRNA levels in mature adipocytes (AD) and in the stromal vascular fraction (STV) obtained from human subcutaneous WAT. Data are means ± s.e.m.; $n = 14$ independent samples of AD and STV. **b**–**f**, Control (C) and TP53INP2-KD 3T3-L1 (KD) cells. Oil Red O staining of adipocytes at day 8 of differentiation (**b**). Scale bars, 100 µm. Perilipin and GLUT4 protein levels in adipocytes (**c**). *PPARG* (which encodes PPAR-γ) (**d**) and *CEBPA* (which encodes C/EBP-α) (**e**) mRNA levels during differentiation. Data are means ± s.e.m. of control and TP53INP3-KD cells. Significance was calculated using two-way ANOVA followed by Sidak's test (*PPARG*: $^*P < 0.0001$; *CEBPA*: $^*P < 0.0001$). Protein expression of PPAR-γ and C/EBP-α during differentiation (**f**). **g**–**k**, Control (C) and TP53INP2-overexpressing (TP53INP2) 3T3-L1CARΔ1 cells. Oil Red O staining of adipocytes at day 8 of differentiation (**g**). Scale bars, 100 µm. Perilipin and GLUT4 protein levels in mature adipocytes (**h**). *PPARG* (**i**) and *CEBPA* (**j**) mRNA levels during differentiation. Data are means ± s.e.m. of control and TP53INP3-overexpressing cells. Significance was calculated using two-way ANOVA followed by Sidak's test (*PPARG*: $^*P < 0.0021$, $^{**}P < 0.0088$, $^{***}P < 0.0151$ and $^{****}P < 0.0001$; *CEBPA*: $^*P < 0.0074$ and $^{**}P < 0.0001$). Protein expression of PPAR-γ and C/EBP-α during differentiation (**k**). **l**,**m**, Control and TP53INP2-overexpressing human adipocytes. Images of human adipocytes at day 14 of differentiation (**l**). Scale bars, 100 µm. Protein expression of PPAR-γ during human adipogenesis (**m**). **b**–**m**: $n = 3$ independent experiments. All unprocessed blots are provided in Supplementary Fig. 8.

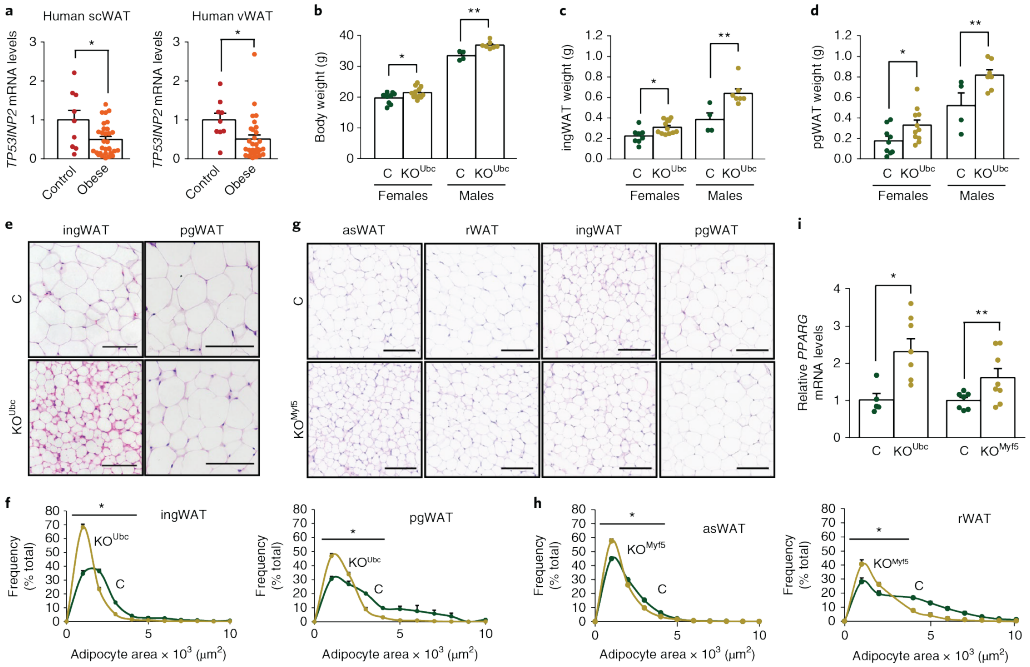

Fig. 2 | TP53INP2 loss of function promotes adipose hyperplasia. a, *TP53INP2* mRNA levels in human scWAT and vWAT from non-obese (control) and obese subjects of study 1. Data are means ± s.e.m. of $n = 9$ control and $n = 30$ obese subjects for scWAT, and $n = 9$ control and $n = 29$ obese subjects for vWAT. Significance was calculated using an unpaired two-tailed *t*-test (scWAT: $^{*}P = 0.0121$ and vWAT: $^{*}P = 0.0244$). **b**–**f**, Control and KO^{Ubc} mice at 4 months of age and subjected to a chow diet. Data are means ± s.e.m. (see details in the 'Statistics and reproducibility' section). Body weight from female and male mice (**b**). Significance was calculated using an unpaired two-tailed *t*-test ($^{*}P = 0.0429$ and $^{**}P = 0.0021$). Weight of ingWAT from female and male mice (**c**). Significance was calculated using an unpaired two-tailed *t*-test ($^{*}P = 0.0127$ and $^{**}P = 0.0081$). Weight of pgWAT from female and male mice (**d**). Significance was calculated using an unpaired two-tailed *t*-test ($^{*}P = 0.0380$ and $^{**}P = 0.0285$). Haematoxylin and eosin staining (**e**) and adipocyte area (**f**) of ingWAT or pgWAT ($n = 3$ control and $n = 3$ KO^{Ubc} mice). Scale bars, 100 μm. In **f**, data are means ± s.e.m. Significance was calculated using two-way ANOVA ($^{*}P < 0.0001$). **g**,**h**, Control and KO^{Myf5} male mice at 3 months of age and subjected to a chow diet. Data represent $n = 7$ control and $n = 6$ KO^{Myf5} samples of asWAT, $n = 8$ control and $n = 8$ KO^{Myf5} of rWAT, $n = 4$ control and $n = 4$ KO^{Myf5} of ingWAT and $n = 5$ control and $n = 6$ KO^{Myf5} of pgWAT. Haematoxylin and eosin staining of asWAT, rWAT, ingWAT and pgWAT (**g**). Scale bars, 100 μm. Adipocyte area of asWAT and rWAT (**h**). Data are means ± s.e.m. Significance was calculated using two-way ANOVA ($^{*}P < 0.0001$). **i**, *PPARG* mRNA expression in ingWAT from KO^{Ubc} and asWAT from KO^{Myf5} mice. Data are means ± s.e.m. of $n = 5$ control and KO^{Ubc} mice, and $n = 8$ control and KO^{Myf5} mice. Significance was calculated using an unpaired two-tailed *t*-test ($^{*}P = 0.0127$ control versus KO^{Ubc} and $^{**}P = 0.0386$ control versus KO^{Myf5}).

of perlipin A/B and glucose transporter type 4 (GLUT4) (Fig. 1c and Supplementary Fig. 1d,e) and greater insulin-stimulated 2-deoxy-glucose uptake (Supplementary Fig. 1f). TP53INP2 deficiency also greatly induced PPAR-γ and C/EBP-α expression during differentiation (Fig. 1d–f and Supplementary Fig. 1g,h). In all, our data indicate that TP53INP2 repression enhances the adipogenic programme in preadipocytes.

Next, we overexpressed TP53INP2 in 3T3-L1CARΔ1 preadipocytes by adenoviral infection (Supplementary Fig. 1i). TP53INP2 overexpression reduced adipogenesis in adipocytes (Fig. 1g). In addition, mature adipocytes showed reduced levels of triglycerides and low expression of adipogenic markers (Fig. 1h, and Supplementary Fig. 1j–l). In agreement with this, TP53INP2 gain of function reduced PPAR-γ and C/EBP-α expression (Fig. 1i–k and Supplementary Fig. 1m,n). TP53INP2 gain of function also blocked human adipogenic differentiation (Fig. 1l) and reduced PPAR-γ expression (Fig. 1m and Supplementary Fig. 1o) in human adipocytes.

TP53INP2 loss of function promotes adipose hyperplasia. To determine whether TP53INP2 is regulated during obesity, we studied its expression in subcutaneous and visceral fat in obese and control non-obese human subjects. Obese subjects showed reduced *TP53INP2* mRNA levels compared with the control group in both subcutaneous and visceral fat (Fig. 2a), and a negative correlation was detected when plotting *TP53INP2* mRNA against body mass index (BMI) (Supplementary Fig. 2a,b). Analysis of an independent cohort validated a negative correlation between *TP53INP2* mRNA levels in subcutaneous adipose tissue and BMI (Supplementary Fig. 2c).

To determine whether TP53INP2 deficiency is sufficient to modulate adiposity in vivo, we generated a tamoxifen-inducible total *Tp53inp2*-knockout mouse (KO^{Ubc}) by crossing homozygous *Tp53inp2*$^{loxP/loxP}$ mice[30] with a mouse strain expressing Cre-ERT2 recombinase under the control of the ubiquitin promoter (*UBC*-Cre-ERT2)[32]. Treatment with tamoxifen for 1 month (Supplementary Fig. 2d) caused the ablation of TP53INP2 in all tissues studied including WAT (KO^{Ubc} mice) (Supplemetary Fig. 2e–g). Both

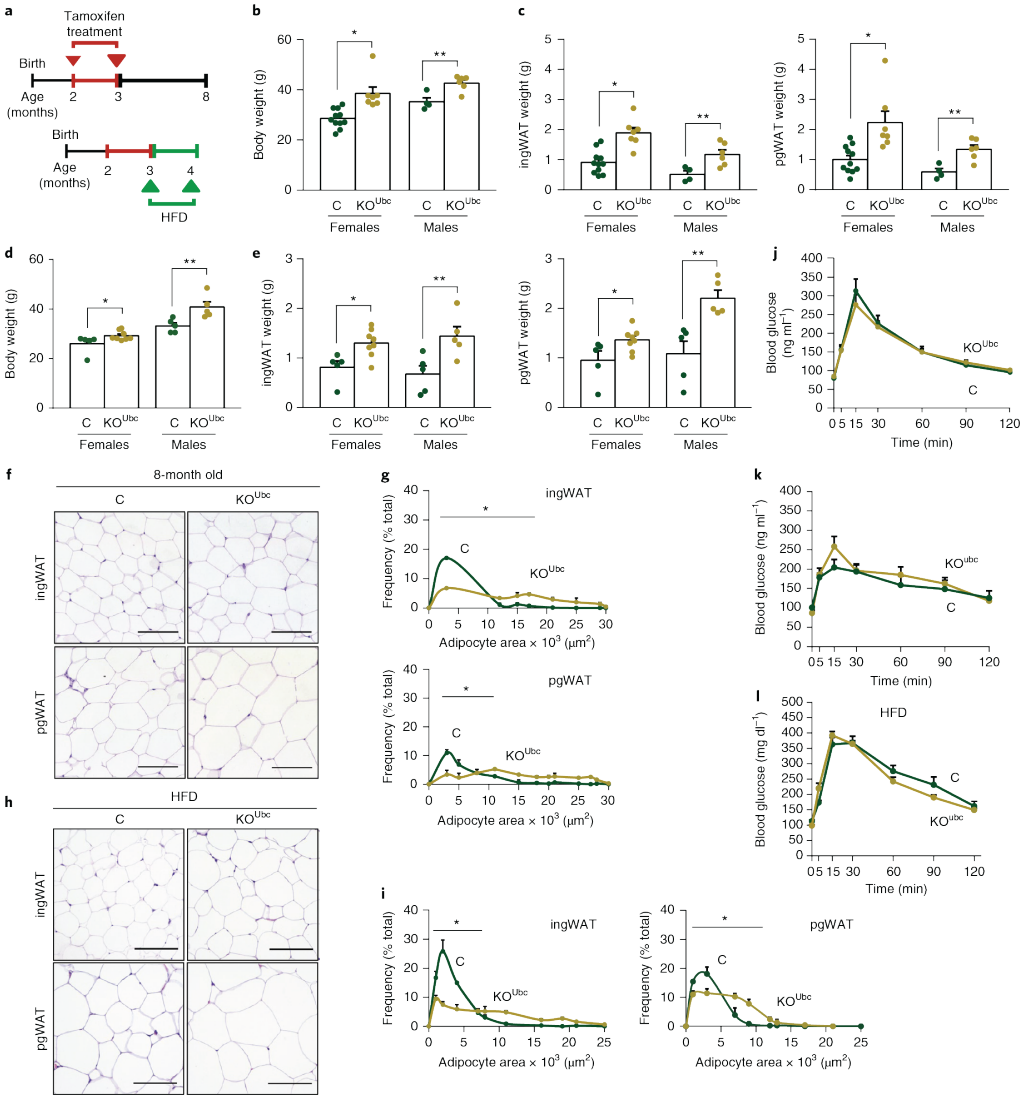

Fig. 3 | TP53INP2 loss of function promotes adiposity. a, Experimental design showing that tissues were collected 6 months after starting the tamoxifen diet (top panel) or 1 month after treatment with a high-fat diet (HFD; bottom panel). **b**,**c**, Control and KO^{Ubc} mice at 8 months of age and subjected to a chow diet. Data are means ± s.e.m. of $n = 11$ control and $n = 7$ KO^{Ubc} female mice, and $n = 4$ control and $n = 6$ KO^{Ubc} male mice. Body weight from female and male mice (**b**). Significance was calculated using an unpaired two-tailed *t*-test (*$P = 0.0009$ and **$P = 0.0061$). Weight of ingWAT and pgWAT (**c**). Significance was calculated using an unpaired two-tailed *t*-test (ingWAT: *$P = 0.0002$ and **$P = 0.0147$; pgWAT: *$P = 0.0024$ and **$P = 0.0051$). **d**,**e**, Control and KO^{Ubc} mice were subjected to a high-fat diet for 1 month. Data are means ± s.e.m. of $n = 5$ control and $n = 8$ KO^{Ubc} female mice, and $n = 5$ control and $n = 5$ KO^{Ubc} male mice. Body weight of female and male mice (**d**). Significance was calculated using an unpaired two-tailed *t*-test (*$P = 0.0471$ and **$P = 0.0138$). Weight of ingWAT and pgWAT (**e**). Significance was calculated using unpaired two-tailed *t*-test (ingWAT: *$P = 0.0118$ and **$P = 0.0175$; pgWAT: *$P = 0.0420$ and **$P = 0.0058$). **f**–**i**, Haematoxylin and eosin staining (**f**,**h**) and adipocyte area (**g**,**i**) of ingWAT and pgWAT of 8-month-old control ($n = 3$) and KO^{Ubc} ($n = 3$) mice (**f**,**g**) or mice fed with a high-fat diet ($n = 3$ control and $n = 3$ KO^{Ubc}) (**h**,**i**). Scale bars, 100 μm. In **g**, data are means ± s.e.m. Significance was calculated using two-way ANOVA (ingWAT: *$P < 0.0001$; pgWAT: *$P = 0.0004$). In **i**, data are means ± s.e.m. Significance was calculated using two-way ANOVA (ingWAT: *$P < 0.0001$; pgWAT: *$P < 0.0001$). **j**, GTT in 4-month-old mice. Data are means ± s.e.m. of $n = 5$ control and $n = 6$ KO^{Ubc} mice. **k**, GTT in 8-month-old mice. Data are means ± s.e.m. of $n = 5$ control and $n = 5$ KO^{Ubc} mice. **l**, GTT in mice fed with a high-fat diet. Data are means ± s.e.m. of $n = 5$ control and $n = 9$ KO^{Ubc} mice.

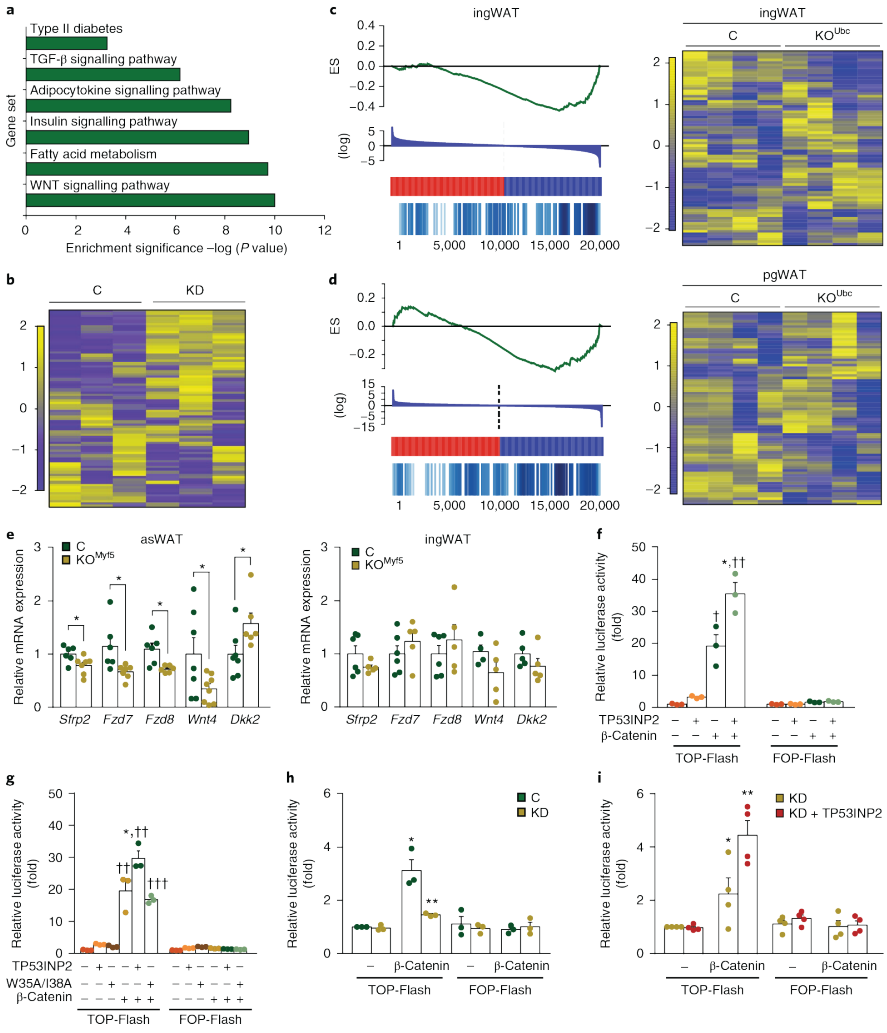

Fig. 4 | TP53INP2 increases WNT signalling. a,**b**, Control and TP53INP2-KD preadipocytes. Gene set enrichment analysis indicates several pathways from KEGG that were deregulated (**a**). Heatmap of the WNT signalling pathway (**b**). **c**,**d**, Gene set enrichment analysis of WNT signalling pathway genes that are downregulated and upregulated and the heatmap of WNT signalling in ingWAT (**c**) or pgWAT (**d**) from KO^{Ubc} and control mice. ES, enrichment score. **e**, mRNA expression of WNT genes in asWAT and ingWAT from control and KO^{Myf5} mice. Data are means ± s.e.m. from independent animals. Significance was calculated using an unpaired two-tailed *t*-test (*Sfrp2*: $n = 6$ control and $n = 7$ KO^{Myf5} mice, $^{*}P = 0.0365$; *Fzd7*: $n = 6$ control and $n = 7$ KO^{Myf5} mice, $^{*}P = 0.0195$; *Fzd8*: $n = 6$ control and $n = 6$ KO^{Myf5} mice, $^{*}P = 0.0093$; *Wnt4*: $n = 7$ control and $n = 8$ KO^{Myf5} mice, $^{*}P = 0.0497$; and *Dkk2*: $n = 7$ control and $n = 6$ KO^{Myf5} mice, $^{*}P = 0.0464$). **f**–**i**, TOP-Flash and FOP-Flash reporter activity. Control and TP53INP2-overexpressing HEK293T cells and the effects of S33Yβ-catenin (**f**). Data are means ± s.e.m. of $n = 3$ independent experiments. Significance was calculated using one-way ANOVA followed by Tukey's test ($^{*}P = 0.0076$ indicates the effects caused by TP53INP2 overexpression; $^{\dagger\dagger}P < 0.0001$ and $^{\dagger}P = 0.0044$ indicate the effects caused by β-catenin). Control HEK293T cells and cells overexpressing wild-type and W35/I38A-mutant TP53INP2, in the presence or absence of β-catenin (**g**). Data are means ± s.e.m. of $n = 3$ independent experiments. Significance was calculated using one-way ANOVA followed by Tukey's test ($^{*}P = 0.0115$ indicates the effects caused by TP53INP2 overexpression; $^{\dagger\dagger\dagger}P = 0.0003$ and $^{\dagger\dagger}P < 0.0001$ indicate the effects caused by β-catenin). Control and TP53INP2-KD preadipocytes in the presence or absence of β-catenin (**h**). Data are means ± s.e.m. of $n = 3$ independent experiments. Significance was calculated using two-way ANOVA ($^{**}P = 0.0154$ indicates the effects caused by TP53INP2 KD and $^{*}P = 0.0033$ indicates the effects caused by β-catenin. Control or TP53INP2-KD preadipocytes upon TP53INP2 re-expression in the presence or absence of β-catenin (**i**). Data are means ± s.e.m. of $n = 4$ independent experiments. Significance was calculated using two-way ANOVA ($^{**}P = 0.0292$ indicates the effects caused by TP53INP2 overexpression and $^{*}P = 0.0014$ indicates the effects caused by β-catenin).

4-month-old male and female KO^{Ubc} mice showed an increased body weight (Fig. 2b), which was a consequence of greater accumulation of subcutaneous (inguinal (ingWAT)) and visceral (perigonadal (pgWAT)) adipose tissues (Fig. 2c,d) and in the absence of major changes in other tissues or organs (Supplementary Fig. 2h,i). Staining of subcutaneous adipose tissue from 4-month-old mice revealed a greater adipocyte number and these cells were smaller in size in KO^{Ubc} mice than their control littermates (Fig. 2e,f), thereby indicating the development of hyperplasic obesity. Furthermore, visceral adipose tissue from 4-month-old mice showed a reduced adipose cell size, which is also coherent with enhanced cellularity (Fig. 2e,f). Subcutaneous adipose tissue from 4-month-old KO^{Ubc} mice showed enhanced expression of the gene encoding PPAR-γ (Fig. 2i). In addition, the expression of genes encoding adipose markers was enhanced in KO^{Ubc} mice (Supplementary Fig. 2j).

To more directly analyse whether the effects of TP53INP2 ablation on adipose tissue were of primary character and to rule out that the effects of TP53INP2 on adipose cells were a consequence of the prolonged presence of tamoxifen upon washout[33], we generated another model of *Tp53inp2*-knockout mouse by crossing homozygous *Tp53inp2*$^{loxP/loxP}$ mice with a mouse strain expressing Cre recombinase under the control of the myogenic factor 5 (*Myf5*) promoter (KO^{Myf5}). It has been reported that Myf5 is expressed in myogenic progenitors but also in cell progenitors detected in anterior subcutaneous (asWAT) and retroperitoneal (rWAT) WAT depots in mice[34]. We detected a reduced *Tp53inp2* expression in asWAT and rWAT from KO^{Myf5} mice, whereas the expression in other subcutaneous or visceral depots was not altered (ingWAT or pgWAT) (Supplementary Fig. 3a). Three-month-old KO^{Myf5} mice showed unaltered body weight (Supplementary Fig. 3b) and unaltered WAT depots weight (Supplementary Fig. 3c). Staining of adipose tissues revealed a smaller adipose cell size in TP53INP2-deficient adipose depots (asWAT and rWAT) in KO^{Myf5} mice (Fig. 2g,h). However, no effects were detected in ingWAT or pgWAT depots with a normal TP53INP2 expression (Fig. 2g and SupplementaryFig. 3d). An enhanced expression of the gene encoding PPAR-γ was also detected in asWAT from KO^{Myf5} mice (Fig. 2i).

TP53INP2 loss of function promotes enhanced adiposity. Eight-month-old KO^{Ubc} mice (Fig. 3a) showed a larger increase in body weight (Fig. 3b) and accumulated more subcutaneous and visceral fat than controls (Fig. 3c). In some studies, 10-week-old control or KO^{Ubc} mice were subjected to a high-fat diet for 1 month. KO^{Ubc} mice were heavier and showed greater fat depots than controls (Fig. 3d,e). Under these conditions, both subcutaneous and visceral adipose depots from 8-month-old mice or after treatment with a high-fat diet showed a larger adipose cell size in KO^{Ubc} mice than their control littermates (Fig. 3f–i), indicating adipose hypertrophy[35]. Despite greater adiposity, KO^{Ubc} mice showed an unaltered glucose tolerance test (GTT) at 4 or 8 months of age or after a high-fat diet (Fig. 3j–l), similar plasma insulin levels (Supplementary Fig. 3e,g) and lower expression of pro-inflammatory genes encoding tumour necrosis factor (TNF) and interleukin-1β (IL-1β) (Supplementary Fig. 3h). Whole-body oxygen consumption was reduced in KO^{Ubc} mice (Supplementary Fig. 3i), with no changes in ambulation (Supplementary Fig. 3j), food or water intake (Supplementary Fig. 3k,l).

TP53INP2 increases WNT signalling. Next, we performed transcriptomic analysis in TP53INP2-deficient 3T3-L1 preadipocytes and in subcutaneous and visceral fat from control and KO^{Ubc} mice. Gene set enrichment analysis indicated several dysregulated KEGG pathways and that the WNT signalling pathway was the most impaired in TP53INP2-deficient 3T3-L1 cells (Fig. 4a,b and Supplementary Table 1). The WNT signalling pathway was also found to be altered in adipose depots from KO^{Ubc} mice (Fig. 4c,d and Supplementary Tables 2,3). WNT target genes were also dysregulated in asWAT depot from KO^{Myf5} mice (Fig. 4e). These alterations were specifically associated with TP53INP2 deficiency, and no changes were detected in ingWAT from KO^{Myf5} mice (Fig. 4e).

Based on these data, we tested whether TP53INP2 inhibits adipogenesis through activation of the WNT pathway. TOP-Flash luciferase reporter activity of the T cell factor/lymphoid enhancer factor (TCF/LEF) transcription factors was assayed. Expression of constitutively active S33Yβ-catenin[36] or the GSK3 inhibitor LiCl enhanced TOP-Flash activity, and this was further stimulated by TP53INP2 (Fig. 4f and Supplementary Fig. 4a). Next, we analysed the impact of the TP53INP2 mutants W35/I38A, L36A/L40A and E97K/D98K, which lack autophagy activity but retain transcriptional activity as a nuclear co-factor[29]. Mutant W35/I38A did not show any capacity to synergize the effects of β-catenin on TOP-Flash activity (Fig. 4g). Similarly, the TP53INP2 mutants L36A/L40A or E97K/D98K lacked the capacity to synergize the effects of LiCl on this activity (Supplementary Fig. 4b).

The expression of constitutively active β-catenin specifically enhanced TOP-Flash activity in control 3T3-L1 cells but not in TP53INP2-deficient cells (Fig. 4h). Furthermore, TP53INP2 re-expression rescued β-catenin-dependent TOP-Flash activity in TP53INP2-deficient cells (Fig. 4i). Thus, TP53INP2 promotes WNT/β-catenin signalling in cells.

TP53INP2 enhances β-catenin levels and its nuclear localization. In preadipocytes, β-catenin translocates to the nucleus to block the transcription of C/EBP-α and PPAR-γ[17,37] and adipogenesis. Thus, we next performed TP53INP2 loss- and gain-of-function studies to address whether this protein modulates β-catenin. TP53INP2-deficient 3T3-L1 preadipocytes showed reduced levels of total β-catenin and of active non-phosphorylated β-catenin (Supplementary Fig. 5a,b), in the absence of changes in the expression of the gene encoding β-catenin (Supplementary Fig. 5c). A reduced abundance of β-catenin was also detected in the fat of KO^{Ubc} mice (Fig. 5a,b and Supplementary Fig. 5d). By contrast, TP53INP2 gain of function caused an increase in the abundance of total and active β-catenin in mouse 3T3-L1 and in human preadipocytes (Fig. 5c,d and Supplementary Fig. 5e,f).

TP53INP2 also altered the cellular localization of β-catenin. In control 3T3-L1 preadipocytes, active β-catenin was mainly nuclear (Fig. 5h), and a reduction in the levels was detectable in TP53INP2-deficient cells (Fig. 5h). Subcellular fractionation also revealed a reduction in the levels of total and active β-catenin in nuclear and cytosolic fractions from TP53INP2-deficient cells (Fig. 5f,g). By contrast, TP53INP2 gain of function increased the levels of active β-catenin in the nucleus (Fig. 5e).

Based on these observations, we analysed whether activation of the WNT signalling pathway could overcome TP53INP2 deficiency. Control or TP53INP2-deficient 3T3-L1 cells were differentiated with or without WNT3a ligand. Indeed, WNT3a caused activation of β-catenin as well as repression of the adipogenic proteins PPAR-γ and C/EBP-α, leading to inhibition of adipogenesis (Fig. 5i,j and Supplementary Fig. 5g,h).

TP53INP2 facilitates the sequestration of GSK3β into a late-endosomal compartment by an ESCRT-dependent mechanism. The activation of WNT signalling requires the sequestration of GSK3β into a late-endosomal compartment to permit cytosolic accumulation of β-catenin and its subsequent nuclear translocation[38,39]. Given our data, we tested the hypothesis that TP53INP2 promotes sequestration of GSK3β into multivesicular endosomes. The expression of an active form of Rab5 (Rab5 Q79L)[40] generated large Rab5-positive (Rab5^{+}) late endosomes (Fig. 6a) in HeLa cells. Under these conditions, TP53INP2 was detected in Rab5^{+} late endosomes (Fig. 6a). Analysis of another marker

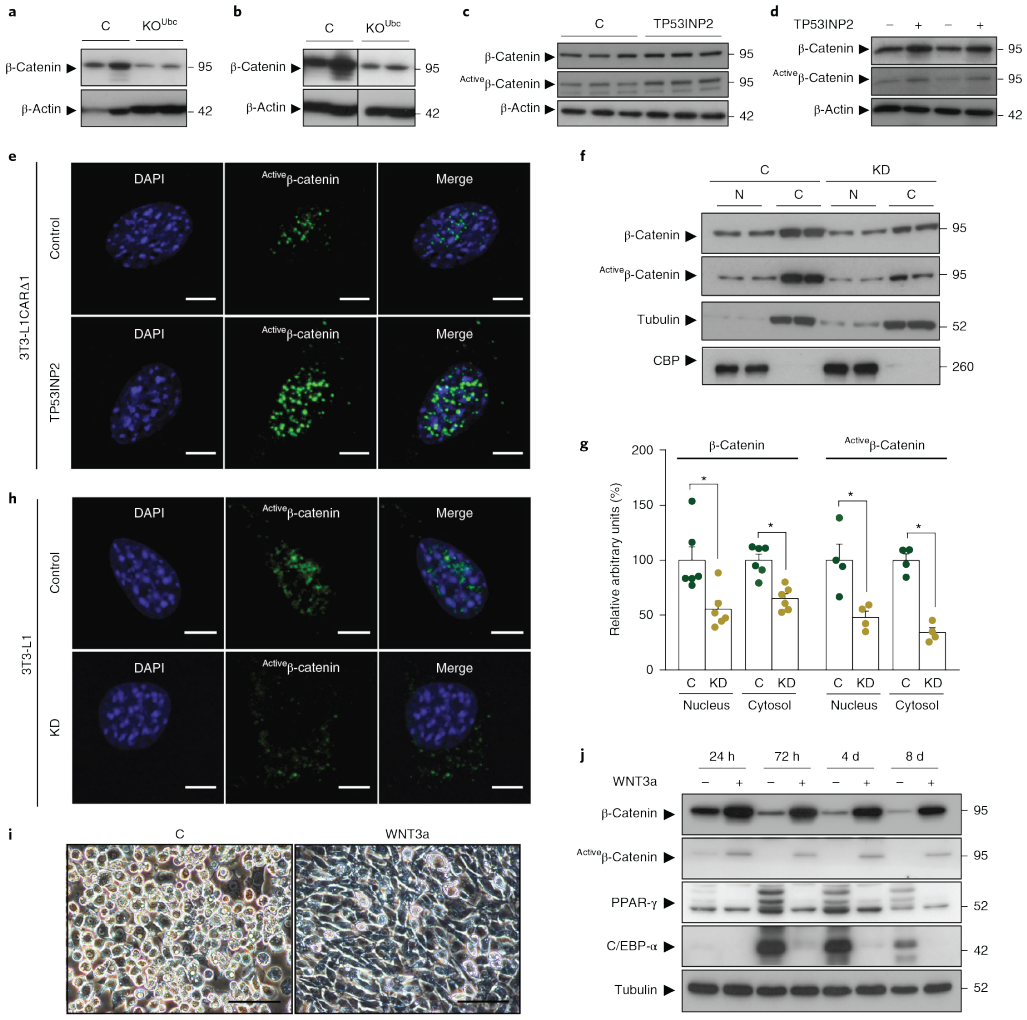

Fig. 5 | TP53INP2 enhances β-catenin levels. a,**b**, Total β-catenin protein levels in ingWAT (**a**) and pgWAT (**b**) depots of control ($n = 4$) and KO^{Ubc} ($n = 4$) mice. Data correspond to different mice. **c**, Protein expression of the total and active form of β-catenin in control and TP53INP2-overexpressing 3T3-L1CARΔ1 preadipocytes. Data correspond to $n = 3$ independent experiments. **d**, Protein expression of the total and active form of β-catenin in control and TP53INP2-overexpressing human preadipocytes. Data correspond to $n = 3$ independent experiments. **e**, Cellular location of active β-catenin in TP53INP2 gain-of-function 3T3-L1CARΔ1 preadipocytes. Scale bar, 5 μm; $n = 3$ independent experiments. **f**,**g**, Abundance of the total and active form of β-catenin in nuclear and cytosolic fractions of control and TP53INP2-KD 3T3-L1 preadipocytes. Tubulin and CBP were used as cytosolic or nuclear controls, respectively. β-catenin data were generated from $n = 6$ independent experiments and ^{Active}β-catenin results were obtained from $n = 4$ independent experiments. In **g**, data are means ± s.e.m. Significance was calculated using one-way ANOVA followed by Tukey's test (for β-catenin: $^{*}P = 0.0036$ nucleus of control versus TP53INP2-KD cells and $^{*}P = 0.0262$ cytosol of control versus TP53INP2-KD cells; for ^{Active}β-catenin: $^{*}P = 0.0057$ nucleus of control versus TP53INP2-KD cells and $^{*}P = 0.0009$ cytosol of control versus TP53INP2-KD cells). **h**, Cellular location of ^{Active}β-catenin in TP53INP2 loss-of-function 3T3-L1 preadipocytes. Scale bars, 5 μm; $n = 3$ independent experiments. **i**,**j**, TP53INP2-KD 3T3-L1 preadipocytes were differentiated in the presence or absence of WNT3a ($n = 3$ independent experiments). The representative images at day 8 of differentiation are shown (**i**). Scale bars, 100 μm. Protein expression of the total and active form of β-catenin, PPAR-γ and C/EBP-α during the differentiation process are shown (**j**). All unprocessed blots are provided in Supplementary Fig. 8.

of late endosomes or multivesicular bodies (MVBs), CD63, also revealed the co-localization of Rab5 Q79L with TP53INP2 (Supplementary Fig. 6a).

Next, we studied the localization of GSK3β in cells expressing Rab5 Q79L. In the absence of TP53INP2, GSK3β was diffuse throughout the cell and was not found in Rab5^{+} endosomes

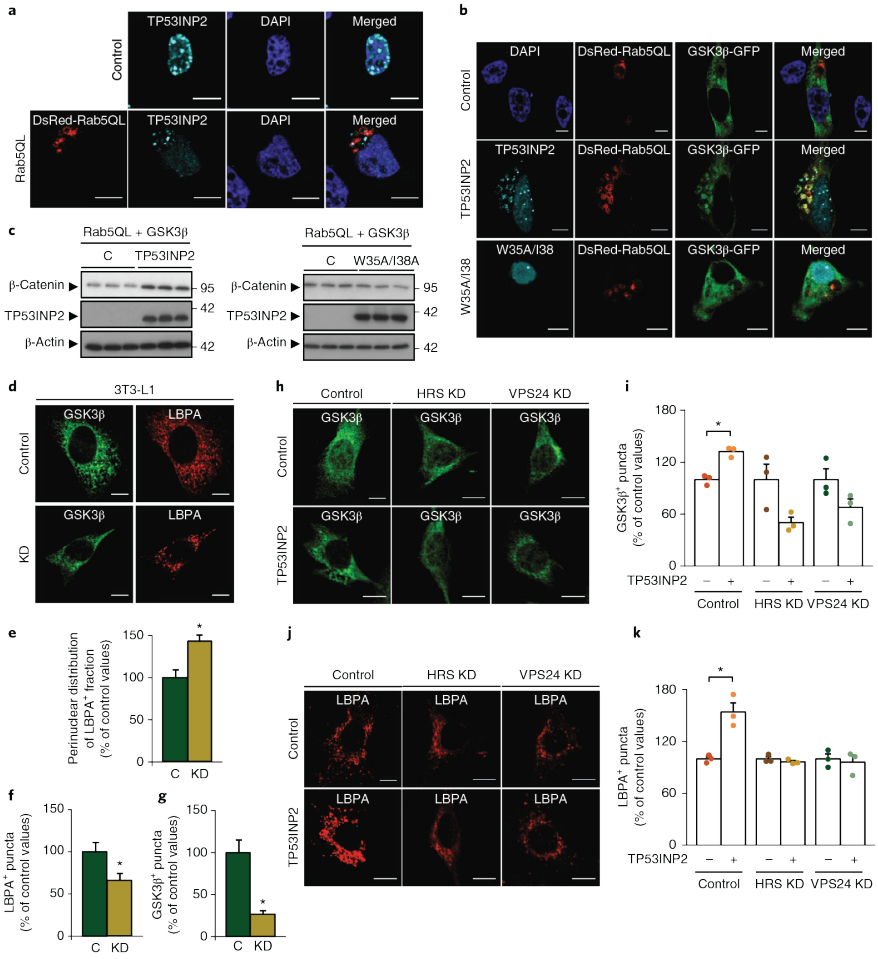

Fig. 6 | TP53INP2 facilitates the sequestration of GSK3β into a late-endosomal compartment in an ESCRT-dependent manner. a, Immunofluorescence of TP53INP2 in Rab5 Q79L-overexpressing HeLa cells. Scale bars, 8 μm; $n = 3$ independent experiments. Confocal images show TP53INP2 (cyan), DsRed-Rab5 Q79L (DsRed-Rab5QL; red) and DAPI (blue). **b**, Cellular localization of GSK3β-GFP in the presence or absence of wild-type or mutant TP53INP2 (W35A/I38A) in Rab5 Q79L-overexpressing HeLa cells. Confocal images show wild-type TP53INP2 or W35A/I38A forms (cyan), DsRed-Rab5 Q79L (red), GSK3β-GFP (green) and DAPI (blue). Scale bars, 8 μm; $n = 3$ independent experiments. **c,** Protein expression of β-catenin in cells expressing wild-type TP53INP2 or W35/I38A; $n = 3$ independent experiments. **d**–**g**, Experiments in control and TP53INP2-KD 3T3-L1 cells are shown. Immunofluorescence staining shows endogenous GSK3β (green) and endogenous LBPA (red) (**d**). Scale bars, 10 μm; $n = 3$ independent experiments. Quantification of the total LBPA⁺ puncta (**e**), the perinuclear distribution of the LBPA⁺ fraction located within 5 μm of the nucleus (**f**) and the total GSK3β⁺ puncta (**g**) are shown. For **e**–**g**, data are means ± s.e.m. Significance was calculated using an unpaired two-tailed *t*-test (*$P = 0.0149$ in panel **e**, *$P = 0.0232$ in panel **f** and *$P = 0.0005$ in panel **g** indicate the effects caused by TP53INP2 KD; $n = 150$ cells). **h**, Immunofluorescence staining shows endogenous GSK3β (green) distribution in the presence or absence of TP53INP2 in control and HRS-KD or VPS24-KD NIH-3T3 cells. Scale bars, 10 μm; $n = 3$ independent experiments. **i**, Quantification of the total GSK3β⁺ puncta in control and HRS-KD or VPS24-KD NIH-3T3 cells is shown. Data are means ± s.e.m.; $n = 3$ independent experiments. Significance was calculated using an unpaired two-tailed *t*-test (*$P = 0.0026$ indicates the effects due to TP53INP2). **j**, Immunofluorescence staining shows endogenous LBPA (red) distribution in the presence or absence of TP53INP2 in control and HRS-KD or VPS24-KD NIH-3T3 cells. Scale bars, 10 μm; $n = 3$ independent experiments. **k**, Quantification of the total LBPA⁺ puncta in control and HRS-KD or VPS24-KD NIH-3T3 cells. Data are means ± s.e.m.; $n = 3$ independent experiments. Significance was calculated using an unpaired two-tailed *t*-test (*$P = 0.0080$ indicates the effects due to TP53INP2). All unprocessed blots are provided in Supplementary Fig. 8.

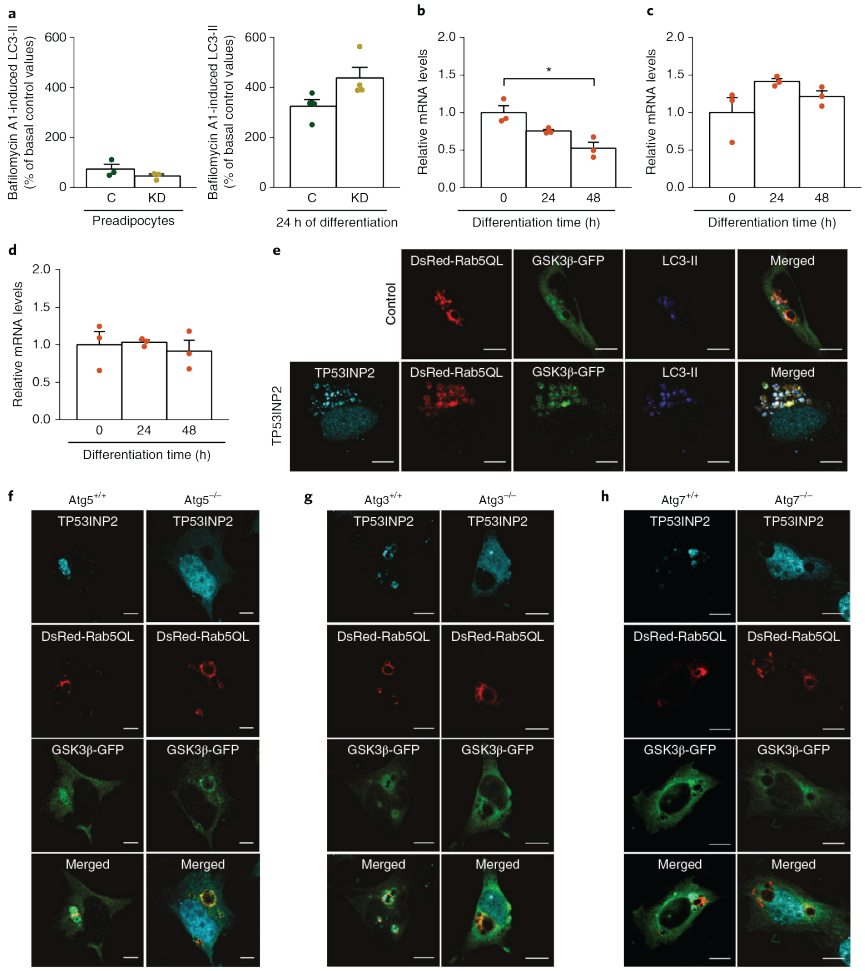

Fig. 7 | Autophagy activity is necessary for the TP53INP2-dependent sequestration of GSK3β. a, Autophagy flux as a build-up of LC3-II upon exposure to bafilomycin A1 in control and TP53INP2-KD 3T3-L1 preadipocytes (left panel) or in cells at 24 h of differentiation (right panel). Data are means ± s.e.m.; $n = 3$ independent experiments for preadipocytes and $n = 4$ independent experiments for cells at 24 h of differentiation. **b**–**d**, Expression of autophagy genes in 3T3-L1 cells upon adipogenic differentiation (*Tp53inp2* in **b**; *Atg12* in **c** and *Ulk1* in **d**). Data are means ± s.e.m.; $n = 3$ independent experiments for **b**–**d**. Significance was calculated using one-way ANOVA followed by Tukey's test (*$P = 0.0149$ 0 h versus 48 h of differentiation in **b**). **e**, Immunofluorescence of endogenous LC3-II in Rab5 Q79L-overexpressing HeLa cells in the presence or absence of TP53INP2. Scale bars, 8 μm; $n = 3$ independent experiments. **f**–**h**, Rab5 Q79L-overexpressing MEF cells. Cellular localization of GSK3β-GFP in the presence of TP53INP2 in Atg5$^{+/+}$ and Atg5$^{-/-}$ (**f**), Atg3$^{+/+}$ and Atg3$^{-/-}$ (**g**), and Atg7$^{+/+}$ and Atg7$^{-/-}$ (**h**) MEF cells. Scale bars, 10 μm; $n = 3$ independent experiments. Confocal images show TP53INP2 (cyan), DsRed-Rab5 Q79L (red), GSK3β-GFP (green) and LC3-II (blue).

(Fig. 6b). TP53INP2 increased the number of Rab5$^+$ endosomes, which were also smaller than control cells (Fig. 6b). In addition, TP53INP2 caused the sequestration of GSK3β into late endosomes that also contained Rab5 and TP53INP2 (Fig. 6b). The TP53INP2 mutant W35/I38A remained in the nucleus and did not promote the internalization of GSK3β into late endosomes (Fig. 6b). The expression of TP53INP2 increased β-catenin levels, whereas the TP53INP2 mutant W35/I38A did not have any effect (Fig. 6c and Supplementary Fig. 6b,c). The expression of a dominant-negative form of Rab5 cancelled out TP53INP2-dependent GSK3β sequestration into late endosomes (Supplementary Fig. 6d).

To further document the role of TP53INP2 as a part of a mechanism involved in GSK3β sequestration, we examined the distribution of another late-endosomal marker, lysobisphosphatidic acid (LBPA), in control and TP53INP2-KD 3T3-L1 cells. TP53INP2-deficient cells showed fewer LBPA$^+$ puncta than controls (Fig. 6d,f), and puncta

were mainly perinuclear (Fig. 6d,e). A marked reduction in the numbers of GSK3β$^+$ puncta was also detected in TP53INP2-deficient cells (Fig. 6d,g). In addition, control cells showed a detectable co-localization of CD63 and GSK3β, thereby suggesting the presence of GSK3β in MVBs (Supplementary Fig. 6e). By contrast, no co-localization of GSK3β and CD63 was detectable under TP53INP2 depletion (Supplementary Fig. 6e). TP53INP2 deficiency did not alter the distribution of the early-endosomal marker EEA1 (Supplementary Fig. 6f). In all, our data are coherent with the notion that TP53INP2 promotes the sequestration of GSK3β into late-endosomal compartments as a fundamental mechanism of WNT pathway activation.

Next, we analysed the role of the ESCRT machinery on TP53INP2-dependent GSK3β sequestration. ESCRT forms endosomal intraluminal vesicles[41] and is involved in WNT-induced GSK3β sequestration into MVBs[38]. We studied the effect of TP53INP2 on the localization of LBPA or GSK3β in HRS (a subunit of the ESCRT-0 complex)-KD 3T3 cells or in VPS24 (a subunit of the ESCRT-III complex)-KD 3T3 cells (Supplementary Fig. 6g). TP53INP2 overexpression enhanced the number of GSK3β$^+$ puncta in control 3T3 cells (Figs. 6H, 6I). In addition, TP53INP2 increased the number of LBPA$^+$ puncta in control cells (Fig. 6j,k). These effects were no longer detectable in HRS-KD or in Vps24-KD cells (Fig. 6h–k). Under these conditions, TP53INP2 increased β-catenin abundance in control but not in HRS-KD or in VPS24-KD 3T3 cells (Supplementary Fig. 6h,i). These data indicate that TP53INP2 promotes the sequestration of GSK3β into late endosomes by a mechanism that requires the ESCRT machinery.

Autophagy activity is necessary for the TP53INP2-dependent sequestration of GSK3β. TP53INP2 promotes autophagosomal formation and enhances autophagy in different cell types[28,30,31]. Basal 3T3-L1 preadipocytes showed a low rate of autophagy flux, and a marked induction of autophagy was detected upon adipogenic differentiation (Fig. 7a). TP53INP2-deficient 3T3-L1 cells showed no changes in autophagy flux during adipogenesis (Fig. 7a), indicating that other factors were key in autophagy control. In line with these data, the expression of the *TP53INP2* gene was markedly repressed upon differentiation (Fig. 7b), under conditions in which other autophagy genes such as *Atg12* or *Ulk1* remained unaltered (Fig. 7c,d). These data indicate that TP53INP2 is repressed during adipogenic differentiation and, under these conditions, autophagy flux is maintained by other autophagy proteins. Thus, TP53INP2 deficiency is not linked to a reduction in non-selective bulk macroautophagy during adipogenic differentiation. In fact, the maintenance of autophagy flux is key in adipogenesis, and submaximal concentrations of the inhibitor chloroquine inhibited C/EBP-α expression (Supplementary Fig. 7a,b).

We studied whether the effects of TP53INP2 in promoting GSK3β sequestration into late endosomes required autophagic activity. TP53INP2 overexpression caused the generation of organelles that were positive for Rab5, TP53INP2, GSK3β and microtubule-associated protein 1 light chain 3, LC3-II (Fig. 7e), suggesting that TP53INP2 promotes the generation of amphisome-like organelles.

To further determine whether the effects of TP53INP2 on sequestering GSK3β depend on autophagy activity, we studied the impact of TP53INP2 in Atg5$^{-/-}$, Atg3$^{-/-}$ or Atg7$^{-/-}$ mouse embryonic fibroblast (MEF) cells. In the presence of Rab5QL, TP53INP2 and GSK3β were recruited to Rab5$^+$ endosomes in control cells (Fig. 7f–h). By contrast, in autophagy-deficient cells, TP53INP2 remained in the nucleus and GSK3β was not internalized in Rab5$^+$ vesicles, some remaining at the periphery of Rab5$^+$ endosomes (Fig. 7f–h). Under these conditions, TP53INP2 increased β-catenin abundance in control but not in Atg5$^{-/-}$ or Atg3$^{-/-}$ MEF cells (Supplementary Fig. 7c–f). Control cells also responded to TP53INP2 by recruiting LC3-II to Rab5$^+$ endosomes. This effect was not observed in Atg5$^{-/-}$ MEF cells (Supplementary Fig. 7g).

Discussion

In this study, we have identified a protein that regulates adipogenesis in human and mouse preadipocytes, as well as adiposity in mice. We document that TP53INP2 negatively modulates adipogenesis in preadipocytes through changes in the expression of PPAR-γ and C/EBP-α. Moreover, TP53INP2 ablation caused a rapid increase in the number of fat depots in mice, which was dependent on age and accelerated by a high-fat diet. At early times after TP53INP2 ablation, a greater adipocyte number and smaller size of adipose cells were detected in both subcutaneous and visceral fat, indicating the development of an adipose hyperplasic phase. At later times or after a high-fat diet, adipose cells from KO^{Ubc} mice were hypertrophic. A phenotype characterized by adipose hyperplasia was also detected in TP53INP2-deficient adipose depots in KO^{Myf5} mice. Because Myf5 is expressed in precursor cells in specific WAT depots[34], we propose that TP53INP2 ablation in precursor cells is a key event responsible for the enhanced adipogenesis and that adipose hyperplasia is not secondary to effects in other tissues. In all, our data indicate that TP53INP2 ablation enhances adipogenic differentiation in fat, leading to initial adipose hyperplasia and further hypertrophic obesity.

Surprisingly, obesity of KO^{Ubc} mice was not accompanied by glucose intolerance, insulin resistance or adipose inflammation. Based on prior observations in mouse models in which an enhanced fat mass is not accompanied by insulin resistance due to reduced inflammation[42–45], we propose that TP53INP2 is a modulator of insulin resistance, serving as a link between fat accumulation, inflammation and insulin resistance in adipose tissue. Future studies are required to analyse the participation of other cells/tissues in the metabolic effects detected in KO^{Ubc} mice.

We also propose the notion that TP53INP2 halts PPAR-γ activity and that TP53INP2 deficiency results in adipose tissue expandability and in an anti-inflammatory macrophage phenotype. In this connection, treatment with PPAR-γ agonists results in weight gain and improved insulin sensitivity in parallel to decreased inflammation[46]. In addition, PPAR-γ controls the alternative activation of macrophages[47].

In this report, we also document a mechanism of inhibition of adipogenesis. We provide evidence that TP53INP2 sequesters GSK3β into MVBs. This sequestration of GSK3β leads to β-catenin activation, its recruitment to the nucleus and the activation of TCF/LEF transcription factors. Consistent with the TP53INP2-induced GSK3β inactivation, the abundance and level of activation of β-catenin increased by TP53INP2 gain of function in preadipocytes, whereas TP53INP2 deficiency reduced the level of active β-catenin. Adipose tissue from TP53INP2-ablated mice also showed a reduced activity and abundance of β-catenin. We should mention that the localization of GSK3β in MVBs was detected upon expression of mutant Rab5 Q79L that enlarges late endosomes, and future studies are needed to validate the localization of GSK3β in the absence of manipulations of the endosomal pathway.

The sequestration of GSK3β induced by TP53INP2 requires the integrity of ESCRT complexes, specifically ESCRT-0 and ESCRT-III complexes. ESCRT complexes participate in sorting ubiquitinated proteins into intraluminal vesicles of MVBs for degradation in lysosomes or exosome release[48,49]. Our data also indicate that the TP53INP2-dependent incorporation of GSK3β into MVBs depends on the integrity of autophagy, and in support of this view, we document that TP53INP2 and LC3 proteins co-localize in the lumen of MVBs and that cells with no autophagy activity do not respond to TP53INP2 by moving GSK3β into MVBs. In all, our data indicate that TP53INP2 promotes the fusion of autophagosomes or autophagosome-like vesicles into endosomes, which triggers the sequestration of GSK3β. The specific pathway followed by GSK3β before being incorporated into MVBs is unknown.

Our data indicate the existence of a complex crosstalk between autophagy and adipogenesis. In preadipocytes, TP53INP2 blocks

adipogenesis through a mechanism that is dependent on autophagy and on the ESCRT machinery and causes GSK3β sequestration and remodelling of MVBs. Under these conditions, TP53INP2 does not modulate global autophagy flux in preadipocytes, which is in contrast to data reported in other cell types[28,30,31]. According to this view, the triggering of adipogenesis is linked to TP53INP2 repression, and under these conditions, a marked activation of autophagy is detected, which must be due to other autophagy factors. This view is coherent with prior observations indicating that deficiency of essential autophagy proteins impairs adipogenic differentiation and reduces adipose depots in mice[23–25].

Methods

Methods, including statements of data availability and any associated accession codes and references, are available at https://doi.org/10.1038/s41556-018-0072-9.

Received: 20 December 2016; Accepted: 23 February 2018;
Published online: 28 March 2018

References

1. Wu, H. & Ballantyne, C. M. Inflammation versus host defense in obesity. *Cell Metab.* **20**, 708–709 (2014).
2. Apovian, C. M. The clinical and economic consequences of obesity. *Am. J. Manag. Care* **19**, s219–s228 (2013).
3. Sun, K., Kusminski, C. M. & Scherer, P. E. Adipose tissue remodeling and obesity. *J. Clin. Invest.* **121**, 2094–2101 (2011).
4. Gustafson, B., Hedjazifar, S., Gogg, S., Hammarstedt, A. & Smith, U. Insulin resistance and impaired adipogenesis. *Trends Endocrinol. Metab.* **26**, 193–200 (2015).
5. Lundgren, M. et al. Fat cell enlargement is an independent marker of insulin resistance and 'hyperleptinaemia'. *Diabetologia* **50**, 625–633 (2007).
6. van Tienen, F. H. et al. Preadipocytes of type 2 diabetes subjects display an intrinsic gene expression profile of decreased differentiation capacity. *Int. J. Obes.* **35**, 1154–1164 (2011).
7. Gustafson, B., Hammarstedt, A., Hedjazifar, S. & Smith, U. Restricted adipogenesis in hypertrophic obesity: the role of WISP2, WNT, and BMP4. *Diabetes* **62**, 2997–3004 (2013).
8. Hammarstedt, A. et al. WISP2 regulates preadipocyte commitment and PPARγ activation by BMP4. *Proc. Natl Acad. Sci. USA* **110**, 2563–2568 (2013).
9. Patel, P. & Abate, N. Body fat distribution and insulin resistance. *Nutrients* **5**, 2019–2027 (2013).
10. Spalding, K. L. et al. Dynamics of fat cell turnover in humans. *Nature* **453**, 783–787 (2008).
11. Cawthorn, W. P., Scheller, E. L. & MacDougald, O. A. Adipose tissue stem cells: the great WAT hope. *Trends Endocrinol. Metab.* **23**, 270–277 (2012).
12. Rosen, E. D. & Spiegelman, B. M. What we talk about when we talk about fat. *Cell* **156**, 20–44 (2014).
13. Rosen, E. D. & MacDougald, O. A. Adipocyte differentiation from the inside out. *Nat. Rev. Mol. Cell Biol.* **7**, 885–896 (2006).
14. Christodoulides, C., Lagathu, C., Sethi, J. K. & Vidal-Puig, A. Adipogenesis and WNT signalling. *Trends Endocrinol. Metab.* **20**, 16–24 (2009).
15. Jin, T. Current understanding on role of the Wnt signaling pathway effector TCF7L2 in glucose homeostasis. *Endocr. Rev.* **37**, 254–277 (2016).
16. Ross, S. E. et al. Inhibition of adipogenesis by Wnt signaling. *Science* **289**, 950–953 (2000).
17. Bennett, C. N. et al. Regulation of Wnt signaling during adipogenesis. *J. Biol. Chem.* **277**, 30998–31004 (2002).
18. Bennett, C. N., Hodge, C. L., MacDougald, O. A. & Schwartz, J. Role of Wnt10b and C/EBPα in spontaneous adipogenesis of 243 cells. *Biochem. Biophys. Res. Commun.* **302**, 12–16 (2003).
19. Cawthorn, W. P. et al. Wnt6, Wnt10a and Wnt10b inhibit adipogenesis and stimulate osteoblastogenesis through a β-catenin-dependent mechanism. *Bone* **50**, 477–489 (2012).
20. Longo, K. A. et al. Wnt10b inhibits development of white and brown adipose tissues. *J. Biol. Chem.* **279**, 35503–35509 (2004).
21. Wright, W. S. et al. Wnt10b inhibits obesity in ob/ob and agouti mice. *Diabetes* **56**, 295–303 (2007).
22. Aslanidi, G. et al. Ectopic expression of Wnt10b decreases adiposity and improves glucose homeostasis in obese rats. *Am. J. Physiol. Endocrinol. Metab.* **293**, E726–E736 (2007).
23. Singh, R. et al. Autophagy regulates adipose mass and differentiation in mice. *J. Clin. Invest.* **119**, 3329–3339 (2009).
24. Baerga, R., Zhang, Y., Chen, P. H., Goldman, S. & Jin, S. Targeted deletion of autophagy-related 5 (atg5) impairs adipogenesis in a cellular model and in mice. *Autophagy* **5**, 1118–1130 (2009).
25. Ro, S. H. et al. Distinct functions of Ulk1 and Ulk2 in the regulation of lipid metabolism in adipocytes. *Autophagy* **9**, 2103–2114 (2013).
26. Zhang, Y. et al. Adipose-specific deletion of autophagy-related gene 7 (*atg7*) in mice reveals a role in adipogenesis. *Proc. Natl Acad. Sci. USA* **106**, 19860–19865 (2009).
27. Kaur, J. & Debnath, J. Autophagy at the crossroads of catabolism and anabolism. *Nat. Rev. Mol. Cell Biol.* **16**, 461–472 (2015).
28. Mauvezin, C. et al. The nuclear cofactor DOR regulates autophagy in mammalian and *Drosophila* cells. *EMBO Rep.* **11**, 37–44 (2010).
29. Sancho, A. et al. *DOR/Tp53inp2* and *Tp53inp1* constitute a metazoan gene family encoding dual regulators of autophagy and transcription. *PLoS ONE* **7**, e34034 (2012).
30. Sala, D. et al. Autophagy-regulating TP53INP2 mediates muscle wasting and is repressed in diabetes. *J. Clin. Invest.* **124**, 1914–1927 (2014).
31. Nowak, J. et al. The TP53INP2 protein is required for autophagy in mammalian cells. *Mol. Biol. Cell* **20**, 870–881 (2009).
32. Ruzankina, Y. et al. Deletion of the developmentally essential gene *ATR* in adult mice leads to age-related phenotypes and stem cell loss. *Cell Stem Cell* **1**, 113–126 (2007).
33. Ye, R. et al. Impact of tamoxifen on adipocyte lineage tracing: inducer of adipogenesis and prolonged nuclear translocation of Cre recombinase. *Mol. Metab.* **4**, 771–778 (2015).
34. Sanchez-Gurmaches, J. et al. *PTEN* loss in the Myf5 lineage redistributes body fat and reveals subsets of white adipocytes that arise from Myf5 precursors. *Cell Metab.* **16**, 348–362 (2012).
35. Gustafson, B. et al. Inflammation and impaired adipogenesis in hypertrophic obesity in man. *Am. J. Physiol. Endocrinol. Metab.* **297**, E999–E1003 (2009).
36. Liu, C. et al. Control of β-catenin phosphorylation/degradation by a dual-kinase mechanism. *Cell* **108**, 837–847 (2002).
37. Okamura, M. et al. COUP-TFII acts downstream of Wnt/β-catenin signal to silence PPARγ gene expression and repress adipogenesis. *Proc. Natl Acad. Sci. USA* **106**, 5819–5824 (2009).
38. Taelman, V. F. et al. Wnt signaling requires sequestration of glycogen synthase kinase 3 inside multivesicular endosomes. *Cell* **143**, 1136–1148 (2010).
39. Vinyoles, M. et al. Multivesicular GSK3 sequestration upon Wnt signaling is controlled by p120-catenin/cadherin interaction with LRP5/6. *Mol. Cell* **53**, 444–457 (2014).
40. Stenmark, H. et al. Inhibition of rab5 GTPase activity stimulates membrane fusion in endocytosis. *EMBO J.* **13**, 1287–1296 (1994).
41. Christ, L., Raiborg, C., Wenzel, E. M., Campsteijn, C. & Stenmark, H. Cellular functions and molecular mechanisms of the ESCRT membrane-scission machinery. *Trends Biochem. Sci.* **42**, 42–56 (2017).
42. Maris, M. et al. Deletion of C/EBP homologous protein (Chop) in C57Bl/6 mice dissociates obesity from insulin resistance. *Diabetologia* **55**, 1167–1178 (2012).
43. Perreault, M. & Marette, A. Targeted disruption of inducible nitric oxide synthase protects against obesity-linked insulin resistance in muscle. *Nat. Med.* **7**, 1138–1143 (2001).
44. Fan, W. et al. Androgen receptor null male mice develop late-onset obesity caused by decreased energy expenditure and lipolytic activity but show normal insulin sensitivity with high adiponectin secretion. *Diabetes* **54**, 1000–1008 (2005).
45. Kalupahana, N. S. et al. Eicosapentaenoic acid prevents and reverses insulin resistance in high-fat diet-induced obese mice via modulation of adipose tissue inflammation. *J. Nutr.* **140**, 1915–1922 (2010).
46. Cariou, B., Charbonnel, B. & Staels, B. Thiazolidinediones and PPARγ agonists: time for a reassessment. *Trends Endocrinol. Metab.* **23**, 205–215 (2012).
47. Odegaard, J. I. et al. Macrophage-specific PPARγ controls alternative activation and improves insulin resistance. *Nature* **447**, 1116–1120 (2007).
48. Bissig, C. & Gruenberg, J. ALIX and the multivesicular endosome: ALIX in Wonderland. *Trends Cell Biol.* **24**, 19–25 (2014).
49. Scourfield, E. J. & Martin-Serrano, J. Growing functions of the ESCRT machinery in cell biology and viral replication. *Biochem. Soc. Trans.* **45**, 613–634 (2017).

Acknowledgements

We thank D. Rossell (Department of Statistics, University of Warwick, Coventry, UK) and C. Stephan-Otto Attolini (Biostatistics and Bioinformatics Unit, Institute for Research in Biomedicine, Barcelona, Spain) for their support with the transcriptomic studies. We also thank L. Bardia (Advanced Digital Microscopy Facility, Institute for Research in Biomedicine, Barcelona, Spain), J. Comas (Cytometry and Genomics Facility, University of Barcelona, Spain), N. Plana, V. Hernández and J. Manuel Seco for their technological assistance. A.Z. is a recipient of an ICREA 'Academia' (Generalitat de Catalunya), M.R. is a researcher hired by CIBERDEM (Instituto de Salud Carlos III) and A.S.-P. is a recipient of a predoctoral fellowship from the Universitat de Barcelona. This

study was supported by research grants from the MINECO (SAF2013-40987R), grant 2014SGR48 from the Generalitat de Catalunya, CIBERDEM ('Instituto de Salud Carlos III') and INTERREG IV-B-SUDOE-FEDER (DIOMED, SOE1/P1/E178). IRB Barcelona is the recipient of a Severo Ochoa Award of Excellence from MINECO (Government of Spain). IRB Barcelona is a member of CERCA.

Author contributions

M.R. conceived and performed the experiments and wrote the manuscript. V.A.F. conceived and performed the experiments. A.S.-P., I.C.-R. A.D.-R., X.D., B.G., A.H., M.S.-F. and J.M.M.-N. performed the experiments. J.V., J.M.F.-R. and U.S. revised the experimental data and contributed to the discussion. M.P. contributed to the discussion. A.Z. directed the research, revised the experimental data and wrote the manuscript.

Competing interests

The authors declare no competing interests.

Additional information

Supplementary information is available for this paper at https://doi.org/10.1038/s41556-018-0072-9.

Reprints and permissions information is available at www.nature.com/reprints.

Correspondence and requests for materials should be addressed to A.Z.

Publisher's note: Springer Nature remains neutral with regard to jurisdictional claims in published maps and institutional affiliations.